Ghent University, Faculty of Medicine and Health Sciences

Unraveling the MYCN-driven transcriptional landscape of neuroblastoma

a cross-species integrated transcriptome approach

Anneleen Beckers


FACULTY OF MEDICINE AND HEALTH SCIENCES

Ghent University, Faculty of Medicine and Health Sciences

Unraveling the MYCN-driven transcriptional landscape of neuroblastoma

a cross-species integrated transcriptome approach

This thesis is submitted as fulfillment of the requirements for the degree of Doctor in Biomedical Sciences by Anneleen Beckers, 2015

Promotor

prof. dr. Frank Speleman

Co-promotor

prof. dr.ir. Katleen De Preter

Center for Medical Genetics

Ghent University Hospital, Medical Research Building

De Pintelaan 185, 9000 Ghent, Belgium

+32-9-332-6979

anneleen.beckers@ugent.be

Thesis is submitted to fulfill the requirements for the degree of doctor in Biomedical Sciences

Promoter: prof. dr. Frank Speleman
Ghent University, Belgium

Co-promoter: prof. dr. ir. Katleen De Preter
Ghent University, Belgium

Members of the examination committee:

dr Frank Westermann
German Cancer Research Center, Germany

prof dr Rogier Versteeg
University of Amsterdam, The Netherlands

prof dr Jean-Christophe Marine
KULeuven, Belgium

dr Yvan Saeys
Ghent University, Belgium

prof dr Kathleen Claes
Ghent University, Belgium

dr Pieter Van Vlierberghe
Ghent University, Belgium

dr Pieter Rondou
Ghent University, Belgium

The research described in this thesis was conducted at the Center for Medical Genetics, Ghent University, Ghent, Belgium. This work was supported by the agency for Innovation by Science and Technology (IWT).

Contents

Summary

Summary

Since its identification in neuroblastoma, increasing evidence points towards a central role for MYCN in the biology of neuroblastoma tumors. As a consequence, targeting MYCN and its downstream functions would be a promising strategy to treat neuroblastoma patients. However, the development of inhibitors targeting MYC proteins has been challenging, as MYC/MYCN proteins are composed of two extended alpha-helices with no obvious surfaces for small molecule binding. Therefore, a thorough understanding of MYCN's functions and the upstream mechanisms regulating its expression would contribute to the development of compounds specifically targeting the impact of MYCN in neuroblastoma cells.

To address this issue, I initiated this thesis with the construction of an *in vivo* time-resolved miRNA and gene expression dataset of MYCN-driven neuroblastoma development, using the well-established TH-MYCN mouse model. After extensive validation of the dataset, I applied an exiting transcriptome-wide cross-species approach to search for transcriptional regulators that can be regarded as master regulators of neuroblastoma development. The corresponding miRNA expression dataset was exploited during the characterization of the complete MYCN-miRNA interactome in neuroblastoma using the powerful combination of this dataset and an unbiased 3'UTR reporter screen. I next characterized how MYCN affects the expression of LIN28B, a highly conserved RNA-binding protein, which is shown to induce MYCN expression in neuroblastoma via the suppression of the MYCN-targeting let-7 family of miRNAs.

Throughout this project, studying the genetic landscape of the well-established TH-MYCN mouse model has provided great insights in the perturbed miRNA-mRNA networks in neuroblastoma. Although representing an excellent and broadly used tool, this mouse model holds some limitations related to the transgene integration site, the anatomical location of the observed tumors, implementation of *in vivo* imaging and tumor incidence in different genetic backgrounds. I therefore present a novel mouse model with targeted Cre-conditional *MYCN* expression in the neural crest. Molecular characterization showed that the tumors arising in this model, strongly resemble the existing TH-MYCN mouse model and human neuroblastoma tumors. We expect that this new model, which addresses some of the major limitations of the TH-MYCN model, will play a major role in the investigation of neuroblastoma.

Samenvatting

Sinds de identificatie van amplificatie van MYCN in neuroblastoom, duidt toenemend bewijs op een centrale rol voor MYCN in de biologie van neuroblastoom tumoren. Bijgevolg lijkt het veelbelovende strategie om therapieën te ontwikkelen die de activiteit en de functies van MYCN ondermijnen. Echter, de ontwikkeling van MYC inhibitoren is uitdagend, aangezien MYC/MYCN eiwitten bestaan uit twee lange alpha-helices zonder duidelijke oppervlakken waarop kleine moleculen zouden kunnen binden. Om deze beperking te kunnen omzeilen, zou een grondig begrip van de functies van MYCN en de stroomopwaartse mechanismen die MYCN reguleren, kunnen bijdragen tot de ontwikkeling van geneesmiddelen die specifiek gericht zijn om de activiteit van MYCN in neuroblastoom cellen uit te schakelen.

Om dit probleem aan te pakken, heb ik dit proefschrift aangevat met de bouw van een dynamische miRNA en gen expressie dataset van MYCN-gedreven neuroblastoom ontwikkeling. Na uitgebreide validatie van de dataset, heb ik een veelbelovende data mining strategie toegepast om te zoeken naar belangrijke sleutel genen in de ontwikkelen van neuroblastoom tumoren. De bijbehorende miRNA expressie dataset werd benut tijdens de karakterisatie van het volledige MYCN-miRNA interactoom in neuroblastoom met behulp van de krachtige combinatie van deze dataset en een 3'UTR reporter screen. Daarnaast heb ik verder in kaart gebracht hoe MYCN een impact heeft op LIN28B, een recent geïdentificeerd oncogen in neuroblastoom tumoren.

Doorheen dit project, heeft de studie van het genetische landschap van het gevestigde TH-MYCN muismodel, nieuwe inzichten gebracht in de verstoorde miRNA-mRNA-netwerken in neuroblastoom. Het gebruikte TH-MYCN muismodel is een belangrijk model dat reeds vaak gebruikt werd voor dergelijke studies, maar dit model houdt enkele beperkingen in. Daarom heb ik, in samenwerking met het labo van prof Schulte (Essen, Duitsland), een nieuw muismodel ontwikkeld met een gerichte en conditionele over expressie van MYCN in de cellen van de neurale lijst. Moleculaire karaterisatie toont aan dat de tumoren die in dit model ontstaan, sterke gelijkenissen vertonen met het bestaande TH-MYCN muis model en humane neuroblastoom tumoren. We verwachten dat dit nieuwe model, die enkele belangrijke beperkingen van het TH-MYCN model aanpakt, in de toekomst een belangrijke rol zal spelen in het onderzoek naar neuroblastoom.

Chapter 1

Introduction

Contents

An introduction to neuroblastoma biology

I believe there is no need to demonstrate that cancer is a devastating disease; during our lifetime, each of us will be confronted with its consequences – either directly or through someone close by. Fortunately, as our understanding of normal and deregulated cellular biology increased, cancer research has resulted in means for curing cancer patients. In contrast to many other tumor entities, however, understanding the genetic basis of neuroblastoma has lagged behind, which is in part due to its infrequent appearance and the heterogenic nature of the disease. In the past decennium, the genetic landscape and the molecular implications have become increasingly clear, generating opportunities for the development of targeted therapies.

The first part of this introduction is devoted to neuroblastoma biology, more specifically describing its cellular origin and its genetic landscape. The second part zooms in on the broad involvement of the oncogenic transcription factor MYCN in the biology of neuroblastoma tumors and highlights emerging therapeutic strategies that aim to tackle MYCN activity in a targeted fashion. Finally, this introduction also brings microRNAs (miRNAs) into the picture.

Neuroblastoma

Neuroblastoma is a rare childhood malignancy that originates from precursor cells of the sympatho-adrenal lineage of the peripheral nervous system. Neuroblastoma tumors arise at various sites of the developing sympathetic nervous system: at least half of the primary tumors are found in the adrenal gland while others originate in the paraspinal sympathetic ganglia or in pelvic ganglia (**Figure 1.1**). Neuroblastoma is the most common extra-cranial solid tumor in children and accounts for 8 to 10% of all childhood cancers. This disease is characterized by clinical and genetic heterogeneity: while young children (< 18 months) with favorable tumors have good survival chances due to spontaneous regression or differentiation of the tumor, older patients are often confronted with aggressive metastatic disease and rapid progression with fatal outcome, despite multimodal therapy.

The following sections highlight the developmental origin of neuroblastoma tumors and the genetic defects that occur during neuroblastoma oncogenesis.

When development goes wrong

Childhood malignancies are typically disorders of normal development. Embryonal development, beginning with a single population of stem cells and culminating in organogenesis, is marked by stages of proliferation and differentiation and is dependent upon communication between distinct populations of precursor cells. Strong mitogenic signals drive expansion and limit the ability of cells to terminally differentiate in G0-phase of the cell cycle. Changes in the concentrations of certain key regulators promote cell-cycle exit and the beginning of differentiation. The inability of progenitor cells to exit from a proliferative phase can potentially drive tumor formation. [1]

This paradigm of embryonal neoplasms contrasts that of adult cancers not only in dramatically shortened latency, but also in the cell populations from which tumors are currently thought to originate. Tumor formation in adults has been attributed classically to a reactivation of persistent cellular proliferation through genetic perturbations such as oncogenic activation and loss of apoptotic regulators. In contrast, childhood malignancies arise from progenitor cells which are already rapidly dividing as part of the normal developmental process. Embryonal tumors arise from embryonic or fetal tissues and develop through aberrations in normal developmental processes. [1]

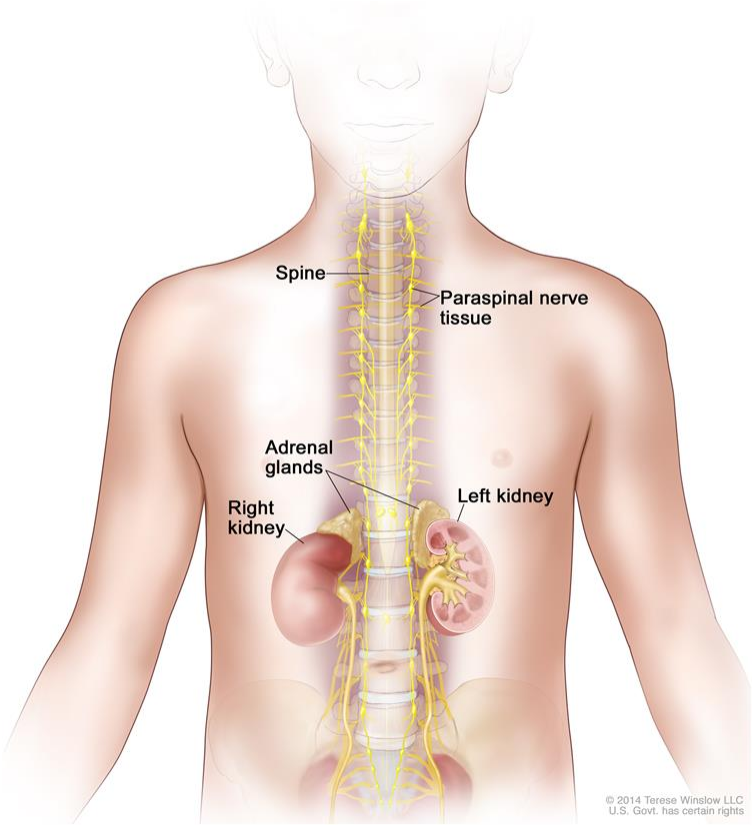

Figure 1.1: Anatomical location of neuroblastoma tumors.
Neuroblastoma may be found in the adrenal glands and paraspinal nerve tissue from the neck to the pelvis. Image from www.cancer.gov

From neuronal precursor to neuroblastoma tumor

Neuroblastoma tumors develop from precursor cells of the sympatho-adrenal lineage that arise from the neural crest. The neural crest is a transient component of the ectoderm, and gives rise to diverse cell types, ranging from the peripheral nervous system to the craniofacial skeleton and pigment cells. Initially, at the end of the third and the beginning of the fourth week of embryonic development, the cells of the neural crest are located at the edge of the neural folds that arise during neurulation – the development of the neural tube from the neural plate. Shortly after neurulation, the neural crest cells migrate out of the neural tube to give rise to various structures, including the sympathetic nervous system that develops from the fate-restricted sympatho-adrenal progenitor cells, so-called neuroblasts, one of the major derivatives of the neural crest. Upon migration, these neuroblasts start expressing a series of factors that further allow their differentiation into either the ganglionic or the chromaffin lineage. Together, they form the differentiated cells that populate the sympathetic ganglia, paraspinal ganglia and the adrenal medulla. [2]

Studying the genetic differences between the neuroblasts and neuroblastoma tumors could provide insight in the aberrations that transform a sympatho-adrenal precursor into a malignant tumor. However, neuroblasts have long remained inaccessible for research, because they fully maturate or undergo apoptosis during development. In 2006, the pioneering isolation of neuroblasts from human fetal adrenal glands, performed by De Preter and colleagues [3], generated a benchmark dataset for the exploration of perturbed genetic networks in neuroblastoma development, and confirmed the hypothesis that neuroblasts are the progenitor cells of neuroblastoma tumors [3]. Indeed, many genes involved in the development of the sympathetic nervous system have now been implicated in neuroblastoma development, further corroborating the link between neuroblastoma and its cell-of-origin.

Oncogenic neuroblastoma driver genes and genetically engineered animal models

Genetically, the majority of neuroblastoma tumors is characterized by loss and/or gain of genomic regions: numerical whole-chromosomal gains are typically found in low-risk tumors, whereas segmental chromosomal gains or losses are associated with high-risk disease. Recurrent structural chromosomal alterations commonly associated with advanced stage of disease and poor outcome in neuroblastoma include amplification of the oncogene *MYCN*, deletion of chromosome arms 1p, 3p, 4p and 11q, and gain of chromosome arm 17q. Recently, whole genome and exome next generation sequencing studies [4-6] have revealed that, besides these genomic regions, few single genes are recurrently affected in

neuroblastoma patients. This is in line with the general observation that pediatric tumors acquire far less genetic alterations compared to adult cancers. Three genes have been convincingly shown to act as oncogenic drivers: MYCN, ALK and LIN28B, all of which are involved in early sympathetic nervous system development.

MYCN – v-myc avian myelocytomatosis viral oncogene neuroblastoma derived homolog

Amplification of *MYCN*, an oncogenic transcription factor on 2p24, was the first genetic aberration established in neuroblastoma [7,8]. High-level amplification of *MYCN* defines approximately 20% of all neuroblastoma tumors and 45% of high-risk cases [9], and is frequently associated with loss of 1p and gain of 17q, together delineating a subgroup of patients with unfavorable prognosis [10]. Oncogenes of the MYC family – to which *MYCN* belongs – are important in normal development; perturbed expression may give rise to deregulated growth and proliferation of cells, ultimately leading to cancer development (see below). Interestingly, high-risk neuroblastoma tumors without *MYCN* amplification often express elevated levels of *MYC* [11], which similarly results in activation of MYCN/MYC signaling pathways inferring a poor outcome similar as in *MYCN* amplified cases [11,12]. This highlights the importance of both MYC and MYCN signaling in neuroblastoma.

To proof a causal relationship between *MYCN* amplification or overexpression and high-risk neuroblastoma, a first neuroblastoma mouse model was developed by targeting *MYCN* overexpression to the cells of the developing sympathetic nervous system [13]. These transgenic TH-MYCN mice develop tumors that faithfully recapitulate biological and genetic features of human high-risk neuroblastoma, thus serving as a useful pre-clinical model [13,14]. However, being a transcription factor, MYCN has proven difficult to target therapeutically, warranting the search for new, drugable neuroblastoma oncogenes.

ALK – anaplastic lymphoma kinase

The genetic study of familial neuroblastoma tumors, comprising <2% of all neuroblastoma cases [15], led to the identification of mutations in the *ALK* gene in the majority of familial cases [16-19]. Subsequent analysis of sporadic tumors showed that *ALK* is an important neuroblastoma predisposition gene, with activating mutations occurring in about 8% of sporadic cases [17]. ALK is tyrosine kinase receptor which is preferentially expressed in the developing peripheral and central nervous systems [20], and mutations result in constitutive receptor activation and subsequent signaling to pro-survival pathways [16,18,19]. More recently, chromosome 2 copy gain, including the *ALK* locus, was shown to be associated with an increased *ALK* expression and a significantly worse out-come in the global population [21,22].

Interestingly, ALK appears to be functionally connected to MYCN: initially, the *ALK*^{F1174L} mutant, which shows increased transforming capacity as compared to the *ALK*^{R1275Q} mutant [19], was observed more often in tumors with *MYCN* amplification, suggesting a cooperative effect between both aberrations in neuroblastoma tumors [21]. Shortly after these observations, mutant *ALK* was found to accelerate neuroblastoma tumorigenesis in MYCN-driven tumors in mice [23-25] and zebrafish [26] by stabilizing MYCN protein. ALK activates the PI3K/AKT/mTOR pathway resulting in inactivation of GSK3ß and PP2A, two proteins involved in MYCN degradation [27] (see below). This direct effect on MYCN stabilization was shown to be complemented by an anti-apoptotic effect of *ALK*^{F1174L} that allows transformed cells to evade MYCN-induced apoptosis [23,26] (see below). Indeed, early in the embryogenesis of MYCN transgenic zebrafish, *MYCN* overexpression results in a profound loss of neural crest-derived cells within the sympatho-adrenal cell lineage. Nevertheless, these animals can develop neuroblastoma, and both the onset and penetrance of the disease are markedly enhanced by constitutively expressed ALK^{F1174L} (ref. 26). Furthermore, *ALK* was recently found to be a MYCN target gene [28], and ALK can, in its turn, stimulate initiation of *MYCN* transcription in neuroblastoma [29], thus creating a strong feed-forward loop in which *MYCN* and *ALK* enhance each others expression and activity.

In the abovementioned animal models, constitutively activated ALK is not able to generate neuroblastoma tumors in absence of prior driving events. This observation is contradicted by the findings of Heukamp and colleagues [24] who showed that targeted expression of *ALK* can induce neuroblastoma tumors, albeit with low penetrance. However, as the mutant ALK construct in this model is integrated in the mouse genome by random insertion, and as this insertion location is not known, it cannot be excluded that the disruption of a potential neuroblastoma tumor suppressor co-operates with ALK in these mice to cause neuroblastoma.

LIN28B – lin-28 homolog B (C. elegans)

More recently, *LIN28B* was identified as a *bona fide* neuroblastoma oncogene [30], although it had been associated to neuroblastoma susceptibility through genome-wide association studies [31]. LIN28B and its paralog LIN28A are highly conserved RNA-binding proteins that play important roles in development and stem cell reprogramming by regulating the self-renewal of stem cells [32], and in glucose metabolism [33]. They mediate these pleiotropic functions by enhancing the translation of target mRNAs and by inhibiting let-7 miRNA biogenesis, both in a sequence-specific manner (reviewed in ref. 34). The let-7 family of miRNAs comprises a group of 9 sequence-related miRNAs, processed from 12 transcripts encoded in 8 genomic loci. In a myriad of tumor entities, decreased let-7 expression levels –

through LIN28 overexpression or other mechanisms – cause the activation of multiple *bona fide* oncogenes, including RAS and MYC (reviewed in ref. 35).

Initially, over-expression of *LIN28B* was found to be associated with the presence of an intronic SNP in neuroblastoma.[31] Recently, elevated *LIN28B* expression was found to contribute to neuroblastoma tumorigenesis via let-7 dependent de-repression of *MYCN* [30], connecting yet another neuroblastoma oncogene to *MYCN*. Indeed, murine and human tumors overexpressing *LIN28B* show a drastic reduction in expression levels of the let-7 family of miRNAs and subsequent loss of *MYCN* repression.[30] Of note, MYCN itself has been suggested to induce *LIN28B* transcription, which would create another feed-forward mechanism.[36,37] However, as MYCN-mediated regulation of *LIN28B* in various neuroblastoma cell line models and TH-MYCN tumors could not be confirmed [30], this remained an unresolved interaction. In Chapter 5, we present evidence that MYCN does regulate LIN28B expression in neuroblastoma tumors, via both direct and indirect mechanisms.

MYCN as central nexus of neuroblastoma biology

Since its first discovery of amplification in high-risk neuroblastoma tumors (in 1983), MYCN has been a central theme in neuroblastoma research. The transcriptional activities of MYCN have far-reaching consequences for neuroblastoma tumorigenesis, and as such, the promise of finding a targeted therapy against MYCN fueled relentless efforts to gain a deeper understanding of MYCN function and regulation. The recent lessons from neuroblastoma animal models have only strengthened the central position of MYCN in neuroblastoma tumor biology: all roads appear to lead to MYCN. This chapter zooms in on MYCN, its transcriptional activities and impact on neuroblastoma biology, and illustrates the promising progression of MYCN-targeting therapies towards the clinic.

MYCN is a MYC family member

MYCN is a member of the MYC-family of proto-oncogenic transcription factors that comprises three members: *MYC*, *MYCN* and *MYCL*. The MYC proteins are one of the most widely studied proto-oncogenes, and are part of the larger MYC/MAX/MAD network that comprises a group of transcription factors whose distinct interactions result in transcriptional activation or repression [38]. Initially isolated from chicken tumor DNA as the human homologue of a retroviral oncogene (v-*myc*), MYC is now documented to be involved broadly in many cancers, in which its expression is estimated to be elevated or deregulated in up to 70% of human cancers. Early *in vitro* studies of MYC revealed its potential to transform normal embryonic fibroblasts in cooperation with other oncogenes. [39] Nowadays, it is clear that the proto-oncogene MYC lies at the crossroads of many growth-promoting signal transduction pathways and is an early response gene immediately downstream of many ligand-membrane receptor complexes. [40]

MYCN was identified as an amplified gene homologous to v-*myc* but distinct from *MYC*, in human neuroblastoma. [7,41] Structurally, the coding regions of both *MYC* and *MYCN* are highly homologous, particularly around the functional domains of the resulting proteins. Because of the structural and sequence homology between the MYC-family genes, the function and biochemical properties of MYC proteins are closely related. [42] Biologically, MYCN, like MYC, was found to promote transformation in rat embryo fibroblasts, and to induce proliferation and cell cycle progression in quiescent fibroblasts. [43,44] Furthermore, cloning of MYCN into the MYC locus in MYC knockout mice could rescue embryonic lethality and restore immune functions. Of note, MYCN knock-in animals were smaller, developed dystrophy of skeletal muscles, and showed differences in growth responses in some cell

types. These findings suggest that MYC and MYCN show prominent, albeit incomplete, redundancy. [45]

The inability of endogenous MYCN and MYC to fully compensate for the abovementioned knockout phenotypes may be due to the distinct spatiotemporal expression patterns displayed by MYC family proteins. MYC is ubiquitous and highly expressed in most rapidly proliferating cells during development and continues to be expressed in dividing cells of adult tissues. [40] MYCN, on the other hand, has a more restricted expression pattern: it is expressed during embryogenesis in pre-B cells, kidney, forebrain, hindbrain, and intestine, with highest expression in the developing brain. After embryonic development, MYCN is downregulated and it is not significantly expressed in adult tissues. In accordance, *MYCN* amplification or overexpression is often restricted to tumors of embryonic or neuro-ectodermal origin such as neuroblastoma, retinoblastoma [46], Wilm's tumor [47], glioblastoma [48] and medulloblastoma [49], while MYC is activated in a broad range of tumors. Further supporting functional differences between both family members, is their differential preference for binding to similar, yet distinct, DNA sequences in the promoters of target genes. [50] As a consequence, despite that MYC genes may share many related targets, at the same time they retain other, unique ones, suggesting that they may have independent and tissue-specific functions. [42]

Transcriptional regulation by MYC proteins

MYC family members are transcription factors that bind to DNA at conserved elements within the promoters of an extensive network of genes, either directly inducing gene transcription or silencing of expressed genes. [40]

MYC proteins as transcriptional activators

Transcriptional activation of MYC target genes occurs via sequence-specific (E-box = CA*NN*TG) DNA binding upon MYC-MAX dimerization. [40,51] In line with the diverging functional implications of MYC and MYCN, MYCN preferentially binds the E-box CATGTG as well as the canonical CACGTG. Under MYCN–amplified conditions, however, MYCN becomes less specific and can bind additional non-canonical E-box motifs. [50] The binding of MYC-MAX heterodimers to DNA initiates the organized recruitment of many associated factors into a large, chromatin-associated complex whose precise constituents may be determined by a variety of both cell- and growth-specific conditions. [52] A crucial role in the recruitment and assembly of these complexes seems to be assigned to the bromodomain and extraterminal (BET) family of adaptor proteins, which comprises BDR2, BRD3, BRD4, and BRDT and performs diverse roles in regulating transcription by RNA polymerase II.

Common to all four BET proteins are two conserved N-terminal bromodomains – BD1 and BD2, which are chromatin interaction modules that recognize acetylated lysine residues on histone tails and other nuclear proteins [53], and an extraterminal domain, which has been linked to transcriptional regulation by interacting with several histone modifiers. Recruitment of the MYC-MAX heterodimer and its associated proteins to the DNA seems to be associated with enhanced histone acetylation, an event which appears crucial for the binding of BET proteins through their bromodomains [54,55].

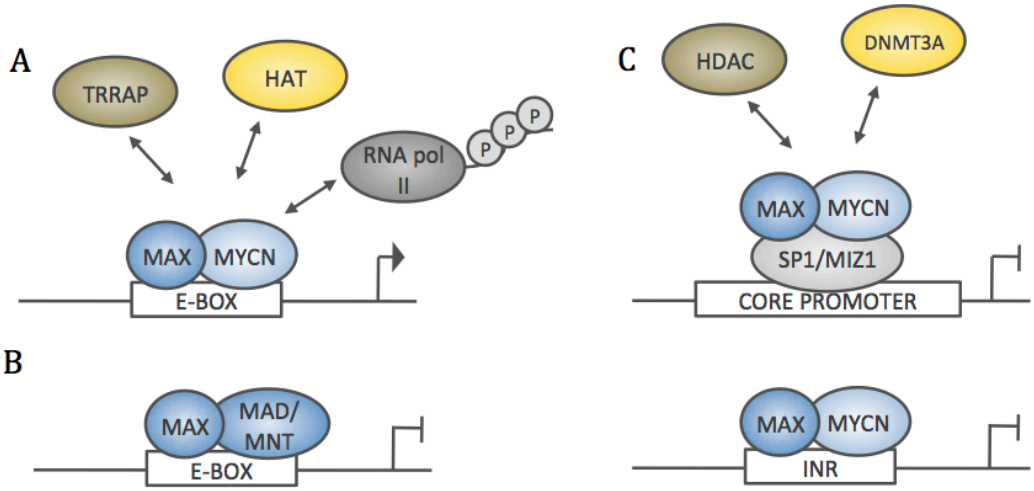

Figure 1.2: Transcriptional regulation by MYC proteins. (A) Transcriptional activation of target genes occurs via binding of the MYC-MAX heterodimer to an E-box sequence in the target promoter region, and subsequent recruitment of many associated factors into a large, chromatin-associated complex. **(B)** E-box dependent transcriptional repression occurs via displacement of the MYC-MAX heterodimer by a repressive MAX-MAD heterodimer. **(C)** E-box independent transcriptional silencing occurs via interaction of the MYC-MAX heterodimer with basal transcription factors, upon which silencing chromatin modifiers are recruited.

MYC proteins as transcriptional repressors

As described above, the role of MYC as a positive regulator of gene expression is well-established, mechanistically diverse and important for transformation. [40] However, genome-wide analyses demonstrate that MYC represses at least as many targets as it activates. [56] One of the first indicators that MYC might also function as a transcriptional repressor came from studies published in the 1980s that suggested that MYC participates in a negative feedback loop. [40] The present mechanistic model includes E-box dependent and E-box independent mode of actions that can co-exist (**Figure 1.2**). In E-box dependent gene silencing, MYC-MAX complexes are displaced by MAX-MAD complexes that recruit the mSin3 repressor complex, which will lead to histone deacetylation and increased chromatin compaction. [38] In E-box independent gene silencing, MYC-MAX complexes interact with

basal transcription factors such as SP1 and MIZ1. [57] Occurrence of this E-box independent process is supported by the observation that more than 40% of MYC binding sites lack recognizable E-box sequences. [58] More recently, Valentijn and colleagues [59] showed that genes downregulated by MYCN are not enriched for MYCN binding, supporting a mechanism in which MYC proteins indirectly associated with repressed genes via intermediate factors such as SP1 and MIZ1. [59] There is evidence that E-box independent MYC-mediated transcriptional repression involves DNA-methylation and silencing chromatin modifications: MYC can recruit the DNA methyltransferase DNMT3A to the promoter region of genes to induce gene silencing. [60] The proposed model involves MYC binding to the cofactor MIZ1 to form a ternary complex with DNMT3A, inducing methylation. Although structural differences exist between MYC and MYCN within the N-terminal domain, both proteins contain the functional domains which are required to associate with DNMT3A [60], indicating that MYCN could interact in a similar manner. In addition, MYCN directly interacts with the histon methyltransferase EZH2 [61], implicated in the trimethylation of histone H3 on lysine 27, a transcriptional silencing mark. Finally, MYCN can indirectly mediate the repression of multiple genes simultaneously via activation of noncoding RNAs, such as miRNAs and long noncoding RNAs (see below).

Identification of MYC target genes

Knowledge of MYCN target genes provides insight in the molecular mechanisms that contribute to the transforming effect of MYCN. Analysis of gene expression in neuroblastoma cell lines where MYCN levels can be experimentally manipulated have identified many genes and miRNAs whose expression is altered in response to changes in MYCN levels. [62-64] Distinguishing direct versus indirect effects based on expression profiling, however, is difficult since MYCN regulates other transcription factors as well as regulatory RNAs. In recent years, the chromatin immunoprecipitation assay (ChIP) has allowed researchers to better identify true direct targets of MYCN. [11,50,59,65,66]

Transcriptional regulation of non-coding RNAs, including miRNAs, contributes to the overall effect of MYCN on the cellular transcriptome (see below). The identification of miRNAs as transcriptional targets of MYCN, however, has been complicated by the difficulty of predicting promoters from short conserved sequence features. [67,68] miRNAs, whether they are located in intergenic regions or embedded within introns of protein-coding genes, are – in most cases – generated from long primary transcripts. The rapid processing of these transcripts, which can be up to several kb long, by DROSHA presents a technical barrier for large-scale identification of miRNA transcription start sites, as they can be located very far away from the mature miRNA and therefore cannot be easily inferred from the genomic

location of the mature miRNA. The difficulty of experimentally detecting and consequently annotating miRNA promoters has limited our ability to identify the regulatory circuits that control miRNA expression. [69]

The heterogeneous nature of MYCN and its impact on neuroblastoma biology

Via activation or repression of its target genes, MYCN leaves a profound footprint on neuroblastoma biology, affecting all hallmarks of cancer (**Figure 1.3**). The observed oncogenic effects in neuroblastoma are the net result of all affected pathways.

One of the key biological functions of MYC proteins contributing to cell proliferation, is their ability to promote cell-cycle progression. [40,70] Specifically, MYCN amplified neuroblastoma tumors show an inability to arrest in G1-phase in response to irradiation and DNA damage, possibly via up-regulation of both CDK4 [71] and SKP2 [72], allowing CDK2 to escape p21 inhibition. This results in hyperphosphorylation of RB1 and subsequent release of E2F transcription factors that activate genes encoding many of the proteins involved in G1 progression and DNA and RNA synthesis. [70] Furthermore, MYCN-mediated upregulation of CHK1, an important regulator of S-phase and G2/M checkpoints, has been suggested as a mechanism through which *MYCN* amplified neuroblastoma becomes refractory to standard chemotherapy. [73] In parallel, MYCN also exerts important influences on the cell cycle by repressing genes: the CDK inhibitors INK4B[p15] and WAF1[p21] — which are involved in cell-cycle arrest — are inactivated because the MYC–MAX heterodimer interferes with positively acting transcription factors such as MIZ1 [74] and/or SP1.

Intriguingly, MYCN – like MYC – not only activates proliferation, it also sensitize cells to apoptosis. [40,70] Ectopic MYCN expression increases apoptosis in response to DNA damage in MYCN non-amplified cell lines [75] and MYCN amplified neuroblastoma cell lines were found to undergo significantly higher levels of apoptosis after DNA damage than MYCN non-amplified neuroblastoma cell lines [76]. Whether MYCN promotes a net proliferative response is dependent on the status of cooperating factors, such as the anti-apoptotic protein BCL2 [77] or p53 [78]. Interestingly, *TP53* mutations are rare in neuroblastoma at diagnosis [79], suggesting that MYCN likely cooperates with suppressors of p53 signaling. A number of these p53 signaling suppressors are directly regulated by MYCN, supporting its dual role in cellular hemostasis: miRNA-380-5p [80], CUL7 [81], BMI1 [82], TWIST1 [83], and the primary p53 antagonist MDM2 [65] are MYCN target genes. In contrast, mutations in *TP53* and p53 pathway members occur in neuroblastoma at relapse, consistent with the idea that such mutations, which drive therapy-resistant disease, may arise in response to cytotoxic chemotherapy[79].

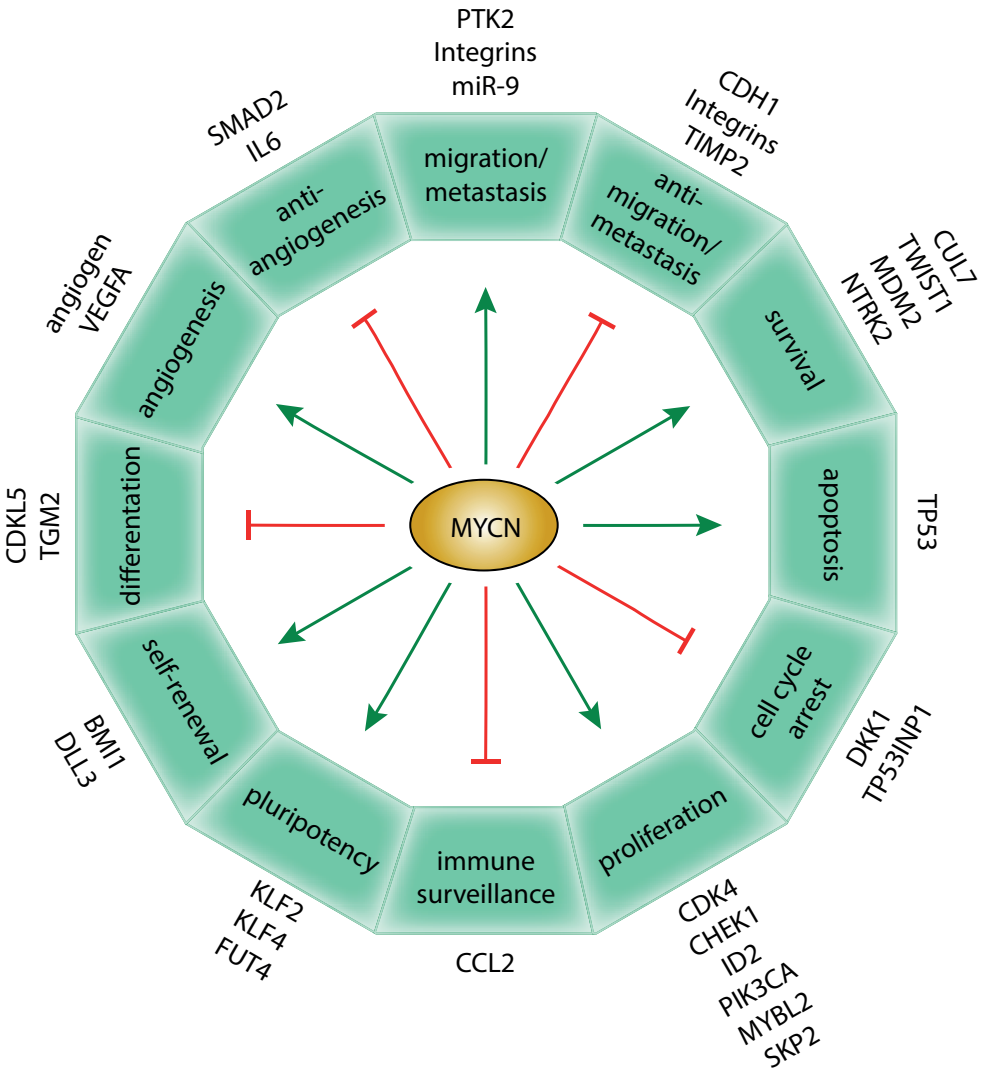

Figure 1.3: The impact of MYCN on neuroblastoma biology. MYCN plays multiple roles in malignancy and maintenance of stem-like state. MYCN can activate transcription of genes involved in metastasis, survival, proliferation, pluripotency, self-renewal, and angiogenesis. Additionally, MYCN can suppress expression of genes that promote differentiation, cell cycle arrest, immune surveillance, and genes that antagonize metastasis and angiogenesis. [Adapted from Huang, M. and Weiss W. A. *Cold Spring Harb Perspect Med* (2013), Figure 2 [84]]

Besides its seemingly contradictory involvement in both cell proliferation and apoptosis, MYCN also exerts opposing roles in the differentiation process. Downregulation of MYCN is necessary to induce retinoic acid mediated differentiation in neuroblastoma cells. [85] The regulation of the MYCN/MAD/MAX network is important in this process: during differentiation the turnover of MYCN and the expression of MAD are increased, resulting in a shift from MYCN-MAX promoter occupancy to MAD-MAX at MYCN target genes involved in cell cycle progression. [86] In contrast, Guglielmi and colleagues [87] recently showed that MYCN protein expression is required to activate the differentiation processes in neuroblastoma cells. The authors hypothesize that MYCN is necessary during the activation of neuroblastoma

differentiation to induce apoptosis in cells that are not committed to differentiation but are still proliferating. [87]

These opposing roles of MYCN in differentiation are illustrated by the relative high frequency of spontaneous tumor regression in disseminated neuroblastoma tumors – termed stage 4S tumors. [88] These tumors display higher MYCN mRNA and protein levels than low-risk localized MYCN non-amplified tumors, despite their lack of *MYCN* amplification. It has been suggested that moderate MYCN function gain in this subtype is still compatible with, or might even favor, spontaneous regression [11] that resembles the concurrence of massive apoptosis and differentiation of a few neurons along the sympatho-adrenal cell lineage in the normal development of the sympathetic nervous system.

Despite the apparently incompatible functions of MYCN, its amplification or overexpression ultimately leads to tumor formation in sympathetic precursor cells. In this process, the balance of MYCN activity is shifted towards an oncogenic nature (summarized in **Figure 1.3**); in parallel, the pro-apoptotic functions of MYCN are repressed via the acquisition of additional aberrations – be there chromosomal imbalances, point mutations, epigenetic alterations – as illustrated by the cooperative effects of ALK activation in mouse en zebrafish models of MYCN-driven neuroblastoma. [23]

Therapeutic targeting of MYCN in neuroblastoma

Giving the enormous impact of MYCN on neuroblastoma biology and that several observations point towards a central role for MYCN, therapeutic targeting of MYCN seems a very promising option in neuroblastoma. There is indeed a need for novel therapies in neuroblastoma: 50% of neuroblastoma patients are classified as high-risk, and outcome remains poor in this patient cohort despite intensified multimodal treatment. [89] A considerable proportion of patients experience disease relapse and are refractory to conventional treatment approaches. [89] The impact of inhibiting MYCN on neuroblastoma tumor progression is evident from RNAi-mediated knockdown of MYCN expression in MYCN amplified neuroblastoma, where it results in increase in apoptosis and differentiation, and suppression of cell growth. [90,91] However, direct inhibition of MYCN *in vivo* is cumbersome, as MYC proteins are composed of two extended alpha-helices with no obvious surfaces for small molecule binding. Therefore the regulatory mechanisms governing MYCN transcription, translation and function are currently being explored as therapeutic targets. Strategies to circumvent blocking MYCN directly include: (1) targeting transcription of MYCN, (2) targeting regulators of MYCN mRNA and protein stability, and (3) triggering differentiation (**Figure 1.4**).

Targeting transcription of MYCN

Recently, interest in the MYC-targeting field increased following the recognition that BET family adaptor proteins (see above) localize to MYC promoters: the development of BET inhibitors appeared to be a promising therapeutic strategy for targeting MYC in different tumor entities. Unfortunately, BET inhibition does not inhibit MYC expression to a similar extent in all tumor cells, likely due to different unique regulatory mechanisms regulating MYC expression in different entities. For instance, in multiple myeloma and acute myeloid leukemia, the expression of MYC is enhanced from unique distant BRD4-occupied enhancers, making these specific cases highly sensitive to BET inhibition.[92] In neuroblastoma cell lines, responses to BET inhibition varied from highly sensitive to resistant[93], suggesting that the transcriptional control of MYCN occurs via different mechanisms, either BET-dependent or -independent. Given that BET proteins might enhance MYCN expression from distant enhancer sites, resistance to BET inhibition in MYCN amplified cells could be explained by a disconnection from MYCN and its enhancing elements, uncoupling MYCN from BET-mediated control. Currently, a number of BET inhibitors are undergoing early-phase clinical testing, for different tumor entities. †

Targeting regulators of MYCN mRNA and protein stability

The occurrence of high nuclear MYCN protein levels, even in cases in which MYCN is not amplified or overexpressed at the mRNA level[59], supports MYCN protein stability as another relevant mechanism for MYCN regulation. MYCN protein turnover is cell-cycle dependent with MYCN degradation occurring during mitosis.[42] MYC and MYCN proteins are proteolyzed through a stepwise set of phosphorylation events. Initially, MYC and MYCN are phosphorylated at serine 62 (S62) via kinases in the RAS signaling pathway, such as MAPK[94] – which lies downstream of ALK – and CDK1[95]. This post-translational modification stabilizes MYCN and primes it for subsequent phosphorylation at threonine 58 (T58) via GSK-3ß[96], a direct target of the PI3K/AKT/mTOR pathway. Dephosphorylation of S62 via PP2A next sensitizes MYCN phosphorylated at T58 to bind a proteasomal degradation complex that includes AURKA, E3 ubiquitin ligases (FBXW7 and HUWE1) and undefined additional proteins, leading to the ubiquitination and degradation in the proteasome[97-99] (**Figure 1.4**). Consequently, inhibition of PI3K or mTOR and subsequent GSK-3ß activation can decrease MYCN protein levels by promoting T58 phosphorylation. A number of compounds active against either PI3K or mTOR are currently in clinical development.[100]

† https://clinicaltrials.gov

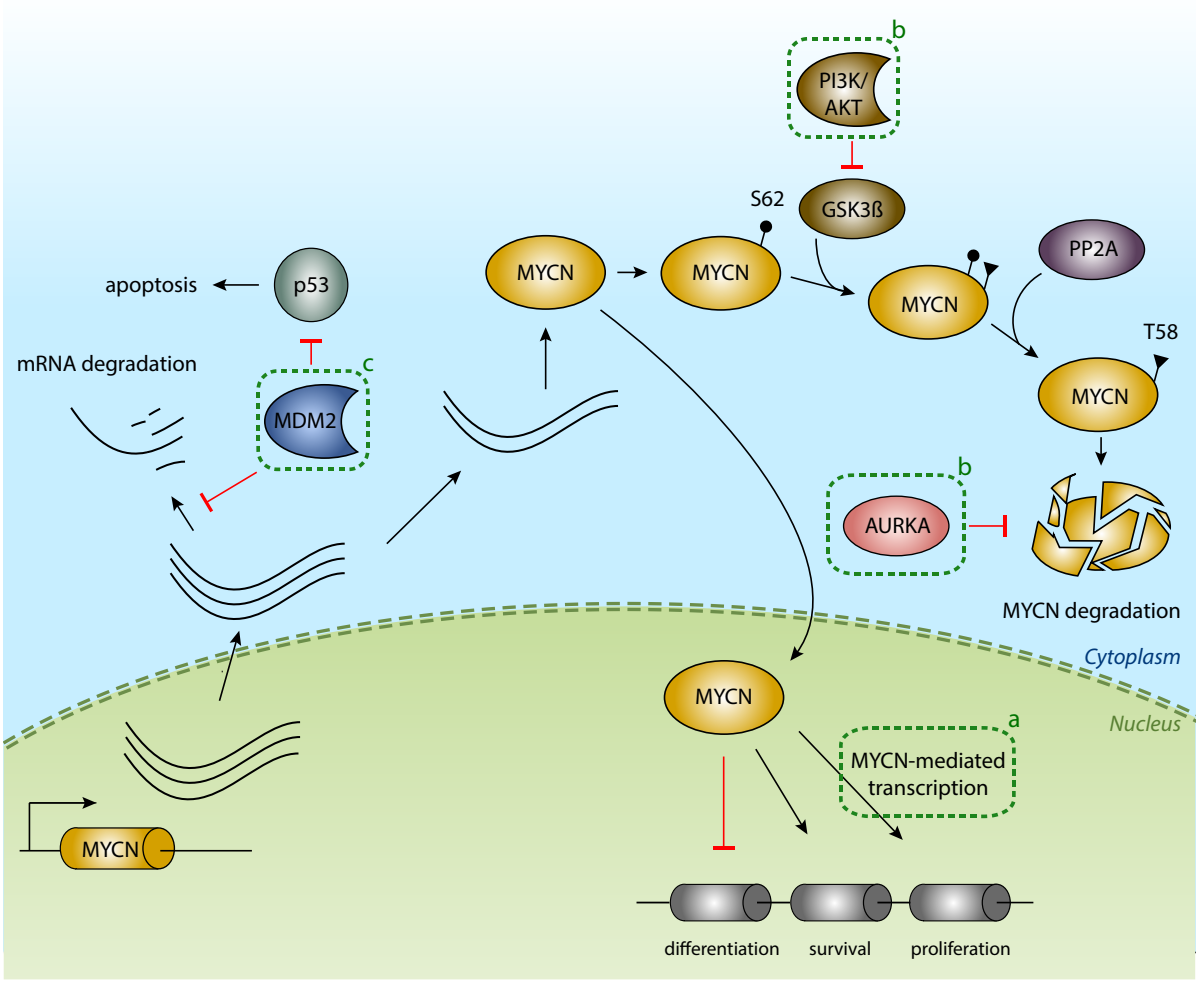

Figure 1.4: Therapeutic targeting of MYCN in neuroblastoma. Possible strategies to treat MYCN- amplified neuroblastoma patients include **(a)** blocking MYCN-dependent transcription with BET-bromodomain inhibitors, **(b)** antagonizing proteins involved in stabilizing MYCN protein and **(c)** suppressing MDM2 that stabilizes MYCN mRNA and disrupts p53-mediated apoptosis. [Adapted from Huang, M. and Weiss, W. A. *Cold Spring Harb Perspect Med* (2013), Figure 4. Ref. [84]]

Proteins that prevent dephosphorylation at T58 stabilize MYCN, which may be the case with AURKA in neuroblastoma. [101] Interestingly, increased expression of *AURKA* is found in MYCN amplified neuroblastoma, mediated potentially by MYCN itself. [102] Therefore, promoting dissociation of the AURKA-MYCN complex, which results in rapid proteasomal degradation of MYCN, represent another strategy to target oncogenic stabilization of MYCN. Certain AURKA inhibitors, such as MLN8237, induce a particular conformational change in the kinase that actively reinitiates MYCN degradation through this mechanism, independent of any requirement for enzymatic inhibition of the kinase itself. [103] MLN8237 was identified as a promising agent for neuroblastoma [104] but has not displayed robust antitumor activity in early-phase pediatric studies [105], warranting the development of improved inhibitors.

The majority of drugs described here are in early-phase clinical testing in adult and pediatric settings [100], making targeted therapeutics a reality for neuroblastoma cure. It is anticipated, however, that a number of drugs might induce secondary mutations rendering a tumor insensitive to a promising targeted therapy. Therefore, further scrutinizing MYCN functions and interactors remains of interest to the field. In this respect, the implementation of non-coding RNAs – playing key roles in normal development and oncogenesis – in the MYCN network holds great promise.

The role of microRNAs in cancer

The discovery that non-coding RNAs (ncRNAs) – once believed to be genomic trash – interfere with the expression of coding genes implicated in virtually all biological processes, has revolutionized the field of molecular biology in the last decades. miRNAs, a specific class of small ncRNAs, have drawn particular attention. miRNAs are very short non-coding transcripts that act by regulating protein expression during cellular processes such as growth, development, and differentiation at the transcriptional, posttranscriptional, and/or translational level. The exact role of an individual miRNA strictly depends on its spatiotemporal expression pattern and that of its target genes. Given the involvement of miRNAs in a myriad of biological processes, researchers investigated consequences of deregulated miRNA expression and found implication in multiple diseases such as inflammatory [106] and cardiovascular disease [107] and cancer [108].

miRNA biogenesis and function

Most miRNAs are transcribed by RNA polymerase II from intergenic, intronic or polycistronic loci to long primary transcripts (pri-miRNAs). Pri-miRNAs are processed sequentially first in the nucleus by the Drosha–DGCR8 complex to approximately 70 nt pre-miRNA hairpin structures and then in the cytoplasm by the Dicer–TRBP complex to approximately 22 nt miRNA duplexes. In addition to the canonical miRNA biogenesis pathway, many Drosha-DGCR8-independent pathways can produce pre-miRNAs. The most common alternative pathway involves short intronic hairpins that are spliced and debranched to form pre-miRNA hairpins. In the cytoplasm, miRNA duplexes are incorporated into an Argonaute protein-containing miRNA-induced silencing complex (miRISC), followed by unwinding of the duplex and retention of the mature miRNA strand in miRISC, while the complementary strand is released and degraded. Recent work has identified a battery of proteins that regulate processing – positively or negatively – either by interacting with Drosha or Dicer or by binding to miRNA precursors. Although the activity of some of the regulators is restricted to specific miRNA families, most affect the processing of a broader range of miRNA precursors, suggesting that their activity can affect the expression of entire gene networks. One such miRNA-specific regulator is LIN28A and its paralog LIN28B that affect pri- and pre-let-7 levels by sequence-specific interaction and subsequent blocking of processing or pre-miRNA degradation (see above). [109]

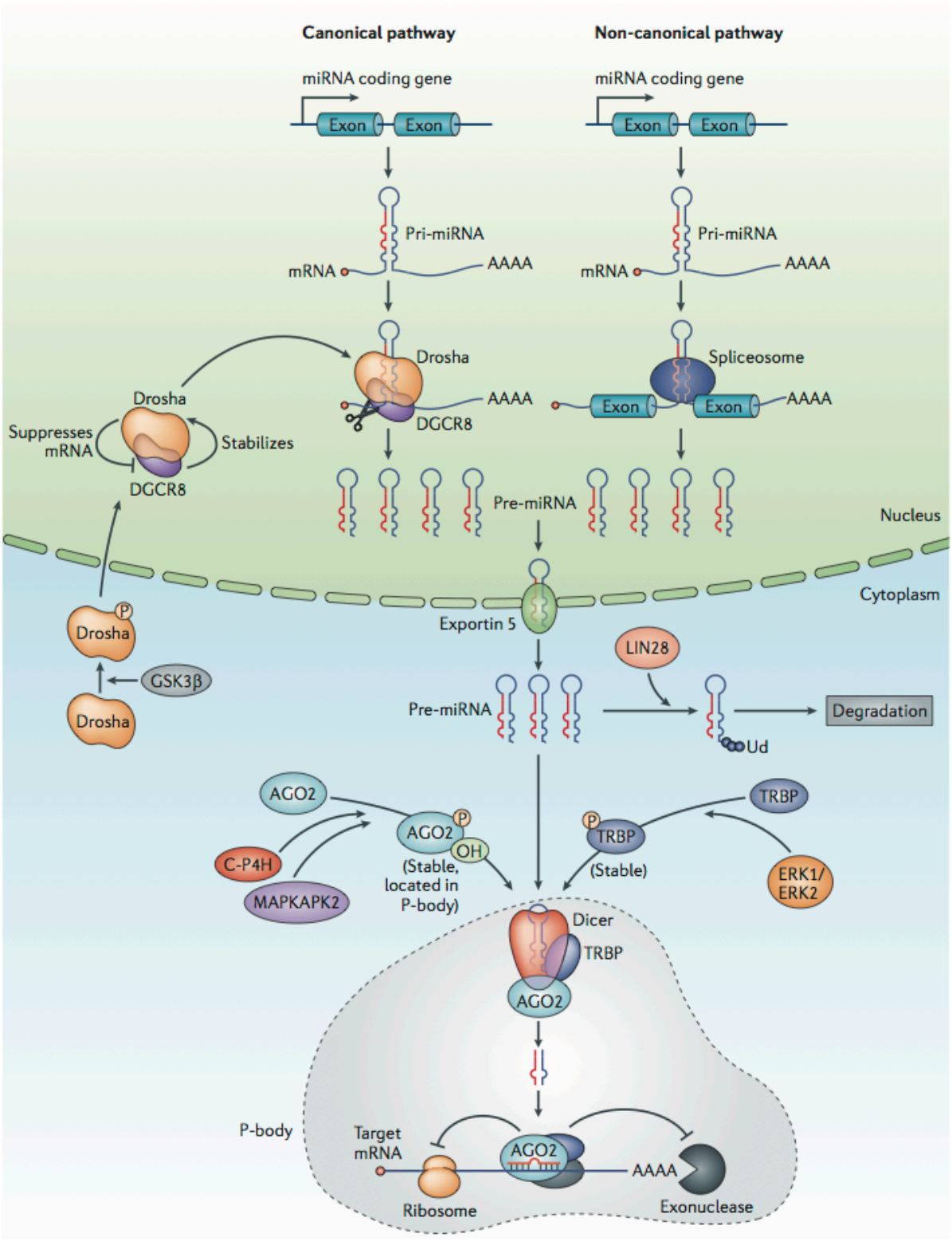

Figure 1.4: Canonical and non-canonical miRNA biogenesis pathways. In the canonical pathway, microRNAs (miRNAs) are typically transcribed by RNA polymerase II to produce primary miRNA (pri-miRNA) hairpins, which are then processed by the Drosha–DGCR8 (DiGeorge syndrome critical region 8) complex to generate precursor miRNAs (pre-miRNAs). These molecules are transported by exportin 5 into the cytoplasm, where they are further processed by Dicer–TRBP (TAR RNA-binding protein 2) and loaded into Argonaute 2 (AGO2)-containing RNA-induced silencing complexes (RISCs) to suppress downstream target gene expression. miRNAs are also produced though non-canonical pathways, such as spliceosome-dependent mechanisms, as shown here. The miRNA biogenesis pathway is a tightly regulated process. For example, Drosha is dependent on phosphorylation by glycogen synthase kinase 3β (GSK3β) for proper nuclear localization168; Drosha

regulates DGCR8 expression by suppressing DGCR8 mRNA20; DGCR8 stabilizes Drosha protein20; AGO2 is hydroxylated by C-P4H169 and phosphorylated by MAPK-activated protein kinase 2 (MAPKAPK2)170, which stabilizes the protein and regulates its localization to processing bodies (P-bodies); and TRBP is stabilized by extracellular signal-regulated kinase 1 (ERK1) or ERK2 phosphorylation25. miRNAs themselves are regulated by a number of modifications, including uridylation (Ud)171. [From Li, Z. and Rana, T. M. *Nat Rev Drug Discov* (2014), Figure 1 [109]]

Upon processing, the miRNA incorporated in the miRISC acts as a guide and leads the miRISC to mRNA transcripts with complementary sequences in their 3' untranslated region (3'UTR). The miRISC may affect its target genes in two non-mutually exclusive ways: repression of translation and degradation of the mRNA. [110] Experimental bioinformatics approaches have shown that the major determinant of target recognition by a miRNA is the perfect or nearly perfect complementarity between the proximal 5' region of the miRNA, the so-called seed, and the mRNA. [111] The region in the 3'UTR of the target gene that is complementary to the miRNA seed, comprising nucleotides 2 to 7 of the miRNA, is called the miRNA recognition element and may exhibit different degrees of complementarity with the miRNA seed. [112] Bioinformatics algorithms designed to detect potential mRNA targets of miRNAs suggest that a single miRNA can regulate up to 200 coding genes. [113] In total, more than 60% of the protein coding fraction of the genome is under the influence of one or more miRNAs. [114] Of these, only a minor portion of target genes is so far confirmed by experimental research. The verified target genes are often involved in signal transduction pathways that are essential for the proper homeostasis of all cell types. As such, they are amongst others involved in regulation of differentiation, control of cell proliferation and apoptosis, which are important processes in cancer.

Deregulated miRNA expression in cancer

In 2004, Calin and colleagues found that more than half of miRNA genes, known at that time, are located at cancer-associated genomic regions or in fragile sites. [115] It can be assumed that genes – or ncRNAs – located in cancer-associated genomic regions contribute to the development of cancer. For instance, 13q14 deletions are observed in 50% of patients with chronic lymphocytic leukemia (CLL), suggesting that one or more genes in this locus play a key role in the pathogenesis of CLL. [116] However, for long, a causal gene contributing to CLL could not be identified. The breakthrough came with the discovery that two miRNAs, miR-15 and miR-16, reside in this genomic locus and that both miRNAs are downregulated in the majority of CLL cases. [116] Several research groups confirmed these results and pointed to the involvement of these and other miRNAs in various tumor entities. [117-119] Besides the location at cancer-associated genomic regions, aberrant miRNA expression in tumors can arise from additional mechanisms, including perturbed

transcriptional regulation, defects in miRNA-processing machinery and mutations in miRNA genes and miRNA binding sites within target genes. [120] As transcription of miRNA genes occurs in a similar fashion as regular gene transcription, the mechanisms leading to perturbed expression of coding genes also apply to miRNAs: a deregulated balance of activating and repressing transcription factors, such as p53 or MYC(N) (see below) and altered epigenetic regulation, such as DNA and histone modifications (reviewed in [121]) can lead to aberrant miRNA expression. Downstream of miRNA transcription, defects in miRNA processing machinery can further contribute to perturbed miRNA profile. Somatic and germ-line mutations in *DICER1*, *TARBP2* – part of the Dicer-containing complex – or *EXPO5* – which mediates the nuclear export of pre-miRNAs – result in impaired miRNA maturation in different tumor entities. [122-124] Finally, genetic variations within miRNA binding sites can modulate gene expression and protein output levels and affect phenotypes or cause disease. [125,126]

The importance of miRNA function and dysfunction in various cancer entities suggest that modulation of miRNA expression may serve as a novel therapeutic modality for these malignancies. [109]

miRNAs in cancer therapy

The research community has turned towards the implementation of miRNAs in cancer therapy for several reasons. Conventional chemotherapy is known to induce severe cytotoxicity in normal dividing cells. The targeted therapies that were developed in an attempt to circumvent this general cytotoxicity, can display off-target effects (small molecule inhibitors), might be difficult to deliver to tumor cells (monoclonal antibodies) and are confronted with secondary mutations rendering a tumor insensitive to the administered drug. [127] In this respect, there are two major advantages in using miRNAs in cancer therapy: first, miRNAs occur as “natural” molecules produced in human cells, showing reduced immune response and low toxicity when compared to protein-based drug molecules [127], and second, they can target multiple genes from the same pathway and therefore they can act at multiple levels in the same pathway, significantly reducing the development of resistance because multiple mutations in multiple genes would be needed. [128]

In using miRNAs as cancer therapeutics, there are two main strategies that can be followed: restoring the miRNAs that are downregulated – with miRNA mimics or miRNAs encoded in expression vectors – and silencing the miRNAs that are upregulated – via miRNA sponges, small molecule inhibitors and antisense oligonucleotides. [109,128] In 2013, MRX34, a miRNA therapeutic, has entered clinical trials for cancer therapy. MRX34 is a liposome-formulated

mimic of the tumor suppressor miR-34, and has been developed in a clinical phase 1 trial for patients with advanced or metastatic liver cancer. [129]

Several problems encountered in clinical development of miRNA delivery, however, limit the further application of miRNAs as a therapeutic option to treat cancer [127]: the penetration of miRNAs into tumor tissues is modest due to mechanical and biological barriers, miRNAs still have some potential to induce immunotoxicity, and unmodified miRNA antagonists and miRNA mimics are quickly degraded and cleared in the blood circulation, and are associated with off-target effects of miRNAs. Therefore, several chemical modifications that can enhance the stability of miRNA modulators and improve the target specificity and systemic delivery efficacy, are currently under development. [109,127]

miRNAs in neuroblastoma

A number of expression profiling studies have demonstrated dysregulation of miRNAs in neuroblastoma. During the last decade, distinct miRNAs were shown to be differentially expressed in favorable versus unfavorable tumor subtypes [130], in MYCN amplified neuroblastoma versus non-amplified cases [131,132] and low-risk versus high-risk tumors [133-135]. Interestingly, a significant number of dysregulated miRNAs in neuroblastoma now appear to be transcriptional targets of MYCN [133,136], suggesting that regulation of these miRNAs could serve as an additional mechanism for MYCN-induced transcriptional changes. A more global study of miRNAs in neuroblastoma observed that MYCN/MYC signaling, rather than MYCN amplification alone, underlies the differential expression of miRNAs in neuroblastoma. Furthermore, MYCN/MYC activated miRNAs contribute to widespread transcriptional repression, in contrast to MYCN/MYC downregulated miRNAs that were not associated with transcriptional activation. [133] However, also global miRNA downregulation by MYC activation was previously reported to significantly contribute to tumorigenesis. [137]

In follow-up of some of the abovementioned profiling studies, interesting candidates were further studied for their involvement in neuroblastoma biology. The two most commonly reported miRNAs are miR-34a-5p and the miR-17-92 cluster. The miR-17-92 cluster was among the first miRNAs to be validated as showing oncogenic potential. The precursor transcript derived from the mir-17-92 gene contains six tandem stem-loop hairpin structures that ultimately yield 12 mature miRNAs: miR-17-5p, -17-3p, -18a-5p, -18a-3p, -19a-3p, -19a-5p, -20a-5p, -20a-3p, -19b-3p, -19b-1-5p, -92a-3p, and -92a-1-5p. Amplification or overexpression of this locus was observed in different cancer entities [138-140] and its role in oncogenesis was further substantiated when MYC proteins were shown to directly activate the cluster, inducing high miR-17-92 expression in MYC(N) activated tumors and cell lines,

including neuroblastoma. [64,133,141,142] Being a MYCN target gene, the miR-17-92 cluster was found to be overexpressed in unfavorable [131] and MYCN amplified [143,144] neuroblastoma tumors. Overexpressing the miR-17-92 cluster in a MYCN non-amplified neuroblastoma cell line led to increased tumorigenicity *in vitro* and *in vivo.* [143] Furthermore, i*n vitro* or *in vivo* inhibition of miR-17-5p abolishes the growth of MYCN amplified and therapy-resistant neuroblastoma through de-repression of *CDKN1A* and *BCL2L11*, leading to cell cycling blockade and activation of apoptosis, respectively. In line with this observation, the majority of primary neuroblastoma tumors show a rise of miR-17-5p level leading to *CDKN1A* repression, which is particularly severe in patients with MYCN amplification and poor prognosis. [144] Interestingly, Kumps and colleagues [145] found a focal 5 kb genomic gain encompassing the miR-17-92 cluster as sole affected gene, in a neuroblastoma cell line. Furthermore, they demonstrated that focal genomic losses in MYCN amplified tumors harbor miR-17-92 target genes. These observations suggest that focal genomic aberrations in MYCN amplified neuroblastoma tumors reinforce MYCN oncogene addiction by altering the expression of direct and indirect MYCN target genes. [145]

miR-34a-5p, another extensively studied miRNA in neuroblastoma, is located on 1p36, a region often deleted in high-risk neuroblastoma tumors. Consequently, miR-34a-5p is expressed at lower levels in primary tumors with a hemizygous deletion of the mir-34a locus compared with those without a 1p36 deletion. [146] miR-34a-5p is a direct transcriptional target of p53 [147] and contributes to p53-mediated apoptosis via repression of *BCL2, SYT1, STX1A, E2F3* and *MYCN* [148]. In line with the great potential of miRNAs as cancer therapeutics, Tivnan and colleagues [149] demonstrated that *in vivo* delivery of nanoparticles encapsulating miR-34a results in significantly decreased tumor growth, increased apoptosis and a reduction in vascularization. These nanoparticles were conjugated to an antibody directed against GD_2, a glycolipid highly expressed on the cell surface of neuroblastoma and several other cancers [150]; this facilitated tumor-specific delivery following systemic administration into tumor bearing mice. The authors further establish a novel, multi-step molecular mechanism by which miR-34a-5p leads to increased levels of TIMP2, an inhibitor of matrix metalloproteinases, accounting for the highly reduced vascularization noted in miR-34a-5p-treated tumors. [149]

Additional miRNAs downregulated in neuroblastoma tumors include miR-27b-3p [151], miR-29a-3p, miR-29b-3p, and miR-29c-3p [152], miR-128-3p [153], miR-137 [154], miR-145-5p [155], miR-149-3p [156], miR-200b-3p [157], miR-204-5p [158] and miR-542-3p [159].

Further understanding the mechanisms by which MYCN alters the expression of miRNAs, and through which targets and pathways deregulated miRNAs may subsequently contribute to oncogenic transformation in aggressive neuroblastoma, will possibly explain missing molecular links in the pathogenesis of this disease, and further elucidate how oncogenic MYCN signaling is executed.

References

1. Grimmer, M. R. & Weiss, W. A. Childhood tumors of the nervous system as disorders of normal development. *Curr Opin Pediatr* **18,** 634–638 (2006).
2. Jiang, M., Stanke, J. & Lahti, J. M. *Chapter 4 - The Connections Between Neural Crest Development and Neuroblastoma*. *Current Topics in Developmental Biology: Cancer and Development* **94,** 77–127 (Elsevier Inc., 2011).
3. De Preter, K. *et al.* Human fetal neuroblast and neuroblastoma transcriptome analysis confirms neuroblast origin and highlights neuroblastoma candidate genes. *Genome Biology* **7,** R84 (2006).
4. Pugh, T. J. *et al.* The genetic landscape of high-risk neuroblastoma. *Nature* **45,** 279–284 (2013).
5. Sausen, M. *et al.* Integrated genomic analyses identify ARID1A and ARID1B alterations in the childhood cancer neuroblastoma. *Nat Genet* **45,** 12–17 (2013).
6. Molenaar, J. J. *et al.* Sequencing of neuroblastoma identifies chromothripsis and defects in neuritogenesis genes. *Nature* **483,** 589–593 (2012).
7. Schwab, M. *et al.* Amplified DNA with limited homology to myc cellular oncogene is shared by human neuroblastoma cell lines and a neuroblastoma tumour. *Nature* **305,** 245–248 (1983).
8. Schwab, M. *et al.* Enhanced expression of the human gene N-myc consequent to amplification of DNA may contribute to malignant progression of neuroblastoma. *Proc Natl Acad Sci U S A* **81,** 4940–4944 (1984).
9. Brodeur, G. M., Seeger, R. C., Schwab, M., Varmus, H. E. & Bishop, J. M. Amplification of N-myc in untreated human neuroblastomas correlates with advanced disease stage. *Science* **224,** 1121–1124 (1984).
10. Vandesompele, J. Unequivocal Delineation of Clinicogenetic Subgroups and Development of a New Model for Improved Outcome Prediction in Neuroblastoma. *J Clin Oncol* **23,** 2280–2299 (2005).
11. Westermann, F. *et al.* Distinct transcriptional MYCN/c-MYC activities are associated with spontaneous regression or malignant progression in neuroblastomas. *Genome Biology* **9,** R150 (2008).
12. Maris, J. M., Hogarty, M. D., Bagatell, R. & Cohn, S. L. Neuroblastoma. *Lancet* **369,** 2106–2120 (2007).
13. Weiss, W. A., Aldape, K., Mohapatra, G., Feuerstein, B. G. & Bishop, J. M. Targeted expression of MYCN causes neuroblastoma in transgenic mice. *EMBO J* **16,** 2985–2995 (1997).
14. Chesler, L. & Weiss, W. A. Genetically engineered murine models--contribution to our understanding of the genetics, molecular pathology and therapeutic targeting of neuroblastoma. *Semin Cancer Biol* **21,** 245–255 (2011).
15. Maris, J. M. *et al.* Evidence for a hereditary neuroblastoma predisposition locus at chromosome 16p12-13. *Cancer Res* **62,** 6651–6658 (2002).
16. Chen, Y. *et al.* Oncogenic mutations of ALK kinase in neuroblastoma. *Nature* **455,** 971–974 (2008).
17. Mossé, Y. P. *et al.* Identification of ALK as a major familial neuroblastoma predisposition gene. *Nature* **455,** 930–935 (2008).
18. Janoueix-Lerosey, I. *et al.* Somatic and germline activating mutations of the ALK kinase receptor in neuroblastoma. *Nature* **455,** 967–970 (2008).
19. George, R. E. *et al.* Activating mutations in ALK provide a therapeutic target in neuroblastoma. *Nature* **455,** 975–978 (2008).
20. Iwahara, T., Fujimoto, J., Wen, D., Cupples, R. & Bucay, N. Molecular characterization of ALK, a receptor tyrosine kinase expressed specifically in the nervous system. *Oncogene* **14,** 439–449 (1997).
21. De Brouwer, S. *et al.* Meta-analysis of neuroblastomas reveals a skewed ALK mutation spectrum in tumors with MYCN amplification. *Clin Cancer Res* **16,** 4353–4362 (2010).
22. Schulte, J. H. *et al.* High ALK receptor tyrosine kinase expression supersedes ALK mutation as a determining factor of an unfavorable phenotype in primary neuroblastoma. *Clin Cancer Res* **17,** 5082–5092 (2011).
23. Berry, T. *et al.* The ALK(F1174L) Mutation Potentiates the Oncogenic Activity of MYCN in Neuroblastoma. *Cancer Cell* **22,** 117–130 (2012).

24. Heukamp, L. C. *et al.* Targeted expression of mutated ALK induces neuroblastoma in transgenic mice. *Sci Transl Med* **4,** 141ra91 (2012).
25. Cazes, A. *et al.* Activated Alk triggers prolonged neurogenesis and Ret upregulation providing a therapeutic target in ALK-mutated neuroblastoma. *Oncotarget* **5,** 2688–2702 (2014).
26. Zhu, S. *et al.* Activated ALK Collaborates with MYCN in Neuroblastoma Pathogenesis. *Cancer Cell* **21,** 362–373 (2012).
27. Gustafson, W. C. & Weiss, W. A. Myc proteins as therapeutic targets. *Oncogene* **29,** 1249–1259 (2010).
28. Hasan, M. K. *et al.* ALK is a MYCN target gene and regulates cell migration and invasion in neuroblastoma. *Sci Rep* **3,** 3450 (2013).
29. Schönherr, C. *et al.* Anaplastic Lymphoma Kinase (ALK) regulates initiation of transcription of MYCN in neuroblastoma cells. *Oncogene* **31,** 5193–5200 (2012).
30. Molenaar, J. J. *et al.* LIN28B induces neuroblastoma and enhances MYCN levels via let-7 suppression. *Nat Genet* **44,** 1199–1206 (2012).
31. Diskin, S. J. *et al.* Common variation at 6q16 within HACE1 and LIN28B influences susceptibility to neuroblastoma. *Nat Genet* **44,** 1126–1130 (2012).
32. Shyh-Chang, N. & Daley, G. Q. Lin28: primal regulator of growth and metabolism in stem cells. *Cell Stem Cell* **12,** 395–406 (2013).
33. van de Bunt, M. *et al.* The miRNA profile of human pancreatic islets and beta-cells and relationship to type 2 diabetes pathogenesis. *PLoS ONE* **8,** e55272 (2013).
34. Zhou, J., Ng, S.-B. & Chng, W.-J. LIN28/LIN28B: an emerging oncogenic driver in cancer stem cells. *Int J Biochem Cell Biol* **45,** 973–978 (2013).
35. Büssing, I., Slack, F. J. & Grosshans, H. let-7 microRNAs in development, stem cells and cancer. *Trends Mol Med* **14,** 400–409 (2008).
36. Helland, Å. *et al.* Deregulation of MYCN, LIN28B and LET7 in a molecular subtype of aggressive high-grade serous ovarian cancers. *PLoS ONE* **6,** e18064 (2011).
37. Cotterman, R. & Knoepfler, P. S. N-Myc regulates expression of pluripotency genes in neuroblastoma including lif, klf2, klf4, and lin28b. *PLoS ONE* **4,** e5799 (2009).
38. Luscher, B. Function and regulation of the transcription factors of the Myc/Max/Mad network. *Gene* **277,** 1–14 (2001).
39. Land, H., Parada, L. F. & Weinberg, R. A. Tumorigenic conversion of primary embryo fibroblasts requires at least two cooperating oncogenes. *Nature* **304,** 596–602 (1983).
40. Meyer, N. & Penn, L. Z. Reflecting on 25 years with MYC. *Nat Rev Cancer* **8,** 976–990 (2008).
41. Kohl, N. E. *et al.* Human N-myc is closely related in organization and nucleotide sequence to c-myc. *Nature* **319,** 73–77 (1986).
42. Beltran, H. The N-myc Oncogene: Maximizing its Targets, Regulation, and Therapeutic Potential. *Mol Cancer Res* **12,** 815–822 (2014).
43. Schwab, M., Varmus, H. E. & Bishop, J. M. Human N-myc gene contributes to neoplastic transformation of mammalian cells in culture. *Nature* **316,** 160–162 (1985).
44. Cavalieri, F. & Goldfarb, M. N-myc proto-oncogene expression can induce DNA replication in Balb/c 3T3 fibroblasts. *Oncogene* **2,** 289–291 (1988).
45. Huang, M. & Weiss, W. A. Neuroblastoma and MYCN. *Cold Spring Harb Perspect Med* **3,** a014415 (2013).
46. Slamon, D. J. *et al.* Identification and characterization of the protein encoded by the human N-myc oncogene. *Science* **232,** 768–772 (1986).
47. Nisen, P. D., Zimmerman, K. A., Cotter, S. V., Gilbert, F. & Alt, F. W. Enhanced expression of the N-myc gene in Wilms' tumors. *Cancer Res* **46,** 6217–6222 (1986).
48. Stenger, A. M. *et al.* N-myc oncogene amplification in a pediatric case of glioblastoma multiforme. *Childs Nerv Syst* **7,** 410–413 (1991).
49. Roussel, M. F. & Robinson, G. W. Role of MYC in Medulloblastoma. *Cold Spring Harb Perspect Med* **3,** (2013).
50. Murphy, D. M. *et al.* Global MYCN transcription factor binding analysis in neuroblastoma reveals association with distinct E-box motifs and regions of DNA hypermethylation. *PLoS ONE* **4,** e8154 (2009).
51. Blackwood, E. M. & Eisenman, R. N. Max: a helix-loop-helix zipper protein that forms a sequence-specific DNA-binding complex with Myc. *Science* **251,** 1211–1217 (1991).
52. Fletcher, S. & Prochownik, E. V. Small-molecule inhibitors of the Myc oncoprotein. *Biochim Biophys Acta* **1849,** 525–543 (2015).

53. Dhalluin, C. *et al.* Structure and ligand of a histone acetyltransferase bromodomain. *Nature* **399,** 491–496 (1999).
54. Fowler, T., Sen, R. & Roy, A. L. Regulation of primary response genes. *Mol Cell* **44,** 348–360 (2011).
55. Zhou, Q., Li, T. & Price, D. H. RNA polymerase II elongation control. *Annu Rev Biochem* **81,** 119–143 (2012).
56. Herkert, B. & Eilers, M. Transcriptional Repression: The Dark Side of Myc. *Genes & Cancer* **1,** 580–586 (2010).
57. Gherardi, S., Valli, E., Erriquez, D. & Perini, G. MYCN-mediated transcriptional repression in neuroblastoma: the other side of the coin. *Front Oncol* **3,** 42 (2013).
58. Zeller, K. I. *et al.* Global mapping of c-Myc binding sites and target gene networks in human B cells. *Proc Natl Acad Sci U S A* **103,** 17834–17839 (2006).
59. Valentijn, L. J. *et al.* Functional MYCN signature predicts outcome of neuroblastoma irrespective of MYCN amplification. *Proc Natl Acad Sci U S A* **109,** 19190–19195 (2012).
60. Brenner, C. *et al.* Myc represses transcription through recruitment of DNA methyltransferase corepressor. *EMBO J* **24,** 336–346 (2005).
61. Corvetta, D. *et al.* Physical interaction between MYCN oncogene and polycomb repressive complex 2 (PRC2) in neuroblastoma: functional and therapeutic implications. *J Biol Chem* **288,** 8332–8341 (2013).
62. Alaminos, M. *et al.* Genome-wide analysis of gene expression associated with MYCN in human neuroblastoma. *Cancer Res* **63,** 4538–4546 (2003).
63. Valentijn, L. J. *et al.* Inhibition of a new differentiation pathway in neuroblastoma by copy number defects of N-myc, Cdc42, and nm23 genes. *Cancer Res* **65,** 3136–3145 (2005).
64. Schulte, J. H. *et al.* MYCN regulates oncogenic MicroRNAs in neuroblastoma. *Int J Cancer* **122,** 699–704 (2008).
65. Slack, A. *et al.* The p53 regulatory gene MDM2 is a direct transcriptional target of MYCN in neuroblastoma. *Proc Natl Acad Sci U S A* **102,** 731–736 (2005).
66. Murphy, D. M. *et al.* Dissection of the oncogenic MYCN transcriptional network reveals a large set of clinically relevant cell cycle genes as drivers of neuroblastoma tumorigenesis. *Mol Carcinog* **50,** 403–411 (2011).
67. Schanen, B. C. & Li, X. Transcriptional regulation of mammalian miRNA genes. *Genomics* **97,** 1–6 (2011).
68. Krol, J., Loedige, I. & Filipowicz, W. The widespread regulation of microRNA biogenesis, function and decay. *Nat Rev Genet* **11,** 597–610 (2010).
69. Marsico, A. *et al.* PROmiRNA: a new miRNA promoter recognition method uncovers the complex regulation of intronic miRNAs. *Genome Biology* **14,** R84 (2013).
70. Pelengaris, S., Khan, M. & Evan, G. c-MYC: more than just a matter of life and death. *Nat Rev Cancer* **2,** 764–776 (2002).
71. Gogolin, S. *et al.* CDK4 inhibition restores G(1)-S arrest in MYCN-amplified neuroblastoma cells in the context of doxorubicin-induced DNA damage. *Cell Cycle* **12,** 1091–1104 (2013).
72. Muth, D. *et al.* Transcriptional repression of SKP2 is impaired in MYCN-amplified neuroblastoma. *Cancer Res* **70,** 3791–3802 (2010).
73. Cole, K. A., Huggins, J. & LaQuaglia, M. RNAi screen of the protein kinome identifies checkpoint kinase 1 (CHK1) as a therapeutic target in neuroblastoma. *Proc Natl Acad Sci U S A* (2011). doi:10.1073/pnas.1012351108/-/DCSupplemental/sd01.xls
74. Herold, S. *et al.* Negative regulation of the mammalian UV response by Myc through association with Miz-1. *Mol Cell* **10,** 509–521 (2002).
75. Bell, E. *et al.* The role of MYCN in the failure of MYCN amplified neuroblastoma cell lines to G1 arrest after DNA damage. *Cell Cycle* **5,** 2639–2647 (2006).
76. Paffhausen, T., Schwab, M. & Westermann, F. Targeted MYCN expression affects cytotoxic potential of chemotherapeutic drugs in neuroblastoma cells. *CANCER LETTERS* **250,** 17–24 (2007).
77. Strasser, A., Harris, A. W., Bath, M. L. & Cory, S. Novel primitive lymphoid tumours induced in transgenic mice by cooperation between myc and bcl-2. *Nature* **348,** 331–333 (1990).
78. Chesler, L., Goldenberg, D. D., Collins, R. & Grimmer, M. Chemotherapy-Induced Apoptosis in a Transgenic Model of Neuroblastoma Proceeds Through< i> p53</i> Induction. *Neoplasia* (2008). doi:10.1593/neo.08778
79. Van Maerken, T., Vandesompele, J., Rihani, A., De Paepe, A. & Speleman, F. Escape from p53-mediated tumor surveillance in neuroblastoma: switching off the p14(ARF)-MDM2-p53 axis. *Cell Death and Differentiation* **16,** 1563–1572 (2009).

80. Swarbrick, A. *et al.* miR-380-5p represses p53 to control cellular survival and is associated with poor outcome in MYCN-amplified neuroblastoma. *Nat Med* **16,** 1134–1140 (2010).
81. Kim, S. S. *et al.* CUL7 is a novel antiapoptotic oncogene. *Cancer Res* **67,** 9616–9622 (2007).
82. Ochiai, H. *et al.* Bmi1 is a MYCN target gene that regulates tumorigenesis through repression of KIF1Bbeta and TSLC1 in neuroblastoma. *Oncogene* **29,** 2681–2690 (2010).
83. Valsesia-Wittmann, S. *et al.* Oncogenic cooperation between H-Twist and N-Myc overrides failsafe programs in cancer cells. *Cancer Cell* **6,** 625–630 (2004).
84. Huang, M. & Weiss, W. A. Neuroblastoma and MYCN. *Cold Spring Harb Perspect Med* **3,** a014415–a014415 (2013).
85. Thiele, C. J., Reynolds, C. P. & Israel, M. A. Decreased expression of N-myc precedes retinoic acid-induced morphological differentiation of human neuroblastoma. *Nature* **313,** 404–406 (1985).
86. Bell, E. *et al.* MYCN oncoprotein targets and their therapeutic potential. *CANCER LETTERS* **293,** 144–157 (2010).
87. Guglielmi, L. *et al.* MYCN gene expression is required for the onset of the differentiation programme in neuroblastoma cells. *Cell Death Dis* **5,** e1081 (2014).
88. Bown, N. Neuroblastoma tumour genetics: clinical and biological aspects. *J Clin Pathol* **54,** 897–910 (2001).
89. Maris, J. M. Recent advances in neuroblastoma. *N Engl J Med* **362,** 2202–2211 (2010).
90. Kang, J.-H. *et al.* MYCN silencing induces differentiation and apoptosis in human neuroblastoma cells. *Biochem Biophys Res Commun* **351,** 192–197 (2006).
91. Burkhart, C. A., Cheng, A. J. & Madafiglio, J. Effects of MYCN antisense oligonucleotide administration on tumorigenesis in a murine model of neuroblastoma. *J Natl Cancer Inst* (2003). doi:10.1093/jnci/djg045
92. Lovén, J. *et al.* Selective inhibition of tumor oncogenes by disruption of super-enhancers. *Cell* **153,** 320–334 (2013).
93. Puissant, A. *et al.* Targeting MYCN in neuroblastoma by BET bromodomain inhibition. *Cancer Discov* **3,** 308–323 (2013).
94. Lutterbach, B. & Hann, S. R. Hierarchical phosphorylation at N-terminal transformation-sensitive sites in c-Myc protein is regulated by mitogens and in mitosis. *Mol Cell Biol* **14,** 5510–5522 (1994).
95. Sjostrom, S. K., Finn, G., Hahn, W. C., Rowitch, D. H. & Kenney, A. M. The Cdk1 Complex Plays a Prime Role in Regulating N-Myc Phosphorylation and Turnover in Neural Precursors. *Developmental Cell* **9,** 327–338 (2005).
96. Pulverer, B. J., Fisher, C., Vousden, K. H., Littlewood, T. D. & Woodgett, J. R. **Site-specific modulation of c-Myc cotransformation by residues phosphorylated in vivo.** *Oncogene* **9,** 50–70 (1994).
97. Sears, R. *et al.* Multiple Ras-dependent phosphorylation pathways regulate Myc protein stability. *Genes & Development* **14,** 2501–2514 (2000).
98. Welcker, M. *et al.* The Fbw7 tumor suppressor regulates glycogen synthase kinase 3 phosphorylation-dependent c-Myc protein degradation. *Proc Natl Acad Sci U S A* **101,** 9085–9090 (2004).
99. Yada, M. *et al.* Phosphorylation-dependent degradation of c-Myc is mediated by the F-box protein Fbw7. *EMBO J* **23,** 2116–2125 (2004).
100. Barone, G., Anderson, J., Pearson, A. D. J., Petrie, K. & Chesler, L. New strategies in neuroblastoma: Therapeutic targeting of MYCN and ALK. *Clin Cancer Res* **19,** 5814–5821 (2013).
101. Otto, T. *et al.* Stabilization of N-Myc is a critical function of Aurora A in human neuroblastoma. *Cancer Cell* **15,** 67–78 (2009).
102. Shang, X. *et al.* Aurora A is a negative prognostic factor and a new therapeutic target in human neuroblastoma. *Mol Cancer Ther* **8,** 2461–2469 (2009).
103. Brockmann, M. *et al.* Small Molecule Inhibitors of Aurora-A Induce Proteasomal Degradation of N-Myc in Childhood Neuroblastoma. *Cancer Cell* **24,** 75–89 (2013).
104. Maris, J. M. *et al.* Initial testing of the aurora kinase a inhibitor MLN8237 by the Pediatric Preclinical Testing Program (PPTP). *Pediatr Blood Cancer* n/a–n/a (2010). doi:10.1002/pbc.22430
105. Mosse, Y. P. *et al.* Pediatric Phase I Trial and Pharmacokinetic Study of MLN8237, an Investigational Oral Selective Small-Molecule Inhibitor of Aurora Kinase A: A Children's Oncology Group Phase I Consortium Study. *Clin Cancer Res* **18,** 6058–6064 (2012).
106. OConnell, R. M., Rao, D. S., Chaudhuri, A. A. & Baltimore, D. Physiological and pathological

roles for microRNAs in the immune system. *Nat Rev Immunol* **10,** 111–122 (2010).
107. Maegdefessel, L. The emerging role of microRNAs in cardiovascular disease. *J Intern Med* n/a–n/a (2014). doi:10.1111/joim.12298
108. Hayes, J., Peruzzi, P. P. & Lawler, S. MicroRNAs in cancer: biomarkers, functions and therapy. *Trends in Molecular Medicine* **20,** 460–469 (2014).
109. Li, Z. & Rana, T. M. Therapeutic targeting of microRNAs: current status and future challenges. *Nat Rev Drug Discov* **13,** 622–638 (2014).
110. Djuranovic, S., Nahvi, A. & Green, R. A parsimonious model for gene regulation by miRNAs. *Science* **331,** 550–553 (2011).
111. Liu, X., Fortin, K. & Mourelatos, Z. MicroRNAs: Biogenesis and Molecular Functions. *Brain Pathol* **18,** 113–121 (2008).
112. Bartel, D. P. MicroRNAs: Target Recognition and Regulatory Functions. *Cell* **136,** 215–233 (2009).
113. Esquela-Kerscher, A. & Slack, F. J. Oncomirs — microRNAs with a role in cancer. *Nat Rev Cancer* **6,** 259–269 (2006).
114. Friedman, R. C., Farh, K. K.-H., Burge, C. B. & Bartel, D. P. Most mammalian mRNAs are conserved targets of microRNAs. *Genome Research* **19,** 92–105 (2009).
115. Calin, G. A. *et al.* Human microRNA genes are frequently located at fragile sites and genomic regions involved in cancers. *Proc Natl Acad Sci U S A* **101,** 2999–3004 (2004).
116. Calin, G. A. *et al.* Frequent deletions and down-regulation of micro- RNA genes miR15 and miR16 at 13q14 in chronic lymphocytic leukemia. *Proc Natl Acad Sci U S A* **99,** 15524–15529 (2002).
117. Cimmino, A. *et al.* miR-15 and miR-16 induce apoptosis by targeting BCL2. *Proc Natl Acad Sci U S A* **102,** 13944–13949 (2005).
118. Garzon, R. *et al.* MicroRNA gene expression during retinoic acid-induced differentiation of human acute promyelocytic leukemia. *Oncogene* **26,** 4148–4157 (2007).
119. Bottoni, A. *et al.* miR-15a and miR-16-1 down-regulation in pituitary adenomas. *J Cell Physiol* **204,** 280–285 (2005).
120. Gregory, R. I. & Shiekhattar, R. MicroRNA biogenesis and cancer. *Cancer Res* **65,** 3509–3512 (2005).
121. Suzuki, H., Maruyama, R., Yamamoto, E. & Kai, M. Epigenetic alteration and microRNA dysregulation in cancer. *Front Genet* **4,** 258 (2013).
122. Melo, S. A. *et al.* A TARBP2 mutation in human cancer impairs microRNA processing and DICER1 function. *Nat Genet* **41,** 365–370 (2009).
123. Melo, S. A. *et al.* A genetic defect in exportin-5 traps precursor microRNAs in the nucleus of cancer cells. *Cancer Cell* **18,** 303–315 (2010).
124. Hill, D. A. *et al.* DICER1 mutations in familial pleuropulmonary blastoma. *Science* **325,** 965 (2009).
125. Ryan, B. M., Robles, A. I. & Harris, C. C. Genetic variation in microRNA networks: the implications for cancer research. *Nat Rev Cancer* **10,** 389–402 (2010).
126. Liu, C. *et al.* Effects of genetic variations on microRNA:target interactions.
127. Chen, Y., Gao, D.-Y. & Huang, L. In vivo delivery of miRNAs for cancer therapy: Challenges and strategies. *Adv Drug Deliv Rev* (2014). doi:10.1016/j.addr.2014.05.009
128. Berindan-Neagoe, I., Monroig, P. D. C., Pasculli, B. & Calin, G. A. MicroRNAome genome: A treasure for cancer diagnosis and therapy. *CA Cancer J Clin* (2014). doi:10.3322/caac.21244
129. Ling, H., Fabbri, M. & Calin, G. A. MicroRNAs and other non-coding RNAs as targets for anticancer drug development. *Nat Rev Drug Discov* **12,** 847–865 (2013).
130. Chen, Y. & Stallings, R. L. Differential Patterns of MicroRNA Expression in Neuroblastoma Are Correlated with Prognosis, Differentiation, and Apoptosis. *Cancer Res* **67,** 976–983 (2007).
131. Schulte, J. H. *et al.* Deep sequencing reveals differential expression of microRNAs in favorable versus unfavorable neuroblastoma. *Nucleic Acids Res* **38,** 5919–5928 (2010).
132. Bray, I. *et al.* Widespread dysregulation of MiRNAs by MYCN amplification and chromosomal imbalances in neuroblastoma: association of miRNA expression with survival. *PLoS ONE* **4,** e7850 (2009).
133. Mestdagh, P. *et al.* MYCN/c-MYC-induced microRNAs repress coding gene networks associated with poor outcome in MYCN/c-MYC-activated tumors. *Oncogene* **29,** 1394–1404 (2010).
134. De Preter, K. *et al.* Accurate outcome prediction in neuroblastoma across independent data sets using a multigene signature. *Clin Cancer Res* **16,** 1532–1541 (2010).

135. Lin, R.-J. *et al.* microRNA signature and expression of Dicer and Drosha can predict prognosis and delineate risk groups in neuroblastoma. *Cancer Res* **70,** 7841–7850 (2010).
136. Shohet, J. M. *et al.* A genome-wide search for promoters that respond to increased MYCN reveals both new oncogenic and tumor suppressor microRNAs associated with aggressive neuroblastoma. *Cancer Res* **71,** 3841–3851 (2011).
137. Chang, T.-C. *et al.* Widespread microRNA repression by Myc contributes to tumorigenesis. *Nat Genet* **40,** 43–50 (2008).
138. Ota, A. *et al.* Identification and characterization of a novel gene, C13orf25, as a target for 13q31-q32 amplification in malignant lymphoma. *Cancer Res* **64,** 3087–3095 (2004).
139. He, L. *et al.* A microRNA polycistron as a potential human oncogene. *Nature* **435,** 828–833 (2005).
140. Hayashita, Y. A Polycistronic MicroRNA Cluster, miR-17-92, Is Overexpressed in Human Lung Cancers and Enhances Cell Proliferation. *Cancer Res* **65,** 9628–9632 (2005).
141. O'Donnell, K. A., Wentzel, E. A., Zeller, K. I., Dang, C. V. & Mendell, J. T. c-Myc-regulated microRNAs modulate E2F1 expression. *Nature* **435,** 839–843 (2005).
142. Lovén, J. *et al.* MYCN-regulated microRNAs repress estrogen receptor-alpha (ESR1) expression and neuronal differentiation in human neuroblastoma. *Proc Natl Acad Sci U S A* **107,** 1553–1558 (2010).
143. Mestdagh, P. *et al.* The miR-17-92 MicroRNA Cluster Regulates Multiple Components of the TGF-β Pathway in Neuroblastoma. *Mol Cell* **40,** 762–773 (2010).
144. Fontana, L. *et al.* Antagomir-17-5p Abolishes the Growth of Therapy-Resistant Neuroblastoma through p21 and BIM. *PLoS ONE* **3,** e2236 (2008).
145. Kumps, C. *et al.* Focal DNA Copy Number Changes in Neuroblastoma Target MYCN Regulated Genes. *PLoS ONE* **8,** e52321 (2013).
146. Cole, K. A. *et al.* A functional screen identifies miR-34a as a candidate neuroblastoma tumor suppressor gene. *Mol Cancer Res* **6,** 735–742 (2008).
147. Raver-Shapira, N. *et al.* Transcriptional Activation of miR-34a Contributes to p53-Mediated Apoptosis. *Mol Cell* **26,** 731–743 (2007).
148. Zhi, F. *et al.* MicroRNAs in Neuroblastoma: Small-Sized Players with a Large Impact. *Neurochem Res* (2014). doi:10.1007/s11064-014-1247-9
149. Tivnan, A. *et al.* Inhibition of Neuroblastoma Tumor Growth by Targeted Delivery of MicroRNA-34a Using Anti-Disialoganglioside GD2 Coated Nanoparticles. *PLoS ONE* **7,** e38129 (2012).
150. Ritter, G. & Livingston, P. O. Ganglioside antigens expressed by human cancer cells. *Semin Cancer Biol* **2,** 401–409 (1991).
151. Lee, J.-J., Drakaki, A., Iliopoulos, D. & Struhl, K. MiR-27b targets PPARγ to inhibit growth, tumor progression and the inflammatory response in neuroblastoma cells. *Oncogene* **31,** 3818–3825 (2012).
152. Xu, H., Cheung, I. Y., Guo, H.-F. & Cheung, N.-K. V. MicroRNA miR-29 modulates expression of immunoinhibitory molecule B7-H3: potential implications for immune based therapy of human solid tumors. *Cancer Res* **69,** 6275–6281 (2009).
153. Evangelisti, C. *et al.* MiR-128 up-regulation inhibits Reelin and DCX expression and reduces neuroblastoma cell motility and invasiveness. *FASEB J* **23,** 4276–4287 (2009).
154. Althoff, K. *et al.* MiR-137 functions as a tumor suppressor in neuroblastoma by downregulating KDM1A. *Int J Cancer* **133,** 1064–1073 (2013).
155. Zhang, H. *et al.* MicroRNA-145 inhibits the growth, invasion, metastasis and angiogenesis of neuroblastoma cells through targeting hypoxia-inducible factor 2 alpha. *Oncogene* **33,** 387–397 (2014).
156. Lin, R.-J., Lin, Y.-C. & Yu, A. L. miR-149* induces apoptosis by inhibiting Akt1 and E2F1 in human cancer cells. *Mol Carcinog* **49,** 719–727 (2010).
157. Ragusa, M. *et al.* MIR152, MIR200B, and MIR338, human positional and functional neuroblastoma candidates, are involved in neuroblast differentiation and apoptosis. *J Mol Med* **88,** 1041–1053 (2010).
158. Ryan, J. *et al.* MicroRNA-204 increases sensitivity of neuroblastoma cells to cisplatin and is associated with a favourable clinical outcome. *Br J Cancer* **107,** 967–976 (2012).
159. Althoff, K. *et al.* miR-542-3p exerts tumor suppressive functions in neuroblastoma by downregulating Survivin. *Int J Cancer* (2014). doi:10.1002/ijc.29091

Chapter 2

Research Outline

Since its identification in neuroblastoma, increasing evidence points towards a central role for MYCN in the biology of neuroblastoma tumors. As a consequence, targeting MYCN and its downstream functions would be a promising strategy to treat neuroblastoma patients. However, the development of inhibitors targeting MYC proteins has been challenging, as MYC/MYCN proteins are composed of two extended alpha-helices with no obvious surfaces for small molecule binding. Therefore, a thorough understanding of MYCN's functions and the upstream mechanisms regulating its expression would contribute to the development of compounds specifically targeting the impact of MYCN in neuroblastoma cells.

To address this issue, I initiated this thesis with the construction of an *in vivo* time-resolved miRNA and gene expression dataset of MYCN-driven neuroblastoma development, using the well-established TH-MYCN mouse model. After extensive validation of the dataset, I applied an exiting transcriptome-wide cross-species approach to search for transcriptional regulators that can be regarded as master regulators of neuroblastoma development (**chapter 3**, paper 1). The corresponding miRNA expression dataset was exploited during the characterization of the complete MYCN-miRNA interactome in neuroblastoma using the powerful combination of this dataset and an unbiased 3'UTR reporter screen (**chapter 4**, paper 2). In **chapter 5** (i.e. paper 3), I next characterized how MYCN affects the expression of LIN28B, a highly conserved RNA-binding protein, which is shown to induce MYCN expression in neuroblastoma via the suppression of the MYCN-targeting let-7 family of miRNAs.

Throughout this project, studying the genetic landscape of the well-established TH-MYCN mouse model has provided great insights in the perturbed miRNA-mRNA networks in neuroblastoma. Although representing an excellent and broadly used tool, this mouse model holds some limitations related to the transgene integration site, the anatomical location of the observed tumors, implementation of *in vivo* imaging and tumor incidence in different genetic backgrounds. In **chapter 6** (i.e. paper 4), we therefore present a novel mouse model with targeted Cre-conditional *MYCN* expression in the neural crest.

Comparing the implications of perturbed MYCN activity in this new mouse model with similar insights obtained from ALK- or LIN28B-driven mouse tumors or the insights obtained from **chapter 3**, could contribute to a more thorough understanding of both common and different effects of these important neuroblastoma oncogenes in the biology of this embryonic tumor.

Chapter 3

Master regulators of MYCN-driven neuroblastoma development identified through genome-wide cross-species integrative transcriptome analysis

Anneleen Beckers[1], Daniel R. Carter[2], Shana Claeys[1], Pieter Mestdagh[1], Gert Van Peer[1], Robrecht Cannoodt[1], Belamy B. Cheung[2], Glenn M. Marshall[2], Jo Vandesompele[1], Katleen De Preter[1], Frank Speleman[1]

[1] Center for Medical Genetics (CMGG), Ghent University, Ghent, Belgium;
[2] Children's Cancer Institute, University of New South Wales, Sydney, Australia.

Manuscript in preparation

Abstract

Neuroblastoma is a childhood malignancy with high clinical and genetic heterogeneity. At least half of aggressive neuroblastoma tumors are characterized by *MYCN* amplification. MYCN is a MYC family member and has also been reported to be amplified or overexpressed in other embryonal tumor such as medulloblastoma as well as adult cancers including lung cancer (ref). Until recently, targeted drugging of MYC(N) driven tumor entities was beyond reach but novel insights into gene regulation and MYC(N) mode of action are now opening the way for precision medicine. Discovering additional key interactors and vulnerable nodes in the MYCN network will further contribute to our understanding of neuroblastoma etiology and hence the development of efficient targeted therapy for patients facing aggressive neuroblastoma. To this end, we explored the dynamic transcriptional changes in MYCN-driven tumor development using an established MYCN neuroblastoma mouse model. Integrative cross-species data-analysis of the developmental gene signatures revealed a total of 22 master regulators and 16 synergistic master regulator pairs involved in MYCN-driven neuroblastoma development. Further characterization of these master regulators and their regulated neuroblastoma signatures, highlighted MYB, E2F2, MXD3, EZH2 and PLAGL2 as key master regulators of both MYCN-driven and MYCN-independent neuroblastoma development. Finally, we showed that synergistic master regulator pairs are associated with patient survival and constitute promising targets for combination therapy.

Introduction

Neuroblastoma is a deadly childhood cancer arising from sympatho-adrenergic nervous progenitor cells [1]. The neuroblastoma genomic landscape is dominated by DNA copy number alterations while mutational burden is very low, as observed in other embryonal tumors. In addition to highly recurrent whole chromosome and segmental chromosomal imbalances, MYCN amplification is observed in a substantial proportion of cases and marks poor prognosis. Rare amplifications allowed to uncover two further *bona fide* oncogenes implicated in this disease, namely ALK [2-5] and LIN28B [6]. Both genes are part of developmental regulatory pathways and were shown to activate MYC(N) activity through distinct mechanisms [6,7]. For each of these driver genes, transgenic mouse models have reinforced the causal relationship between aberrant overexpression or somatic mutation and neuroblastoma tumor development. In addition, the established mouse models have been – and continue to be – of great value to the study of neuroblastoma tumor biology and the development of new therapeutic strategies.

The identification of neuroblastoma driver genes and their study in preclinical models has lead to the execution of phase 1 clinical trials testing the safety and clinical activity of compounds targeting ALK [8,9] or MYCN [10]. Regardless of these encouraging findings, intrinsic and acquired resistance almost inevitably occurs when using single compound treatment, warranting the exploration of opportunities for rationally designed combinatorial treatment approaches. While second generation ALK inhibitors are now emerging and insights into down stream signaling is growing [11], allowing further design of optimized drugging, interest for uncovering further venues to drug MYCN or MYCN governed regulatory pathways is a strongly emerging focus of research.

While MYCN clearly plays a central role in neuroblastoma initiation and progression, both its exact mode of action and the critically involved regulatory partners are still under intensive investigation [12]. Recently, the Califano team developed an algorithm coined the MAster Regulator INference algorithm (MARINa) [13,14], in order to identify so-called master regulators. While this is an ill defined term [15], the concept used here is that master regulators act as transcriptional regulators controlling the regulation of multiple genes in a given gene signature of biological or clinical significance. These master regulators are positioned at the top of the regulatory network in the given gene signature and, as such, could constitute vulnerable drugable targets. In this study, we assembled gene signatures reflecting MYCN-driven neuroblastoma development using dynamic gene expression data from murine MYCN-driven neuroblastoma tumorigenesis, and screened for cooperating master regulators in neuroblastoma development using MARINa. Using this approach, we identified

five core master regulators, MYB, E2F2, MXD3, EZH2 and PLAGL2. Our approach thus unraveled for the first time a unique network of master regulators offering the basis for further research to explore novel approaches to drug the MYCN governed oncogenic regulatory network in neuroblastoma.

Results

Composing the hyperplasia dataset reflecting gene expression alterations during neuroblastoma development

To gain insight in neuroblastoma development, we performed gene expression profiling of different stages of tumor development in the TH-MYCN mouse model, a MYCN-driven neuroblastoma model [16]. In brief, we sacrificed TH-MYCN+/+ mice at one (n = 4) and two weeks (n = 4) after birth to harvest superior cervical and celiac ganglia containing foci of neuroblast hyperplasia, and 6-week old (n = 4) TH-MYCN+/+ mice to dissect advanced neuroblastoma tumors, arisen from the neuroblast hyperplasia [17]. Additionally, we dissected the superior cervical and celiac ganglia from TH-MYCN-/- mice at one (n = 4), two (n = 4) and six weeks (n = 4) after birth to control for gene expression changes during normal postnatal development of the sympathetic ganglia. We assayed each individual harvested sample with a murine-specific gene expression microarray.

To obtain a global view of the gene expression patterns in these samples, principal component analysis was performed and the first and second principal component were plotted (**Figure 3.1a**). The first principal component showed a strong genotype effect and accounted for 43.2% of data variability, while the second principal component showed a strong time effect and accounted for an additional 18.7% of data variability. This representation thus shows the main variability of mRNA expression levels of all samples. The first time point (1 week after birth) from both genotypes (TH-MYCN+/+ and TH-MYCN -/-) map together implying that the overall changes of the transcriptome in this set of samples were comparable with the average variability between biological replicates. At later time points (2 and 6 weeks after birth), the overall changes of the transcriptome increase relative to the average variability between replicates and both genotypes cluster further apart, suggesting strong transcriptional differences between neuroblastoma tumors and normal ganglionic tissue. Indeed, as time progresses and as can be expected, an increasing number of genes are significantly differentially expressed between TH-MYCN+/+ and TH-MYCN-/- samples (**Supplemental Figure 3.1a**).

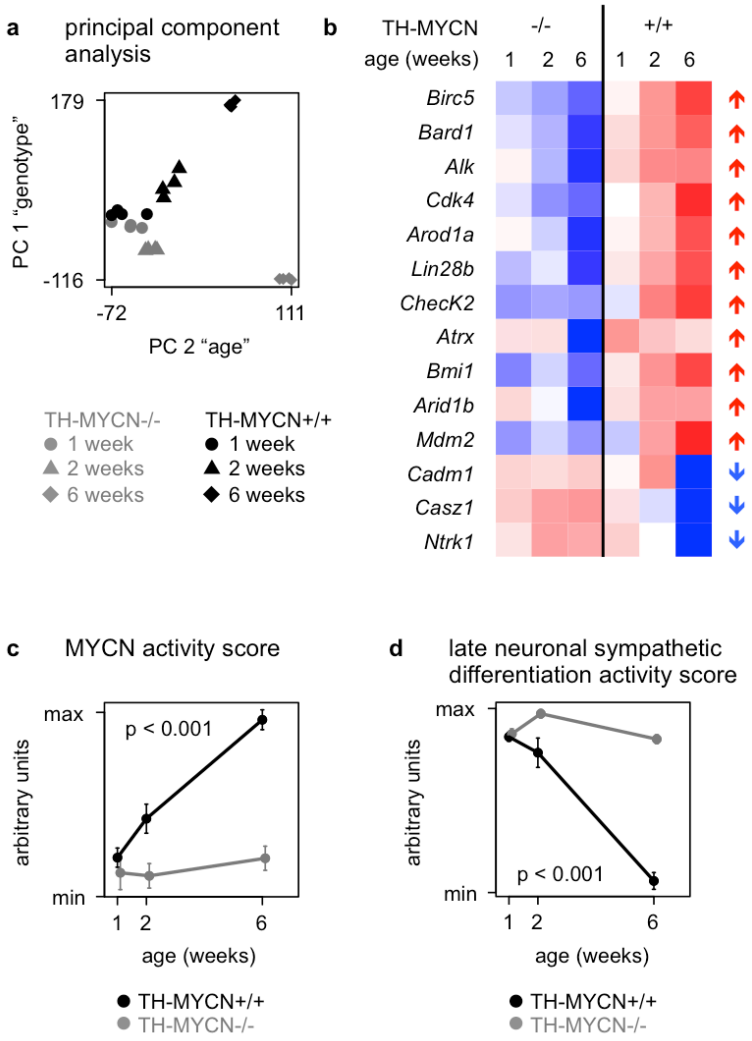

Figure 3.1. Characterization of the hyperplasia dataset. (a) Principal component analysis visualizes the variation in the hyperplasia dataset. The vertical axis corresponds to the first principal component of the mRNA data, mainly discriminating genotypes, and the horizontal axis shows the second principal component, primarily discriminating age of mice. **(b)** The expression of candidate neuroblastoma oncogenes (↑) and tumorsuppressor genes (↓) in the hyperplasia dataset. Each instance in the heatmap represents mean expression of 4 samples. **(c)** Signature score analysis of MYCN activity in the hyperplasia dataset. Data represent mean signature score ± standard deviation of 4 samples. Y-axis represents arbitrary units. Black: TH-MYCN+/+ samples; gray: TH-MYCN-/- samples. P-value corresponds to the interaction term of a two-way ANOVA analysis. **(d)** Signature score analysis of late neuronal sympathetic differentiation (19) in the hyperplasia dataset. Data represent mean signature score ± standard deviation of 4 samples. Y-axis represents arbitrary units. Black: TH-MYCN+/+ samples; gray: TH-MYCN-/- samples. P-value corresponds to the interaction term of a two-way ANOVA analysis.

To validate the biological relevance of the hyperplasia dataset for the study of neuroblastoma tumor biology, we first evaluated the expression of known neuroblastoma oncogenes and tumor suppressor genes in the hyperplasia dataset. The expression of known oncogenes increased, whereas the expression of known tumor suppressor genes decreased over time in the TH-MYCN+/+ samples compared to TH-MYCN-/- samples (**Figure 3.1b**). Subsequently, we assessed the expression of known MYC(N) transcriptional target genes [18] in the hyperplasia dataset, summarized in a MYCN activity score.

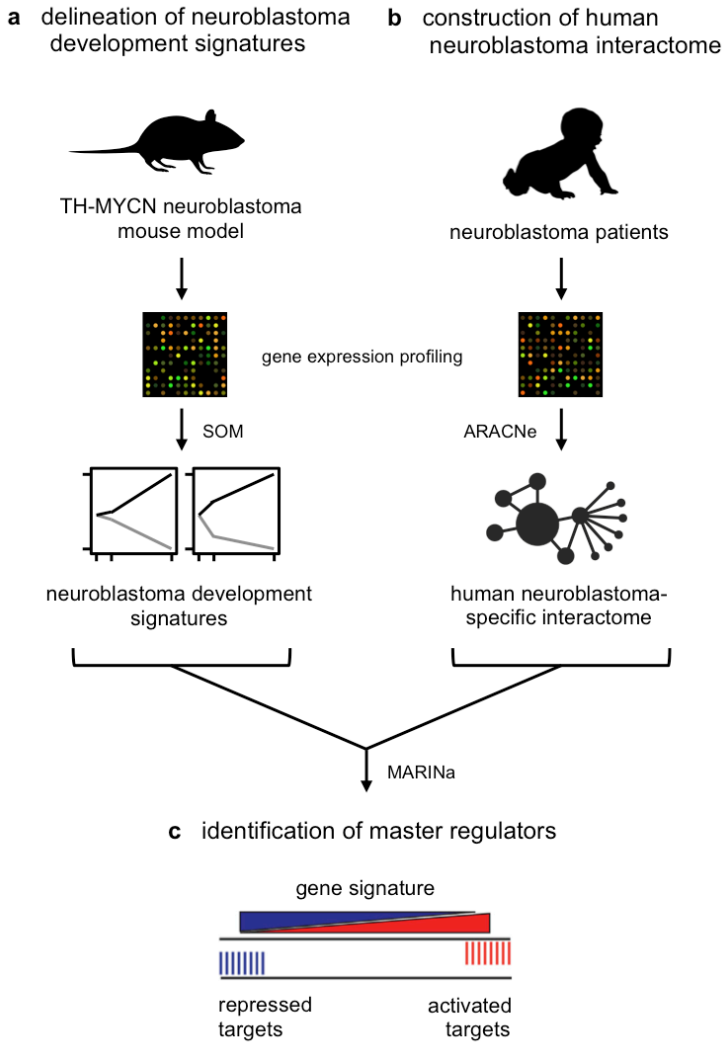

Figure 3.2. Strategy for genome-wide cross-species analysis of neuroblastoma development. Schematic representation of the overall strategy. **(a)** Step I: delineation of murine neuroblastoma signatures via clustering of gene expression data from the hyperplasia dataset with Self Organizing Maps. **(b)** Step II: construction of a human neuroblastoma-specific interactome. **(c)** Step III: identification of master regulators of neuroblastoma development using the murine neuroblastoma development signatures and a human neuroblastoma-specific interactome. Step I and III were iterated 100 times to ensure robust master regulator analysis.

The MYCN activity score increased significantly over time in the TH-MYCN+/+ samples compared to TH-MYCN-/- samples (**Figure 3.1c**). This observation is in keeping with the hypothesis that sustained MYCN activity in the sympathetic ganglia of TH-MYCN+/+ mice gives rise to the appearance of neuroblastoma tumors in these anatomic locations [17]. Furthermore, genes involved in late neuronal sympathetic differentiation [19], summarized in a late neuronal sympathetic differentiation activity score, decreased significantly over time in the TH-MYCN+/+ samples compared to TH-MYCN-/- samples (**Figure 3.1d**), implying that late neuronal sympathetic differentiation markers are suppressed during neuroblastoma development. Together these observations indicate that we have generated a highly

valuable transcriptome dataset reflecting gene expression alterations during MYCN-driven neuroblastoma development.

Inferring master regulators of MYCN-driven neuroblastoma development

Having established a highly valuable transcriptome dataset reflecting gene expression alterations during MYCN-driven neuroblastoma development, we next set out to identify master regulators of MYCN-driven neuroblastoma development. To this end, we first constructed neuroblastoma development signatures through clustering of genes in the hyperplasia dataset in 12 distinct gene signatures according to similar gene expression patterns using Self-Organizing Maps (SOM) (**Figure 3.2a** and **Supplementary Figure 3.2**). To identify master regulators of these neuroblastoma development signatures, we used the MARINa algorithm, which identifies candidate master regulators based on the concerted differential expression of their targets genes [13,14]. To allow for this analysis, we constructed a human neuroblastoma-specific interactome using ARACNe (**Figure 3.2b**). ARACNe is an unbiased algorithm that infers direct transcriptional interactions based on the mutual information between transcriptional regulators and their potential targets, based on gene expression profiles. To assemble a human neuroblastoma-specific interactome, we analyzed the gene expression in a large heterogeneous cohort of primary neuroblastoma tumors (n = 200), enabling optimal ARACNe analysis. This resulted in a regulatory network representing 371,783 interactions between 601 transcriptional regulators and their inferred target genes (**Figure 3.2b**). Thus having established the murine neuroblastoma development signatures and the human neuroblastoma-specific interactome, we screened the 601 transcriptional regulators for their putative role as master regulator of neuroblastoma development, with the MARINa algorithm (**Figure 3.2c**). To ensure robust identification of master regulators of neuroblastoma development, we iterated the process of signature generation (**Figure 3.2a**) and master regulator inference (**Figure 3.2c**) 100 times (see Materials and Methods). Finally, we retained all master regulators that were inferred for neuroblastoma development signatures with a significant increasing or decreasing activity during murine neuroblastoma development, as measured with two-way ANOVA with interaction of the activity score in the hyperplasia dataset (see Materials and Methods).

a

	increasing gene signatures	decreasing gene signatures
MRs inferred	71.7%	12.0%
no MRs inferred	28.3%	88.0%

b

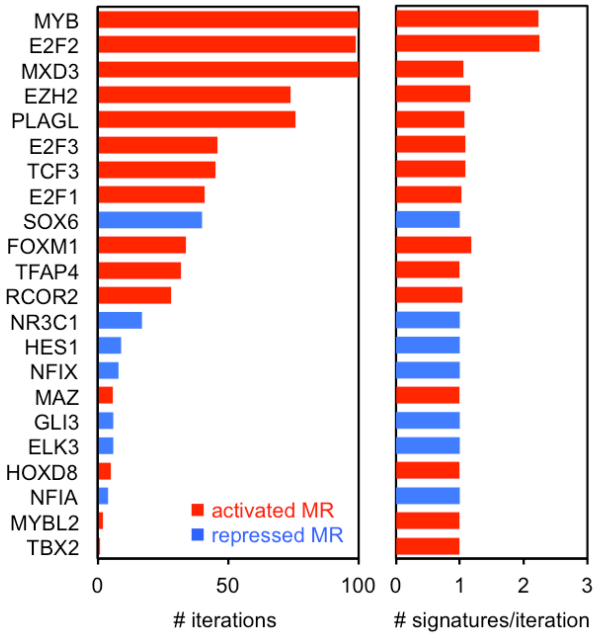

c

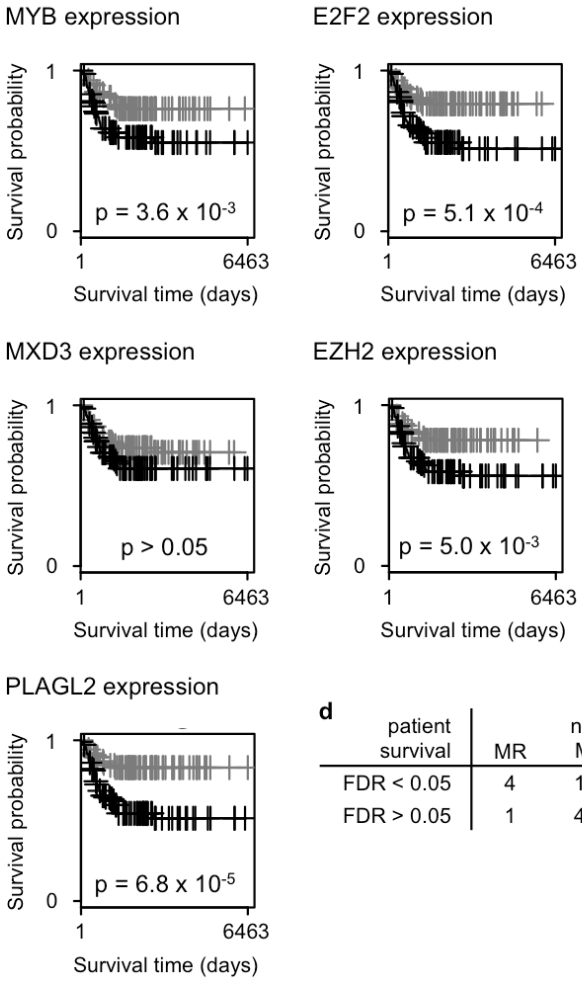

d

patient survival	MR	non-MR
FDR < 0.05	4	134
FDR > 0.05	1	459

Figure 3.3. Master regulator analysis of neuroblastoma development. (a) Percentage of gene signatures with increasing or decreasing pattern in neuroblastoma development, for which master regulators were inferred. Fisher's Exact test, $p < 2.2 \times 10^{-16}$. **(b)** Results of 100 iterations of gene expression clustering with self-organizing maps and subsequent master regulator analysis (including shadow and synergism analysis; see Materials and methods). In total, 22 master regulators were identified in at least 1 SOM analysis (left). Black circles indicated master regulators that are not associated with patient survival (see panel d). The majority of master regulators were found to regulate 1/12 gene signatures per SOM analysis (right). **(c)** Kaplan-Meier survival analysis based on gene expression levels of MYB, E2F2, MXD3, EZH2 or PLAGL2 in a large cohort of primary neuroblastoma patients with respect to time to cancer-specific death (two-sided log rank test). **(d)** Number of master regulators or non-master regulator transcriptional regulators tested in the master regulator analysis (non-master regulator), that are associated with patient survival. FDR value corresponds to a log-rank test with Benjamini-Hochberg multiple testing correction. Fisher's Exact test, $p = 6.6 \times 10^{-8}$.

The constructed neuroblastoma development signatures were highly similar across the 100 iterations (**Supplementary Figure 3.3**). In each of the 100 iterations, on average 11/12 gene signatures (range: 9 - 12) showed significant differential activity between TH-MYCN+/+ and TH-MYCN-/- mice: on average 4.4 signatures (range: 4 - 5) showed increasing and 6.6 signatures (range: 5 - 8) decreasing activity. In each of the 100 iterations, on average 3.2 increasing gene signatures (range: 2 - 4) and 0.8 decreasing gene signatures (range: 0 - 2) were found to be significantly regulated by master regulators (**Figure 3.3a**). Thus, master

regulators were more likely to be inferred from gene signatures with increasing gene signature scores during murine neuroblastoma development.

In total, 22 distinct master regulators could be inferred for at least one neuroblastoma development signature in at least one iteration (**Figure 3.3b** and **Supplementary Table 3.1**). These master regulators were either activated (n = 15) or repressed (n = 7): activated master regulators have induced and repressed target genes significantly enriched among up- and downregulated genes in the neuroblastoma development signatures, respectively, while repressed master regulators show the opposite pattern. We focused our subsequent analysis on the master regulators that were inferred as regulators of neuroblastoma development in at least half of the 100 iterations, each of which is an activated master regulator: MYB, E2F2, MXD3, EZH2 and PLAGL2. We next asked whether expression of these master regulators is associated with neuroblastoma progression and/or outcome by analysis of gene expression in our neuroblastoma patient cohort. Of the five retained master regulators, high expression of four master regulators was significantly associated with adverse outcome of neuroblastoma patients (**Figure 3.3c**). Notably, the five master regulators were more likely to be associated with disease outcome, as assessed by a log-rank test, than transcriptional regulators not inferred as master regulators (**Figure 3.3d**). Thus, genome-wide cross-species integrative transcriptome analysis identified master regulators of MYCN-driven neuroblastoma development of potential clinical relevance.

MYB, E2F2 and EZH2 are MYCN-regulated master regulators

Given that the five master regulators were inferred as regulators of MYCN-driven neuroblastoma development signatures, we set out to investigate the relation between the expression levels of MYCN and each of the master regulators. To this end, we evaluated the gene expression of the master regulators as well as their ARACNe-inferred transcriptional activity in different neuroblastoma models. In the TH-MYCN mouse model, the mRNA expression and inferred activity of each of the five master regulators increased significantly during MYCN-driven tumor development (**Figure 3.4a-b**). These observations were confirmed in a second, independent, murine MYCN-driven neuroblastoma model, the LSL-*MYCN;Dbh-iCre* model [20] as four out of five master regulators were found to be higher expressed and all five master regulators had higher inferred transcriptional activity in tumors as compared to normal adrenal tissue (**Supplementary Figure 3.4**).

To verify that the increased expression of MYB, E2F2, MXD3, EZH2 and PLAGL2 in these *in vivo* models is a direct consequence of increased MYCN activity, we evaluated their expression in public data of an *in vitro* model of MYCN activity in neuroblastoma [21].

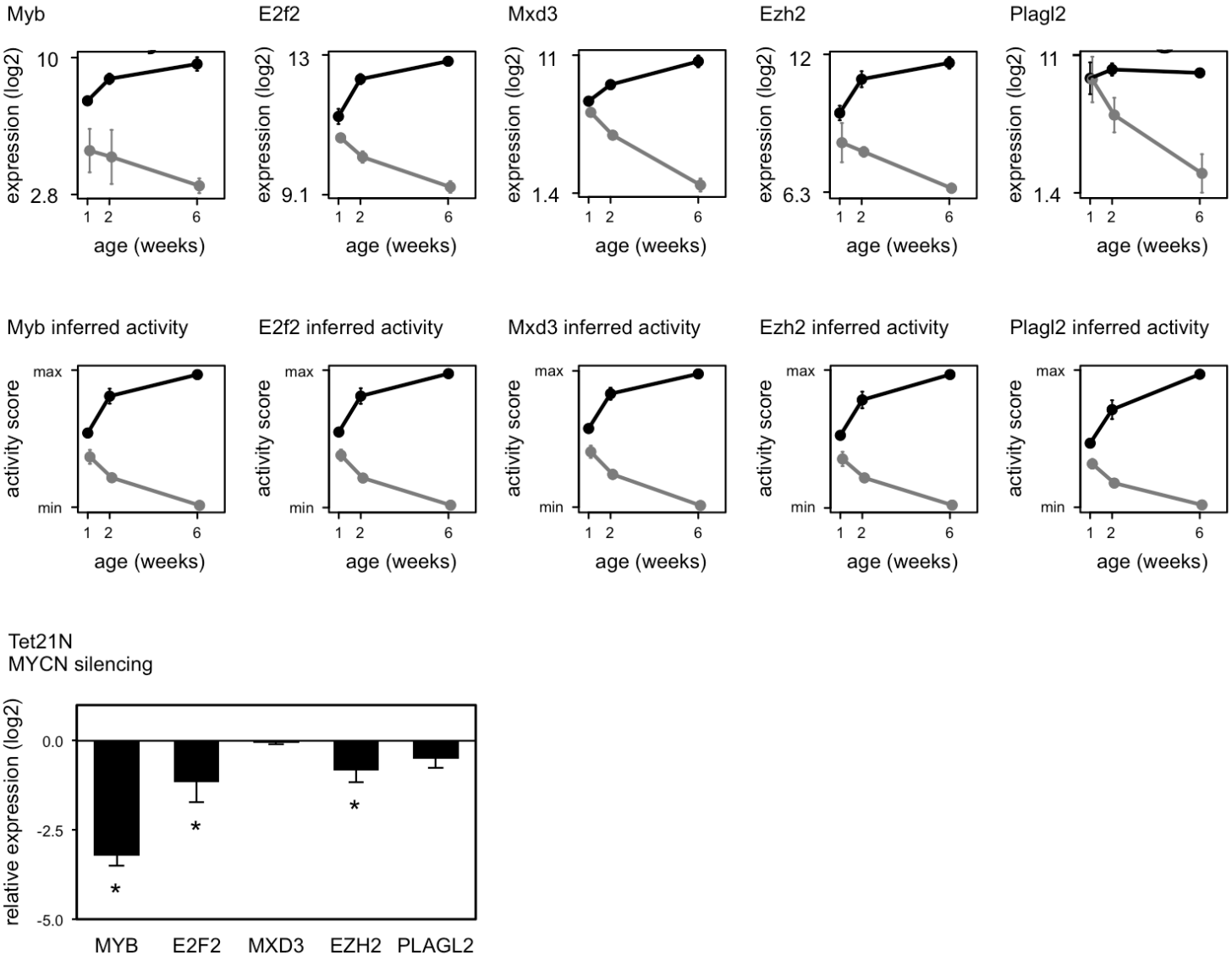

Figure 3.4. Characterization of identified master regulators. (a) Expression of MYB, E2F2, MXD3, EZH2 or PLAGL2 in the hyperplasia dataset. Data represent mean gene expression ± standard deviation of 4 samples. Black: TH-MYCN+/+ samples; gray: TH-MYCN-/- samples. P-value corresponds to the interaction term of a two-way ANOVA analysis. **(b)** Signature score analysis of inferred master regulator activity in the hyperplasia dataset. Data represent mean signature score ± standard deviation of 4 samples. Y-axis represents arbitrary units. Black: TH-MYCN+/+ samples; gray: TH-MYCN-/- samples. P-value corresponds to the interaction term of a two-way ANOVA analysis. **(c)** Expression of MYB, E2F2, MXD3, EZH2 or PLAGL2 upon MYCN silencing in SHEP-Tet21N cells. Asterisk indicates significant differential expression before and after MYCN silencing (paired T-test; $P < 0.05$).

The SHEP-Tet21N system is a conditional tetracycline-regulated MYCN expression system established in the MYCN non-amplified SHEP neuroblastoma cell line [22]. Expression of MYCN is switched off by the addition of tetracycline to the growth medium. Levels of MYCN protein and RNA in the absence of tetracycline are comparable with those present in MYCN amplified cell lines [23]. We observed a significant decrease in the expression of *MYB*, *E2F2* and *EZH2* upon silencing of MYCN, while the expression of *MXD3* and *PLAGL2* did not change significantly (**Figure 3.4c**). Together these *in vivo* and *in vitro* data demonstrate that

MYCN could induce the expression of *MYB*, *E2F2* and *EZH2* in neuroblastoma cells. These data further show that *MXD3* and *PLAGL2* are up-regulated during murine MYCN-driven neuroblastoma development; however, these data do not provide evidence that this is a direct consequence of MYCN activity.

Having studied the relationship between MYCN and the five master regulators, we also assessed whether the master regulators were of clinical relevance for all neuroblastoma patients irrespective of MYCN amplification status. To this end, we evaluated the mRNA expression levels of the master regulators as well as their ARACNe-inferred transcriptional activity in our neuroblastoma patient cohort. For 3 master regulators (E2F2, EZH2 and PLAGL2), the observed clinical impact was independent of MYCN amplification status since high expression of these master regulators was associated with worse outcome in a subgroup of patients without MYCN amplification (**Supplementary Table 3.2**). Moreover, for all five master regulators high ARACNe-inferred transcriptional activity was associated with worse outcome in a subgroup of patients without MYCN amplification (**Supplementary Table 3.2**). Thus, cross-species master regulator analysis revealed master regulators regulating both MYCN-driven and MYCN-independent neuroblastoma development

MYB, E2F2, MXD3, EZH2 and PLAGL2 regulate cancer-related biological processes

To gain insight into the inferred master regulators and their regulated neuroblastoma development signatures, we subsequently focused on one representative iteration, i.e. iteration 31 (**Supplementary Figure 3.3**). Here, MYB, E2F2, MXD3, EZH2 and PLAGL2 were inferred for three gene signatures with increasing activity during neuroblastoma development (**Supplementary Table 3.1**); no master regulators for gene signatures with decreasing activity were found. To attain deeper knowledge of the biological processes that are regulated by the inferred master regulators, we performed Gene Ontology (GO) enrichment analysis of the neuroblastoma development signatures constructed in iteration 31. GO enrichment analysis of gene signatures with increasing activity during neuroblastoma development revealed an overrepresentation of genes involved in DNA metabolism (DNA replication and repair), RNA metabolism (transcription, RNA processing and splicing) and cell cycle regulation, while genes involved in immune response and translation were overrepresented in gene signatures with decreasing activity (**Supplementary Figure 3.5**). In line with these observations, the ARACNe-inferred target genes of the five master regulators were enriched for genes involved in biological processes similar to those enriched in their regulated gene signatures (**Figure 3.5**): the targets of

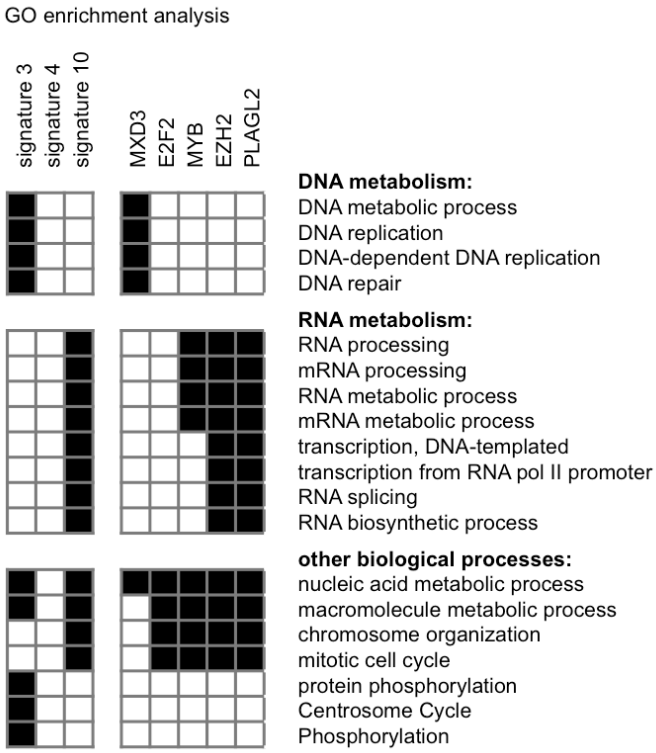

Figure 3.5. Results from Gene Ontology enrichment analysis of the three neuroblastoma development gene signatures in iteration 31 and of the ARACNe-inferred master regulator regulons. Black boxes represent significant enrichment of the GO term (right), in the respective gene signature or regulon (top).

MXD3, master regulator of neuroblastoma development signature 3, were enriched for genes involved in DNA metabolism; while the targets of MYB, E2F2, EZH2 and PLAGL2, master regulators of signature 10, were enriched for genes involved in RNA metabolism.

Synergistic master regulator pairs are associated with patient survival

We further prioritized the five master regulators by computationally evaluating their potential synergistic interactions. In particular, any pair of master regulators was considered ‘‘synergistic’’ if their co-regulated MARINa-inferred targets were more significantly enriched in the co-regulated neuroblastoma development signature than their individual targets [14]. Among all possible pairs of inferred master regulators, two pairs were statistically significant: MYB-PLAGL2 and E2F2-PLAGL2 (**Figure 3.6a** and **Supplementary Table 3.3**).

To more thoroughly investigate the role of these synergistic master regulators pairs in neuroblastoma development, we performed patient survival analysis to assess the potential impact of co-alterations in gene pairs. In this analysis, each gene has one of two states: "high" if the gene in the sample is expressed at a high level relative to the average level of the gene across all samples; and "low" if the gene is expressed at a low level. For each synergistic master regulator pair, we examined each of four scenarios, namely, "high-high",

"high-low", "low-high" and "low-low". By comparing the survival time of patients with high expression of both genes to survival time of patients with high expression of only one gene, we found that for both synergistic master regulator pairs, combined high expression of both master regulators was associated with worse outcome of neuroblastoma patients (**Figure 3.6b**). This property is independent of the MYCN amplification status since the association was also discovered in MYCN non-amplified patients. Notably, the observed association between patient outcome and co-alterations in synergistic master regulator pairs is significant compared to the association between patient outcome and the co-alteration of random selected pairs of transcriptional regulators not inferred as master regulators of neuroblastoma tumor development (data not shown). These data indicate that information on synergistic master regulator pairs can be useful for risk assessment and outcome prediction of neuroblastoma patients.

Discussion

We have identified MYB, E2F2, MXD3, EZH2 and PLAGL2 as master regulators of MYCN-driven neuroblastoma development through genome-wide cross-species integrative transcriptome analysis. The MARINa algorithm [13,14] used for these analyses infers master regulators as genes that most significantly regulate the transcriptional program associated with a particular phenotype – in this case, neuroblastoma development.

Using GO enrichment analysis of master regulator-regulated genes, we showed that the inferred master regulators control cancer-related biological processes. The targets of MXD3 were enriched for genes involved in DNA metabolism (i.e. DNA replication and repair); while the targets of MYB, E2F2, EZH2 and PLAGL2 were enriched for genes involved in RNA metabolism (i.e. transcription, (m)RNA processing and RNA splicing), chromosome organization and mitotic cell cycle. These processes closely relate to the biological processes overrepresented in genes that are required for MYCN-driven neuroblastoma cell proliferation: transcription, cell cycle, and apoptosis [24]. This concordance supports the hypothesis that the inferred Master regulators strongly contribute to, and could be necessary for, MYCN-driven neuroblastoma development.

Interestingly, the MARINa algorithm also provides an effective computational tool for the identification of synergistic interactions among master regulators. Indeed, our unbiased interrogation of 602 transcriptional regulators represented in the human neuroblastoma-specific interactome, led to identification of two synergistic master regulator pairs.

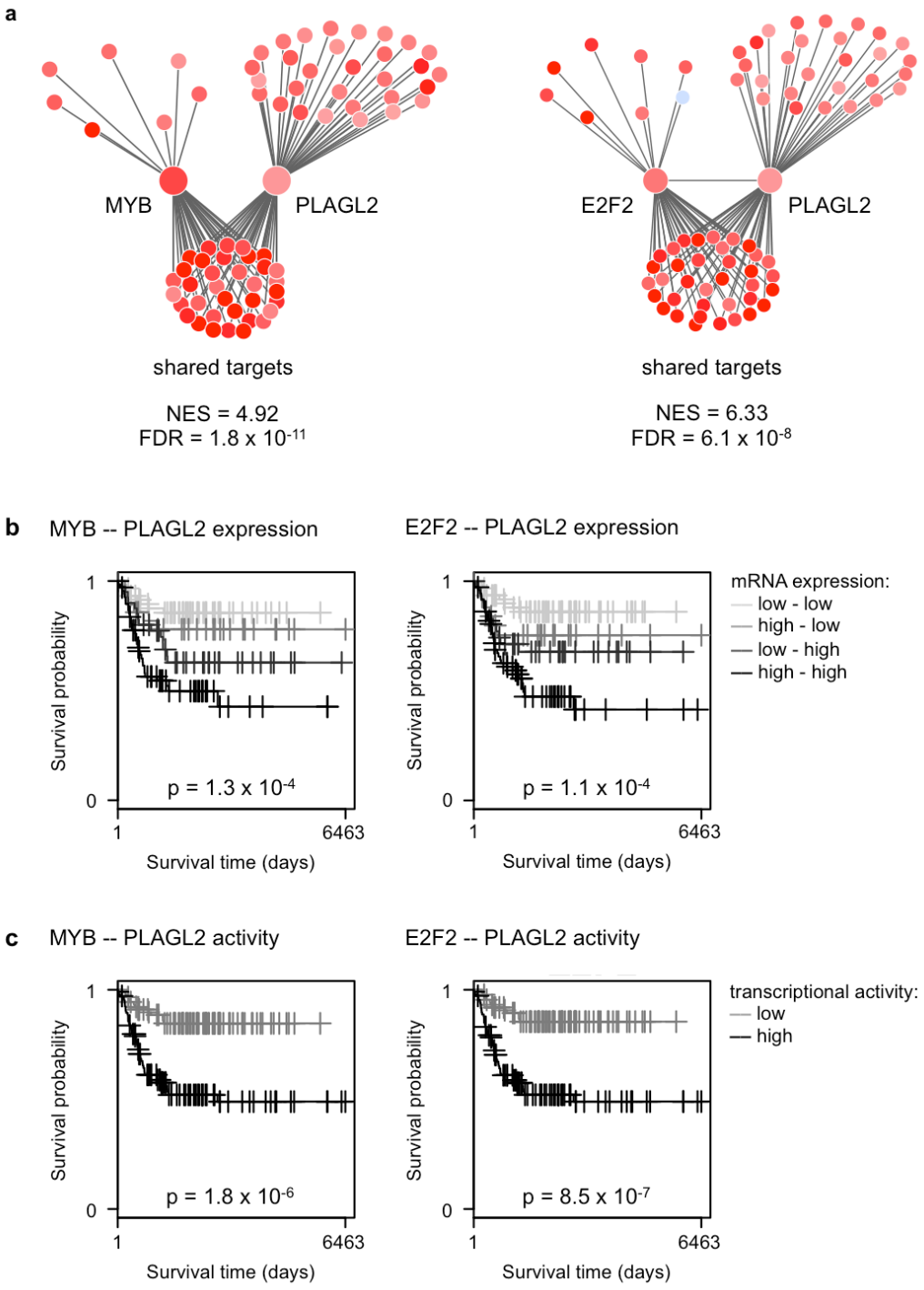

Figure 3.6. Synergistic master regulator pairs are associated with patient survival. (a) Computational synergy analysis depicting PLAGL2 and MYB regulons (left) and PLAGL2 and EF2E regulons (right) showing shared and nonshared targets. Red corresponds to overexpressed targets and blue to underexpressed targets in the hyperplasia dataset; NES = normalized enrichment score; FDR = false discovery rate. **(b)** Kaplan-Meier survival analysis based on combined gene expression levels of PLAGL2 and MYB (left) and PLAGL2 and E2F2 (right) in a large cohort of primary neuroblastoma patients with respect to time to cancer-specific death (two-sided log rank test). **(c)** Kaplan-Meier survival analysis based on combined gene activity of PLAGL2 and MYB (left) and PLAGL2 and E2F2 (right) in a large cohort of primary neuroblastoma patients with respect to time to cancer-specific death (two-sided log rank test).

Both identified synergistic master regulator pairs involved PLAGL2, a ubiquitously expressed C2H2 zinc finger transcription factor that is involved in cellular transformation and apoptosis, and has been reported to have both oncogenic and tumor suppressor functions. PLAGL2 was shown to increase proliferation in acute myeloid leukemia in cooperation with the CBFB-MYH11 fusion gene [25]. Further, in glioblastoma, PLAGL2 expression suppressed cellular differentiation and promoted cellular capacity for self-renewal by activating the Wnt/β-catenin pathway [26]. In contrast, under hypoxic conditions or in response to or iron deficiency, PLAGL2 may have an apoptotic role via induction of the pro-apoptotic factor BNIP3 by promoter activation [27]. The data presented here suggest an oncogenic function for PLAGL2 in neuroblastoma development. Moreover, we hypothesize that PLAGL2 and its the synergistic partners, E2F2 and MYB, may act together to execute (some of) their functions in neuroblastoma development. While these master regulators have been implicated in various cancers, their synergistic actions have been identified here for the first time. The underlying biological mechanism resulting in these *in silico* observed cooperation events can not be deduced from our data, warranting further experiments to elucidate the biological cooperation of these synergistic master regulator pairs. Putative mechanistic models include co-localization at promoters of target genes and / or functional cooperativity as co-repressor or -activator. In analogy with similar studies in other tumor entities [14,28], we anticipate that the combined therapeutic targeting of synergistic master regulators may help to overcome the complex feedback mechanisms that hinder therapeutic targeting of signaling pathways.

Both MYB and E2F2 have previously been associated to neuroblastoma tumor biology, validating the findings of our strategy. MYB is a transcription factor with a well-established role in hematopoiesis, and its oncogenic activation is associated with leukaemogenesis in several species including humans. A key function of MYB in these processes is to maintain the proliferative progenitor-cell phenotype, whereas its downregulation is necessary for differentiation [29]. Similar functions for MYB were reported in neuroblastoma cells, where the expression of MYB declined during retinoic-acid induced maturation [30]. Moreover, it was recently shown that MYCN overexpressing neuroblastoma cells are strongly dependent on high MYB levels to sustain their proliferative state. Upon MYB knock down, MYCN overexpressing cells displayed massive apoptosis, while non-MYCN overexpressing cells were unaffected [24]. Previously, MYBL2 (alias B-MYB), a MYB family member, was shown to be necessary for proliferation of neuroblastoma cells with MYCN amplification [31]. In addition, the same study showed that MYBL2 and MYCN act in a reciprocal regulatory loop, enhancing each others expression levels and maintaining the proliferative state of aggressive neuroblastoma cells. Here, we showed that MYCN induces the expression of MYB in the SHEP-Tet21N model system, which explains increasing MYB expression levels

during neuroblastoma development in the TH-MYCN mouse model. Both the addiction of MYCN overexpressing cells to MYB, and the involvement of MYB in the maintenance of proliferative state of neuroblastoma cells, are in keeping with our identification of MYB as an master regulator of MYCN-driven neuroblastoma development, and support the validity of our approach.

E2F2 belongs to a family of cell-cycle regulated transcription factors that stimulate proliferation. The activating members of the E2F family – E2F-1, E2F-2, and E2F-3 – regulate MYCN transcription and are required for full activity of the MYCN promoter in neuroblastoma cells [32]. In addition, E2F2 and its family member E2F3 are required for MYC to induce S phase in quiescent fibroblasts [33]. Finally, MYC in turn was shown to induce transcription of the activating members of the E2F family, E2F-1, E2F-2, and E2F-3 [33], forming yet another positive feedback loop between MYCN and an inferred master regulator of MYCN-driven neuroblastoma development.

Finally, also for the two remaining inferred master regulators, MXD3 and EZH2, evidence exists for a contributing role to neuroblastoma development. EZH2, a histone–lysine methyltransferase, is the enzymatically active component of the Polycomb Repressor Complex 2 (PRC2) that catalyzes the addition of methyl groups to histone 3 at lysine 27 (H3K27me2/me3), a well-known histone mark associated with gene silencing. In line with our identification of EZH2 as master regulator of neuroblastoma development, high EZH2 expression levels have been associated with poor outcome of neuroblastoma patients [34]. Moreover, silencing of EZH2 inhibited neuroblastoma cell growth and induced neuronal differentiation in KCNR cells [34]. In the same study, EZH2 was found to silence a number of tumor suppressors which control differentiation in neuroblastoma, such as CLU, RUNX3, and NGFR [34]. Notably, in our study, we identified EZH2 as an master regulator of genes activated – rather than repressed – during neuroblastoma development. Indeed, apart from the canonical role of EZH2 as a transcriptional repressor, recent literature reports highlight its less-known function as a transcriptional activator (reviewed in [35]). In castration resistant prostate cancer cells, AKT1 mediated phosphorylation of EZH2 allows EZH2 to methylate the transcriptional activator AR (androgen receptor) and interact with it to induce gene expression [36]. In breast cancer cells, EZH2 has been reported to induce gene transcription in two different ways depending on the ESR1 (estrogen receptor) status. In ESR1-positive breast cancer cells, EZH2 acts as a bridge to physically link ESR1 and Wnt signaling components CTNNB1 (β-catenin) and LEF1, on the CCNB1 (cyclin B1) and MYC promoters [37]. EZH2 further also interacts with Mediator complex and induces transcription by its interaction with RNA polymerase II. In ESR1-negative breast cancer cells, EZH2 forms a ternary complex with NF-κB components RELA and RELB and activates transcription of NF-

κB target genes such as TNF and IL6 [38]. Although EZH2 has been reported to silence the expression of a number of genes in neuroblastoma cells, it is not unlikely that in addition to is repressor activity, EZH2 can also act as a transcriptional activator in neuroblastoma. In order to gain insight in the mode of action of EZH2 in neuroblastoma cells, additional experiments are required, at least including whole-transcriptome gene expression profiling upon EZH2 perturbation.

MXD3 is a member of the MYC/MAX/MAD superfamily of basic helix-loop-helix leucine zipper transcriptional regulators to which MYCN also belongs. Both MYC (MYC, MYCN, MYCL) and MAD (MXD1, MXI1, MXD3, MXD4) proteins form heterodimers with the cofactor MAX thereby permitting binding to specific DNA sequences known as E-boxes in target gene promoters [39]. These MYC/MAX or MAD/MAX DNA-bound heterodimers respectively recruit coactivator or corepressor complexes that generate alterations in chromatin structure and transcriptional activity [39]. Members of the MAD family have been shown to induce cell cycle arrest, inhibit proliferation and promote differentiation in cell lines and in transgenic mice [40]. Together, these and other studies have led to the "switch" model in which MAD/MAX complexes antagonize MYC/MAX complexes to regulate the transition between proliferation and differentiation [41,42]. Several reports, however, suggest that MXD3 is an atypical member of the MAD family. Mice with a targeted deletion of Mxd3 showed a mild phenotype consisting of increased sensitivity to apoptosis in response to DNA damage [43]. In the developing mouse embryo, *Mxd3* is only expressed during the S-phase of the cell cycle while the remaining *Mad* genes are expressed in postmitotic cells [44]. Moreover, MXD3 appears to be an important regulator of Shh-dependent GNP proliferation and MYCN expression, an unexpected role for a MAD family member [45]. Finally, MXD3 is expressed in medulloblastoma cells, where, intriguingly, sustained high levels of the protein negatively influence proliferation by the induction of programmed cell death [46]. These observations are in line with our identification of MXD3 as a master regulator of neuroblastoma development and warrant the further exploration of MXD3 in the context of neuroblastoma.

Notably, MYCN itself was not inferred as an master regulator of the defined neuroblastoma development signatures, although these signatures have been established through analysis of a MYCN-driven neuroblastoma mouse model. We believe it is not unlikely that the large group of MYCN target genes, involved in the execution of MYCN's pleiotropic functions, is distributed across different neuroblastoma development signatures, each of which encompassing a subgroup of MYCN target genes involved in distinct MYCN functions. This would indeed result in a lack of overrepresentation of MYCN target genes in one particular neuroblastoma development signature, as observed in our study.

Thus, our approach unraveled for the first time a unique network of master regulators offering the basis for further research to explore novel approaches to drug the MYCN governed oncogenic regulatory network in neuroblastoma. Cumulatively, our findings suggest that co-expression of PLAGL2 and MYB or E2F2 in neuroblastoma leads to co-regulation of transcriptional programs, which ultimately contributes to neuroblastoma development. Although our findings need wet-lab confirmation, we speculate that therapeutic targeting of these synergistic master regulator pairs will contribute to the regression of MYCN-driven neuroblastoma tumors. However, because transcription factors mediate their action largely through protein-protein and protein-DNA interactions rather than enzymatic activities, they have been traditionally been regarded as undruggable targets. Another challenge of inhibiting transcription factors is their predominant nuclear localization, which makes them less accessible to therapeutic agents. Despite these obstacles, there have been numerous advances in the development of both pharmacologic agents and delivery strategies to specifically target cancer cells [47]. Potential strategies include inhibition of expression via RNA interference or perturbation of regulator microRNAs, targeting protein maturation and stability, interference of protein-protein or protein-DNA interactions by oligonucleotide decoys, and altering the chromatin accessibility via, for example, bromodomain inhibitors [47].

Materials and methods

TH-MYCN neuroblastoma progression model

TH-MYCN+/+ mice [16] were sacrificed at day seven (n = 4) and day fourteen (n = 4) of life to harvest sympathetic ganglia containing foci of neuroblast hyperplasia, and at week 6 of life to harvest advanced neuroblastoma tumors (n = 4). Additionally, we have dissected the same sympathetic ganglia from TH-MYCN-/- mice at day seven (n = 4), day fourteen (n = 4) and week 6 (n = 4) of life to control for miRNA expression changes during normal development. Murine total RNA was isolated using the miRNeasy Mini Kit (Qiagen, 217004) according to the manufacturer's instructions. The samples were profiled on Agilent SurePrint G3 Gene Expression Microarrays according to the manufacturer's protocol. Data were summarized and normalized with the vsn method [48], in the R statistical programming language using the *limma* package. Probes with a log2 expression of less than 4 in more than 20/24 samples were considered not expressed and filtered out. Additionally, for each unique gene symbol, only the probe with the most significant differential expression between TH-MYCN+/+ and TH-MYCN-/- samples (two-way ANOVA, p-value of interaction term) was

retained for further analysis. Microarray profiling results for all samples are available in the ArrayExpress database (www.ebi.ac.uk/arrayexpress) under accession number E-MTAB-3247. Furthermore, the processed data can be visualized via the R2 microarray analysis and visualization platform (http://r2.amc.nl) under experiment "Exp Nb Hyperplasia TH-MYCN - Ghent - 28 - custom - agmge8x60".

Delineation of murine neuroblastoma development signatures

Murine gene expression profiles were clustered using SOM. To this end, per gene, the average group expression was calculated for each of the six sample groups: WT.1week, WT.2weeks, WT.6weeks, TG.1week, TG.2weeks and TG.6weeks (WT = TH-MYCN-/-; TG = TH-MYCN+/+). With the resulting dataset containing average gene expression of 17185 genes in 6 groups, SOM analysis was performed with a 3x4 rectangular grid. Subsequently, a value representing the differential gene expression in TH-MYCN+/+ and TH-MYCN-/- samples over time, was assigned to each gene in each cluster. To this end, for each gene, a two-way ANOVA assessing the interaction between the genotype and the age of the mice, was performed. Subsequently, the resulting p-value and estimate of the interaction term were combined into one π-value per gene as follows: $\pi = - \log_{10}(P) \times \text{estimate}$. While performing 100 iterations of the described SOM analysis, a new random seed was set prior to each analysis to ensure random iterations. Randomness was verified by visual inspection of the profiles of the 100 x 12 SOM clusters. Gene signatures with a significant differential gene signature score during murine neuroblastoma development were retained for further analysis. gene signature scores were calculated as described elsewhere [19] and two-way ANOVA was applied to assess the interaction between the genotype and the age.

Human neuroblastoma expression dataset

In total, 200 primary tumor samples of neuroblastoma patients were collected prior to therapy at the Ghent University Hospital (Ghent, Belgium), the University Children's Hospital Essen (Essen, Germany), the Hospital Clínico Universitario (Valencia, Spain), the Academic Medical Center (University of Amsterdam, Netherlands) and the National Children's Research Centre (Dublin, Ireland). Informed consent was obtained from the patients' relatives. Total RNA was isolated using the miRNeasy Mini Kit (Qiagen, 217004) according to the manufacturer's instructions. The samples were profiled on Affymetrix Human Exon 1.0 ST Microarrays according to the manufacturer's protocol. Exon level expression was recovered using Affymetrix power tools 1.10.0. Expression data from 113 samples is available at the Gene Expression Omnibus (http://www.ncbi.nlm.nih.gov/geo; Accession Numbers GSE32664 & GSE21713).

Assembly of a human neuroblastoma-specific interactome

The human neuroblastoma-specific interactome was assembled by analyzing the aforementioned human neuroblastoma expression dataset with the ARACNe algorithm [49], which is available in geWorkbench v2.5.1. A custom list of HUB markers was provided to the algorithm. To this end, a total of 718 well-characterized sequence-specific TFs were retrieved from Vaquerizas et al. [50], of which 601 were expressed in the aforementioned human neuroblastoma expression dataset. In addition, the following parameters were used: Mode = "Complete", Algorithm = "Adaptive Partitioning", Threshold Type = "P-Value 0.01, Corrected by # of Markers", DPI Tolerance = "Do Not Apply", Bootstrap Number = 1.

Master Regulator Analysis

Master regulator analysis was performed using the MARINa algorithm [13,14] available as an R script from bioconductor in the VIPER package [51]. The default parameters were applied. Upon master regulator analysis, shadow analysis was performed on significantly enriched master regulators to correct for regulon overlap, a frequent event in mammalian networks [13,52] leading to false-positive master regulator inference. Indeed, if the regulons of an master regulator and of a non-master regulator gene overlapped significantly, then the latter would also be enriched in the tested gene signature, yielding a false positive master regulator. These regulators – shadow regulators – can be identified and removed by determining whether their enrichment is significantly reduced when shared targets are disregarded. Finally, synergism analysis was performed on true master regulators (further referred to as master regulator), not being a shadow of any other master regulator. Shadow and synergism analysis are described in detail elsewhere [14] and are available as an R script in the VIPER package [51].

Acknowledgments

We would like to thank Fanny De Vloed for excellent technical support and Mariano Alvarez for help with the MARINa analyses. Further, we would like to thank the Ghent University Hospital (Ghent, Belgium), the University Children's Hospital Essen (Essen, Germany) and the Hospital Clínico Universitario (Valencia, Spain) for collection of primary tumor samples.

Funding: This work was supported by the GOA (grant number 01G01910), by research grants from the European Union (FP7-ASSET project), the Belgian Foundation against Cancer (Stichting Tegen Kanker) [SCIE 2010-177] and the Fund for Scientific Research Flanders (FWO) to F.S. [G.0530.12N], and by research grants from the Belgian Childhood Cancer Fund (vzw Kinderkankerfonds); by a PhD grant from the Agency for Innovation by Science and Technology (IWT) to A.B. [IWT 101506] and a post-doc grant of the FWO to K.D.P. This work was further supported by Program Grants from the NHMRC Australia, the Cancer Institute NSW and the Cancer Council NSW to D.C., B.C. and G.M..

References

1. Louis CU, Shohet JM. Neuroblastoma: Molecular Pathogenesis and Therapy. Annu Rev Med. 2015 Jan 14;66(1):49–63.
2. Chen Y, Takita J, Choi YL, Kato M, Ohira M, Sanada M, et al. Oncogenic mutations of ALK kinase in neuroblastoma. Nature [Internet]. 2008 Oct 16;455(7215):971–4. Available from: http://www.nature.com.ezp-prod1.hul.harvard.edu/nature/journal/v455/n7215/pdf/nature07399.pdf
3. Janoueix-Lerosey I, Lequin D, Brugières L, Ribeiro A, de Pontual L, Combaret V, et al. Somatic and germline activating mutations of the ALK kinase receptor in neuroblastoma. Nature. 2008 Oct 16;455(7215):967–70.
4. Mossé YP, Laudenslager M, Longo L, Cole KA, Wood A, Attiyeh EF, et al. Identification of ALK as a major familial neuroblastoma predisposition gene. Nature. 2008 Aug 24;455(7215):930–5.
5. George RE, Sanda T, Hanna M, Fröhling S, II WL, Zhang J, et al. Activating mutations in ALK provide a therapeutic target in neuroblastoma. Nature. 2008 Oct 16;455(7215):975–8.
6. Molenaar JJ, Domingo-Fernández R, Ebus ME, Lindner S, Koster J, Drabek K, et al. LIN28B induces neuroblastoma and enhances MYCN levels via let-7 suppression. Nat Genet. 2012 Oct 7;44(11):1199–206.
7. Berry T, Luther W, Bhatnagar N, Jamin Y, Poon E, Sanda T, et al. The ALK(F1174L) Mutation Potentiates the Oncogenic Activity of MYCN in Neuroblastoma. Cancer Cell. 2012 Jul 10;22(1):117–30.
8. Carpenter EL, Haglund EA, Mace EM, Deng D, Martinez D, Wood AC, et al. Antibody targeting of anaplastic lymphoma kinase induces cytotoxicity of human neuroblastoma. Oncogene. 2012 Nov 15;31(46):4859–67.
9. Mossé YP, Lim MS, Voss SD, Wilner K, Ruffner K, Laliberte J, et al. Safety and activity of crizotinib for paediatric patients with refractory solid tumours or anaplastic large-cell lymphoma: a Children's Oncology Group phase 1 consortium study. Lancet Oncology. 2013 May;14(6):472–80.
10. Puissant A, Frumm SM, Alexe G, Bassil CF, Qi J, Chanthery YH, et al. Targeting MYCN in neuroblastoma by BET bromodomain inhibition. Cancer Discov. 2013 Mar;3(3):308–23.
11. Pall G. The next-generation ALK inhibitors. Curr Opin Oncol. 2015 Mar;27(2):118–24.
12. Huang M, Weiss WA. Neuroblastoma and MYCN. Cold Spring Harb Perspect Med. Cold Spring Harbor Laboratory Press; 2013 Oct;3(10):a014415–5.
13. Carro MS, Lim WK, Alvarez MJ, Bollo RJ, Zhao X, Snyder EY, et al. The transcriptional network for mesenchymal transformation of brain tumours. Nature. 2010 Jan 21;463(7279):318–25.
14. Lefebvre C, Rajbhandari P, Alvarez MJ, Bandaru P, Lim WK, Sato M, et al. A human B-cell interactome identifies MYB and FOXM1 as master regulators of proliferation in germinal centers. Mol Syst Biol. 2010 Jun 8;6:377.
15. Chan SS-K, Kyba M. What is a Master Regulator? J Stem Cell Res Ther. 2013 May 4;3(02).
16. Weiss WA, Aldape K, Mohapatra G, Feuerstein BG, Bishop JM. Targeted expression of MYCN causes neuroblastoma in transgenic mice. EMBO J. 1997 Jun 2;16(11):2985–95.
17. Hansford LM, Thomas WD, Keating JM, Burkhart CA, Peaston AE, Norris MD, et al. Mechanisms of embryonal tumor initiation: distinct roles for MycN expression and MYCN amplification. Proc Natl Acad Sci U S A. 2004 Aug 24;101(34):12664–9.
18. Westermann F, Muth D, Benner A, Bauer T, Henrich K-O, Oberthuer A, et al. Distinct transcriptional MYCN/c-MYC activities are associated with spontaneous regression or malignant progression in neuroblastomas. Genome Biology. BioMed Central Ltd; 2008;9(10):R150.
19. Fredlund E, Ringnér M, Maris JM, Påhlman S. High Myc pathway activity and low stage of neuronal differentiation associate with poor outcome in neuroblastoma. Proc Natl Acad Sci U S A. National Acad Sciences; 2008 Sep 16;105(37):14094–9.
20. Althoff K, Beckers A, Bell E, Nortmeyer M, Thor T, Sprüssel A, et al. A Cre-conditional MYCN-driven neuroblastoma mouse model as an improved tool for preclinical studies. Oncogene. 2014 Sep 1.
21. Chen L, Iraci N, Gherardi S, Gamble LD, Wood KM, Perini G, et al. p53 is a direct transcriptional target of MYCN in neuroblastoma. Cancer Res. American Association for Cancer Research; 2010 Feb 15;70(4):1377–88.
22. Lutz W, Stöhr M, Schürmann J, Wenzel A, Löhr A, Schwab M. Conditional expression of N-

myc in human neuroblastoma cells increases expression of alpha-prothymosin and ornithine decarboxylase and accelerates progression into S-phase early after mitogenic stimulation of quiescent cells. Oncogene. 1996 Aug 15;13(4):803–12.
23. Bell E, Premkumar R, Carr J, Lu X, Lovat PE, Kees UR, et al. The role of MYCN in the failure of MYCN amplified neuroblastoma cell lines to G1 arrest after DNA damage. Cell Cycle. 2006 Nov;5(22):2639–47.
24. Chayka O, D'Acunto CW, Middleton O, Arab M, Sala A. Identification and pharmacological inactivation of the MYCN gene network as a therapeutic strategy for neuroblastic tumor cells. J Biol Chem. 2015 Jan 23;290(4):2198–212.
25. Landrette SF, Kuo Y-H, Hensen K, Barjesteh van Waalwijk van Doorn-Khosrovani S, Perrat PN, Van de Ven WJM, et al. Plag1 and Plagl2 are oncogenes that induce acute myeloid leukemia in cooperation with Cbfb-MYH11. Blood. 2005 Apr 1;105(7):2900–7.
26. Zheng H, Ying H, Wiedemeyer R, Yan H, Quayle SN, Ivanova EV, et al. PLAGL2 regulates Wnt signaling to impede differentiation in neural stem cells and gliomas. Cancer Cell. 2010 May 18;17(5):497–509.
27. Mizutani A, Furukawa T, Adachi Y, Ikehara S, Taketani S. A zinc-finger protein, PLAGL2, induces the expression of a proapoptotic protein Nip3, leading to cellular apoptosis. J Biol Chem. 2002 May 3;277(18):15851–8.
28. Aytes A, Mitrofanova A, Lefebvre C, Alvarez MJ, Castillo-Martin M, Zheng T, et al. Cross-species regulatory network analysis identifies a synergistic interaction between FOXM1 and CENPF that drives prostate cancer malignancy. Cancer Cell. 2014 May 12;25(5):638–51.
29. Ramsay RG, Gonda TJ. MYB function in normal and cancer cells. Nat Rev Cancer. 2008 Jul;8(7):523–34.
30. Thiele CJ, Cohen PS, Israel MA. Regulation of c-myb expression in human neuroblastoma cells during retinoic acid-induced differentiation. Mol Cell Biol. American Society for Microbiology; 1988 Apr;8(4):1677–83.
31. Gualdrini F, Corvetta D, Cantilena S, Chayka O, Tanno B, Raschellà G, et al. Addiction of MYCN amplified tumours to B-MYB underscores a reciprocal regulatory loop. Oncotarget. 2010 Aug;1(4):278–88.
32. Strieder V, Lutz W. E2F proteins regulate MYCN expression in neuroblastomas. J Biol Chem. 2003 Jan 31;278(5):2983–9.
33. Leone G, Sears R, Huang E, Rempel R, Nuckolls F, Park C-H, et al. Myc requires distinct E2F activities to induce S phase and apoptosis. Mol Cell. 2001 Jul;8(1):105–13.
34. Wang C, Liu Z, Woo C-W, Li Z, Wang L, Wei JS, et al. EZH2 Mediates epigenetic silencing of neuroblastoma suppressor genes CASZ1, CLU, RUNX3, and NGFR. Cancer Res. American Association for Cancer Research; 2012 Jan 1;72(1):315–24.
35. Deb G, Singh AK, Gupta S. EZH2: not EZHY (easy) to deal. Mol Cancer Res. American Association for Cancer Research; 2014 May;12(5):639–53.
36. Xu K, Wu ZJ, Groner AC, He HH, Cai C, Lis RT, et al. EZH2 oncogenic activity in castration-resistant prostate cancer cells is Polycomb-independent. Science. 2012 Dec 14;338(6113):1465–9.
37. Shi B, Liang J, Yang X, Wang Y, Zhao Y, Wu H, et al. Integration of estrogen and Wnt signaling circuits by the polycomb group protein EZH2 in breast cancer cells. Mol Cell Biol. 2007 Jul;27(14):5105–19.
38. Lee ST, Li Z, Wu Z, Aau M, Guan P, Karuturi RKM, et al. Context-specific regulation of NF-κB target gene expression by EZH2 in breast cancers. Mol Cell. 2011 Sep 2;43(5):798–810.
39. Grandori C, Cowley SM, James LP, Eisenman RN. The Myc/Max/Mad network and the transcriptional control of cell behavior. Annu Rev Cell Dev Biol. 2000;16(1):653–99.
40. Ayer DE, Kretzner L, Eisenman RN. Mad: a heterodimeric partner for Max that antagonizes Myc transcriptional activity. Cell. 1993 Jan 29;72(2):211–22.
41. Rottmann S, Luscher B. The Mad side of the Max network: antagonizing the function of Myc and more. Curr Top Microbiol Immunol. 2006;302:63–122.
42. Barisone GA, Yun J-S, Díaz E. From cerebellar proliferation to tumorigenesis: new insights into the role of Mad3. Cell Cycle. 2008 Feb 15;7(4):423–7.
43. Quéva C, McArthur GA, Iritani BM, Eisenman RN. Targeted deletion of the S-phase-specific Myc antagonist Mad3 sensitizes neuronal and lymphoid cells to radiation-induced apoptosis. Mol Cell Biol. American Society for Microbiology; 2001 Feb;21(3):703–12.
44. Fox EJ, Wright SC. S-phase-specific expression of the Mad3 gene in proliferating and differentiating cells. Biochem J. 2001 Oct 15;359(Pt 2):361–7.
45. Yun J-S, Rust JM, Ishimaru T, Díaz E. A novel role of the Mad family member Mad3 in

cerebellar granule neuron precursor proliferation. Mol Cell Biol. 2007 Dec;27(23):8178–89.
46. Barisone GA, Ngo T, Tran M, Cortes D, Shahi MH, Nguyen T-V, et al. Role of MXD3 in Proliferation of DAOY Human Medulloblastoma Cells. Katoh M, editor. PLoS ONE. Public Library of Science; 2012 Jul 10;7(7):e38508.
47. Yeh JE, Toniolo PA, Frank DA. Targeting transcription factors: promising new strategies for cancer therapy. Curr Opin Oncol. 2013 Nov;25(6):652–8.
48. Wu Z, Irizarry RA, Gentleman R, Martinez-Murillo F, Spencer F. A model-based background adjustment for oligonucleotide expression arrays. J Am Stat Assoc. Taylor & Francis; 2004;99(468):909–17.
49. Margolin AA, Nemenman I, Basso K, Wiggins C, Stolovitzky G, Dalla-Favera R, et al. ARACNE: an algorithm for the reconstruction of gene regulatory networks in a mammalian cellular context. BMC Bioinformatics. BioMed Central Ltd; 2006;7 Suppl 1(Suppl 1):S7.
50. Vaquerizas JM, Kummerfeld SK, Teichmann SA, Luscombe NM. A census of human transcription factors: function, expression and evolution. Nat Rev Genet. 2009 Apr;10(4):252–63.
51. Alvarez MJ. viper: Virtual Inference of Protein-activity by Enriched Regulon analysis. 1st ed. 2013.
52. Margolin AA, Palomero T, Sumazin P, Califano A, Ferrando AA, Stolovitzky G. ChIP-on-chip significance analysis reveals large-scale binding and regulation by human transcription factor oncogenes. Proc Natl Acad Sci U S A. National Acad Sciences; 2009 Jan 6;106(1):244–9.

Supplements

Supplementary Tables

The supplementary tables of this manuscript are accessible through the following URL: https://goo.gl/OfGd8K

Supplementary figures

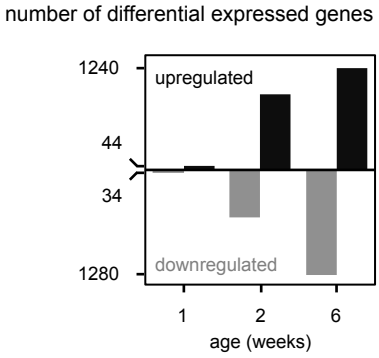

Supplementary Figure 3.1. The number of significantly upregulated (black) and downregulated (gray) genes in TH-MYCN+/+ samples versus TH-MYCN-/- samples per time point. Rank Product analysis

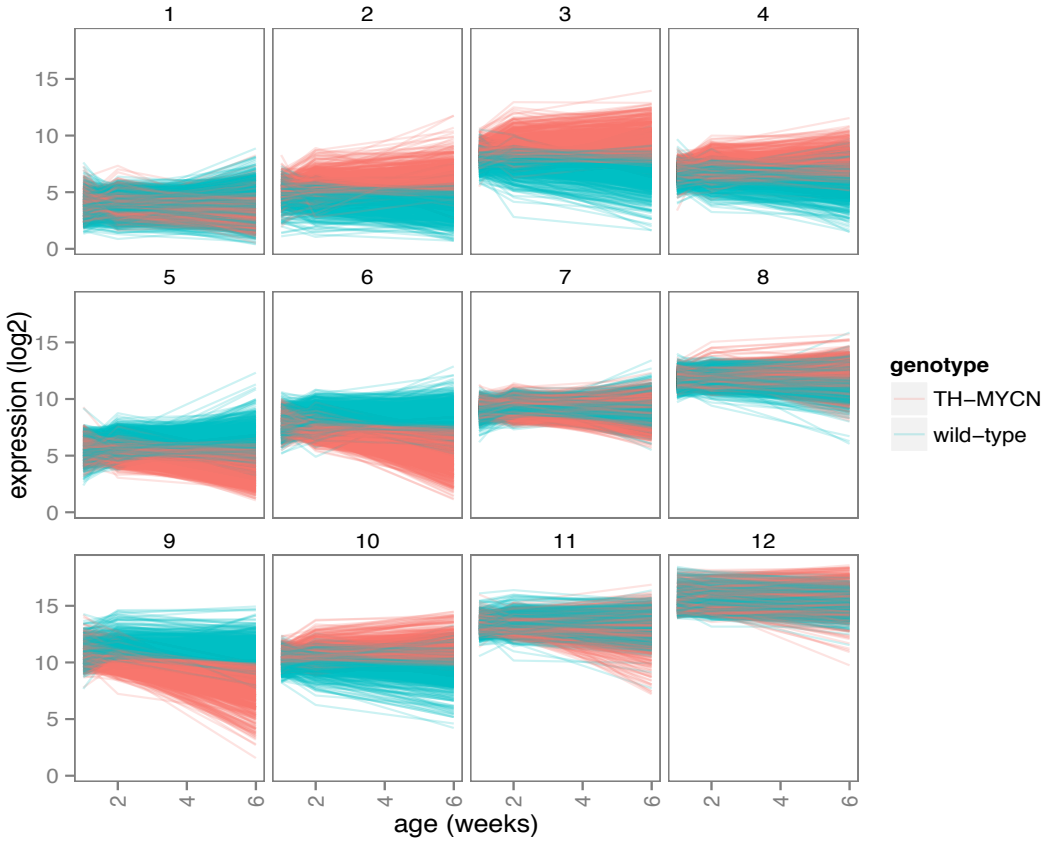

Supplementary Figure 3.2. Representative example of clustering of genes in the hyperplasia dataset in 12 distinct gene signatures according to similar gene expression patterns using Self-Organizing Maps (SOM). Green and red lines represent gene expression in TH-MYCN-/- and TH-MYCN +/+ mice samples respectively., in function of age.

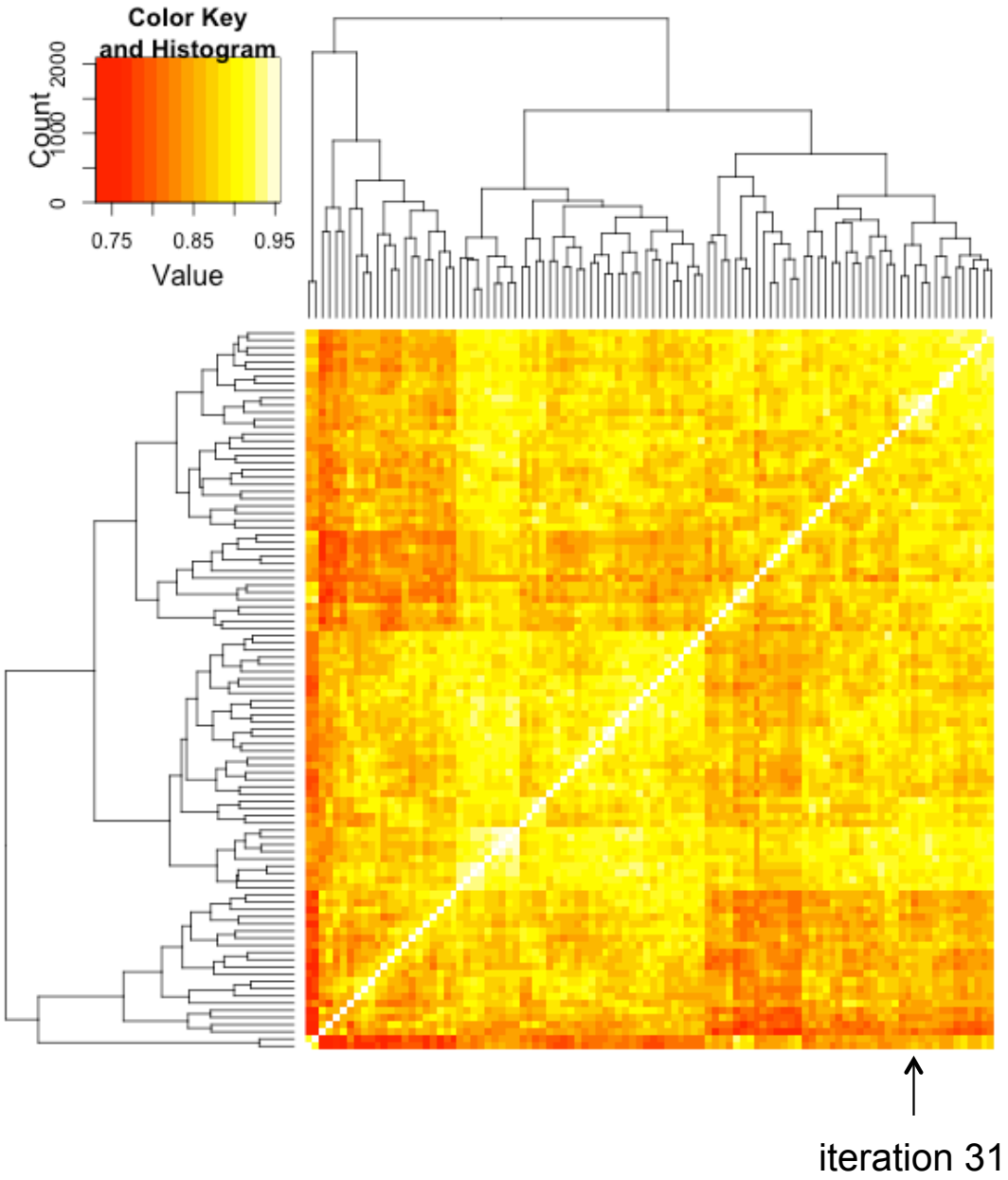

Supplementary Figure 3.3. Comparison of 100 SOM analyses clustering the hyperplasia gene expression data set. The heatmap represent the average Jacquard score (between 0 and 1) for each pairwise comparison of the 12 clusters in the 100 iterations. Iteration 31, which considered to be a representative iteration, is highlighted with a black arrow.

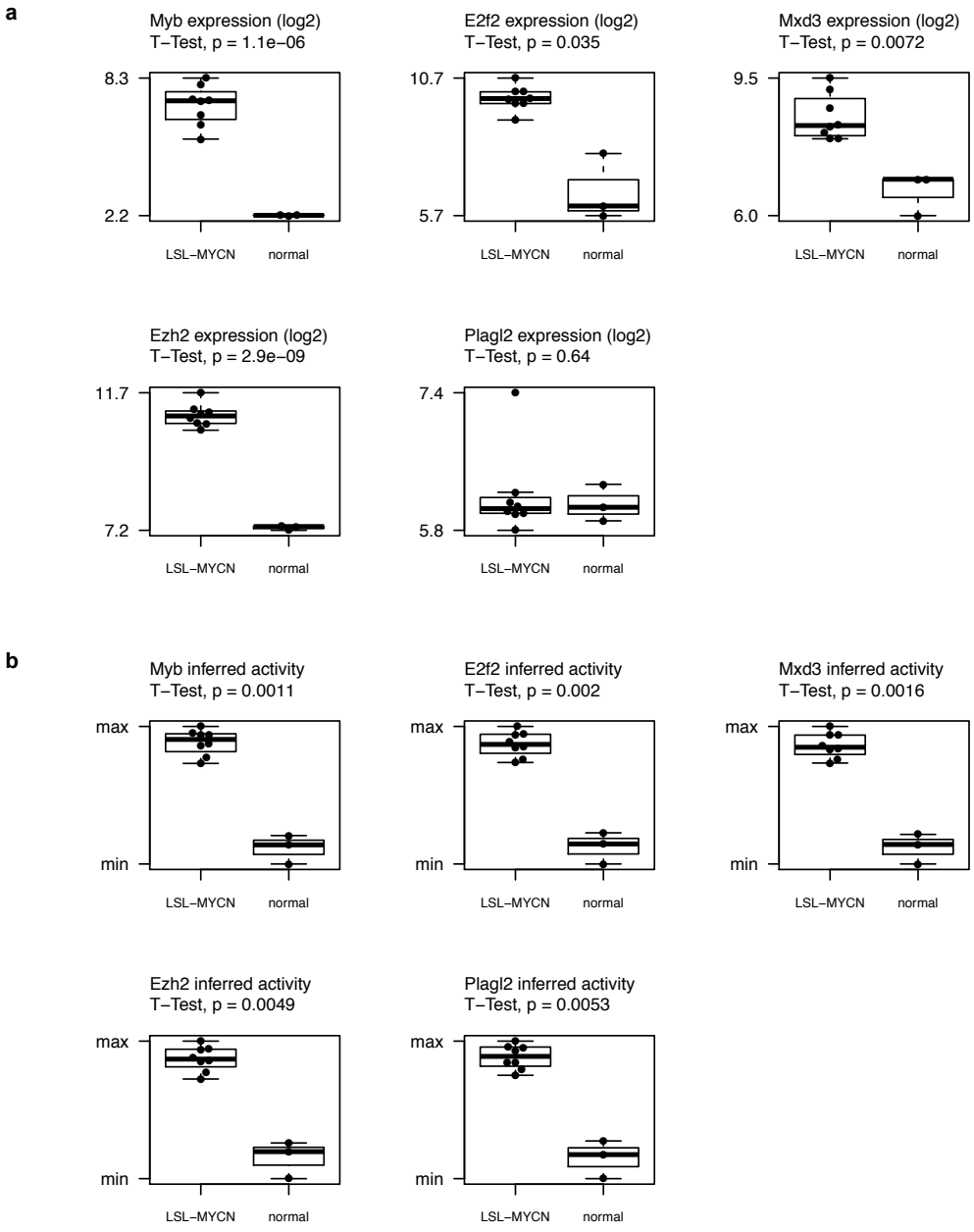

Supplementary Figure 3.4. MR mRNA expression **(a)** and ARACNe-inferred transcriptional MR activity **(b)** in the LSL-MYCN;Dbh-iCre mouse model.

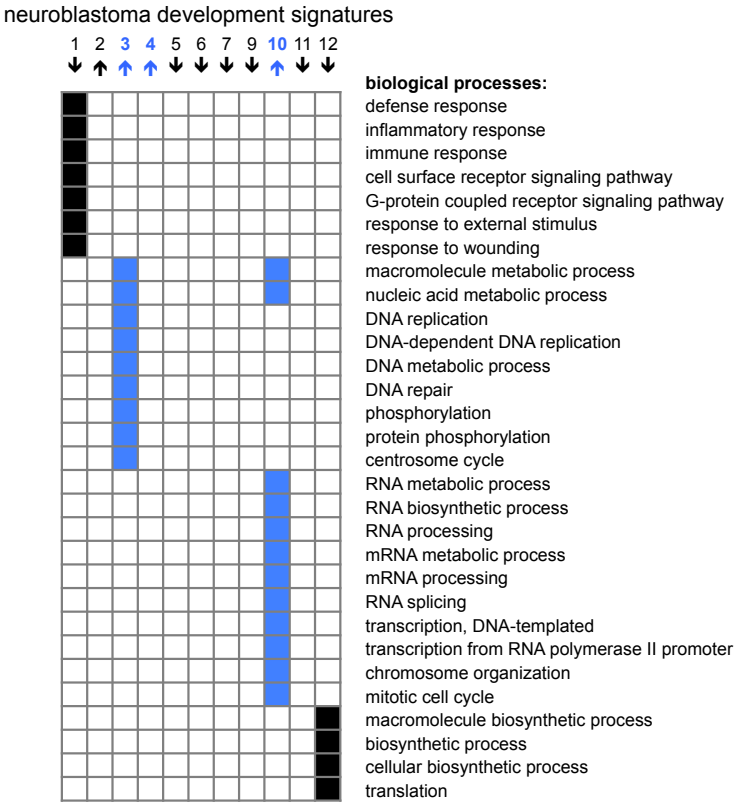

Supplementary Figure 3.5. Overview of enriched biological processes in the 12 distinct neuroblastoma development gene signatures from iteration 31. Blue and black squares represent significant enrichment of the GO term (right), in the respective gene signature (top). For three genes signature (blue) independent MRs could be inferred.

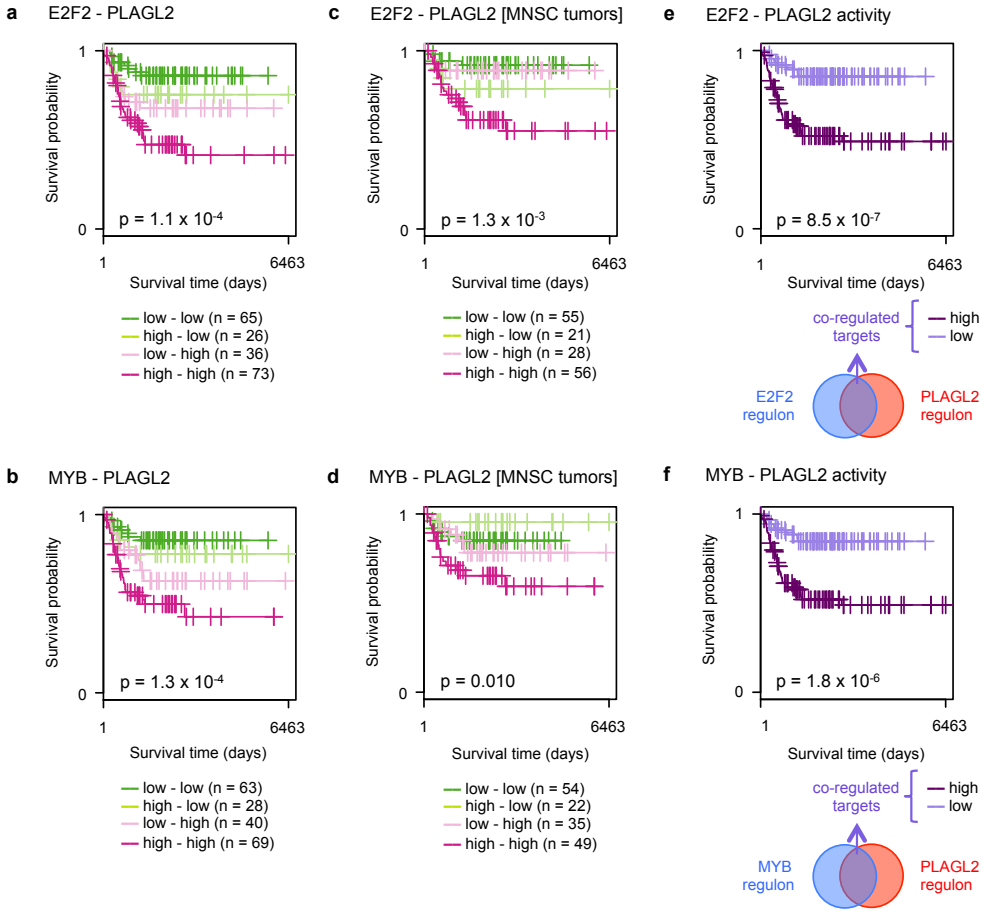

Supplementary Figure 3.6. Co-alterations of synergistic MR pairs are significantly associated with clinical outcome in neuroblastoma patients. **(a)** Kaplan–Meier curves of overall survival in patients with high E2F2 expression, high PLAGL2 expression or both (two-sided log rank test). **(b)** Kaplan–Meier curves of overall survival in patients with high MYB expression, high PLAGL2 expression or both (two-sided log rank test). **(c)** Kaplan–Meier curves of overall survival in patients without MYCN amplification (MNSC), with high E2F2 expression, high PLAGL2 expression or both (two-sided log rank test). **(d)** Kaplan–Meier curves of overall survival in patients without MYCN amplification (MNSC), with high MYB expression, high PLAGL2 expression or both (two-sided log rank test). **(e)** Kaplan–Meier curves of overall survival in patients with high or low E2F2 - PLAGL2 activity as measured by a signature score of the genes co-regulated by E2F2 and PLAGL2 (two-sided log rank test). **(f)** Kaplan–Meier curves of overall survival in patients with high or low MYB - PLAGL2 activity as measured by a signature score of the genes co-regulated by MYB and PLAGL2 (two-sided log rank test).

Chapter 4

MYCN-targeting miRNAs are predominantly downregulated during MYCN-driven neuroblastoma tumor formation

Anneleen Beckers*[1], Gert Van Peer*[1], Daniel R Carter[2], Evelien Mets[1], Kristina Althoff[3,4], Belamy B Cheung[2], Johannes H Schulte[3-6], Pieter Mestdagh[1], Jo Vandesompele[1], Glenn M Marshall[2,7], Katleen De Preter[1] and Frank Speleman[1]

[1] Center for Medical Genetics (CMGG), Ghent University, Ghent, Belgium;
[2] Children's Cancer Institute, University of New South Wales, Sydney, Australia;
[3] Department of Pediatric Oncology and Hematology, University Children's Hospital Essen, Essen, Germany;
[4] German Cancer Consortium (DKTK), Germany;
[5] German Cancer Research Center (DKFZ), Heidelberg, Germany;
[6] Translational Neuro-Oncology, West German Cancer Center, University Hospital Essen, University Duisburg-Essen, Essen, Germany;
[7] Kids Cancer Centre, Sydney Children's Hospital, Sydney, Australia.
** These authors contributed equally to this work*

Oncotarget 2014 Sep 16; [Epub ahead of print]

Abstract

MYCN is a transcription factor that plays key roles in both normal development and cancer. In neuroblastoma, MYCN acts as a major oncogenic driver through pleiotropic effects controlled by multiple protein encoding genes as well as microRNAs (miRNAs). MYCN activity is tightly controlled at the level of transcription and protein stability through various mechanisms. Like most genes, MYCN is further controlled by miRNAs, but the full complement of all miRNAs implicated in this process has not been determined through an unbiased approach. To elucidate the role of miRNAs in regulation of MYCN, we thus explored the MYCN-miRNA interactome to establish miRNAs controlling MYCN expression levels. We combined results from an unbiased and genome-wide high-throughput miRNA target reporter screen with miRNA and mRNA expression data from patients and a murine neuroblastoma progression model. We identified 29 miRNAs targeting MYCN, of which 12 miRNAs are inversely correlated with MYCN expression or activity in neuroblastoma tumor tissue. The majority of MYCN-targeting miRNAs in neuroblastoma showed a decrease in expression during murine MYCN-driven neuroblastoma tumor development. Therefore, we provide evidence that MYCN-targeting miRNAs are preferentially downregulated in MYCN-driven neuroblastoma, suggesting that MYCN negatively controls the expression of these miRNAs, to safeguard its expression.

Introduction

MYCN acts as a major driver oncogene in neuroblastoma, a pediatric tumor of the sympathetic nervous system. Genomic amplification of this gene occurs in about half of all high-stage neuroblastoma tumors and has been associated with poor survival. As such, MYCN amplification has been used as one of the first biomarkers for therapeutic decision-making.

MYC proto-oncogenes (MYC, MYCN, MYCL) are transcription factors that play key roles in both normal development and cancer. The MYC proteins act as direct amplifiers of transcriptionally active genes through sequence-specific binding to consensus E-box DNA binding sites [1-3]. In addition, MYC proteins can also silence genes, by a mechanism that is uncoupled from E-box binding and dependent upon initiator elements in the basal promoter region [1,4]. Apart from the broad impact on transcriptional regulation of protein coding genes, MYCN has also been shown to tightly control the expression of many microRNAs (miRNAs) [1,5].

Numerous signal transduction pathways and regulatory mechanisms keep the expression of MYC family members under tight control. This regulation occurs at multiple levels, including gene transcription, messenger RNA (mRNA) turnover, and protein activity and stability [1-3]. miRNAs have also been shown to contribute to the regulation of MYC expression [2,3]. miRNAs are involved in the regulation of virtually all signaling circuits within a cell, and their dysregulation has been shown to play an essential role in the development and progression of cancer [6,7]. This class of small non-coding RNA molecules typically inhibits the translation and stability of mRNA molecules and thus eventually controls protein levels.

In previous studies, individual miRNAs targeting MYCN have been identified, using miRNA target reporter assays to confirm predicted miRNA target sites in the 3' untranslated region (3'UTR) of MYCN [3,8]. Eleven MYCN-targeting miRNAs have thus been identified, of which miR-34a, miR-101, let-7e and miR-202 were shown to affect neuroblastoma proliferation in vitro [3,8]. Although the applied approach is valuable, it is biased towards canonical miRNA-mRNA interactions, identified by available prediction algorithms.

Here, we performed a comprehensive, genome-wide exploration of the miRNA-MYCN interactome in neuroblastoma. We combined results from an unbiased and genome-wide high-throughput miRNA target reporter screen with miRNA and mRNA expression data from patients and identified 12 MYCN-targeting miRNAs in neuroblastoma tumor tissue. Subsequently, the dynamic regulation of MYCN-targeting miRNAs during neuroblastoma development was evaluated in a murine neuroblastoma progression model. We provide evidence that MYCN targeting miRNAs are preferentially downregulated in MYCN-driven

neuroblastoma tumors, suggesting that MYCN negatively controls the expression of these miRNAs, and as such safeguards its own expression. Hence, our findings further clarify the role of miRNAs in the regulation of MYCN in neuroblastoma and describe a negative feedback loop from MYCN to its targeting miRNAs.

Results

An unbiased MYCN 3'UTR-miRNA library screen identifies 29 miRNAs targeting MYCN.

Potential interactions of 470 miRNAs with the 3'UTR of MYCN were assayed in a high-throughput luciferase reporter screen. In brief, human embryonic kidney cells (HEK293T) were co-transfected with a reporter construct, containing the MYCN 3'UTR downstream of a luciferase reporter gene, and each of the individual miRNA mimics from a 470 miRNA mimic library. Based on the relative luciferase activities in two independent screens (**Supplementary Figure 4.1**), an interaction score was calculated for each miRNA-MYCN combination (see Material and Methods). This effort was part of a large-scale 3'UTR screening in which the interactions of 470 miRNAs with 17 selected cancer- and disease-associated genes were probed (Van Peer *et al.*, submitted).

Applying this strategy, we identified 29 miRNAs with a high probability of targeting MYCN (interaction score < -1.94; see Material and Methods; **Figure 4.1a**, **Figure 4.2a** and **Supplementary Table 4.6**). All 11 previously established miRNA-MYCN interactions [3,8] were validated in our screen (**Figure 4.1a**). In the same studies, 9 miRNAs predicted to target MYCN could not be validated; this is now confirmed by our data. Additionally, 18 new MYCN targeting miRNAs were identified, of which only 2 are predicted to target MYCN by MirTarget2, underscoring the value of this screening method to detect novel, predicted as well as non-predicted, miRNA-target gene interactions. The top 5 miRNAs (miR-449b-5p, miR-767-5p, miR-98-5p, let-7b-5p and let-7f-5p) not reported in literature were validated by demonstrating rescue of reporter gene downregulation upon mutation of potential binding sites (Van Peer *et al.*, submitted). Among the strongest hits in the screen, a significant enrichment was observed for both miRNAs with seed-matched sites present in the MYCN 3'UTR (**Figure 4.1b**) and MirTarget2 (**Supplementary Figure 4.2**) predicted miRNAs, thus further underscoring the sensitivity and robustness of the screen.

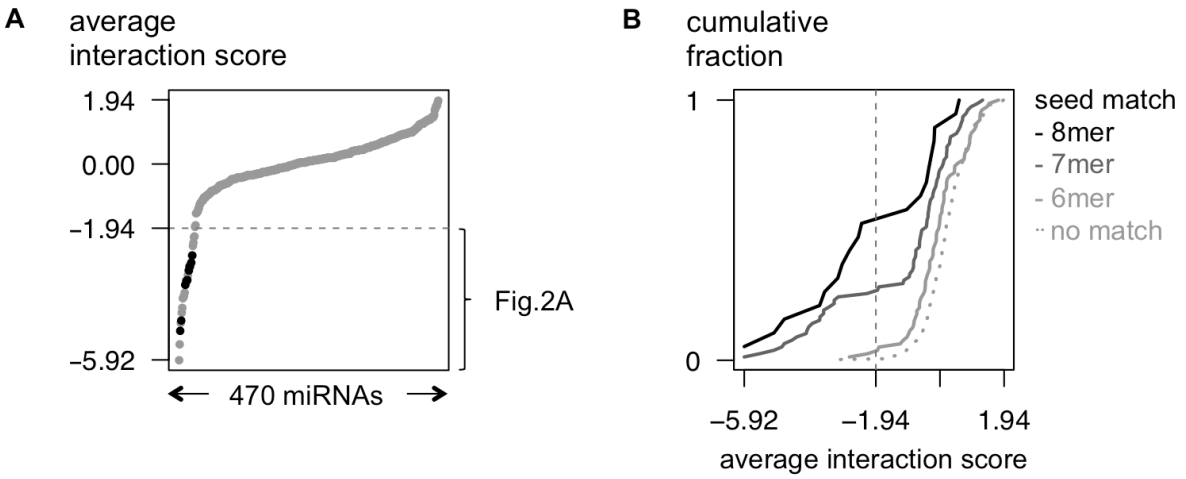

Figure 4.1: An unbiased MYCN 3'UTR-miRNA library screen identifies 29 miRNAs potentially targeting MYCN. (a) Average interaction scores are plotted (Y-axis) for 470 tested miRNAs (X-axis). The 29 miRNAs with an interactions core of < -1.94 are listed in Figure 4.2A. The 11 interactions that have been reported in literature, are indicated in black. **(b)** Cumulative distributions (Y-axis) of the interaction scores (X-axis) of miRNAs that respectively have 6-, 7- or 8-mer seed-matches in the MYCN 3'UTR.

Integration of 3'UTR-miRNA library screen and patient expression data identifies 12 MYCN-targeting miRNAs in neuroblastoma.

miRNAs are known to regulate their target genes in a highly tissue- and cell type specific manner [9]. As the MYCN 3'UTR-miRNA library screen was performed in HEK293T cells, we next aimed to specifically select miRNAs targeting MYCN in neuroblastoma cells by integrating the obtained screen results with miRNA expression data from primary neuroblastoma tumors. We reasoned that the expression of a targeting miRNA is inversely correlated to MYCN mRNA expression levels or MYCN activity in primary tumor samples. Assuming that miRNAs would have more impact on MYCN expression levels and activities in MYCN non-amplified cells, we chose to assess miRNA correlations with MYCN mRNA levels and activity only in this tumor subset to infer a potential regulatory relationship.

Correlation to MYCN mRNA expression

Overall, MYCN targeting miRNAs showed stronger inverse correlation to MYCN mRNA levels compared to non-targeting miRNAs (**Figure 4.2b**), as indicated by a shift of the cumulative distribution of π-values (-log10 p-value x Pearson correlation coefficient) to more negative values. Of the 25 MYCN-targeting miRNAs that were included on the human miRNA expression platform, 8 miRNAs showed statistically significant inverse correlation to MYCN mRNA expression, suggesting that they can indeed downregulate MYCN expression in primary MYCN non-amplified tumors.

A

negatively correlated MYCN-targeting miRNAs			
hsa-let-7a-5p		-0.21	1 (-)
hsa-let-7b-5p		-0.32	1 (-)
hsa-let-7c-5p		-0.32	1 (-)
hsa-let-7d-5p		n.s.	2 (-)
hsa-let-7f-5p		n.s.	1 (-)
hsa-let-7g-5p		n.s.	1 (-)
hsa-let-7i-5p		n.s.	1 (-)
hsa-miR-29a-3p	(3)	-0.27	1 (-)
hsa-miR-29b-3p	(3)	-0.34	1 (-)
hsa-miR-29c-3p	(3)	-0.28	1 (-)
hsa-miR-34a-5p	(3,28)	-0.24	0
hsa-miR-98-5p		n.s.	1 (-)
positively correlated MYCN-targeting miRNAs			
hsa-miR-19a-3p	(3)	0.21	4 (+)
hsa-miR-19b-3p	(3)	0.21	4 (+)
hsa-miR-34c-5p	(3)	n.s.	1 (+)
hsa-miR-449a	(3)	n.s.	1 (+)
hsa-miR-494-3p		0.36	1 (+)
remaining MYCN-targeting miRNAs			
hsa-let-7e-5p	(3)	n.s.	0
hsa-miR-101-3p	(3)	n.s.	0
hsa-miR-193a-3p		n.s.	0
hsa-miR-193b-3p		n.s.	0
hsa-miR-202-3p	(3)	n.s.	0
hsa-miR-206		n.s.	0
hsa-miR-34b-5p		-0.32	1 (+)
hsa-miR-449b-5p		n.s.	0
hsa-miR-571		n.d.	
hsa-miR-617		n.d.	
hsa-miR-767-5p		n.d.	
hsa-miR-770-5p		n.d.	

reference

correlation to MYCN expression
Spearman correlation coefficient

correlation to MYCN activity
number of negative (-) and positive (+) enriched MYC(N) gene sets

B

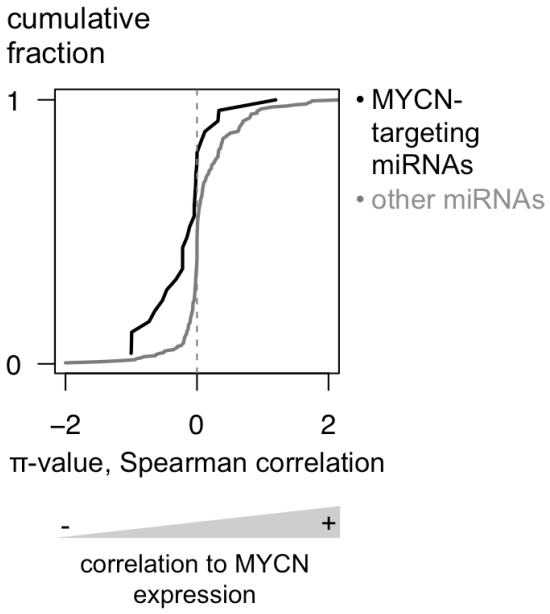

C

	negative enrichment of MYC(N) gene sets	
	yes	no
MYCN-targeting miRNAs	11	14
other miRNAs	64	188

$p = 4.6 \times 10^{-2}$

Figure 4.2: Integration of 3'UTR-miRNA library screen and patient expression data identifies 12 MYCN-targeting miRNAs in neuroblastoma. (A) MYCN targeting miRNAs are filtered for their relevance in neuroblastoma according to two criteria: significant negative correlation to MYCN expression in a MYCN non-amplified neuroblastoma patient cohort and negative enrichment for MYC(N) gene sets, using Gene Set Enrichment Analysis. 12/29 miRNAs match with at least one of these criteria and are considered to be relevant for neuroblastoma. n.s.: not significant (Spearman correlation, Benjamini & Hochberg multiple testing corrected p-value > 0.05); n.d.: no data available. **(B**) The cumulative distribution (Y-axis) of the π-value for the correlation between miRNA and MYCN expression (X-axis) of miRNAs that were identified as either MYCN-targeting (black) or not MYCN-targeting (gray). Kolmogorov-Smirnov test, p-value = 1.4 x 10-3. **(C)** 2x2 contingency table for negative enrichment of MYC(N) gene sets of MYCN-targeting and other miRNAs. Chi-Square test.

Three miRNAs were positively correlated to MYCN expression. Two of these miRNAs, miR-19a-3p and miR-19b-3p, are part of the oncogenic miR-17-92 cluster and were already known to be directly induced by MYCN in neuroblastoma cells [10].

Correlation to MYCN activity

miRNAs are known to regulate their targets by inducing mRNA destabilization and translational inhibition. Assessing the correlation between miRNA and MYCN mRNA levels, however, will not identify potential regulatory effects at protein level. Therefore, we additionally evaluated which miRNAs are inversely correlated to MYCN activity as a surrogate for MYCN protein levels. MYCN activity is reflected in the expression of MYCN regulated genes and can be assessed using Gene Set Enrichment Analysis (GSEA) [11]. In brief, for each miRNA, mRNAs were ranked according to decreasing expression correlation in MYCN non-amplified neuroblastoma tumors. Subsequently, GSEA was performed using six selected gene sets of MYC(N) upregulated genes [12-17] (see Materials and Methods). A miRNA negatively correlated to MYCN protein levels – and thus activity – is expected to be negatively correlated to genes that are positively regulated by MYCN. In this case an enrichment of MYCN upregulated genes can be expected among the most negatively correlated genes at the bottom of the ranked list. Here, a miRNA was considered to be negatively correlated to MYCN activity in case such negative enrichment could be observed for at least one MYC(N) gene set (normalized enrichment score < -2 and false discovery rate < 0.25). As expected, the MYCN-targeting miRNAs identified in the 3'UTR-miRNA library screen were significantly enriched for miRNAs that showed negative enrichment for at least one MYC(N) gene set and thus for miRNAs that are negatively correlated to MYCN activity (**Figure 4.2c**). Of the 25 MYCN-targeting miRNAs that were included on the human miRNA expression platform, 11 miRNAs showed this inverse relation to MYCN activity, whereas 6 miRNAs showed a positive relation to MYCN activity (**Figure 4.2a**, **Supplementary Table 4.7**).

In summary, 12 of 29 MYCN-targeting miRNAs were inversely correlated to either MYCN expression or MYCN activity in MYCN non-amplified tumor samples, and therefore likely regulate MYCN in neuroblastoma (**Figure 4.2a**, **Table 4.1**).

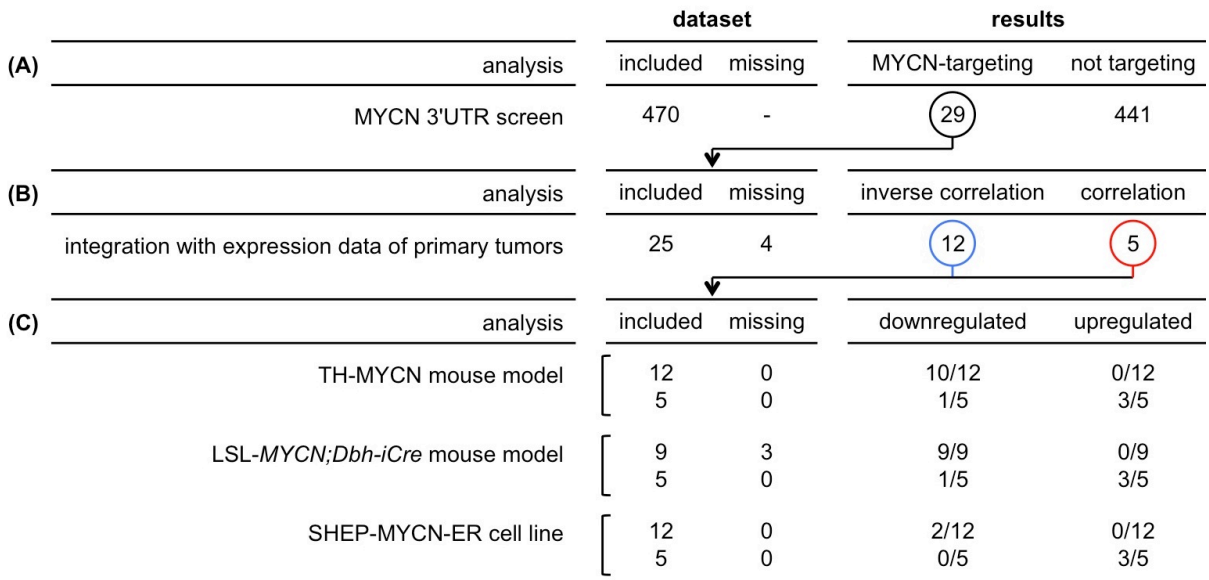

Figure 4.3: Overview of results from different analyses. Numbers listed represent the number of miRNAs. (A) Of 470 screened miRNAs, 29 miRNAs interact with the 3'UTR of MYCN. **(B)** Of these 29 miRNAs, 25 miRNAs could subsequently be analyzed in primary neuroblastoma tumors: 12 miRNAs are inversely correlated to MYCN expression or activity, whereas 5 miRNAs are positively correlated to MYCN expression or activity**. (C)** Of the 12 miRNAs inversely correlated to MYCN expression or activity, 10 miRNAs are downregulated during MYCN-driven tumor development in the TH-MYCN mouse model, 9 miRNAs are lower expressed in LSL-MYCN;Dbh-iCre tumors compared to wild-type adrenals, and 2 miRNAs are repressed upon induction of MYCN in the SHEP-MYCN-ER model system. On the other hand, of the 5 miRNA correlated to MYCN expression or activity, 3 miRNAs are upregulated during MYCN- driven tumor development in the TH-MYCN mouse model, these miRNAs are also higher expressed in LSL-MYCN;Dbh-iCre tumors compared to wild-type adrenals, and 3 miRNAs are induced upon induction of MYCN in the SHEP-MYCN-ER model system.

Interestingly, 5 MYCN-targeting miRNAs were positively correlated to MYCN expression or activity (**Figure 4.2a**), suggesting that MYCN induces their expression in neuroblastoma. One miRNA, miR-34b-5p, shows both negative correlation to MYCN mRNA levels and positive correlation to MYCN activity (**Figure 4.2a**) and is therefore excluded from further analyses.

miRNAs that regulate MYCN are downregulated during murine MYCN-driven neuroblastoma tumor formation.

In a next step, we explored how expression levels of miRNAs that target MYCN are dynamically regulated during MYCN-driven tumor formation. To this end, we performed miRNA expression profiling of the TH-MYCN mouse model, a murine MYCN-driven neuroblastoma progression model [18]. In brief, we sacrificed TH-MYCN+/+ mice one and two weeks after birth to harvest superior cervical and celiac ganglia containing foci of neuroblast hyperplasia, and 6-week old TH-MYCN+/+ mice to dissect advanced neuroblastoma tumors, arising from the neuroblast hyperplasia [19].

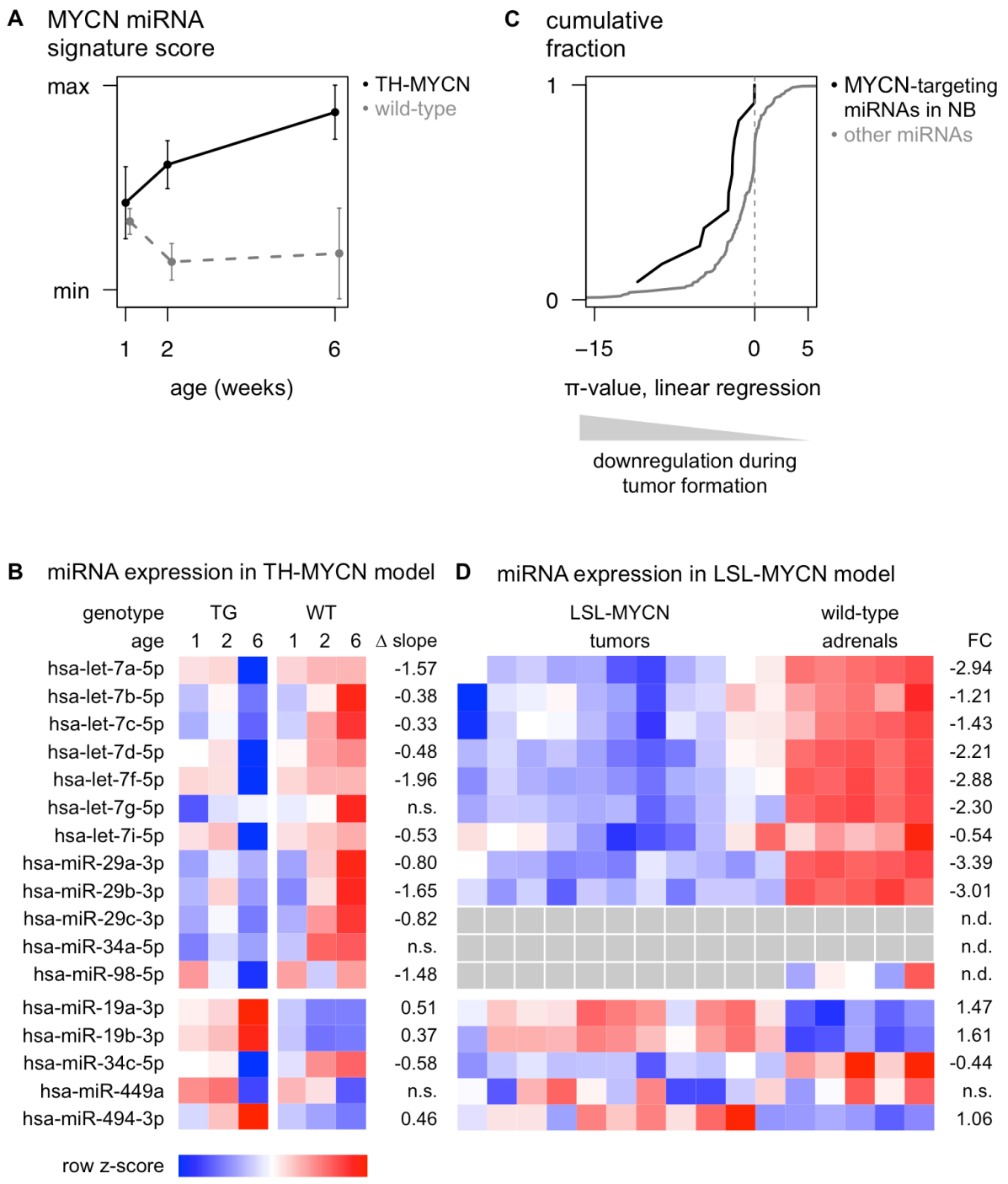

Figure 4.4: miRNAs that regulate MYCN are downregulated during murine MYCN-driven neuroblastoma tumor formation. (a) The MYCN miRNA signature score, representing expression of known MYC(N)-regulated miRNAs, increases during neuroblastoma progression in ganglia from TH-MYCN mice (TG, black) compared to ganglia from wild-type mice (WT, gray dashed). Data are presented as mean ± standard deviation of four samples. **(b)** Heatmap of average miRNA expression levels during murine MYCN-driven neuroblastoma development. Data are presented as row normalized. TG: transgenic; WT: wild-type; Δ slope: the difference in regression slope between TG and WT samples; n.s.: non-significant difference (Benjamini & Hochberg multiple testing corrected p-value > 0.05). **(c)** The 12 MYCN-targeting miRNAs in neuroblastoma show significantly more downregulation during MYCN-driven tumor development, compared to non-targeting miRNAs. Kolmogorov-Smirnov test, p-value = 9.2 x 10-3. **(d)** Heatmap of miRNA expression levels in 11 LSL-MYCN;Dbh-iCre tumors and 5 normal adrenals. For miR-29c-3p and -34a-5p, no expression data was available; miR-98-5p was not expressed in LSL-MYCN;Dbh-iCre tumors. Data are presented as row normalized. gray: no data available. FC: log2 fold change; n.d.: no data available; n.s.: non-significant fold change (Student T-test, Benjamini & Hochberg multiple testing corrected p-value > 0.05).

Additionally, we dissected the superior cervical and celiac ganglia from TH-MYCN-/- mice one, two and six weeks after birth to control for miRNA expression changes during normal postnatal development of the sympathetic ganglia. In the following analyses we only considered those murine miRNA assays that target sequences similar to the sequences of the human miRNAs included in our 3'UTR-miRNA library screen (n = 187, **Supplementary Table 4.6**). To validate this MYCN-driven neuroblastoma progression model, we evaluated the expression of 50 known MYC(N)-regulated miRNAs [5], summarized in a MYCN signature score. This MYCN signature score increases significantly throughout tumor progression from tumor-prone ganglia to tumors in transgenic mice, compared to wild-type ganglia (**Figure 4.3a** and **Supplementary Figure 4.3**). This observation is in keeping with the hypothesis that sustained MYCN activity in the sympathetic ganglia of homozygous transgenic mice gives rise to the appearance of neuroblastoma tumors in these anatomic locations [19].

The majority of the MYCN-targeting miRNAs in neuroblastoma (10 out of 12) showed a significantly decreased expression during tumor development in TH-MYCN+/+ mice compared to normal development, while 2 of them showed no significantly different expression pattern (**Figure 4.3b**, **Table 4.1**). Interestingly, of the 5 MYCN-targeting miRNAs with positive correlation to MYCN expression or activity, 3 miRNAs, miR-19a-3p, miR-19b-3p and miR-494-3p, showed significantly increased expression during tumor development (**Figure 4.3b**), further supporting the hypothesis that MYCN induces the expression of these miRNAs. The 2 remaining positively correlated miRNAs, miR-34c-5p and miR-449a, are, respectively, significantly downregulated and not regulated during tumor development (**Figure 4.3b**). Overall, the 12 MYCN-targeting miRNAs in neuroblastoma, show significantly more downregulation during MYCN-driven tumor development, compared to non-targeting miRNAs, as indicated by a shift of the cumulative distribution of the π-values (-log10 p-value x Δ slope) to more negative values (**Figure 4.3c**).

The above findings could be confirmed in an additional, recently developed, MYCN-driven neuroblastoma mouse model, the LSL-MYCN;Dbh-iCre mouse model [20]. All 9 MYCN-targeting miRNAs that could be evaluated are significantly lower expressed in LSL-MYCN;Dbh-iCre tumors compared to wild-type adrenals (**Figure 4.3d**, **Table 4.1**). Considering the 5 MYCN-induced miRNAs, the data in the LSL-MYCN;Dbh-iCre tumors again fully recapitulated the findings from the TH-MYCN progression model: miR-19a-3p, miR-19b-3p and miR-494-3p showed increased expression in tumors compared to wild-type control

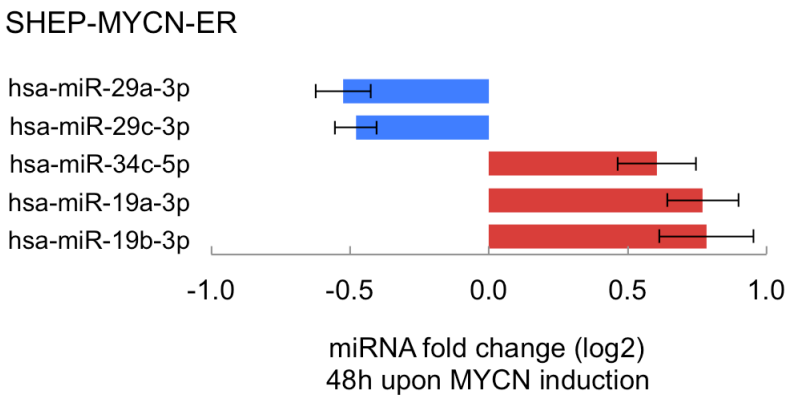

Figure 4.5: Induction of MYCN activity is associated with altered expression levels of particular miRNAs that target its 3'UTR. Summary of significantly differentially expressed miRNAs upon MYCN induction relative to control treatment (Student t-test, Benjamini & Hochberg multiple testing corrected p-value < 0.05). Data are represented in a horizontal bar graph as log 2 fold changes ± standard error of the mean (5 biological replicates).

tissue (**Figure 4.3d**), whereas miR-34c-5p and miR-449a are respectively significantly downregulated and not regulated in LSL-MYCN;Dbh-iCre tumors.

MYCN can directly modulate the expression levels of particular miRNAs that target its 3'UTR.

In a final step, we explored to what extent MYCN directly controls, as transcriptional activator and repressor, the expression levels of the 12 selected MYCN-targeting miRNAs. To this end we measured miRNA expression levels in a MYCN-inducible model system. Two out of 12 MYCN-targeting miRNAs in neuroblastoma (**Figure 4.2a**), miR-29a-3p and miR-29b-3p, showed significant reduction in expression 48h after MYCN activation (**Figure 4.4**, **Table 4.1**).

Of the five MYCN-targeting miRNAs with positive correlation to MYCN expression or activity (**Figure 4.2a**), three miRNAs, miR-19b-3p, miR-19a-3p and miR-34c-5p, showed induction of expression (**Figure 4.4**), supporting the assumption that MYCN induces the expression of these miRNAs.

Discussion

Previous studies have highlighted the importance of miRNAs in the regulation of MYCN, a major driver oncogene in neuroblastoma. Nonetheless, a comprehensive, genome-wide exploration of the miRNA-MYCN interactome has not yet been performed. Thus far, studies have only focused on individual miRNAs or a small subset of miRNAs predicted to target MYCN by algorithms that are biased towards the limited knowledge of miRNA binding site architecture. Here, we report on the first unbiased and genome-wide high-throughput

miRNA target reporter screen to identify miRNAs targeting MYCN. From the total of 29 MYCN-targeting miRNAs identified in this study, 18 interactions were novel whereas all 11 previously established MYCN-targeting miRNAs [3,8] were confirmed, thus underscoring the validity of our genome-wide high-throughput screen.

Previously identified MYCN-targeting miRNAs have not been confirmed to regulate MYCN in primary neuroblastoma tumor cells. To address this shortcoming, we integrated our screen results with matching miRNA and mRNA expression profiles from primary neuroblastoma tumors. For 12 MYCN-targeting miRNAs we observed significant inverse correlation to MYCN expression or activity and thus provide evidence that they regulate MYCN in a neuroblastoma tissue context: eight let-7 family miRNAs (let-7a-5p, let-7b-5p, let-7c-5p, let-7d-5p, let-7f-5p, let-7g-5p, let-7i-5p and miR-98), three miR-29 family miRNAs (miR-29a-3p, miR-29b-3p, miR-29c-3p) and miR-34a-5p.

In a next step, we investigated the dynamic regulation of these miRNAs during the process of MYCN-driven tumor formation, using the extensively validated TH-MYCN mouse model. Notably, we observe that MYCN-targeting miRNAs are preferentially downregulated during MYCN-driven tumor development, suggesting that MYCN negatively regulates the miRNAs by which it is targeted, to safeguard its own expression. Growing evidence suggests that MYCN predominantly acts repressively on the overall miRNA composition [5,21-24] and we indeed observed widespread downregulation of miRNA expression during murine MYCN-driven neuroblastoma development (**Figure 4.3c**, gray line). Nonetheless, the fraction of MYCN-targeting miRNAs that is downregulated is larger than expected by chance (**Figure 4.3c**, black line). The mechanisms by which MYCN directly represses transcription are not fully understood. Several lines of evidence suggest that it acts in a protein complex including SP1 and/or MIZ-1 [25-29] to recruit histone writers [25,27-30] and/or DNA-methyltransferases [26,30] to the promoter regions of its repressed target genes. Whether binding of MYCN to the canonical E-box sequence is required for this process is still unclear [26,31]. Notably, only two MYCN-targeting miRNAs in neuroblastoma (miR-29a-3p and miR-29c-3p) are directly downregulated upon induction of MYCN in a neuroblastoma cell line model, suggesting that downregulation of MYCN-targeting miRNAs during tumor formation is likely to result from secondary (epi)genetic events downstream of increased MYCN activity.

The integration of the screen results with miRNA expression data from MYCN non-amplified primary neuroblastoma tumors further identified 5 MYCN-targeting miRNAs with positive correlation to MYCN expression or activity. Subsequent analysis of these miRNAs in in vivo MYCN model systems showed that activation of MYCN is associated to increased expression of miR-19a-3p, miR-19b-3p and miR-494-3p. Indeed, miR-19a-3p and miR-19b-3p, members of the oncogenic miR-17-92 cluster, have been shown to be direct

transcriptional targets of MYCN in neuroblastoma cells [5,24], and the region upstream to miR-494-3p contains E-box sequences (data not shown), suggesting that MYCN can induce its expression. It is conceivable that these miRNAs act both in a MYCN negative regulatory feed-back loop as well as via repression of important neuroblastoma tumor suppressor genes: indeed, miR-19a-3p targets ESR1 [32], a ligand-inducible transcription factor implicated in neuronal differentiation, whereas miR-19b-3p represses DKK3 expression [33], a marker of tumor differentiation with elevated expression levels in favorable tumors. The MYCN model systems, however, cannot confirm the positive correlation between miR-34c-5p and miR-449a and MYCN expression or activity observed in primary neuroblastoma tumors: miR-34c-5p is consistently downregulated in the murine models, whereas the expression of miR-449a is not altered. Furthermore, there is no evidence that MYCN could induce the expression of these miRNAs directly. Although the expression of miR-34c-5p increases upon MYCN activation in the in vitro SHEP-MYCN-ER model system, the upstream region of miR-34c-5p does not contain E-box sequences (data not shown), and miR-449a, residing in the second intron of CDC20B, was not identified by Shohet and colleagues [24] in their screen for intronic miRNAs regulated by MYCN. Nevertheless, the different relation between MYCN and miR-34c-5p expression in MYCN non-amplified versus amplified environment should not be surprising: activation of miR-34c-5p, either direct or indirect, could be one of the mechanisms through which normal physiological levels of MYCN affect apoptosis. In cases where MYCN exceeds its physiological levels and oncogene-induced apoptosis is triggered, a transforming cell will need to circumvent MYCN-mediated apoptosis, for instance via downregulation of miR-34c-5p, which seems to occur in TH-MYCN and LSL-MYCN;Dbh-iCre tumors.

Of further notice, 17 out of 29 identified MYCN-targeting miRNAs were considered not to be relevant for MYCN regulation in the context of neuroblastoma, due to lack of inverse correlation to MYCN expression and/or activity, or due to unavailable expression data. Given the tissue specific nature of miRNA function, it is not excluded that these miRNAs regulate MYCN in an other cellular context, such as that of normal brain development [34] and a number of childhood malignancies with demonstrated involvement of MYCN: medulloblastoma [31,35], retinoblastoma [35,36], Wilms' tumor [36,37], rhabdomyoscaroma [37,38] and T-cell acute lymphoblastic leukemia [38]. Notably, three of these excluded miRNAs, let-7e-5p, miR-101-3p and miR-202-3p, have been reported to target MYCN in a MYCN amplified neuroblastoma cell line [3]. This discrepancy between literature and our data could be explained by the fact that our integrative approach identifies MYCN-targeting miRNAs in neuroblastoma using gene expression data from MYCN non-amplified primary tumors. Buechner and colleagues [3] showed that let-7e-5p, miR-101-3p and miR-202-3p are able to

affect MYCN expression in a MYCN amplified neuroblastoma cell line, whereas we found no evidence that they are regulating MYCN in MYCN non-amplified primary neuroblastoma tumors.

In conclusion, we identify 12 MYCN-targeting miRNAs in with regulatory effects on MYCN expression levels or activity in MYCN non-amplified neuroblastoma (Figure 4.2A). Furthermore, we provide evidence that these miRNAs are preferentially downregulated during MYCN-driven neuroblastoma tumor formation, suggesting that MYCN negatively controls the expression of these miRNAs, and as such safeguards its own expression. Understanding this regulatory miRNAome upstream of MYCN in neuroblastoma can open new perspectives for targeting the MYCN pathway in neuroblastoma tumors, a strategy that holds great promise [39]. Moreover, the identification of additional target genes of the miRNAs in the described MYCN-miRNA interactome might prove useful in the search for novel therapeutic targets.

Methods

MYCN 3'UTR-miRNA library screen

HEK293T cells were seeded at a density of 10 000 cells/well in 96-well plates. Twenty-four hours after seeding, cells were co-transfected with 100 ng of a reporter vector with the wild-type MYCN 3'UTR (ENST00000281043, Ensembl release 75) cloned downstream of the Firefly luciferase gene (SwitchGear Genomics, S207230) and 20 ng of pRL-TK control vector containing the Renilla luciferase gene (Promega) together with a library of 470 miRNA mimics (2.5 pmol) (Ambion's Pre-miR miRNA Precursor Library - Human V3, design based on miRBase v9.2 with exclusion of hsa-miR-122a). Lipid based transfections were performed using 0.4 µl Dharmafect Duo reagent (Dharmacon). Forty-eight hours post-transfection, luciferase reporter gene activities were assayed using the Dual-Luciferase Reporter assay system (Promega) according to the manufacturer's protocol with minor changes (LARII and Stop & Glo buffer volumes were reduced to 50 µl). Firefly reporter gene activities were normalized to Renilla values and then log-transformed. Subsequently, robust z-scores were calculated and median centered to the distribution of robust z-scores from 36 analogous screens (of 17 selected cancer and disease associated genes) on a per miRNA basis in order to remove potential systematic bias. The resulting interaction scores are thus more negative for miRNAs that interact with the 3'UTR. In order to determine the interaction score cutoff that separates interactions from non-interactions, the scores for a set of validated miRNA interactions, probed in the MYCN screen or any of the analogous screens,

were used together with the scores for a set of negative control interactions from an empty-3'UTR vector miRNA library screen to perform ROC-curve analysis and determine the point of highest accuracy (interaction score = -1.94, specificity = 99%, sensitivity = 51%). MYCN 3'UTR-miRNA library screen results were replicated in two independent experiments. For a more detailed description of the 3'UTR-miRNA library screen setup and data-analysis we refer to Van Peer et al. (in preparation).

miRNA target analysis

Potential miRNA target sites in the MYCN 3'UTR were identified as reported previously [40]. In addition, miRNAs targeting MYCN were predicted using the MirTarget2 algorithm [41].

miRNA and mRNA expression in patient cohort

160 MYCN non-amplified primary tumor samples of neuroblastoma patients were collected prior to therapy at the Ghent University Hospital (Ghent, Belgium), the University Children's Hospital Essen (Essen, Germany), the Hospital Clínico Universitario (Valencia, Spain), the Academic Medical Center (University of Amsterdam, Netherlands) and the National Children's Research Centre (Dublin, Ireland). Informed consent was obtained from the patients' relatives. mRNA data from 75 primary neuroblastoma tumors is available at the Gene Expression Omnibus (http://www.ncbi.nlm.nih.gov/geo; Accession Number: GSE32664). Correlation of miRNA expression levels and MYCN mRNA levels was evaluated with Spearman's rank correlation coefficient. In order to find miRNAs that show negative correlation to MYCN activity and hence MYCN protein levels, mRNAs were ranked according to decreasing Spearman's rank correlation coefficient for each miRNA. Ranked gene lists were used for Gene Set Enrichment Analysis (GSEA) [11] with selected gene sets of MYC(N) regulated genes from the chemical and genetic perturbations gene set collections in the GSEA Molecular Signatures Database. From all gene sets in this collection that have either MYC or MYCN in their name, the six gene sets that contain MYC(N) upregulated genes were used for this analysis: COLLER MYC TARGETS UP [12], DANG MYC TARGETS UP [13], DANG REGULATED BY MYC UP [13], KIM MYC AMPLIFICATION TARGETS UP [14], LEE LIVER CANCER MYC UP [42], SCHUHMACHER MYC TARGETS UP [16] and YU MYC TARGETS UP [17]. Gene sets with a false discovery rate (FDR) below 25% and a normalized enrichment score (NES) below -2 were considered significantly negatively enriched.

miRNA annotation

In this study we used data obtained with three different analytical miRNA platforms. Platform designs are based on different releases of the miRBase database for miRNA

annotation, resulting in non-overlapping annotation of data sets. To allow for correct integration of miRNA data, we used miRBase Tracker, an in-house developed web tool for miRNA reannotation [43] and applied the most up-to-date annotation at time of publication (miRBase release 21). Details of reannotation of the different miRNA platforms, including cross-species comparison, can be found in Supplementary Tables S1 - S5.

SHEP-MYCN-ER model system

The MYCN-inducible SHEP-MYCN-ER cell model [44] was kindly provided by Johannes H Schulte (Department of Pediatric Oncology and Hematology, University Children's Hospital Essen, Germany). Cell line authenticity was validated by Short Tandem Repeat (STR) genotyping prior to performing the described experiments. In the SHEP-MYCN-ER cell line, the cDNA of MYCN is fused to a mutated estrogen responsive domain (ER) which can bind 4-hydroxy-tamoxifen (4-OHT), but is unable to bind with natural estrogen [44]. Addition of 4-OHT to the culture medium (200 nM final concentration) activates the MYCN-ER expression. SHEP-MYCN-ER cells were seeded at 100 000 cells per 6-well and treated with 4-OHT after 48 h. Subsequently, cells were pelleted for RNA isolation 48 h after treatment. In parallel, cells were treated with equal amounts of the 4-OHT solvent (70 % ethanol) as a negative control. RNA was isolated using the miRNeasy Mini Kit (Qiagen; 217004) according to manufacturer's instructions. Five replicate experiments were performed and analyzed.

RT-qPCR

RT-qPCR reactions were performed and reported according to the MIQE guidelines [45]. For quantification of individual miRNA expressions, cDNA was synthesized from 500 ng total RNA with 4 µl of HiSpec Buffer, 2 µl of Nucleics Mix and 2 µl miScript RT Mix (miScript II RT Kit, Qiagen; 218161) in a final volume of 20 µl. This reaction mix was incubated for 60' at 37°C and 5' at 95°C using an iCycer instrument (Bio-Rad). qPCR reactions contained 3 ng of cDNA, 2.5 µl QuantiTeckt Mastermix, 0.5 µl miScript Universal Primer and 0.5 µl miRNA-specific miScript Primer Assay (Qiagen, miScript Primer Assays used are listed in Supplementary Table S2) in a total volume of 5 µl. Expression levels were normalized against three stably expressed reference miRNAs (hsa-miR-125a, hsa-miR-423 and hsa-miR-92) validated with GeNorm [46] and analyzed using qbase+ software version 2.6 (http://www.biogazelle.com/qbaseplus) [47].

TH-MYCN neuroblastoma progression model

TH-MYCN+/+ mice [18] were sacrificed at day seven (n=4) and day fourteen (n=4) of life to harvest sympathetic ganglia containing foci of neuroblast hyperplasia, and at week 6 of life to harvest advanced neuroblastoma tumors (n=4). Additionally, we have dissected the same sympathetic ganglia from TH-MYCN-/- mice at day seven (n=4), day fourteen (n=4) and week 6 (n=4) of life to control for miRNA expression changes during normal development. Murine total RNA was isolated using the miRNeasy Mini Kit (Qiagen, 217004) according to the manufacturer's instructions. Mature miRNA expression levels were quantified using a stem-loop RT-qPCR platform. Briefly, 99 ng of total RNA was reverse transcribed using Megaplex™ RT Primers, Rodent Pool Set v3.0 (Life Technologies - Applied Biosystems; 4444746) followed by a 12-cycle pre-amplification according to the manufacturer's instructions. Pre-amplified cDNA was diluted four times and quantified using the TaqMan Array Rodent MicroRNA A+B Cards Set v3.0 (Life Technologies - Applied Biosystems; 4444909) according to the manufacturer's instructions on a ViiA 7 Real-Time PCR System (Life Technologies - Applied Biosystems). Only C_q values lower than 32 were retained and normalized using global mean normalization, as previously described [48]. Furthermore, to allow for cross-species comparison of miRNA expression data, we only considered those murine miRNA assays that target sequences similar to the sequences of the human miRNAs included in our 3'UTR-miRNA library screen (see Supplementary Tables S3 - S4). Linear regression analysis was performed to evaluate the differential temporal expression pattern in ganglia from wild-type mice and ganglia and tumors from transgenic mice. A π-value metric was subsequently calculated as the difference in regression slopes between transgenic and wild-type samples, multiplied with the statistical significance of this difference: $\pi - \text{value} = -\log_{10} \text{p-value} \times \Delta_{slope\ regression}$.

LSL-MYCN;Dbh-iCre tumors

The LSL-MYCN;Dbh-iCre mouse model is described elsewhere [20] along with details on tumor dissection and miRNA expression profiling. In brief, 60 ng of total RNA of normal adrenals and LSL-MYCN;Dbh-iCre tumors, isolated with the miRNeasy Mini kit (Qiagen), was used to quantify murine mature miRNA expression levels using a stemloop RT-qPCR platform (Life Technologies-Applied Biosystems).

Statistical methods

All statistical analyses were performed using R Bioconductor software (version 3.0.2). If not further specified in the results section, statistical significance was defined as p-value < 0.05 for all statistical tests.

Data accessibility

mRNA data from 75 primary neuroblastoma tumors are available at the Gene Expression Omnibus (http://www.ncbi.nlm.nih.gov/geo) under accession number GSE32664. miRNA expression data from the TH-MYCN neuroblastoma progression model are available in the ArrayExpress database (www.ebi.ac.uk/arrayexpress) under accession number E-MTAB-2618. Furthermore, the processed data can be visualized via the R2 microarray analysis and visualization platform (http://r2.amc.nl) under experiment "Exp Nb Hyperplasia TH-MYCN - Ghent - 24 - custom - mirbase19mm2".

Acknowledgments

We would like to thank the Ghent University Hospital (Ghent, Belgium), the University Children's Hospital Essen (Essen, Germany) and the Hospital Clínico Universitario (Valencia, Spain) for collection of primary tumor samples. Further, we would like to thank F. De Vloed for excellent technical support and J.J.B. Koster for loading the murine miRNA expression data and accompanying statistics in R2.

Funding. This work was supported by the GOA (grant number 01G01910), by research grants from the European Union (FP7-ASSET project) to F.S., from the Belgian Foundation against Cancer (Stichting Tegen Kanker) to J.V. [SCIE 2010-177], and from the Fund for Scientific Research Flanders (FWO) to F.S. [G.0530.12N]; by a PhD grant from the Agency for Innovation by Science and Technology (IWT) to A.B. [IWT 101506]; an Emmanuel van der Schueren research grant from the Flemish League against Cancer (Vlaamse Liga tegen Kanker) to G.V.P.; a PhD grant from the Ghent University to G.V.P. [BOF 01D35609]; and a post-doc grant of the FWO to P.M. and K.D.P. This work was further supported by Program Grants from the NHMRC Australia, the Cancer Institute NSW and the Cancer Council NSW to D.C., B.C. and G.M..

References

1. Meyer N, Penn LZ. Reflecting on 25 years with MYC. Nat Rev Cancer. 2008 Dec;8(12):976–90.
2. Molenaar JJ, Domingo-Fernández R, Ebus ME, Lindner S, Koster J, Drabek K, et al. LIN28B induces neuroblastoma and enhances MYCN levels via let-7 suppression. Nat Genet. 2012 Oct 7;44(11):1199–206.
3. Buechner J, Tomte E, Haug BH, Henriksen JR, Løkke C, Flaegstad T, et al. Tumour-suppressor microRNAs let-7 and mir-101 target the proto-oncogene MYCN and inhibit cell proliferation in MYCN-amplified neuroblastoma. British Journal of Cancer. 2011 Jul 12;105(2):296–303.
4. Peukert K, Staller P, Schneider A, Carmichael G, Hänel F, Eilers M. An alternative pathway for gene regulation by Myc. The EMBO Journal. 1997 Sep 15;16(18):5672–86.
5. Mestdagh P, Fredlund E, Pattyn F, Schulte JH, Muth D, Vermeulen J, et al. MYCN/c-MYC-induced microRNAs repress coding gene networks associated with poor outcome in MYCN/c-MYC-activated tumors. Oncogene. 2010 Mar 4;29(9):1394–404.
6. Ramaswami R, Harding V, Newsom-Davis T. Novel cancer therapies: treatments driven by tumour biology. Postgrad Med J. 2013 Nov;89(1057):652–8.
7. Di Leva G, Garofalo M, Croce CM. MicroRNAs in cancer. Annu Rev Pathol. 2014;9:287–314.
8. Wei JS, Song YK, Durinck S, Chen Q-R, Cheuk ATC, Tsang P, et al. The MYCN oncogene is a direct target of miR-34a. Oncogene. 2008 Sep 4;27(39):5204–13.
9. Mestdagh P, Lefever S, Pattyn F, Ridzon D, Fredlund E, Fieuw A, et al. The microRNA body map: dissecting microRNA function through integrative genomics. Nucleic Acids Research. Oxford University Press; 2011 Nov 1;39(20):e136–6.
10. Fontana L, Fiori ME, Albini S, Cifaldi L, Giovinazzi S, Forloni M, et al. Antagomir-17-5p Abolishes the Growth of Therapy-Resistant Neuroblastoma through p21 and BIM. Maas S, editor. PLoS ONE. 2008 May 21;3(5):e2236.
11. Subramanian A, Tamayo P, Mootha VK, Mukherjee S, Ebert BL, Gillette MA, et al. Gene set enrichment analysis: a knowledge-based approach for interpreting genome-wide expression profiles. Proceedings of the National Academy of Sciences of the United States of America. 2005 Oct 25;102(43):15545–50.
12. Coller HA, Grandori C, Tamayo P, Colbert T, Lander ES, Eisenman RN, et al. Expression analysis with oligonucleotide microarrays reveals that MYC regulates genes involved in growth, cell cycle, signaling, and adhesion. Proceedings of the National Academy of Sciences of the United States of America. 2000 Mar 28;97(7):3260–5.
13. Zeller KI, Jegga AG, Aronow BJ, O'Donnell KA, Dang CV. An integrated database of genes responsive to the Myc oncogenic transcription factor: identification of direct genomic targets. Genome Biology. 2002 Dec 31;4(10):R69–9.
14. Kim J, Woo AJ, Chu J, Snow JW, Fujiwara Y, Kim CG, et al. A Myc network accounts for similarities between embryonic stem and cancer cell transcription programs. Cell. 2010 Oct 15;143(2):313–24.
15. Lee RC. An Extensive Class of Small RNAs in Caenorhabditis elegans. Science. 2001 Oct 26;294(5543):862–4.
16. Schuhmacher M, Kohlhuber F, Hölzel M, Kaiser C, Burtscher H, Jarsch M, et al. The transcriptional program of a human B cell line in response to Myc. Nucleic Acids Research. 2001 Jan 15;29(2):397–406.
17. Yu D, COZMA D, PARK A, Thomas-Tikhonenko A. Functional validation of genes implicated in lymphomagenesis: an in vivo selection assay using a Myc-induced B-cell tumor. Ann N Y Acad Sci. 2005 Nov;1059:145–59.
18. Weiss WA, Aldape K, Mohapatra G, Feuerstein BG, Bishop JM. Targeted expression of MYCN causes neuroblastoma in transgenic mice. The EMBO Journal. 1997 Jun 2;16(11):2985–95.
19. Hansford LM, Thomas WD, Keating JM, Burkhart CA, Peaston AE, Norris MD, et al. Mechanisms of embryonal tumor initiation: distinct roles for MycN expression and MYCN amplification. Proceedings of the National Academy of Sciences of the United States of America. 2004 Aug 24;101(34):12664–9.
20. Althoff K, Beckers A, Bell E, Nortmeyer M, Thor T, Sprüssel A, et al. A Cre-conditional MYCN-driven neuroblastoma mouse model as an improved tool for preclinical studies. Oncogene. 2014 Sep 1.
21. Chen Y, Stallings RL. Differential Patterns of MicroRNA Expression in Neuroblastoma Are Correlated with Prognosis, Differentiation, and Apoptosis. Cancer Research. 2007 Feb

1;67(3):976–83.
22. Bray I, Bryan K, Prenter S, Buckley PG, Foley NH, Murphy DM, et al. Widespread dysregulation of MiRNAs by MYCN amplification and chromosomal imbalances in neuroblastoma: association of miRNA expression with survival. PLoS ONE. 2009;4(11):e7850.
23. Schulte JH, Schowe B, Mestdagh P, Kaderali L, Kalaghatgi P, Schlierf S, et al. Accurate prediction of neuroblastoma outcome based on miRNA expression profiles. Int J Cancer. 2010 Nov 15;127(10):2374–85.
24. Shohet JM, Ghosh R, Coarfa C, Ludwig A, Benham A, chen Z, et al. A genome-wide search for promoters that respond to increased MYCN reveals both new oncogenic and tumor suppressor microRNAs associated with aggressive neuroblastoma. Cancer Research. 2011 Jun 1;71(11):3841–51.
25. Liu T, Tee AEL, Porro A, Smith SA, Dwarte T, Liu PY, et al. Activation of tissue transglutaminase transcription by histone deacetylase inhibition as a therapeutic approach for Myc oncogenesis. Proceedings of the National Academy of Sciences of the United States of America. 2007 Nov 20;104(47):18682–7.
26. Gherardi S, Valli E, Erriquez D, Perini G. MYCN-mediated transcriptional repression in neuroblastoma: the other side of the coin. Front Oncol. 2013;3:42.
27. Iraci N, Diolaiti D, Papa A, Porro A, Valli E, Gherardi S, et al. A SP1/MIZ1/MYCN repression complex recruits HDAC1 at the TRKA and p75NTR promoters and affects neuroblastoma malignancy by inhibiting the cell response to NGF. Cancer Research. 2011 Jan 15;71(2):404–12.
28. Lodrini M, Oehme I, Schroeder C, Milde T, Schier MC, Kopp-Schneider A, et al. MYCN and HDAC2 cooperate to repress miR-183 signaling in neuroblastoma. Nucleic Acids Research. 2013 Jul;41(12):6018–33.
29. Corvetta D, Chayka O, Gherardi S, D'Acunto CW, Cantilena S, Valli E, et al. Physical interaction between MYCN oncogene and polycomb repressive complex 2 (PRC2) in neuroblastoma: functional and therapeutic implications. Journal of Biological Chemistry. American Society for Biochemistry and Molecular Biology; 2013 Mar 22;288(12):8332–41.
30. Brenner C, Deplus R, Didelot C, Loriot A, Viré E, De Smet C, et al. Myc represses transcription through recruitment of DNA methyltransferase corepressor. The EMBO Journal. 2005 Jan 26;24(2):336–46.
31. Roussel MF, Robinson GW. Role of MYC in Medulloblastoma. Cold Spring Harb Perspect Med. 2013 Nov;3(11).
32. Lovén J, Zinin N, Wahlström T, Müller I, Brodin P, Fredlund E, et al. MYCN-regulated microRNAs repress estrogen receptor-alpha (ESR1) expression and neuronal differentiation in human neuroblastoma. Proceedings of the National Academy of Sciences of the United States of America. 2010 Jan 26;107(4):1553–8.
33. De Brouwer S, Mestdagh P, Lambertz I, Pattyn F, De Paepe A, Westermann F, et al. Dickkopf-3 is regulated by the MYCN-induced miR-17-92 cluster in neuroblastoma. Int J Cancer. 2011 Jul 27.
34. Hurlin PJ. N-myc functions in transcription and development. Birth Defect Res C. 2005 Dec;75(4):340–52.
35. Rushlow DE, Mol BM, Kennett JY, Yee S, Pajovic S, Thériault BL, et al. Characterisation of retinoblastomas without RB1 mutations: genomic, gene expression, and clinical studies. Lancet Oncol. 2013 Apr;14(4):327–34.
36. Nisen PD, Zimmerman KA, Cotter SV, Gilbert F, Alt FW. Enhanced expression of the N-myc gene in Wilms' tumors. Cancer Research. 1986 Dec;46(12 Pt 1):6217–22.
37. Driman D, Thorner PS, Greenberg ML, Chilton-MacNeill S, Squire J. MYCN gene amplification in rhabdomyosarcoma. Cancer. 1994 Apr 15;73(8):2231–7.
38. Astolfi A, Vendemini F, Urbini M, Melchionda F, Masetti R, Franzoni M, et al. MYCN is a novel oncogenic target in pediatric T-cell acute lymphoblastic leukemia. Oncotarget. 2014 Jan;5(1):120–30.
39. Barone G, Anderson J, Pearson ADJ, Petrie K, Chesler L. New strategies in neuroblastoma: Therapeutic targeting of MYCN and ALK. Clin Cancer Res. 2013 Nov 1;19(21):5814–21.
40. Grimson A, Farh KK-H, Johnston WK, Garrett-Engele P, Lim LP, Bartel DP. MicroRNA targeting specificity in mammals: determinants beyond seed pairing. Molecular Cell. 2007 Jul 6;27(1):91–105.
41. Wang X, Naqa El IM. Prediction of both conserved and nonconserved microRNA targets in animals. Bioinformatics. 2008 Feb 1;24(3):325–32.
42. Lee J-S, Chu I-S, Mikaelyan A, Calvisi DF, Heo J, Reddy JK, et al. Application of comparative

functional genomics to identify best-fit mouse models to study human cancer. Nat Genet. 2004 Dec;36(12):1306–11.
43. Van Peer G, Lefever S, Anckaert J, Beckers A, Rihani A, Van Goethem A, et al. miRBase Tracker: keeping track of microRNA annotation changes. Database. Oxford University Press; 2014 Jan 9;2014(0):bau080–0.
44. Schulte JH, Horn S, Otto T, Samans B, Heukamp LC, Eilers U-C, et al. MYCN regulates oncogenic MicroRNAs in neuroblastoma. Int J Cancer. 2008 Feb 1;122(3):699–704.
45. Bustin SA, Benes V, Garson JA, Hellemans J, Huggett J, Kubista M, et al. The MIQE guidelines: minimum information for publication of quantitative real-time PCR experiments. Clinical chemistry. 2009. pp. 611–22.
46. Vandesompele J, De Preter K, Pattyn F, Poppe B, Van Roy N, De Paepe A, et al. Accurate normalization of real-time quantitative RT-PCR data by geometric averaging of multiple internal control genes. Genome Biology. 2002 Jun 18;3(7):R34.
47. Hellemans J, Mortier G, De Paepe A, Speleman F, Vandesompele J. qBase relative quantification framework and software for management and automated analysis of real-time quantitative PCR data. Genome Biology. 2007;8(2):R19.
48. Mestdagh P, Van Vlierberghe P, De Weer A, Muth D, Westermann F, Speleman F, et al. A novel and universal method for microRNA RT-qPCR data normalization. Genome Biology. 2009;10(6):R64.

Supplements

Supplementary Tables

Supplementary tables from this manuscript are accessible through the following URL: https://goo.gl/OfGd8K

Supplemental Figures

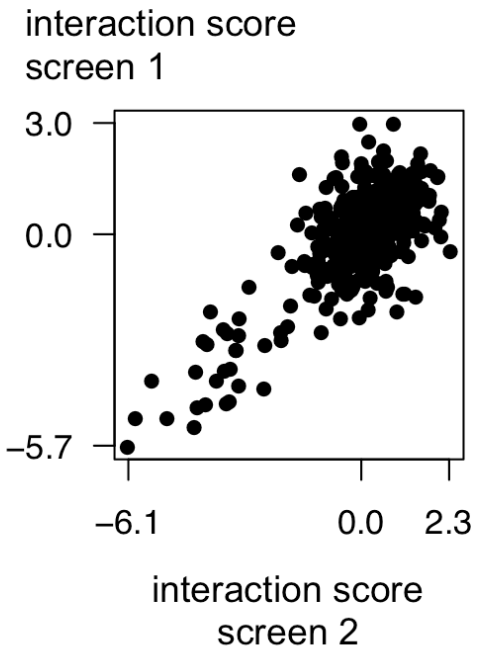

Supplementary Figure 1. Correlation between the interaction scores from two independent MYCN 3' UTR screens. The interaction scores resulting from the two screens show high correlation, underlining the reproducibility of the generated data. Spearman correlation coefficient = 0.86, p = 2.2 x 10-16.

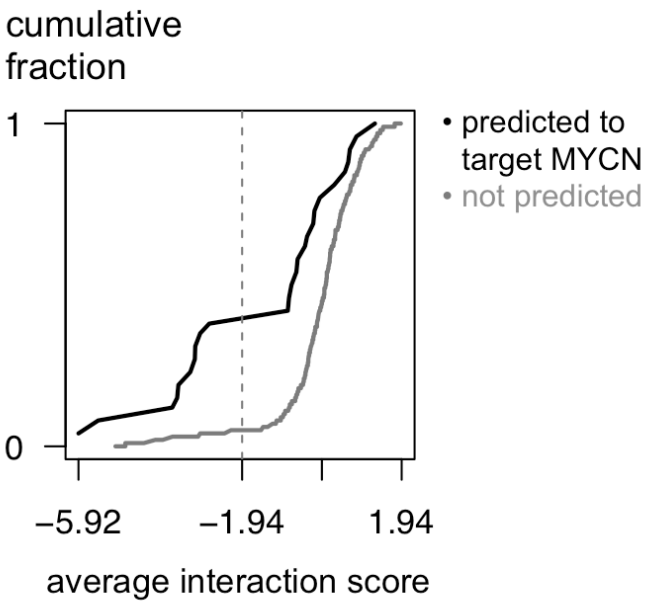

Supplementary Figure 2. Enrichment of miRNAs predicted to target MYCN among the miRNAs with a more negative interaction score. Kolmogorov-Smirnov test, p = 5.3 x 10-4.

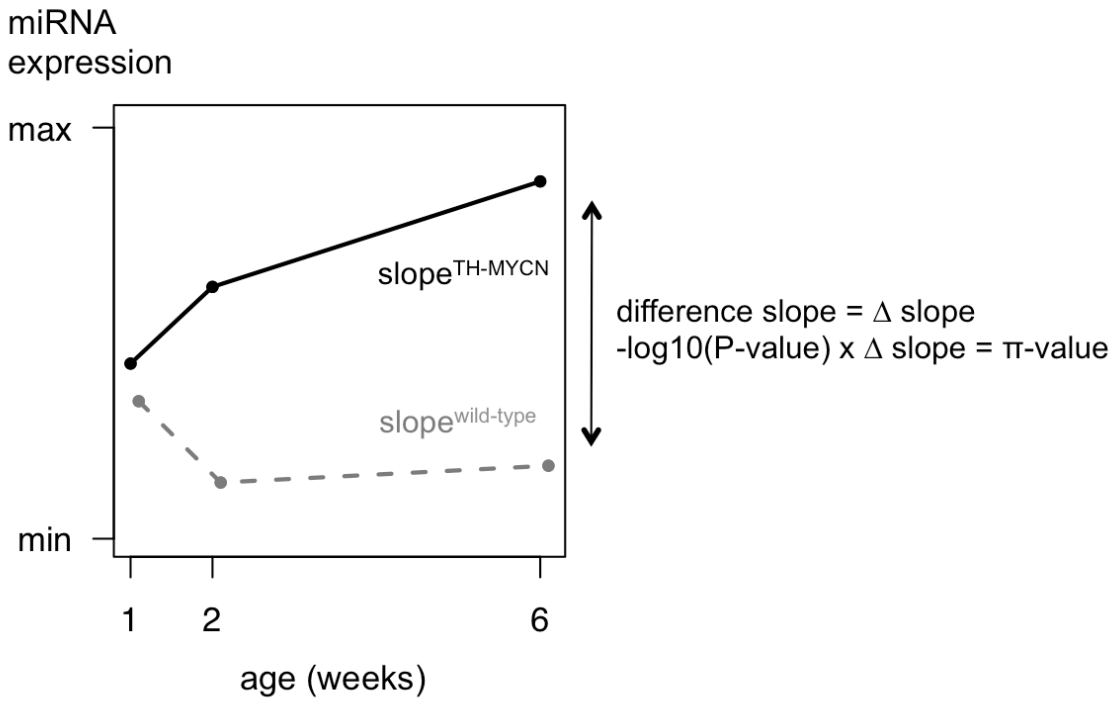

Supplementary Figure 3. Schematic overview of the metrics calculated to study the dynamic miRNA expression changes during neuroblastoma development in the TH-MYCN mouse model. Linear regression analysis was used to calculate the slope of the regression line of miRNA expression in either transgenic (TG; black) or wild-type (WT; gray) samples. The difference between these slopes, Δ slope, is a measure for the difference in dynamic expression pattern: negative Δ slope values are indicative for decreased miRNA expression in TH- MYCN+/+ versus wild-type samples.

Chapter 5

MYCN-driven regulatory mechanisms controlling LIN28B in neuroblastoma

Anneleen Beckers[1], Gert Van Peer[1], Daniel R Carter[2], Moritz Gartlgruber[3], Carl Herrmann[4,5], Saurabh Agarwal[6], Hetty H Helsmoortel[1,7], Kristina Althoff[8,9], Jan J Molenaar[10], Belamy B Cheung[2], Johannes H Schulte[3,8,9,11,12], Yves Benoit[7], Jason M Shohet[6], Frank Westermann[3], Glenn M Marshall[2], Jo Vandesompele[1], Katleen De Preter[1], Frank Speleman[1]

1 Center for Medical Genetics (CMGG), Ghent University, Belgium;
2 Children's Cancer Institute, University of New South Wales, Sydney, Australia;
3 Division of Neuroblastoma Genomics, DKFZ, Heidelberg, Germany;
4 Division of Theoretical Bioinformatics, DKFZ, Heidelberg, Germany;
5 Institute of Pharmacy and Molecular Biotechnology, University of Heidelberg, Germany;
6 Division of Pediatric Hematology-Oncology Baylor College of Medicine, Houston, USA;
Department of Pediatric Hematology-Oncology and Stem Cell Transplantation, Ghent University Hospital, Ghent, Belgium;
Department of Pediatric Oncology and Hematology, University Children`s Hospital Essen, Germany;
German Consortium for Translational Cancer Research (DKTK), Essen, Germany;
Department of Oncogenomics, Academic Medical Center, Amsterdam, Netherlands;
West German Cancer Center (WTZ), University Hospital Essen, Germany;
Centre for Medical Biotechnology, University Duisburg-Essen, Essen, Germany.

Accepted for publication in Cancer Letters

Abstract

LIN28B has been identified as an oncogene in various tumor entities, including neuroblastoma, a childhood cancer that originates from neural crest-derived cells, and is characterized by amplification of the MYCN oncogene. Recently, elevated LIN28B expression levels were shown to contribute to neuroblastoma tumorigenesis via let-7 dependent de-repression of MYCN. However, additional insight in the regulation of LIN28B in neuroblastoma is lacking. Therefore, we have performed a comprehensive analysis of the regulation of LIN28B in neuroblastoma, with a specific focus on the contribution of miRNAs.

We show that MYCN regulates LIN28B expression in neuroblastoma tumors via two distinct parallel mechanisms. First, through an unbiased LIN28B-3'UTR reporter screen, we found that miR-26a-5p and miR-26b-5p regulate LIN28B expression. Next, we demonstrated that MYCN indirectly affects the expression of miR-26a-5p, and hence regulates LIN28B, therefor establishing a MYCN-miR-26a-5p-LIN28B regulatory axis. Second, we provide evidence that MYCN regulates LIN28B expression via interaction with the LIN28B promotor, establishing a direct MYCN-LIN28B regulatory axis. We believe that these findings mark LIN28B as an important effector of the MYCN oncogenic phenotype and underlines the importance of MYCN-regulated miRNAs in establishing the MYCN-driven oncogenic process.

Introduction

The highly conserved RNA-binding proteins LIN28A and LIN28B play important roles in glucose metabolism [1] and during development and stem cell reprogramming by regulating the self-renewal of stem cells [2]. They mediate these pleiotropic functions by modulating the translation of target messenger RNAs (mRNAs) and by inhibiting let-7 microRNA (miRNA) biogenesis – their main mode of action studied. The let-7 family of miRNAs comprises a group of 12 sequence-related miRNAs, encoded by 8 distinct genomic loci. Because these miRNAs regulate multiple stemness regulators and bona fide proto-oncogenes, such as RAS, HMGA2 and MYC, they play an essential role in stem cell differentiation and tumor-suppression. As a consequence, deregulated LIN28A or LIN28B expression contributes to abnormal development and tumorigenesis.

Recently, elevated LIN28B expression levels were shown to contribute to neuroblastoma tumorigenesis via let-7 dependent de-repression of MYCN [3]. Neuroblastoma is a pediatric tumor of the sympathetic nervous system and is characterized by high MYCN activity through genomic amplification, which occurs in about half of high-stage neuroblastoma tumors and marks poor survival. LIN28B is frequently overexpressed in high-risk neuroblastoma, and high-level amplifications of the 6q21 region including the LIN28B gene occur at a low frequency. In addition, increased expression of LIN28B is associated with poor outcome of neuroblastoma patients [3]. This prominent LIN28B expression results in a strong increase in the amount of MYCN protein via repression of the MYCN-targeting let-7 miRNAs, as shown by expression analysis of murine Lin28b-driven tumors and a series of in vitro LIN28B model systems [3].

Increased LIN28B expression in neuroblastoma tumors could be attributed to genomic amplification in only a few samples. Therefore, additional mechanisms are likely to be involved, such as alterations in upstream regulatory pathways as well as transcriptional and post-transcriptional control. Indeed, several miRNAs, including the let-7 family miRNAs, were reported to target the LIN28B 3' untranslated region (3'UTR) [4-8]. Interestingly, also MYCN has been proposed to induce LIN28B transcription [9,10] but other studies could not confirm these findings [3]. Taken together, the present data point at an intimate regulatory interconnection between MYCN and LIN28B, let-7 and possibly also other miRNAs.

In this study, we set about to elucidate the regulation of LIN28B expression in neuroblastoma tumors, with particular focus on the contribution of MYCN and miRNAs. To this end, we performed a comprehensive, genome-wide exploration of the miRNA-LIN28B interactome in neuroblastoma. We combined results from an unbiased and genome-wide high-throughput miRNA target reporter screen with miRNA and mRNA expression data from

200 neuroblastoma patients and identified twelve LIN28B-targeting miRNAs in neuroblastoma. Subsequent integration of the screen results and clinical data from neuroblastoma patients prioritized miR-26a-5p and miR-26b-5p for further analysis. Using different MYCN-driven in vitro and in vivo model systems, we show that MYCN induces the expression of LIN28B via indirect repression of miR-26a-5p and miR-26b-5p. In addition, we provide evidence that MYCN further enhances the expression of LIN28B via direct binding to the LIN28B promoter region. Hence, our findings clarify the role of MYCN and miRNAs in the upstream regulation of LIN28B in neuroblastoma and describe a double feed-forward loop between MYCN and LIN28B.

Results

An unbiased LIN28B 3'UTR-miRNA library screen identifies 28 miRNAs targeting LIN28B

Potential interactions of 470 miRNAs with the 3'UTR of LIN28B were assayed in a high-throughput luciferase reporter screen. In brief, human embryonic kidney cells (HEK293T) were co-transfected with a reporter construct, containing the LIN28B 3'UTR downstream of a luciferase reporter gene, and each of the individual miRNA mimics from a 470 miRNA mimic library. Based on the relative luciferase activities in two independent screens (**Supplementary Figure 5.1**), a robust z-score was calculated for each miRNA-LIN28B combination (see Material and Methods). Applying this strategy, we identified 28 miRNAs with a high probability of targeting LIN28B (average robust z-score score < -3.05; see Material and Methods; **Figure 5.1a** and **Supplementary Table 5.1**). According to miRTarBase 4.0, an experimentally validated microRNA-target interactions database [11], scientific literature holds weak (n = 8) [4,5,12] or strong (n = 2) [6,7,13] evidence for 10 miRNAs as regulator of LIN28B. Both miRNAs with strong evidence to target LIN28B, let-7b-5p and miR-125b-5p, were validated in our screen (**Figure 5.1a**, red), whereas only 3 out of 8 miRNAs with weak evidence to target LIN28B, let-7d-5p, miR-125a-5p and miR-484, could be confirmed (**Figure 5.1a**, blue). Additionally, 23 new LIN28B targeting miRNAs were identified, of which 14 are predicted to target LIN28B by MirTarget2 [14] (**Supplementary Table 5.1**), underscoring the value of our screening method to detect novel, predicted as well as non-predicted, miRNA-target gene interactions. Among the strongest hits in the screens, a significant enrichment was observed for miRNAs with seed-matched sites present in the LIN28B 3'UTR (**Figure 5.1b**), thus further underscoring the sensitivity and robustness of the 3'UTR-miRNA library screen.

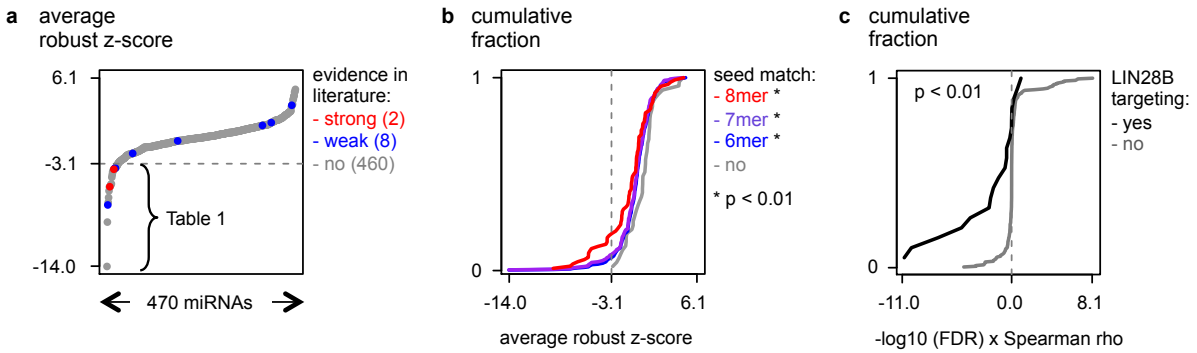

Figure 5.1: An unbiased MYCN 3'UTR-miRNA library screen identifies 29 miRNAs potentially targeting MYCN. (a) Average interaction scores are plotted (Y-axis) for 470 tested miRNAs (X-axis). The 29 miRNAs with an interactions core of < -1.94 are listed in Figure 5.2A. The 11 interactions that have been reported in literature, are indicated in black. **(b)** Cumulative distributions (Y-axis) of the interaction scores (X-axis) of miRNAs that respectively have 6-, 7- or 8-mer seed-matches in the MYCN 3'UTR.

miR-26a-5p and miR-26b-5p are top candidate LIN28B-targeting miRNAs in neuroblastoma

miRNAs are known to regulate their target genes in a highly tissue- and cell type specific manner [15]. As the LIN28B 3'UTR-miRNA library screens were performed in HEK293T cells, we next aimed to identify miRNAs specifically targeting LIN28B in neuroblastoma cells by integrating the obtained screen results with miRNA expression data from a large cohort primary neuroblastoma tumors We reasoned that the expression of a LIN28B-targeting miRNA is inversely correlated to LIN28B mRNA expression levels in primary tumor samples. Of the 19 LIN28B-targeting miRNAs that were included on the human miRNA expression platform, 12 miRNAs showed significant inverse correlation to LIN28B mRNA expression (**Table 5.1**), suggesting that they can indeed downregulate LIN28B expression in primary neuroblastoma tumors. In addition, three of the 19 LIN28B-targeting miRNAs that were included on the human miRNA expression platform were positively correlated to MYCN expression (**Table 5.1**). Overall, LIN28B targeting miRNAs identified in our screen showed stronger inverse correlation to LIN28B mRNA levels compared to non-targeting miRNAs (**Figure 5.1c**), as indicated by a shift of the cumulative distribution of π-values (-log10 p-value x Pearson correlation coefficient) to more negative values.

Next, we reasoned that miRNAs with a putative tumor suppressive role in neuroblastoma are lower expressed in more aggressive neuroblastoma tumors. Therefore, we assessed the relationship between expression of the LIN28B-targeting miRNAs and the outcome of high-risk neuroblastoma patients (International Neuroblastoma Staging System stage 4, n = 92). For three LIN28B-targeting miRNAs, miR-26a-5p, miR-26b-5p and miR-125b-5p, low expression is associated with poor outcome (**Figure 5.2a-b** and **Supplementary Fig 5.2**).

Table 5.1: Overview of 28 LIN28B-targeting miRNAs, categorized according to LIN28B-targeting potential in primary neuroblastoma tumors. LIN28B-targeting miRNAs are filtered for their relevance in neuroblastoma according to significant negative correlation to LIN28B expression in a neuroblastoma patient cohort. In total, 12 out of 28 miRNAs show negative correlation to LIN28B expression and are considered to be relevant for neuroblastoma, while 3 out of 28 miRNAs show positive correlation to LIN28B expression. Four miRNAs lack correlation to LIN28B expression (n.s.: not significant, Spearman correlation, Benjamini & Hochberg multiple testing corrected p-value > 0.05), and for 9 miRNAs no expression data was available (n.d.: no data available). In addition, of the 15 miRNAs showing correlation to LIN28B expression, the expression of 3 miRNAs is associated to poor outcome of stage 4 neuroblastoma patients (n = 92). n.s.: not significant (log-rank test, p-value > 0.05)

miRNA	mirBase Accession	Reference	Spearman rho	log-rank OR
miRNA's with negative correlation to LIN28B expression				
hsa-let-7a-5p	MIMAT0000062		-0.35	n.s.
hsa-let-7b-5p	MIMAT0000063	[6,8]	-0.36	n.s.
hsa-let-7c-5p	MIMAT0000064		-0.23	n.s.
hsa-let-7d-5p	MIMAT0000065	[4]	-0.59	n.s.
hsa-let-7f-5p	MIMAT0000067		-0.45	n.s.
hsa-let-7g-5p	MIMAT0000414		-0.54	n.s.
hsa-let-7i-5p	MIMAT0000415		-0.60	n.s.
hsa-miR-125b-5p	MIMAT0000423	[7]	-0.25	14.43
hsa-miR-26a-5p	MIMAT0000082		-0.37	12.48
hsa-miR-26b-5p	MIMAT0000083		-0.31	13.00
hsa-miR-363-3p	MIMAT0000707		-0.23	n.s.
hsa-miR-98-5p	MIMAT0000096		-0.49	n.s.
miRNA's with positive correlation to LIN28B expression				
hsa-miR-516b-3p	MIMAT0002860		0.17	n.s.
hsa-miR-550a-3p	MIMAT0003257		0.28	n.s.
hsa-miR-641	MIMAT0003311		0.29	n.s.
miRNA's without correlation to LIN28B expression				
hsa-let-7e-5p	MIMAT0000066		n.s.	-
hsa-miR-125a-5p	MIMAT0000443	[5]	n.s.	-
hsa-miR-367-3p	MIMAT0000719		n.s.	-
hsa-miR-383-5p	MIMAT0000738		n.s.	-
miRNA's with missing data				
hsa-miR-182-3p	MIMAT0000260		n.d.	-
hsa-miR-208a-3p	MIMAT0000241		n.d.	-
hsa-miR-484	MIMAT0002174	[5]	n.d.	-
hsa-miR-499a-5p	MIMAT0002870		n.d.	-
hsa-miR-552-3p	MIMAT0003215		n.d.	-
hsa-miR-561-3p	MIMAT0003225		n.d.	-
hsa-miR-569	MIMAT0003234		n.d.	-
hsa-miR-605-5p	MIMAT0003273		n.d.	-
hsa-miR-92b-3p	MIMAT0003218		n.d.	-

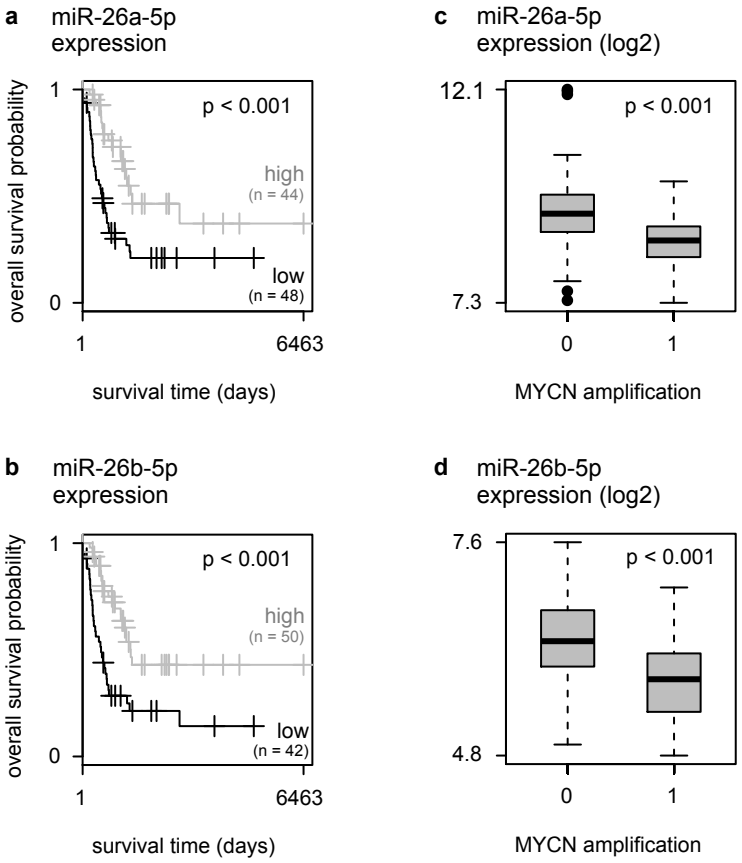

Figure 5.2: miR-26a-5p and miR-26b-5p are top candidate LIN28B-targeting miRNAs in neuroblastoma. (a) Kaplan-Meier curves for miR-26a-5p in a cohort of primary neuroblastoma tumors. Patients are split in two groups with either miR-26a-5p expression above (= high) or below (= low) the average miR-26a-5p expression. Log-rank test, OR = 12.48, p = 2.4 x 10^{-3}. **(b)** Kaplan-Meier curves for miR-26b-5p in a cohort of primary neuroblastoma tumors. Patients are split in two groups with either miR-26b-5p expression above (= high) or below (= low) the average miR-26b-5p expression. Log-rank test, OR = 13.00, p = 1.4 x 10^{-3}. **(c)** Expression (log2) of miR-26a-5p in primary neuroblastoma tumors with MYCN amplification (= 1) versus tumors without MYCN amplification (= 0). T-test, p = 4.3 x 10^{-7}. **(d)** Expression (log2) of miR-26b-5p in primary neuroblastoma tumors with MYCN amplification (= 1) versus tumors without MYCN amplification (= 0). T-test, p = 1.9 x 10^{-6}.

In addition, two miRNAs, miR-26a-5p and miR-26b-5p, were previously reported to be lower expressed in neuroblastoma tumors with MYCN amplification, a marker of aggressive neuroblastoma (**Figure 5.2c-d**) [16]. These observations highlight miR-26a-5p and miR-26b-5p as interesting candidate regulators of LIN28B in neuroblastoma.

Overexpression of miR-26a-5p or miR-26b-5p reduces LIN28B expression

Following the selection of miR-26a-5p and miR-26b-5p as candidate miRNAs in the context of neuroblastoma, we assessed whether these miRNAs regulate LIN28B expression levels in the neuroblastoma cell line NGP. As expected from the luciferase reporter screen, overexpression of either miR-26a-5p or miR-26b-5p induced downregulation of LIN28B expression levels compared with a non-targeting miRNA control (**Figure 5.3a**).

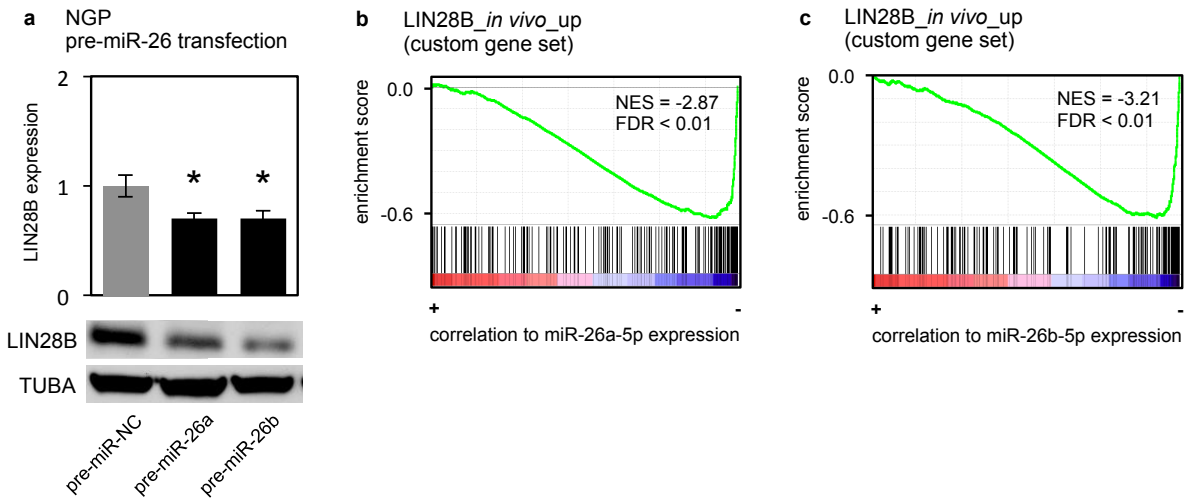

Figure 5.3. Overexpression of miR-26a-5p or miR-26b-5p reduces LIN28B expression. (a) mRNA (upper panel) and protein (lower panel) expression of LIN28B upon overexpression of miR-26a-5p or miR-26b-5p in NGP cells. T-test, pre-miR-26a: $p = 2.7 \times 10^{-2}$; pre-miR-26b: $p = 3.5 \times 10^{-2}$. **(b-c)** Result of GSEA. Red-blue color bars denote genes ranked based on correlation to miR-26a-5p **(b)** or miR-26b-5p **(c)** expression in primary neuroblastoma tumors (n = 200). Each vertical bar corresponds to genes upregulated in LSL-LIN28B tumors vs. normal adrenal glands. The green line represents the running enrichment score calculated in GSEA.

Finally, we investigated whether the functions of these miRNAs in neuroblastoma are related to the functions of LIN28B using a Gene Set Enrichment Approach (GSEA). To this end, we first constructed a gene set of genes upregulated by LIN28B in the LSL-Lin28b mouse model [3]. This gene set contains 256 genes that are significantly upregulated in LSL-Lin28B tumors compared to normal adrenal glands. Next, we calculated the Spearman correlation coefficient between the expression of miR-26a-5p or miR-26b-5p and all mRNAs expressed in a large cohort of primary neuroblastoma tumors (n = 200). Finally, we performed GSEA on these ranked lists to assess the enrichment of LIN28B regulated genes among the genes negatively correlated with miR-26a-5p or miR-26b-5p expression in primary neuroblastoma tumors. As expected for miRNAs that regulate the expression of LIN28B, the GSEA analysis for both miRNAs results in strong negative enrichment for the LSL-Lin28b gene set (**Figure 5.3b-c**). This suggests that the functions miR-26a-5p and miR-26b-5p in neuroblastoma are strongly related to those of LIN28B. Hence, the putative tumor-suppressors miR-26a-5p and miR-26b-5p affect the LIN28B expression levels in neuroblastoma and show inverse correlation to LIN28B-induced gene expression patterns.

miR-26a-5p and miR-26b-5p are downregulated in MYCN-driven neuroblastoma

Given the decreased expression of miR-26a-5p and miR-26b-5p in neuroblastoma tumors with MYCN amplification as compared to neuroblastoma tumors that lack MYCN amplification [16], we sought to investigate whether miR-26a-5p and miR-26b-5p were regulated by the oncoprotein MYCN.

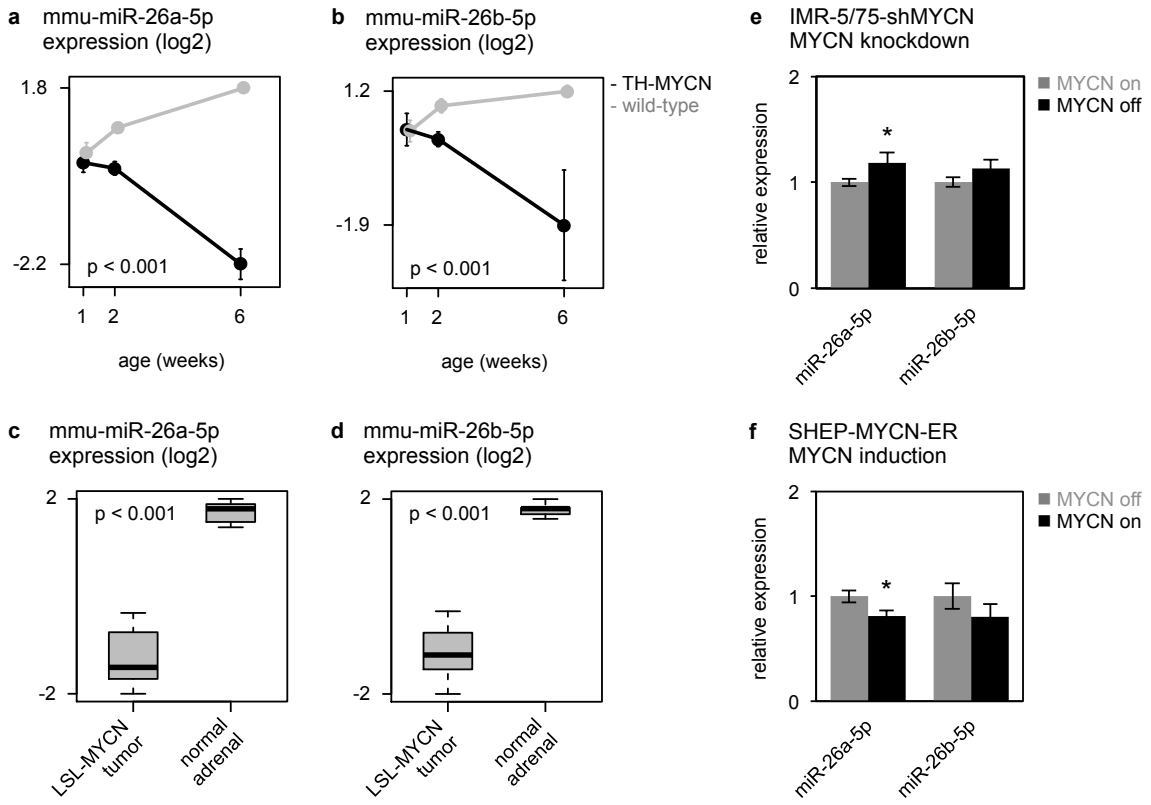

Figure 5.4. miR-26a-5p and miR-26b-5p are downregulated in MYCN-driven neuroblastoma. (a-b) Expression (log2) of mmu-miR-26a-5p **(a)** and mmu-miR-26b-5p **(b)** in sympathetic ganglia containing hyperplastic lesions, and advanced tumors from TH-MYCN+/+ mice at, respectively, 1 and 2 weeks and 6 weeks of age (black), and in normal sympathetic ganglia from wild-type mice at 1, 2 and 6 weeks of age (gray). Data are presented as mean ± standard deviation of four samples. Two-way ANOVA interaction, mmu-miR-26a-5p: $p = 6.2 \times 10^{-13}$; mmu-miR-26b-5p: $p = 1.1 \times 10^{-5}$. **(c-d)** Expression of miR-26a-5p **(c)** and miR-26b-5p **(d)** in LSL-MYCN tumors compared to normal adrenal tissue. T-test, miR-26a-5p: $p = 7.6 \times 10^{-10}$; miR-26b-5p: $p = 8.0 \times 10^{-10}$. **(e)** Relative expression of miR-26a-5p and miR-26b-5p in IMR-5/75-shMYCN cells before (gray bars) and after (black bars) silencing of MYCN. Data are presented as mean ± standard deviation of three replicate experiments. T-test, miR-26a-5p: $p = 0.041$; miR-26b-5p: $p > 0.05$. **(f)** Relative expression of miR-26a-5p and miR-26b-5p in SHEP-MYCN-ER cells before (gray bars) and after (black bars) activation of MYCN. Data are presented as mean ± standard deviation of three replicate experiments. T-test, miR-26a-5p: $p = 0.041$; miR-26b-5p: $p > 0.05$.

To this end, we evaluated the expression of both miRNAs in MYCN-driven neuroblastoma models. First, we interrogated a murine neuroblastoma progression model, consisting of pre-tumorigenic lesions and advanced neuroblastoma tumors from the TH-MYCN+/+ mouse model, in combination with matching reference tissue from wild-type mice. Both miR-26a-5p and miR-26b-5p expression strongly decreased during TH-MYCN+/+ neuroblastoma development as compared to normal development (**Figure 5.4a-b**). Next, these results were confirmed in a second, independent, murine MYCN-driven neuroblastoma model, the LSL-MYCN;Dbh-iCre model [17] – further referred to as the LSL-MYCN model – as both miRNAs were found to be lower expressed in LSL-MYCN tumors compared to normal adrenal tissue (**Figure 5.4c-d**).

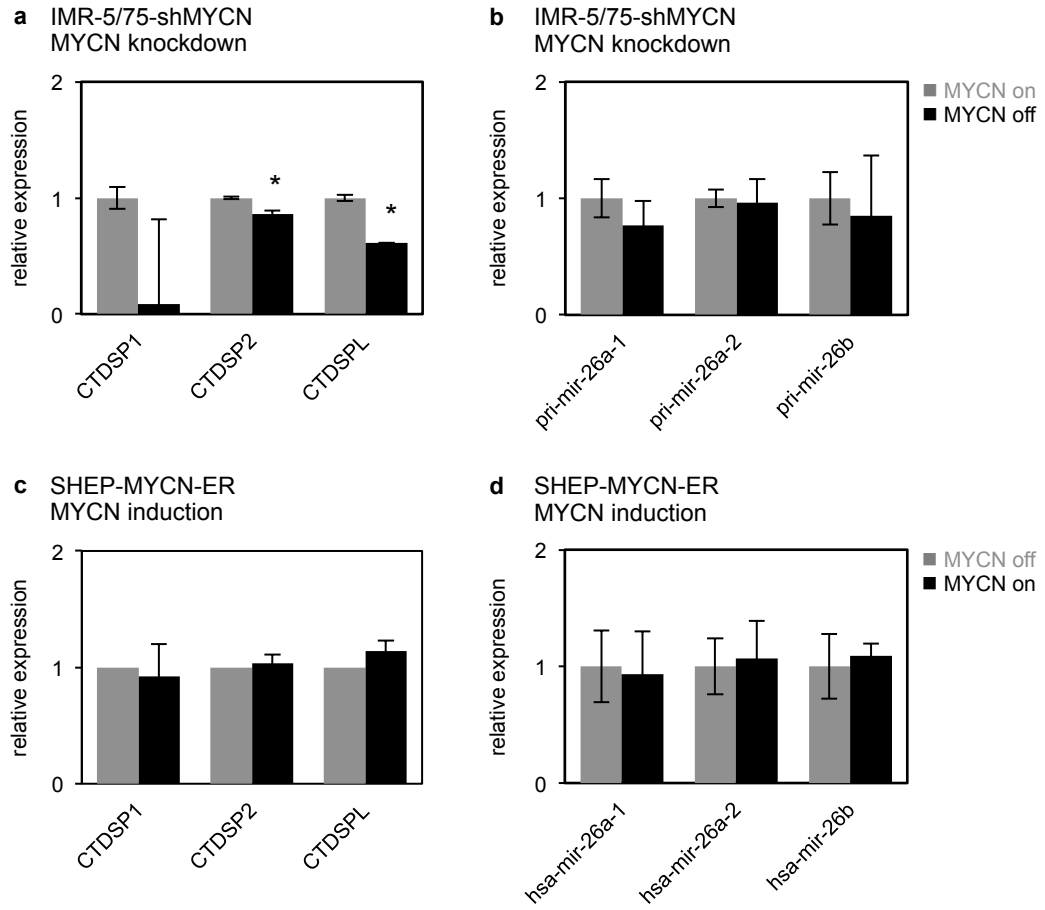

Figure 5.5. MYCN does not inhibit transcription of pri-mir-26a-1, pri-mir-26a-2 or pri-mir-26b in neuroblastoma cells. (a) Relative expression of pri-mir-26a-1, pri-mir-26a-2 and pri-mir-26b in IMR-5/75-shMYCN cells before (gray bars) and after (black bars) silencing of MYCN. Data are presented as mean ± standard deviation of three replicate experiments. T-test, pri-mir-26a-1: $p > 0.05$; pri-mir-26a-2: $p > 0.05$; pri-mir-26b: $p > 0.05$. **(b)** Relative expression of CTDSP1, CTDSP2 and CTDSPL in IMR-5/75-shMYCN cells before (gray bars) and after (black bars) silencing of MYCN. Data are presented as mean ± standard deviation of three replicate experiments. T-test, CTDSP1: $p > 0.05$; CTDSP2: $p = 6.2 \times 10^{-3}$; CTDSPL: $p = 6.2 \times 10^{-5}$. **(c)** Relative expression of pri-mir-26a-1, pri-mir-26a-2 and pri-mir-26b in SHEP-MYCN-ER cells before (gray bars) and after (black bars) induction of MYCN activity. Data are presented as mean ± standard deviation of three replicate experiments. T-test, pri-mir-26a-1: $p > 0.05$; pri-mir-26a-2: $p > 0.05$; pri-mir-26b: $p > 0.05$. **(d)** Relative expression of CTDSP1, CTDSP2 and CTDSPL in SHEP-MYCN-ER cells before (gray bars) and after (black bars) induction of MYCN activity. Data are presented as mean ± standard deviation of three replicate experiments. T-test, CTDSP1: $p > 0.05$; CTDSP2: $p > 0.05$; CTDSPL: $p > 0.05$.

To verify that the decreased expression of miR-26a-5p and miR-26b-5p in these in vivo models is a consequence of increased MYCN activity, we evaluated the expression of both miRNAs in multiple in vitro models of MYCN activity in neuroblastoma. First, the effect of MYCN knockdown on miRNA expression was evaluated in the IMR5-75-shMYCN model system. These cells stably express a tetracycline-inducible MYCN shRNA that, upon induction, reduced MYCN protein to 44% (**Supplementary Figure 5.3**) [18]. We observed a modest but significant increase in the expression of miR-26a-5p upon silencing of MYCN, while the expression of miR-26b-5p did not change (**Figure 5.4e**). Next, we assessed the effect of MYCN activation in the SHEP-MYCN-ER cell line. Here, miR-26a-5p expression

level was decreased by 20% (**Figure 5.4f**) upon 4-hydroxy-tamoxifen-mediated activation of the MYCN-ER fusion protein, whereas, again, no significant regulation of miR-26b-5p expression levels was observed (**Figure 5.4f**). Together these in vivo and in vitro data support the hypothesis that MYCN could regulate the expression of miR-26a-5p in neuroblastoma cells. Furthermore, these data show that miR-26b-5p is downregulated during murine MYCN-driven neuroblastoma development; however, they do not provide evidence that this is a direct consequence of MYCN activity.

MYCN does not inhibit transcription of primary mir-26 transcripts in neuroblastoma cells

Both miR-26a-5p and miR-26b-5p are intronic miRNAs that are transcribed from three genomic regions, residing within the introns of three coding genes: CTDSP1, CTDSP2 and CTDSPL, host genes of mir-26b, mir-26a-2 and mir-26a-1 respectively; both mir-26a-1 and mir-26a-2 are processed into the mature miR-26a-5p. In order to evaluate whether transcriptional activity of MYCN directly regulates miR-26a-5p and miR-26b-5p, we measured the expression of the primary miRNA transcripts and the host genes in the IMR-5/75-shMYCN and SHEP-MYCN-ER cell lines. Knockdown of MYCN in IMR-5/75-shMYCN cells resulted in decreased expression of miR-26a-5p host genes CTDSP2 and CTDSPL, but did not affect the expression of pri-mir-26 transcripts (**Figure 5.5a-b**). Induction of MYCN activity in the SHEP-MYCN-ER cells, did not affect miR-26 host gene expression levels, nor the expression of the pr-mir-26 transcripts (**Figure 5.5c-d**). These data suggest that downregulation of miR-26a-5p by MYCN in neuroblastoma cells is not the consequence of transcriptional silencing of mir-26a-1 or mir-26a-2.

MYCN induces LIN28B expression in neuroblastoma cells

Given that MYCN affects the expression levels of miR-26a-5p, and that both miR-26a-5p and miR-26b-5p regulate the expression of LIN28B, we postulated that MYCN affects LIN28B expression in neuroblastoma cells. To investigate this premise, we measured the effect of MYCN activation and silencing on LIN28B mRNA and protein expression in the above-mentioned in vitro models. In the SHEP-MYCN-ER cell line, LIN28B expression increased by 1.7-fold 48h upon activation of MYCN (**Figure 5.6a**). Correspondingly, knockdown of MYCN resulted in a 2-fold decrease in LIN28B expression levels (**Figure 5.6b**). In addition, we evaluated the relationship between MYCN and LIN28B expression levels in the murine MYCN-driven model systems.

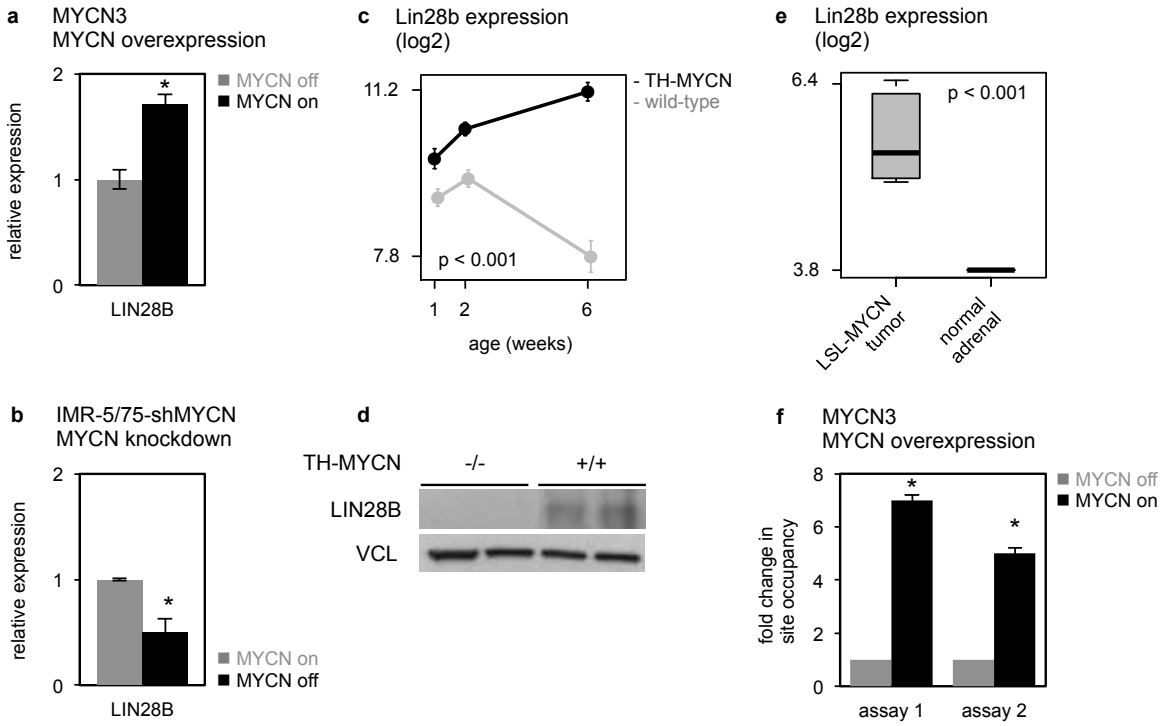

Figure 5.6. MYCN induces LIN28B expression in neuroblastoma cells. (a) Relative expression of LIN28B in SHEP-MYCN-ER cells before (gray bars) and after (black bars) induction of MYCN activity. Data represent average fold change of three independent biological replicates +/- standard deviation. T-test, $p = 4.2 \times 10^{-3}$. **(b)** Relative expression of LIN28B in IMR-5/75-shMYCN cells before (gray bars) and after (black bars) silencing of MYCN. Data are presented as mean ± standard deviation of three replicate experiments T-test, $p = 5.7 \times 10^{-3}$. **(c)** Lin28b expression (log2) in sympathetic ganglia containing hyperplastic lesions, and advanced tumors from TH-MYCN+/+ mice at, respectively, 1 and 2 weeks and 6 weeks of age (black), and in normal sympathetic ganglia from wild-type mice at 1, 2 and 6 weeks of age (gray). Data are presented as mean ± standard deviation of four samples. Two-way ANOVA, interaction $p = 1.9 \times 10^{-8}$. **(d)** Lin28b protein levels in advanced tumors from TH-MYCN+/+ mice at 6 weeks of age (indicated as "+/+"), and in normal sympathetic ganglia from wild-type mice at 6 weeks of age (indicated as "-/-"). **(e)** MYCN ChIP was performed on MYCN3 cell line either doxycycline treated (MYCN high) or untreated (MYCN low). Two assays (Supplementary Table 5) for MYCN binding site at LIN28B promoter was designed by analyzing MYCN ChIP-Sequencing database. Negative control IgG ChIP and Input material was also analyzed and used for normalizing the MYCN ChIP data. Two sets of control primers were used to confirm the specificity of immunoprecipitated genomic DNA. Fold enrichment in site occupancy was calculated by comparing normalized MYCN ChIP Cq values between treatments. ChIP-qPCR reactions were performed in triplicates and represented here as mean ± SEM. T-test, $p < 0.001$.

As expected from the *in vitro* data, LIN28B mRNA expression levels strongly increased during MYCN-driven murine neuroblastoma development in the TH-MYCN+/+ model compared to normal development (**Figure 5.6c**). Accordingly, we detected LIN28B protein in murine neuroblastoma tumors, whereas expression was absent in wild-type sympathetic ganglia (**Figure 5.6d**). In addition, LSL-MYCN tumors were characterized by 1.8-fold higher LIN28B mRNA levels as compared to normal adrenal tissue (**Figure 5.6e**). Finally, LIN28B expression showed significant correlation to MYCN expression in a large cohort of primary neuroblastoma tumors (n = 200) from different clinical stages (**Supplementary Figure 5.4a**) and was higher expressed in MYCN amplified neuroblastoma tumors (n = 40) versus MYCN non-amplified tumors (n = 160) (**Supplementary Figure 5.4b**).

Thus far, our study supports a mechanistic model in which MYCN can enhance LIN28B expression in neuroblastoma via indirect repression of miR-26a-5p, which regulates LIN28B expression levels. Several studies, however, have reported that MYC, a family member of MYCN, can directly induce LIN28B expression via binding to an E-box sequence in its promoter region [19,20], and a similar mode of action for MYCN has been proposed [9,21]. To verify whether MYCN indeed binds the LIN28B promoter region and activates its transcription, we have evaluated direct interaction in the MYCN3 cell line, a neuroblastoma model of doxycycline-inducible MYCN overexpression. Here, overexpression of MYCN resulted in a 1.7-fold increase in LIN28B expression levels (**Supplementary Figure 5.5**) and a > 5-fold increase in LIN28B promoter occupancy by MYCN as demonstrated by ChIP-qPCR with two independent assays (**Figure 5.6f**). Together these data support an additional mechanistic model in which MYCN enhances LIN28B expression via induction of LIN28B transcription through direct promoter interaction.

Discussion

The elucidation of the LIN28B–let-7–MYCN axis in neuroblastoma and its role in sustaining proliferation and cell viability and suppression of differentiation of neuroblasts, offered exciting insights in MYCN-regulating pathways in neuroblastoma [3]. However, little is known about the regulation of LIN28B expression in neuroblastoma. Given the importance of miRNAs in regulating key oncogenes [22,23], we believe that the contribution of miRNAs to the regulation of LIN28B in neuroblastoma is underexplored. Here, we report on the first unbiased and genome-wide high-throughput miRNA target reporter screen to identify miRNAs targeting LIN28B. From the total of 28 LIN28B-targeting miRNAs identified in this study, 23 interactions were novel, whereas 5 out of 8 previously established LIN28B-targeting miRNAs were confirmed (**Table 5.1**). Subsequent filtering of the screen results through clinical data of neuroblastoma patients highlighted two miRNAs, miR-26a-5p and miR-26b-5p, for their potential tumor suppressive activity in neuroblastoma. To our knowledge, these miRNAs have not been associated to neuroblastoma tumor biology before.

The most studied LIN28B-targeting miRNAs are the let-7 family members [32]. In our 3'UTR library screen, we identified all let-7 family members as LIN28B-targeting miRNAs. Moreover, these miRNAs displayed negative correlation to LIN28B expression levels in primary neuroblastoma tumors (**Table 5.1**), thus confirming previous data and validating our 3'UTR library screen. However, in contrast to both miR-26a-5p and miR-26b-5p, the let-7

family members did not show association to patient outcome in a cohort of aggressive neuroblastoma tumors.

We revealed that induction or knockdown of MYCN activity in vitro respectively represses or induces the expression of miR-26a-5p, and that both miR-26a-5p and miR-26b-5p show decreased expression levels in murine MYCN-driven mouse tumors. The observed effects of MYCN perturbation on miR-26a-5p expression levels are modest (~ 20%); this could raise questions regarding the relevance of such regulation. However, it has been suggested that the capability of miRNAs to regulate multiple targets within the same pathway can amplify their biological effects [24]. As a result, even relatively small changes in miRNA expression may be biologically significant [25,26]. Therefore, it is our opinion that MYCN does affect the expression levels of miR-26a-5p and that this regulation could have significant biological consequences. However our observations do not fully support the regulation of miR-26b-5p expression levels: we observed no significant changes in miR-26b-5p expression levels upon perturbation of MYCN expression in in vitro models. Additional experimentation in cell culture systems may be useful to identify the exact role of miR-26b-5p in the proposed regulatory network.

Several reports have demonstrated that MYC, a MYCN family member, is capable of down-regulating expression of miR-26a-5p and miR-26b-5p in breast cancer [27] and hepatocellular carcinoma [28]. For miR-26a-5p, it has been demonstrated that this down-regulation occurs through a cooperative effect of MYC and EZH2 and the promoter region of its host genes CTDSPL (mir-26a-1 host gene) and CTDSP2 (mir-26a-2 host gene) in aggressive lymphomas [29]. However, our data do not support a similar mode of action in neuroblastoma as we did not observe direct regulation of the primary mir-26a-1, mir-26a-2 nor the mir-26b transcript by MYCN. This observation indicates that regulation of miR-26a-5p by MYCN is rather in keeping with an indirect mechanism, possibly via regulation of genes that contribute to or inhibit the stability of miR-26a-5p. For instance, nuclear modifiers that recognize unique motifs on pre-miR-26a can regulate the export of pre-miR-26a. If pre-miR-26a cannot be exported into cytoplasm and is retained in the nucleus, mature miR-26a-5p cannot be produced. Alternatively, Dicer processing can be blocked by cytoplasmic modifiers that bind to pre-miR-26a, or, as in the case of pre-let-7 regulation, Dicer processing efficiency can be decreased by TUT-mediated uridylation [30]. The discrepancy between pri-mir-26 and mature miR-26 levels may also result from the turnover rate of mature miR-26a-5p. Mature miRNAs have been thought to be very stable. However, studies have shown that extracellular signals can induce the rapid degradation of specific miRNAs [31,32]. Unknown modifiers may work on mature miR-26a-5p to affect its stability.

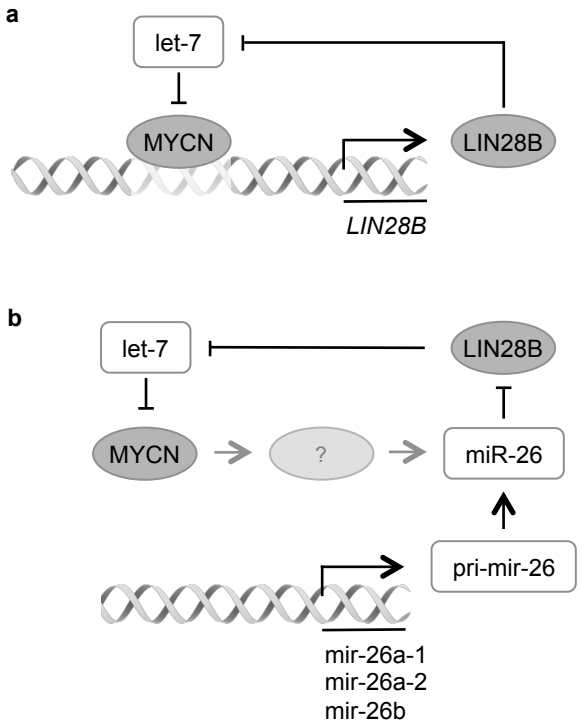

Figure 5.7. Proposed working hypothesis for the regulation of LIN28B in neuroblastoma. (a) MYCN enhances the expression of LIN28B via direct binding at the LIN28B promoter region. In turn, LIN28B inhibits the processing of the let-7 miRNAs, which results in loss of MYCN repression [3]. **(b)** MYCN indirectly represses the expression of miR-26a-5p via an unknown factor, indicated as "?". Reduced miR-26a-5p expression levels results in increased LIN28B expression, which again, in turn, inhibits the processing of the let-7 miRNAs, resulting in loss of MYCN repression [3].

Finding such modifiers of miR-26a-5p will be instrumental in understanding the nature of miR-26a-5p regulation. Further experimentation in cell culture systems may be useful to identify miR-26a-5p post-transcriptional regulators.

Our LIN28B-3'UTR library screen and subsequent validation experiments showed that miR-26a-5p regulate LIN28B expression levels in neuroblastoma. In addition, we showed that MYCN activation, both *in vitro* and *in vivo*, leads to decreased miR-26a-5p and increased LIN28B expression levels. From these observations, we concluded that MYCN can regulate LIN28B expression levels via indirect repression of miR-26a-5p. However, we further showed that MYCN regulates LIN28B mRNA levels via a second mechanism: MYCN can directly control LIN28B expression thorough binding of its promoter as shown by ChIP-analysis. This result is not unexpected as it had been reported that MYC induces LIN28B expression levels in B-cell lymphoma [19], while induction of LIN28B expression by MYCN in neuroblastoma had been suggested by several additional reports [9,21].

In conclusion, our integrated analyses uncovered a double regulatory feed-forward loop, enhancing the expression of both LIN28B and MYCN in neuroblastoma. The proposed molecular model consists of two alternative paths that are probably not mutually exclusive,

but appear to differ between different cellular contexts, such as the different model systems analyzed here. The shortest path involves direct regulation of LIN28B by MYCN through binding at its promoter region (**Figure 5.7a**). Subsequent induction of LIN28B expression results in reduced levels of mature let-7 miRNAs due to inhibition of miRNA processing by LIN28B. Finally, reduced let-7 levels results in loss of MYCN repression, which closes the proposed loop. The second path involves an intermediate step where MYCN indirectly represses the expression of the LIN28B-targeting miRNA miR-26a-5p (**Figure 5.7b**). Again, subsequent induction of LIN28B expression results in reduced levels of mature let-7 miRNAs due to inhibition of miRNA processing by LIN28B.

Understanding this regulatory mechanism upstream of LIN28B in neuroblastoma can open new perspectives for targeting the MYCN-LIN28B pathway in neuroblastoma tumors, a strategy that holds great promise. Moreover, the identification of additional target genes of the miRNAs in the described LIN28B-miRNA interactome might prove useful in the search for novel therapeutic targets.

Methods

LIN28B 3'UTR-miRNA library screen

Since the wild-type LIN28B (ENST00000345080, Ensemble release 78) 3' UTR is longer than 3.5kb, GeneCopoeia (Rockville, MD, U.S.A) provided the UTR into two constructs with overlapping sequence; further referred to as construct A (1 - 3084bp, catalog number: HmiT010363a-MT01) and construct B (2905 - 4548bp, catalog number: HmiT010363b-MT01). HEK293T cells were seeded at a density of 1x104 cells/well in 96-well plates. Twenty-four hours after seeding, cells were co-transfected with 100 ng of one of the two LIN28B reporter vectors and 20 ng of pRL-TK control vector containing the Renilla luciferase gene (Promega, Madison, WI, USA) together with a library of 470 miRNA mimics (2.5 pmol) (Ambion's Pre-miR miRNA Precursor Library - Human V3, design based on miRBase v9.2 with exclusion of hsa-miR-122a; Life Technologies, Carlsbad, CA, USA). Lipid based transfections were performed using 0.4 µl Dharmafect Duo reagent (GE Dharmacon, Lafayette, CO, USA). Forty-eight hours post-transfection, luciferase reporter gene activities were assayed using the Dual-Luciferase Reporter assay system (Promega) according to the manufacturer's protocol with minor changes (LARII and Stop & Glo buffer volumes were reduced to 50 µl). Firefly reporter gene activities were normalized to Renilla values and then log-transformed. Subsequently, robust z-scores were calculated; the robust z-score is a variation of the outlier-sensitive z-score that substitutes the outlier-insensitive median and

median absolute deviation (MAD) for mean and standard deviation in the z-score calculation. In order to determine the robust z-score cutoff that separates interactions from non-interactions, the scores for a set of validated miRNA interactions, probed in the LIN28B screen and in 36 analogous screens (of 17 cancer and disease associated genes), were used together with the scores for a set of negative control interactions from an empty-3'UTR vector miRNA library screen to perform ROC-curve analysis and determine the point of highest accuracy (z-score = -3.05, specificity = 97%, sensitivity = 31%, accuracy = 86%). LIN28B 3'UTR-miRNA library screen results were replicated in two independent experiments for both reporter constructs. To allow for correct integration of miRNA data, we used miRBase Tracker, an in-house developed web tool for miRNA reannotation [33], to re-annotate the miRNAs in the miRNA mimic library to the most up-to-date annotation at time of publication (miRBase release 21) (Supplementary Table 2).

miRNA target analysis

Potential miRNA target sites in the LIN28B 3'UTR were identified as reported previously [34]. In addition, miRNAs targeting LIN28B were predicted using the MirTarget2 algorithm [35].

miRNA and mRNA expression in patient cohort

200 primary tumor samples of neuroblastoma patients were collected prior to therapy at the Ghent University Hospital (Ghent, Belgium), the University Children's Hospital Essen (Essen, Germany), the Hospital Clínico Universitario (Valencia, Spain), the Academic Medical Center (University of Amsterdam, Netherlands) and the National Children's Research Centre (Dublin, Ireland). Informed consent was obtained from the patients' relatives. mRNA data from 75 primary neuroblastoma tumors is available at the Gene Expression Omnibus (http://www.ncbi.nlm.nih.gov/geo; Accession Number: GSE32664). Correlation of miRNA expression levels and LIN28B mRNA levels was evaluated with Spearman's rank correlation coefficient.

Tissue culture

Human neuroblastoma cell lines were cultured in RPMI 1640 medium (Invitrogen, Waltham, MA, USA) supplemented with fetal bovine serum (10%), kanamycin (1%), penicillin/streptomycin (1%), L-glutamine (1%) and HEPES (25mM) (Life Technologies). Cells were kept at 37°C in a 5% C02 / 95 %02 humidified environment. Cell line authenticity was validated by Short Tandem Repeat (STR) genotyping prior to performing the described experiments. Experiments with the IMR5-75-shMYCN, SHEP-MYCN-ER and MYCN3 cell

lines were performed as previously published [18,36,37]. In all cases, three replicate experiments were performed and analyzed.

RT-qPCR

Total RNA was isolated using the miRNeasy Mini Kit (Qiagen, Venlo, Netherlands) according to manufacturer's instructions, including on-column DNase treatment. RT-qPCR reactions were performed and reported according to the MIQE guidelines [38]. For quantification of gene expression, cDNA was synthetized from 500 ng total RNA with the iScript cDNA Synthesis Kit (Bio-Rad, Hercules, CA, USA) according to the manufacturer's instructions. qPCR reactions were performed with Sybr green detection chemistry, using the LC480 real-time PCR detection system (Bio-Rad). qPCR reactions were performed in a total volume of 5 µl consisting of 2.5 µl of SsoAdvance Universal SYB Green Supermix (Bio-Rad), 0.5 µl forward and reverse primer (5 µM; primer sequences are listed in Supplementary Table 3) and 2 µl of 2.5 ng/µl cDNA (total RNA equivalents). Cycling conditions were as follows: 2 minutes at 95 °C followed by 44 cycles of 5 seconds at 95 °C, 30 seconds at 60 °C and 1 second at 72 °C. Expression levels of LIN28B were normalized to reference genes. Expression analysis as well as error propagation was done using qbase+ software version 3.0 (http://www.biogazelle.com/qbaseplus) (Biogazelle, Zwijnaarde, Belgium) [39]. Measuring the primary miRNAs transcripts was done using stem-loop TaqMan assays. qPCR was performed according to the manufacturer's protocol using 10 ng of the RT product, TaqMan universal master mix (2x) and TaqMan Pri-miRNA assays (20x) (Applied Biosystems) in 8 µl reaction volume. The following cycling conditions were applied: 95°C for 10 min followed by 40 cycles of 95°C for 15 s and 60°C for 1 min. Expression levels were normalized to reference genes. Expression analysis as well as error propagation was done using qbase+ software version 3.0. For quantification of individual miRNA expressions, cDNA was synthesized from 500 ng total RNA with 4 µl of HiSpec Buffer, 2 µl of Nucleics Mix and 2 µl miScript RT Mix (miScript II RT Kit, Qiagen) in a final volume of 20 µl. This reaction mix was incubated for 60' at 37°C and 5' at 95°C using an iCycer instrument (Bio-Rad). qPCR reactions contained 3 ng of cDNA, 2.5 µl QuantiTeckt Mastermix, 0.5 µl miScript Universal Primer and 0.5 µl miRNA-specific miScript Primer Assay (Qiagen, miScript Primer Assays used are listed in Supplementary Table 4) in a total volume of 5 µl. Expression levels were normalized against two stably expressed reference miRNAs (hsa-miR-423-5p and hsa-miR-92) validated with GeNorm [40] and analyzed using qbase+ software version 3.0.

Protein isolation, antibodies and Western blotting

Total protein lysates were harvested after washing with ice-cold PBS and total protein isolation was carried out using RIPA lysis buffer, containing cOmplete Protease Inhibitor Cocktail Tablet (Roche Diagnostics, Basel, Switzerland) and PhosSTOP Phosphatase Inhibitor Cocktail Tablets (Roche Diagnostics). 30 µg of protein lysate was loaded. The antibody directed against LIN28B (4196), secondary anti-rabbit and anti-mouse antibodies were obtained from Cell Signaling Technologies (Danvers, MA, USA). The antibody directed against VCL (V9131) was obtained from Sigma-Aldrich (St. Louis, MO, USA).

anti-MYCN ChIP-qPCR in MYCN3 cells

MYCN ChIP was performed on 1x107 MYCN3 cells either treated or untreated with doxycycline for 24 h using ChIP-IT Express Chromatin Immunoprecipitation Kit (53008; Active Motif, Carlsbad, CA, USA) according to manufacturer's instructions. Samples were sonicated for 20 cycles of 30 sec intervals in a Bioruptor UCD-200 sonicator (Diagenode). ChIP-grade Anti-MYCN anti-body (ab16898, abcam), IgG control anti-body (12-370; EMD-Millipore, Billerica, MA, USA) antibodies were used for ChIP and input was generated by purifying DNA from the sonicated lysates of each sample. ChIP-qPCR primers were designed by analyzing putative MYCN binding sites on LIN28B promoter from previous MYCN ChIP-seq data [37] and are listed in Supplementary Table 5. Control primers for a non-specific genomic region and a distal site on LIN28B promoter was also designed and used to validate the specificity of ChIP DNA. Real-time qPCR reactions were performed in triplicates. The amount of genomic DNA co-precipitated with specific antibody was calculated by normalizing and comparing Cq values of MYCN CHIP with input and control IgG.

Statistical methods

All statistical analyses were performed using R Bioconductor software (version 3.0.2). If not further specified in the results section, statistical significance was defined as p-value < 0.05 for all statistical tests.

Acknowledgments

We would like to thank the Ghent University Hospital (Ghent, Belgium), the University Children's Hospital Essen (Essen, Germany) and the Hospital Clínico Universitario (Valencia, Spain) for collection of primary tumor samples. Further, we would like to thank F. De Vloed for excellent technical support.

Funding: This work was supported by the GOA (grant number 01G01910), by research grants from the European Union (FP7-ASSET project) to F.S., from the Belgian Foundation against Cancer (Stichting Tegen Kanker) [SCIE 2010-177 and 2012-199], from the Fund for Scientific Research Flanders (FWO) to F.S. [G.0530.12N] and the Belgian Childhood Cancer Fund (vzw Kinderkankerfonds); by a PhD grant from the Agency for Innovation by Science and Technology (IWT) to A.B. [IWT 101506]; an Emmanuel van der Schueren research grant from the Flemish League against Cancer (Vlaamse Liga tegen Kanker) to G.V.P.; a PhD grant from the Ghent University to G.V.P. [BOF 01D35609]; and a post-doc grant of the FWO to K.D.P. This work was further supported by Program Grants from the NHMRC Australia, the Cancer Institute NSW and the Cancer Council NSW to D.C., B.C. and G.M.; by grants from NIH (R01-CA174808), Alex's Lemonade Stand Foundation and the Gillson-Longenbaugh Foundation to J.S.

References

1. van de Bunt M, Gaulton KJ, Parts L, Moran I. The miRNA profile of human pancreatic islets and beta-cells and relationship to type 2 diabetes pathogenesis. PLoS ONE. 2013.
2. Shyh-Chang N, Daley GQ. Lin28: primal regulator of growth and metabolism in stem cells. Cell Stem Cell. 2013 Apr 4;12(4):395–406.
3. Molenaar JJ, Domingo-Fernández R, Ebus ME, Lindner S, Koster J, Drabek K, et al. LIN28B induces neuroblastoma and enhances MYCN levels via let-7 suppression. Nat Genet. 2012 Oct 7;44(11):1199–206.
4. Hafner M, Landthaler M, Burger L, Khorshid M, Hausser J, Berninger P, et al. Transcriptome-wide identification of RNA-binding protein and microRNA target sites by PAR-CLIP. Cell. 2010 Apr 2;141(1):129–41.
5. Helwak A, Kudla G, Dudnakova T, Tollervey D. Mapping the human miRNA interactome by CLASH reveals frequent noncanonical binding. Cell. 2013 Apr 25;153(3):654–65.
6. Johnson CD, Esquela-Kerscher A, Stefani G, Byrom M, Kelnar K, Ovcharenko D, et al. The let-7 microRNA represses cell proliferation pathways in human cells. Cancer Research. 2007 Aug 15;67(16):7713–22.
7. Liang L, Wong C-M, Ying Q, Fan DN-Y, Huang S, Ding J, et al. MicroRNA-125b suppressesed human liver cancer cell proliferation and metastasis by directly targeting oncogene LIN28B2. Hepatology. Wiley Subscription Services, Inc., A Wiley Company; 2010 Nov;52(5):1731–40.
8. Guo Y, Chen Y, Ito H, Watanabe A, Ge X, Kodama T, et al. Identification and characterization of lin-28 homolog B (LIN28B) in human hepatocellular carcinoma. Gene. 2006 Dec 15;384:51–61.
9. Helland Å, Anglesio MS, George J, Cowin PA, Johnstone CN, House CM, et al. Deregulation of MYCN, LIN28B and LET7 in a molecular subtype of aggressive high-grade serous ovarian cancers. PLoS ONE. Public Library of Science; 2011;6(4):e18064.
10. Cotterman R, Knoepfler PS. N-Myc regulates expression of pluripotency genes in neuroblastoma including lif, klf2, klf4, and lin28b. PLoS ONE. 2009.
11. Hsu S-D, Tseng Y-T, Shrestha S, Lin Y-L, Khaleel A, Chou C-H, et al. miRTarBase update 2014: an information resource for experimentally validated miRNA-target interactions. Nucleic Acids Research. 2014 Jan;42(Database issue):D78–85.
12. Chi SW, Zang JB, Mele A, Darnell RB. Argonaute HITS-CLIP decodes microRNA-mRNA interaction maps. Nature. Nature Publishing Group; 2009 Jul 13;460(7254):479–86.
13. Guo Y, Chen Y, Ito H, Watanabe A, Ge X, Kodama T, et al. Identification and characterization of lin-28 homolog B (LIN28B) in human hepatocellular carcinoma. Gene. 2006 Dec 15;384:51–61.
14. Wang X, Naqa El IM. Prediction of both conserved and nonconserved microRNA targets in animals. Bioinformatics. 2008 Jan 31;24(3):325–32.
15. Mestdagh P, Lefever S, Pattyn F, Ridzon D, Fredlund E, Fieuw A, et al. The microRNA body map: dissecting microRNA function through integrative genomics. Nucleic Acids Research. Oxford University Press; 2011 Nov 1;39(20):e136–6.
16. Mestdagh P, Fredlund E, Pattyn F, Schulte JH, Muth D, Vermeulen J, et al. MYCN/c-MYC-induced microRNAs repress coding gene networks associated with poor outcome in MYCN/c-MYC-activated tumors. Oncogene. 2010 Mar 4;29(9):1394–404.
17. Althoff K, Beckers A, Bell E, Nortmeyer M, Thor T, Sprüssel A, et al. A Cre-conditional MYCN-driven neuroblastoma mouse model as an improved tool for preclinical studies. Oncogene. 2014 Sep 1.
18. Muth D, Ghazaryan S, Eckerle I, Beckett E, Pöhler C, Batzler J, et al. Transcriptional repression of SKP2 is impaired in MYCN-amplified neuroblastoma. Cancer Research. American Association for Cancer Research; 2010 May 1;70(9):3791–802.
19. Chang T-C, Zeitels LR, Hwang H-W, Chivukula RR, Wentzel EA, Dews M, et al. Lin-28B transactivation is necessary for Myc-mediated let-7 repression and proliferation. Proceedings of the National Academy of Sciences of the United States of America. 2009 Mar 3;106(9):3384–9.
20. You X, Liu F, Zhang T, Lv N, Liu Q, Shan C, et al. Hepatitis B virus X protein upregulates Lin28A/Lin28B through Sp-1/c-Myc to enhance the proliferation of hepatoma cells. Oncogene. 2014 Jan 23;33(4):449–60.
21. Cotterman R, Jin VX, Krig SR, Lemen JM, Wey A, Farnham PJ, et al. N-Myc regulates a widespread euchromatic program in the human genome partially independent of its role as a classical transcription factor. Cancer Research. 2008 Dec 1;68(23):9654–62.

22. Garzon R, Calin GA, Croce CM. MicroRNAs in Cancer. Annu Rev Med. 2009 Feb;60(1):167–79.
23. Di Leva G, Garofalo M, Croce CM. MicroRNAs in cancer. Annu Rev Pathol. 2014;9:287–314.
24. Calin GA, Croce CM. MicroRNA-cancer connection: the beginning of a new tale. Cancer Research. 2006 Aug 1;66(15):7390–4.
25. Peltier HJ, Latham GJ. Normalization of microRNA expression levels in quantitative RT-PCR assays: identification of suitable reference RNA targets in normal and cancerous human solid tissues. RNA. Cold Spring Harbor Lab; 2008 May;14(5):844–52.
26. Chang K, Mestdagh P, Vandesompele J, Kerin MJ, Miller N. MicroRNA expression profiling to identify and validate reference genes for relative quantification in colorectal cancer. BMC Cancer. BioMed Central Ltd; 2010;10(1):173.
27. Tan S, Ding K, Li R, Zhang W, Li G, Kong X, et al. Identification of miR-26 as a key mediator of estrogen stimulated cell proliferation by targeting CHD1, GREB1 and KPNA2. Breast Cancer Research. BioMed Central Ltd; 2014 Apr 15;16(2):R40.
28. Zhu Y, Lu Y, Zhang Q, Liu J-J, Li T-J, Yang J-R, et al. MicroRNA-26a/b and their host genes cooperate to inhibit the G1/S transition by activating the pRb protein. Nucleic Acids Research. 2012 May;40(10):4615–25.
29. Zhao X, Lwin T, Zhang X, Huang A, Wang J. Disruption of the MYC-miRNA-EZH2 loop to suppress aggressive B-cell lymphoma survival and clonogenicity. Leukemia. 2013.
30. Zhang Z, Zha Y, Hu W, Huang Z, Gao Z, Zang Y, et al. The autoregulatory feedback loop of microRNA-21/programmed cell death protein 4/activation protein-1 (MiR-21/PDCD4/AP-1) as a driving force for hepatic fibrosis development. Journal of Biological Chemistry. 2013 Dec 27;288(52):37082–93.
31. Hwang H-W, Wentzel EA, Mendell JT. A hexanucleotide element directs microRNA nuclear import. Science. 2007 Jan 5;315(5808):97–100.
32. Krol J, Busskamp V, Markiewicz I, Stadler MB, Ribi S, Richter J, et al. Characterizing light-regulated retinal microRNAs reveals rapid turnover as a common property of neuronal microRNAs. Cell. 2010 May 14;141(4):618–31.
33. Van Peer G, Lefever S, Anckaert J, Beckers A, Rihani A, Van Goethem A, et al. miRBase Tracker: keeping track of microRNA annotation changes. Database. Oxford University Press; 2014 Jan 9;2014(0):bau080–0.
34. Grimson A, Farh KK-H, Johnston WK, Garrett-Engele P, Lim LP, Bartel DP. MicroRNA targeting specificity in mammals: determinants beyond seed pairing. Molecular Cell. 2007 Jul 6;27(1):91–105.
35. Wang X, Naqa El IM. Prediction of both conserved and nonconserved microRNA targets in animals. Bioinformatics. 2008 Feb 1;24(3):325–32.
36. Schulte JH, Horn S, Otto T, Samans B, Heukamp LC, Eilers U-C, et al. MYCN regulates oncogenic MicroRNAs in neuroblastoma. Int J Cancer. 2008 Feb 1;122(3):699–704.
37. Shohet JM, Ghosh R, Coarfa C, Ludwig A, Benham A, chen Z, et al. A genome-wide search for promoters that respond to increased MYCN reveals both new oncogenic and tumor suppressor microRNAs associated with aggressive neuroblastoma. Cancer Research. American Association for Cancer Research; 2011 Jun 1;71(11):3841–51.
38. Bustin SA, Benes V, Garson JA, Hellemans J, Huggett J, Kubista M, et al. The MIQE guidelines: minimum information for publication of quantitative real-time PCR experiments. Clinical chemistry. 2009. pp. 611–22.
39. Hellemans J, Mortier G, De Paepe A, Speleman F, Vandesompele J. qBase relative quantification framework and software for management and automated analysis of real-time quantitative PCR data. Genome Biology. 2007;8(2):R19.
40. Vandesompele J, De Preter K, Pattyn F, Poppe B, Van Roy N, De Paepe A, et al. Accurate normalization of real-time quantitative RT-PCR data by geometric averaging of multiple internal control genes. Genome Biology. 2002 Jun 18;3(7):R34.

Supplements

Supplementary figures

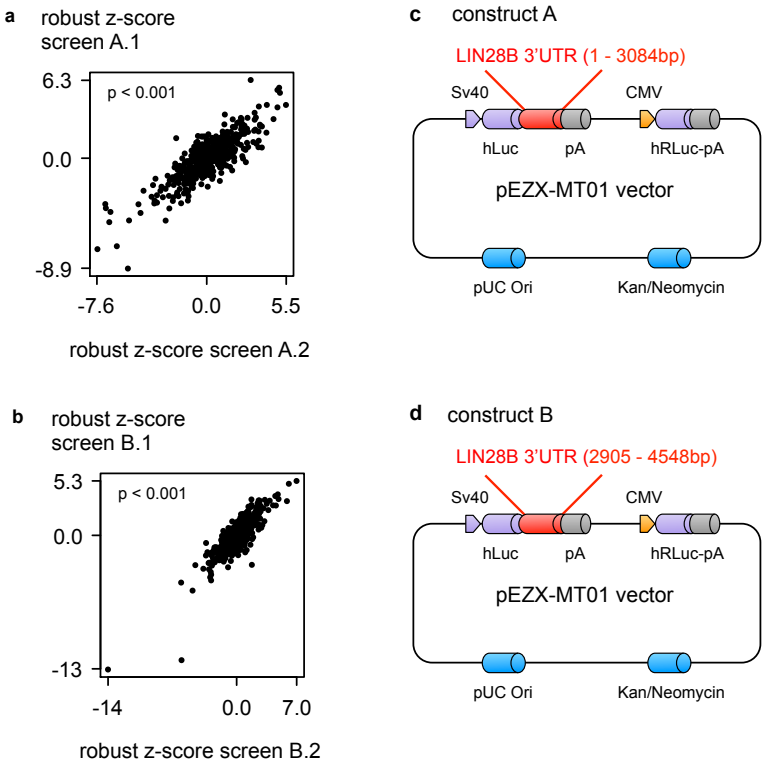

Supplementary Figure 1: Correlation between the robust z-scores from two independent replicate LIN28B 3' UTR screens for two constructs (A and B). Since the wild-type LIN28B (ENST00000345080, Ensemble release 78) 3' UTR is longer than 3.5kb, GeneCopoeia provided the 3'UTR into two constructs with overlapping sequence (referred to as construct A and construct B). The robust z-scores resulting from two independent replicate screens of construct A **(a)** and construct B **(b)** show high correlation, highlighting the reproducibility of the generated data. Spearman correlation; construct A: $r = 0.84$, $p < 2.2 \times 10^{-16}$; construct B: $r = 0.86$, $p < 2.2 \times 10^{-16}$. **(c-d)** Schematic overview of the two LIN28B 3'UTR luciferase reporter constructs.

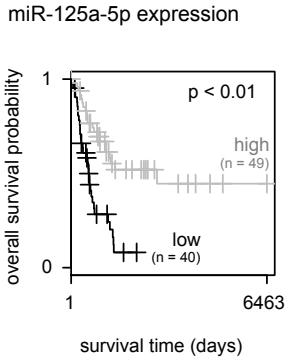

Supplementary Figure 2: Kaplan-Meier curve for the expression of miR-125a-5p in high-risk (INSS stage 4, n = 92) primary neuroblastoma tumors. high (gray lines): expression higher than mean expression; low (black lines): expression lower than mean expression. Log-rank test; $p = 1.6 \times 10^{-5}$

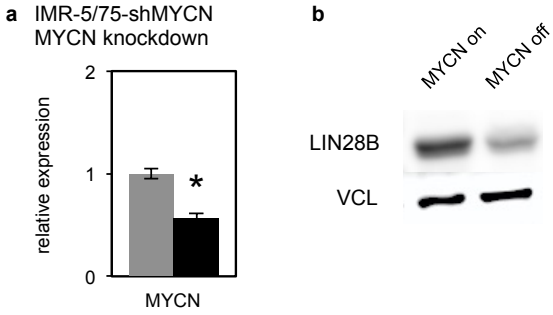

Supplementary Figure 3: Knockdown of MYCN in the IMR-5/75-shMYCN cell line. mRNA **(a)** and protein **(b)** levels of MYCN before (gray bar) and after (black bar) knockdown of MYCN. T-test; $p = 1.2 \times 10^{-3}$.

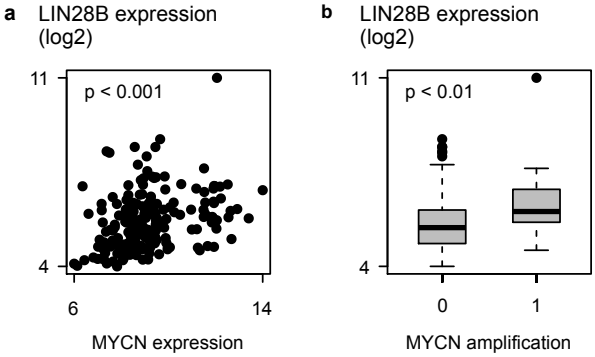

Supplementary Figure 4: Expression of *LIN28B* in primary neuroblastoma tumors. (a) Correlation between MYCN and LIN28B expression in primary neuroblastoma tumors. Spearman correlation coefficient = 0.31, $p = 8.6 \times 10^{-6}$. **(b)** Expression of LIN28B in primary neuroblastoma tumors with and without MYCN amplification. T-test, $p = 2.6 \times 10^{-3}$.

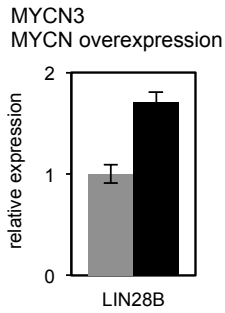

Supplementary Figure 5: Relative expression of LIN28B in MYCN3 cells before (gray bars) and after (black bars) induction of MYCN. Data represent average fold change of three independent biological replicates +/- standard deviation. T-test, $p = 5.0 \times 10^{-3}$.

Supplementary Tables

Supplementary Table 5.1: Results from two independent LIN28B-3'UTR library screens. For each assayed miRNA, the average z-score (av. rob. z score) and the standard deviation (st. dev. int. score) are disclosed. Furthermore, it is indicated (x) whether the miRNA is predicted to target MYCN according to MirTarget V3, used in the web tool miRDB version 5.0

see https://goo.gl/OfGd8K

Supplementary Table 5.2: Annotation update of miRNAs from Ambion's Pre-miR miRNA Precursor Library - Human V3. The most up-to-date annotation at the time of publication (miRBase release 21) of Ambion's Pre-miR miRNA Precursor Library - Human V3 (design based on miRBase release 9.2) was retrieved using the *miRBase release comparison* query option of the miRBase Tracker.

see https://goo.gl/OfGd8K

Supplementary Table 5.3: RT-qPCR primers. Target type: TOI = target of interest, REF = reference target. Fwd = forward, Rev = reverse.

Primer Name	Target Type	Sequence Fwd Primer	Sequence Rev Primer
LIN28B	TOI	ATATCGGTGTGCTGTGATGC	TGAGCAACGCTTATCATGTTTT
CTDSP1	TOI	GTGTGCTGTTCACTGCTA	TCACTCATGTTGTCAAACCA
CTDSP2	TOI	AAGGCCTCTTGAGCACATA	CAACAATGCTGACTTCATAGTG
CTDSPL	TOI	GGAGCTGAGCAAAGTGAT	CACAGGCACTGCATTCTC
SDHA	REF	TGGGAACAAGAGGGCATCTG	CCACCACTGCATCAAATTCATG
TBP	REF	CACGAACCACGGCACTGATT	TTTTCTTGCTGCCAGTCTGGAC
UBC	REF	ATTTGGGTCGCGGTTCTTG	TGCCTTGACATTCTCGATGGT
YWHAZ	REF	ACTTTTGGTACATTGTGGCTTCAA	CCGCCAGGACAAACCAGTAT
B2M	REF	TGCTGTCTCCATGTTTGATGTATCT	TCTCTGCTCCCCACCTCTAAGT

Supplementary Table 5.4: Qiagen miScript primers. Target type: TOI = target of interest, REF = reference target. Fwd = forward, Rev = reverse.

Primer Name	Target Type	Qiagen Catalog Number
hsa-miR-26a-5p	TOI	MS00029239 (Hs_miR-26a_2)
hsa-miR-26b-5p	TOI	MS00003234 (Hs_miR-26b_1)
hsa-miR-423-5p	REF	MS00009681 (Hs_miR-423-5p_1)
hsa-miR-99b-3p	REF	MS00032165 (Hs_miR-99b_2)

Supplementary Table 5.5: ChIP-qPCR primers. Target type: TOI = target of interest, REF = reference target. Fwd = forward, Rev = reverse.

Primer Name	Target Type	Sequence Fwd Primer	Sequence Rev Primer
LIN28B assay 1	TOI	CGCAGTTTCAGTTAGTGATTCC	TTTCAGCGAAACTATTCTCTCC
LIN28B assay 2	TOI	TTGTGTGAGTGTGATTAAGCG	GGAGGAAAGAGAAATCGTGAAG
Control1	REF	CCTGGAGGGCTTGGAGATG	GATCCTACGGCTGGCTGTGA
Control2	REF	TTCTGTGAAAGAAGCACTCTAGG	GGAAGTTGGAAAGGGAGAGAAG

Chapter 6

A Cre-conditional MYCN-driven neuroblastoma mouse model as an improved tool for preclinical studies

Kristina Althoff[1,2,*], Anneleen Beckers[3,*], Emma Bell[4], M Nortmeyer[4], Theresa Thor[1,2,4,5], Annika Sprüssel[1,2,4,5], Sven Lindner[1,2,4,5], Katleen De Preter[3], A Florin[6], Lukas C Heukamp[6,7], Ludger Klein-Hitpass[8], Katty Astrahantseff[9], Candy Kumps[3], Frank Speleman[3], Angelika Eggert[9], Frank Westermann[4], Alexander Schramm[1] and Johannes H Schulte[1,2,3,4,5]

[1] Department of Pediatric Oncology and Hematology, University Children's Hospital Essen, Essen, Germany;

[2] German Cancer Consortium (DKTK), Partner Site Essen/Duesseldorf, Germany;

[3] Center for Medical Genetics Ghent (CMGG), Ghent University Hospital, Ghent, Belgium;

[4] German Cancer Research Center (DKFZ), Heidelberg, Germany;

[5] Translational Neuro-Oncology, West German Cancer Center, University Hospital Essen, University Duisburg-Essen, Essen, Germany;

[6] Institute of Pathology, University Hospital Cologne, Cologne, Germany;

[7] New Oncology -a division of Blackfield AG, Köln, Germany;

[8] Institute of Cell Biology (Cancer Research), Faculty of Medicine, University of Duisburg-Essen, Essen, Germany;

[9] Department of Pediatric Oncology, Hematology and BMT, Charité University Medicine, Berlin, Germany.

[*] These authors contributed equally to this work

Oncogene 2014 Sep 1; [Epub ahead of print]

Abstract

Neuroblastoma, a childhood cancer that originates from neural crest-derived cells, is the most common deadly solid tumor of infancy. Amplification of the MYCN oncogene, which occurs in approximately 20–25% of human neuroblastomas, is the most prominent genetic marker of high-stage disease. The availability of valid preclinical in vivo models is a prerequisite to develop novel targeted therapies. We here report on the generation of transgenic mice with Cre-conditional induction of MYCN in dopamine β-hydroxylase-expressing cells, termed LSL-MYCN;Dbh-iCre. These mice develop neuroblastic tumors with an incidence of 475%, regardless of strain background. Molecular profiling of tumors revealed upregulation of the MYCN-dependent miR-17–92 cluster as well as expression of neuroblastoma marker genes, including tyrosine hydroxylase and the neural cell adhesion molecule 1. Gene set enrichment analyses demonstrated significant correlation with MYC-associated expression patterns. Array comparative genome hybridization showed that chromosomal aberrations in LSL-MYCN;Dbh-iCre tumors were syntenic to those observed in human neuroblastomas. Treatment of a cell line established from a tumor derived from a LSL-MYCN;Dbh-iCre mouse with JQ1 or MLN8237 reduced cell viability and demonstrated oncogene addiction to MYCN. Here we report establishment of the first Cre-conditional human MYCN-driven mouse model for neuroblastoma that closely recapitulates the human disease with respect to tumor localization, histology, marker expression and genomic make up. This mouse model is a valuable tool for further functional studies and to assess the effect of targeted therapies.

Introduction

Neuroblastoma is the most common deadly solid tumor of infancy, and accounts for 15% of pediatric cancer deaths.[1,2] Primary tumors derive from precursor cells of the sympathetic nervous system along the sympathetic chain.[3] Neuroblastoma most frequently arises in the adrenal, but also develops from the superior cervical or celiac ganglia.[4] The most prominent genetic marker of high-stage disease is amplification of the MYCN oncogene, which occurs in 20–25% of all neuroblastomas.[5] Mouse models for human neuroblastoma can be helpful to understand the molecular mechanisms underlying pathogenesis and serve as important tools for preclinical studies. Weiss et al. has previously demonstrated that MYCN has the potential to drive murine neuroblastoma in a transgenic model, in which MYCN expression is driven by a rat tyrosine hydroxylase (TH) promoter.[6] Transgenic mice expressing MYCN in the abdominal ganglia developed neuroblastoma. Although representing an excellent and broadly used tool, some limitations exist: (i) the transgene integration site and its genomic context is ill-defined, potentially resulting in less robust MYCN expression, (ii) tumors predominantly originate from abdominal ganglion structures, thus resembling only a subset of human neuroblastoma, (iii) no intrinsic option for in vivo tumor imaging is included and (iv) tumor incidence of heterozygous TH-MYCN mice is 70% in the 129 × 1/SvJ strain background, but only 5% in C57Bl6/N background, reducing the potential for combination with other cancer-relevant alleles. We aimed to overcome these limitations by developing a novel mouse model with targeted Cre-conditional MYCN expression in the neural crest.

Results

Characterization of LSL-MYCN mice

LSL-MYCN transgenic mice were viable and fertile without obvious physiological or morphological phenotypes. Offspring resulting from breeding LSL-MYCN mice with wild-type mice were born according to the expected Mendelian ratio (data not shown). We next confirmed the molecular integration site and localization of the transgene. Representative examples of PCR analyses validating transgene integration in heterozygous and homozygous LSL-MYCN mice are shown in **Figure 6.1b**. PCR analyses validating the presence of a wild-type allele at the ROSA26 locus in wild-type and heterozygous LSL-MYCN mice are shown in **Figure 6.1c**.

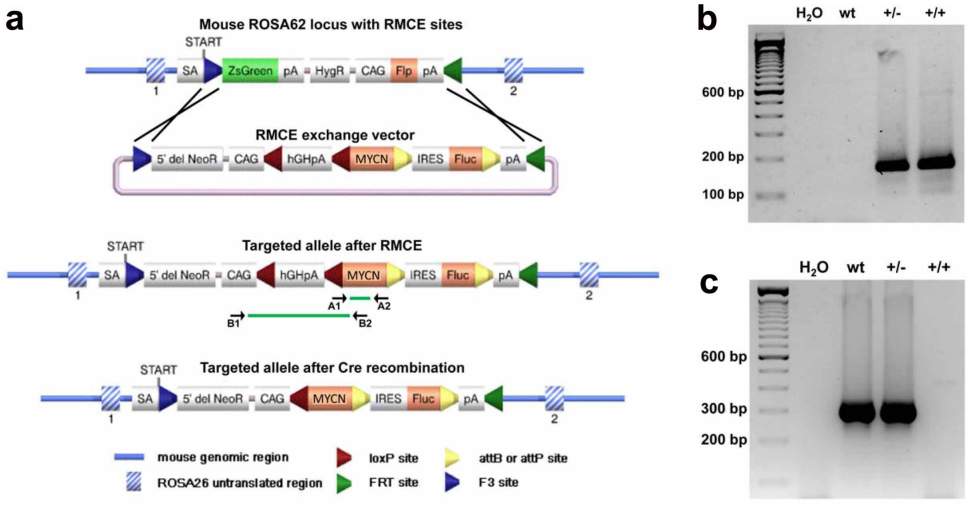

Figure 6.1. Generation of transgenic LSL-MYCN mice. (a) Graphical representation of the ROSA26 locus with recombinase-mediated cassette exchange (RMCE) sites used to introduce the RMCE exchange vector containing the MYCN transgene. The Rosa26 locus is displayed before (top) and after (center) insertion of MYCN by RMCE, and after cre-recombinase-mediated removal of the transcription termination site 5′ to the MYCN allele (bottom). Localizations of primers used for genotyping (A1 and A2) and the PCR-based validation of floxing out the transcriptional site 5′ of the MYCN allele (B1 and B2) are displayed. Splice acceptor site (SA), polyadenylation signal (pA), internal ribosome entry site (IRES), chicken actin gene promotor (CAG), transcriptional STOP cassette made of the human Growth Hormone polyadenylation signal (hGHpA), human MYCN open reading frame (MYCN). **(b)** Representative genotyping PCR validating the MYCN knock-in allele in heterozygous and homozygous LSL-MYCN mice (primers used: A1 and A2); wild type (wt), heterozygous LSL-MYCN (+/−), homozygous LSL-MYCN (+/+). **(c)** Representative PCR validating absence or presence of the transgene inserted into the ROSA26 locus in wt, heterozygous (+/−) and homozygous (+/+) LSL-MYCN mice.

Targeted expression of MYCN in the neural crest causes abdominal tumor formation in double-transgenic LSL-MYCN;Dbh-iCre mice

Double-transgenic LSL-MYCN;Dbh-iCre mice developed palpable abdominal tumors with an incidence of 76% in a mixed C57/Bl6/129 × 1/SvJ strain background (n = 38). Tumor onset was detectable between 26–337 days of age, and the mean age at tumor onset was 79.6 days (**Figure 6.2a**). Interestingly, Kaplan–Meier analysis revealed a significantly prolonged tumor-free survival of mice heterozygous for TH-MYCN compared with LSL-MYCN;Dbh-iCre mice (P = 0.001; **Supplementary Figure 6.1**). Of note, none of the single transgenic LSL-MYCN or Dbh-iCre mice developed a tumor (**Figure 6.2a**); P<0.0001. Cre-mediated recombination in tumors, but not in control tissue from LSL-MYCN;Dbh-iCre mice was validated using B1 and B2 primers (**Figure 6.1a**). In the presence of the transcriptional termination site, a 2241-bp band was present in control tissue, whereas Cre-mediated excision of the transcriptional termination site upstream of the MYCN allele was indicated by the presence of a 703-bp band (**Figure 6.2b** and **Supplementary Figure 6.2**).

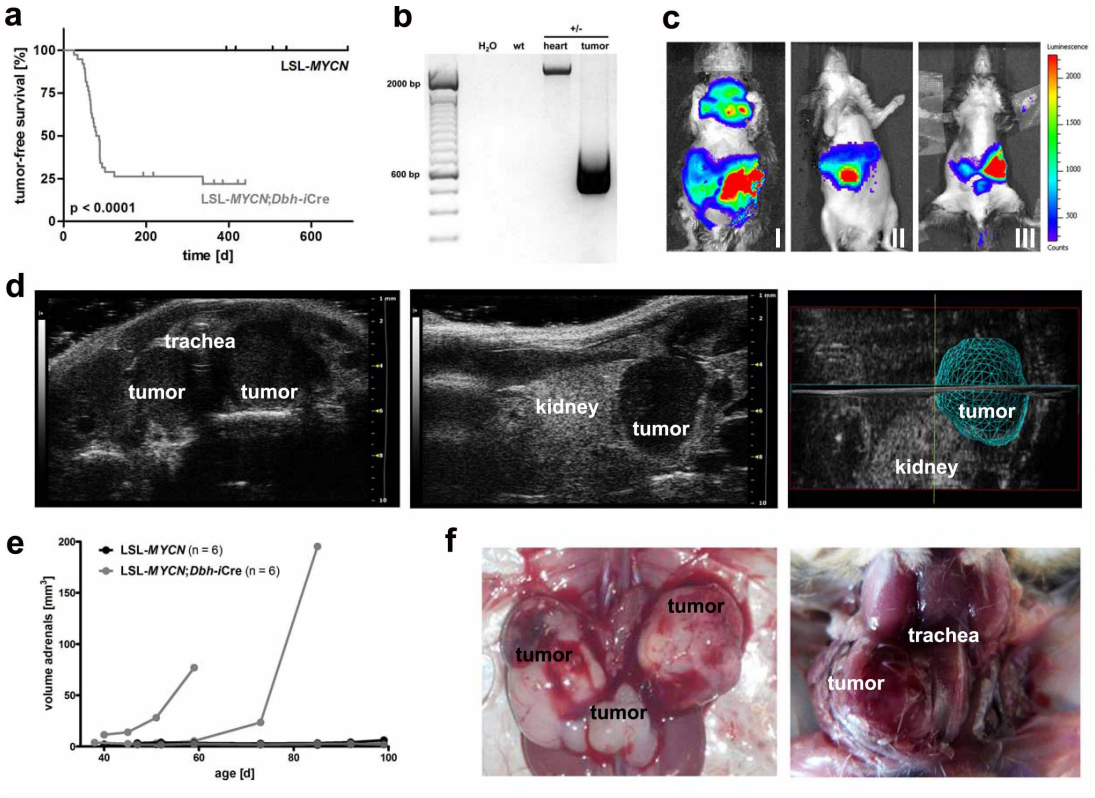

Figure 6.2. Double-transgenic LSL-MYCN;Dbh-iCre mice develop tumors derived from the neural crest. **(a)** Kaplan–Meier analysis indicating the presence and the time to detection of palpable tumors in mice (that is, tumor-free survival) heterozygous for LSL-MYCN and mice double transgenic for LSL-MYCN and Dbh-iCre (Log-rank test). **(b)** Representative result of PCR validating the removal or presence of the transcriptional termination site 5′ to the MYCN transgene in tumor and control tissues, respectively. Wild type (wt), double-transgenic LSL-MYCN;Dbh-iCre (+/−). **(c)** Bioluminescence imaging of three representative LSL-MYCN;Dbh-iCre mice carrying palpable tumors at the superior cervical ganglion (I), adrenals (I, II, III) or celiac ganglion (III). Color code indicates luciferase activity (low = blue; high = red). **(d)** High frequency ultrasound images of palpable tumors arising from superior cervical ganglion (left) and adrenal (middle), and three-dimensional reconstruction of adrenal tumor (right). **(e)** Growth curves of tumors, as detected by high-frequency ultrasound. **(f)** Macroscopic images during autopsy of mice carrying palpable tumors arising from both adrenals and the celiac ganglion (left) and from the superior cervical ganglion (right).

Tumor localization, histology and expression of marker genes in LSL-MYCN;Dbh-iCre mice recapitulate the patterns of human neuroblastoma

In vivo bioluminescence imaging (**Figure 6.2c**) revealed that tumors in LSL-MYCN;Dbh-iCre mice arose from the superior cervical ganglion (I), the adrenals (I, II, III) or the celiac ganglion (III). Several tumors were shown to originate from adrenal structures using high-frequency ultrasound imaging (**Figure 6.2d-e**). Macroscopic images acquired during dissection of mice carrying palpable tumors (**Figure 6.2f**) also confirmed that tumors arose from both adrenals and the celiac ganglion (left) and from the superior cervical ganglion (right).

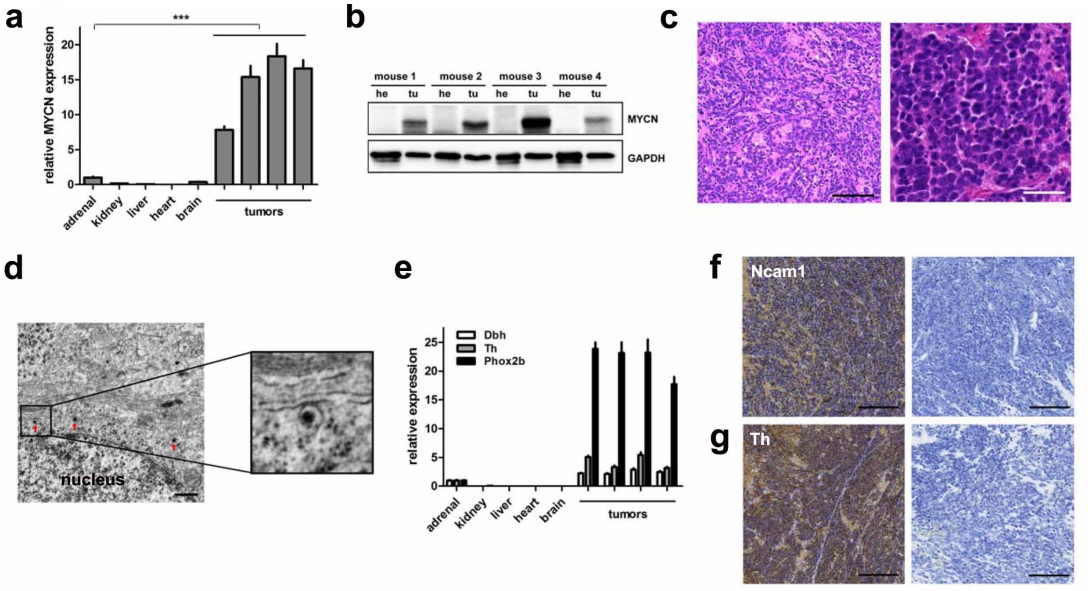

Figure 6.3. Tumors of LSL-MYCN;Dbh-iCre mice resemble human neuroblastoma in terms of histology and molecular expression patterns. (a) MYCN expression (qPCR) in four representative tumors from LSL-MYCN;Dbh-iCre mice compared with control tissues. Expression was normalized to normal adrenal glands. Student's t-test: ***P<0.001. **(b)** Western blot analysis confirms MYCN expression in tumors (tu) compared with heart (he) tissue collected from four representative double-transgenic mice. **(c)** Hematoxylin and eosin (H&E) staining shows small, round blue cells typical for neuroectodermal tumors. Scale bars=100µm (left) and 50µm (right). **(d)** Electron micrographs show neuronal structures, including neurosecretory vesicles (red arrows). Scale bar = 500 nm. **(e)** RT-qPCR confirms significantly increased expression of the murine orthologs of the human neuroblastoma marker genes dopamine β-hydroxylase (Dbh), tyrosine hydroxylase (Th) and paired-like homeobox 2b (Phox2b) in tumors compared with normal control tissues (Student's t-test; Dbh: P = 0.005, Th: P = 0.02, Phox2b: P = 0.0006). **(f, g)** Immunohistochemistry confirms expression of neuroblastoma markers, Ncam1 and Th. Scale bars = 200 µm.

Table 6.1. Genomic aberrations in tumors from LSL-MYCN;Dbh-iCre mice compared with tail

LSL-MYCN; Dbh-iCre tumors			Human neuroblastoma			
Chromosomal region	Genomic aberration	Frequency (%)	Syntenic region	Genomic aberration	Frequency (%)	Reference
1	Partial gain	8	2q	Gain	12	(43)
1	Focal loss	8	1q41, 1q32.2, 1q32.3			
3	Gain	69	1q	Gain	Often	(10)
6	Gain	38	7	Gain	40	(9)
6	Focal gain	15	3p25.3			
8	Fical loss	15	-			
11	Partial gain	31	17q	Gain	50	(8)
12	Gain	23	7q	Gain	12	(9)
16	Focal loss/gain	8	16q13.3			
16	Focal Gain	8	21q22.13, 21q22.2, 21q22.3			

Tumors had elevated expression of both MYCN mRNA and protein compared with normal tissues (**Figure 6.3a-b**). Hematoxylin and eosin staining of histological tumor sections and electron microscopy showed a small round blue cell tumor with cells harboring neurosecretory vesicles (**Figure 6.3c-d**), indicative of neuroblastoma. Furthermore, tumors strongly expressed the neuroblastoma-specific marker genes, dopamine β-hydroxylase (*Dbh*), tyrosine hydroxylase (*Th*) and paired-like homeobox 2b (*Phox2b*), as observed by quantitative PCR (RT-qPCR; **Figure 6.3e**). The neural cell adhesion molecule, *Ncam1*, a marker for neuroendocrine tissues, was strongly expressed in tumors from LSL-MYCN;Dbh-iCre mice (**Figure 6.3f**). Expression of tyrosine hydroxylase was also confirmed on the protein level (**Figure 6.3g**). To analyze early or even premalignant stages of neuroblastoma development in our mouse model, we collected adrenals for histological examinations at day of birth, at days 14 and 28 of life. Hyperplastic cells were present in the adrenal medulla of some, but not all, of adrenal glands from 0-day-old transgenic mice and most 14- and 28-day-old transgenic mice.

Especially at day 28, the adrenal medulla of LSL-MYCN;Dbh-iCre mice had an atypical, nodal tissue architecture. In contrast, no hyperplasia was observed in adrenal glands from control mice of any age. The observed hyperplasia is in line with the hyperplastic lesions (in superior cervical ganglia) previously described in TH-MYCN mice by Hansford *et al.*[7] Taken together, we demonstrate that LSL-MYCN;Dbh-iCre mice develop neuroblastomas that arise from the adrenal medulla and other neural crest derivatives.

Murine MYCN-driven neuroblastomas are characterized by genomic aberrations syntenic to human neuroblastomas

An overview of all genomic aberrations detected in tumors from heterozygous LSL-MYCN;Dbh-iCre mice compared with tail DNA is depicted in **Table 6.1** and **Figure 6.4a**. A partial gain of murine chromosome 11q was detected in the tumors of four mice (**Figure 6.4a-c**). This region is syntenic to human chromosome 17 (**Figure 6.4c**), for which gain or partial gain (17q) occurs in the majority of human neuroblastomas.[8] Five tumors exhibited gain of the entire murine chromosome 6 (**Figure 6.4a** and **Supplementary Figure 6.3c**), which is partially syntenic to human chromosomes 7p, 7q and 12p. In human neuroblastomas, gain of an entire chromosome 7 occurs in 40% of tumors and appears to be prevalent in all tumor stages, whereas gain of 7q, observed in 12% of human tumors, is more common in higher stage tumors.[9] Three tumors harbored a gain of the entire mouse chromosome 12, which is syntenic to human chromosome 2p and includes the MYCN locus, as well as human chromosome 14q and parts of human chromosome 7p and 7q (**Figure 6.4a** and **Supplementary Figure 6.3d**).

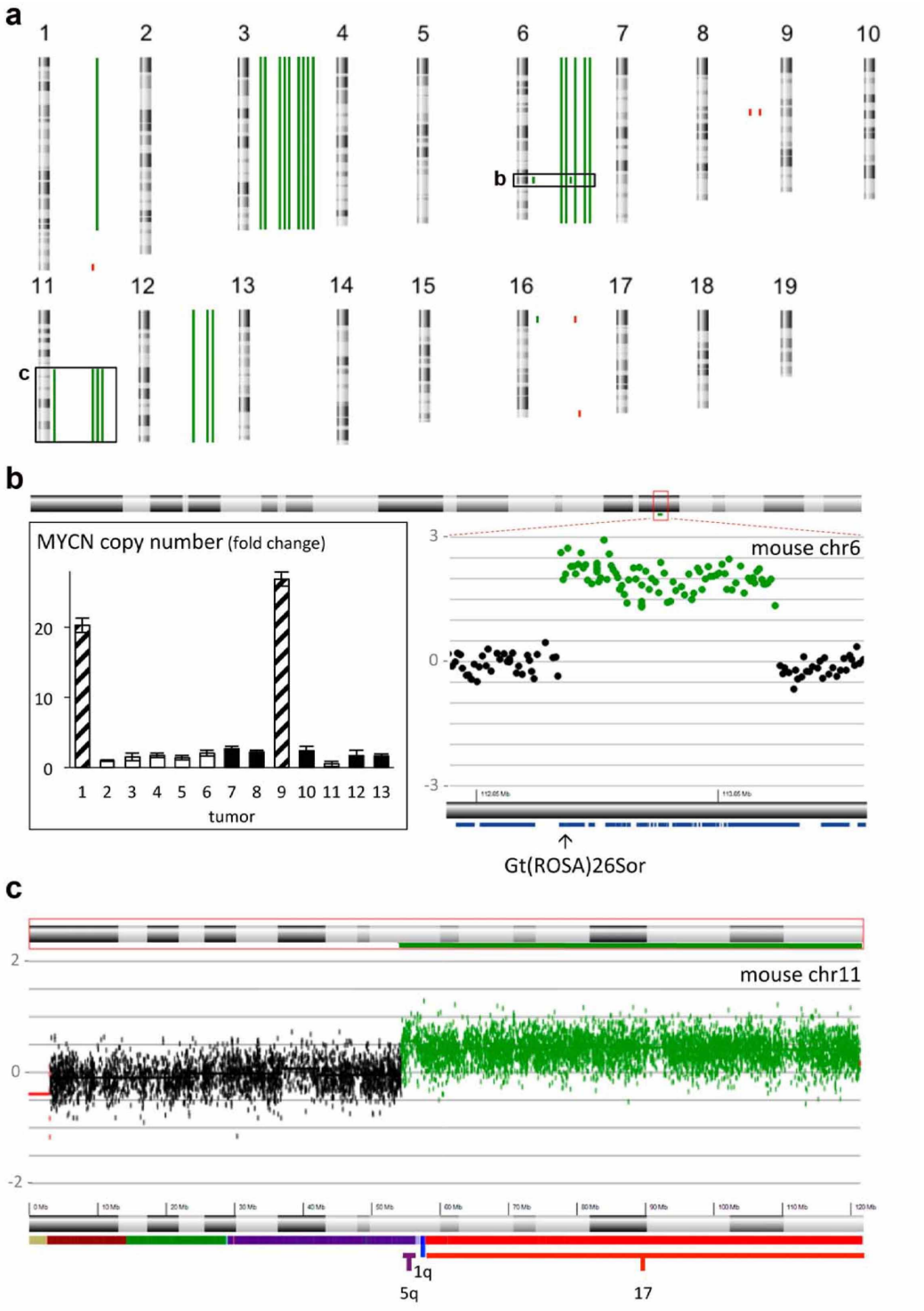

Figure 6.4. Murine neuroblastomas recapitulate genomic aberrations of human neuroblastomas. (a) Mouse karyotype overview of all genomic imbalances detected in 13 murine neuroblastomas (green bars: gained regions, red bars: lost regions). **(b)** Partial ratio plot for the mouse chromosome 6 region encompassing the ROSA26 amplicon in tumor 9 (right) and copy number of the MYCN transgene in 13 tumors from heterozygous LSL-MYCN;Dbh-iCre mice (+/ −), as assessed by qPCR (insert left). Bars represent mice with normal chromosome 6 copy number (white), with whole chromosome 6 gain (black) and with focal chromosome 6 amplification (striped). **(c)** Tumor/control ratio plot for mouse chromosome 11 in tumor 9 showing partial chromosome 11q gain, corresponding to gain of almost the entire human chromosome 17.

Eight tumors displayed gain of the entire chromosome 3 (**Figure 6.4a** and **Supplementary Figure 6.3b**), which is partially syntenic to human chromosome 1q, a region often gained in human neuroblastomas.[10] Interestingly, two tumors showed a focal gain on chromosome 6 that encompassed the ROSA26 locus, in which the human MYCN transgene was integrated (**Figure 6.4a-b**). This focal gain resulted in a 20- to 25-fold increase in MYCN transgene copy number in these two tumors, as measured by qPCR (inset **Figure 6.4b**). Consequently, the two tumors containing this aberration had elevated expression of the human MYCN mRNA (**Supplementary Figure 6.3e**), as assessed by RT-qPCR.

No chromosomal deletions and only few focal deletions were observed in the tumors from heterozygous LSL-MYCN;Dbh-iCre mice. The region on murine chromosome 8 that was lost in two murine tumors, which is syntenic to human chromosome 4, does not harbor any annotated genes (data not shown). Each of the remaining focal losses were only observed in one tumor, and are not syntenic to regions often lost in human neuroblastomas. From these data, it appears that chromosomal and focal losses observed in human neuroblastomas are less well represented in the LSL-MYCN;Dbh-iCre mouse model. Nevertheless, the spectrum of chromosomal aberrations in these MYCN-driven murine tumors recapitulates many of the observed chromosomal imbalances observed in human neuroblastomas.

Murine MYCN-driven neuroblastoma transcriptomes show patterns of canonical MYC-related mRNA and microRNA (miRNA) signatures

The consequences of MYCN overexpression on downstream gene expression were analyzed using transcriptional profiles obtained from normal murine adrenal gland and tumors from LSL-MYCN;Dbh-iCre mice. Unsupervised hierarchical clustering using the 1% of genes with the highest standard deviation in expression across all samples revealed distinct clustering of normal adrenal medulla and MYCN-driven tumors (**Supplementary Figure 6.4**). Interestingly, a similar hierarchical clustering approach revealed that tumors from LSL-MYCN;Dbh-iCre mice are very similar to tumors from the well-established TH-MYCN mouse model,[6] both at the level of mRNA and miRNA expression (**Supplementary Figure 6.5**). Consistent with the role of MYCN as a transcriptional activator, there was a predominance of upregulated over downregulated genes: 2315 genes, represented by 3680 probe sets, were significantly upregulated, whereas 1190 genes, represented by 1726 probe sets, were significantly downregulated (false discovery rate < 0.05; **Supplementary Table 6.2**).

a

Gene Set	Rank	Size	NES	FDR
upregulated in LSL-*MYCN*;*Dbh-i*Cre tumors				
WHITEFORD PEDIATRIC CANCER MARKERS	7	95	2.30	0.00
WHITFIELD CELL CYCLE LITERATURE	25	42	2.18	0.00
REACTOME DNA REPLICATION	31	154	2.11	0.00
REACTOME CELL CYCLE MITOTIC	38	253	2.06	0.00
REACTOME CELL CYCLE	49	298	2.02	0.00
YU MYC TARGETS UP	65	32	1.95	0.00
EGUCHI CELL CYCLE RB1 TARGETS	66	20	1.96	0.00
LE NEURONAL DIFFERENTIATION DN	75	19	1.91	0.00
KEGG DNA REPLICATION	93	32	1.82	0.00
REACTOME CELL CYCLE CHECKPOINTS	103	99	1.82	0.00
downregulated in LSL-*MYCN*;*Dbh-i*Cre tumors				
DANG REGULATED BY MYC DN	412	220	-1.60	0.03
YU MYC TARGETS DN	498	42	-1.56	0.04
DANG MYC TARGETS DN	554	30	-1.54	0.04
LEE LIVER CANCER MYC DN	694	53	-1.49	0.06
LEE LIVER CANCER MYC UP	1012	50	-1.37	0.13
ELLWOOD MYC TARGETS DN	1064	31	-1.36	0.14
PID MYC REPRESSPATHWAY	1143	61	-1.33	0.16

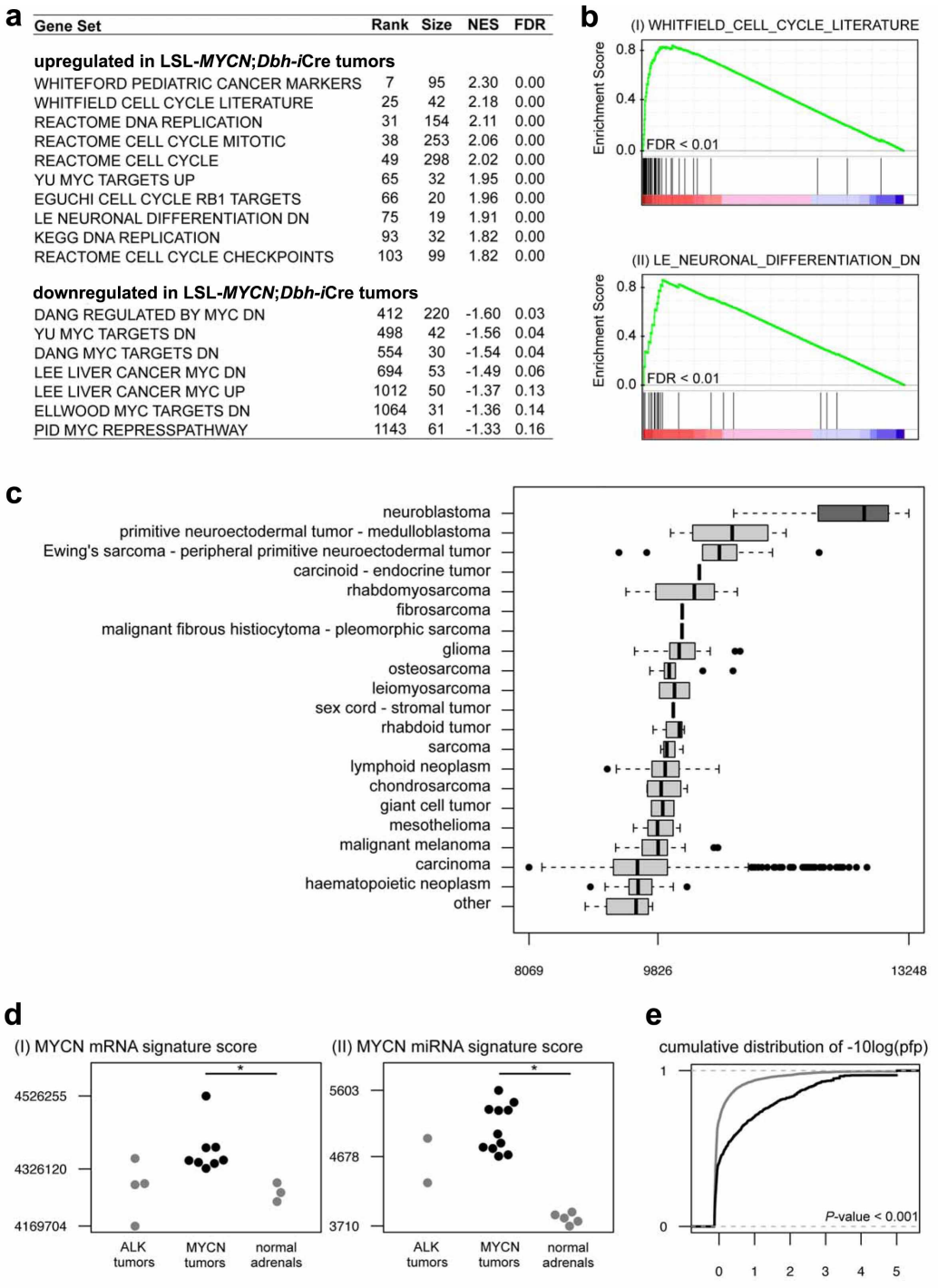

Figure 6.5. Tumors from heterozygous LSL-MYCN;Dbh-iCre mice recapitulate human neuroblastoma at transcriptional level. (a) Table of selected gene sets from the MSigDB C2 collection, enriched among genes upregulated in the tumors from heterozygous LSL-MYCN;Dbh-iCre mice based on GSEA. (Rank of gene set in overall list of gene sets, ranked according to decreasing normalized enrichment score (NES; rank), number of genes in each set (size), NES). **(b)** GSEA enrichment plots showing upregulation of a gene set representing cell cycle (I) and markers downregulated during neuronal differentiation (II) in the transcriptional profiles of neuroblastoma tumors from heterozygous LSL-MYCN;Dbh-iCre mice. Depicted is the plot of the running sum for the MSigDB gene set within the LSL-MYCN;Dbh-iCre neuroblastoma data set, including the maximum enrichment score and the leading edge subset of enriched genes. FDR = false discovery rate. **(c)** The LSL-MYCN;Dbh-iCre signature score in the 967 cell lines in the Cancer Cell Line Encyclopedia[13] showing the highest signature score in neuroblastoma cell lines, followed by medulloblastoma cell lines. **(d)** The MYCN mRNA (I) and miRNA (II) gene signature in normal adrenal medulla and MYCN- and ALK^{F1174L}-driven tumors. $P < 0.05$ (*) was considered significant. **(e)** The cumulative distribution of the significance score [-10log(pfp)] associated with

differential expression in tumors from heterozygous LSL-MYCN;Dbh-iCre mice (+/ −) versus normal adrenals, for genes in the human non- MYCN-amplified neuroblastoma signature (black) and all other genes (gray). Genes in the human non-MYCN-amplified neuroblastoma signature show more significant differential expression compared with all remaining genes (Kolmogorov–Shmirnov test, $P < 0.001$).

The differential expression profiles of regulated transcripts were functionally annotated using Gene Set Enrichment Analysis (GSEA),[11] which seeks to estimate the significance of overrepresentation of an independently defined set of genes in gene expression data sets. LSL-MYCN;Dbh-iCre tumors were characterized by a strong association with MYC-upregulated target genes, whereas MYC-downregulated target genes were enriched in the normal adrenal glands (**Figure 6.5a**). In addition, a large number of DNA replication-related gene sets were statistically enriched among genes upregulated in LSL-MYCN;Dbh-iCre tumors (**Figure 6.5a-b(I)**). Furthermore, upregulation of a gene set representing genes repressed during neuronal differentiation is in line with the undifferentiated phenotype of LSL-MYCN;Dbh-iCre tumors (**Figure 6.5a-b(II)**). Finally, one of the most strongly enriched gene sets among genes upregulated in the MYCN-driven tumors is the WHITEFORD_PEDIATRIC_ CANCER_MARKERS gene set, consisting of differentially expressed genes in a panel of xenografts representing eight common pediatric tumors (neuroblastoma, rhabdomyosarcoma, Ewing sarcoma, acute lymphoblastic leukemia, Wilms' tumor, osteosarcoma, medulloblastoma and ependymona), compared with normal tissues[12] (**Figure 6.5a**). This pediatric cancer phenotype is also apparent when comparing a LSL-MYCN;Dbh-iCre signature in 967 cancer cell lines from Cancer Cell Line Encyclopedia,[13] representing more than 20 tumor entities. The LSL-MYCN;Dbh-iCre signature, composed of the top 100 most differentially up- and downregulated genes in LSL-MYCN;Dbh-iCre tumors compared with normal adrenal gland, is significantly higher in neuroblastoma cell lines than in any other cancer cell line (Kruskal–Wallis rank sum test, $P < 0.001$; **Figure 6.5c**). To specifically evaluate the magnitude of MYCN activity on transcriptional profiles both at mRNA and miRNA level, a MYCN signature score[14] was calculated for all samples. As an additional reference, profiles from neuroblastoma tumors arising from targeted overexpression of mutated ALK[15] were included. The MYCN signature score was significantly higher in MYCN-driven tumors than in the ALK^{F1174L}-driven tumors and normal murine adrenals, demonstrating that MYCN is strongly activated in the tumors arising in transgenic mice with targeted MYCN expression (**Figure 6.5d(I)**, **Supplementary Figure 6.6a** and **Supplementary Table 6.3**). Known human MYCN-upregulated (*Cad*, *Cdk4*, *Odc1*) and MYCN-downregulated (*Dkk3*, *Rgs5*) target genes were also significantly regulated in LSL-MYCN;Dbh-iCre tumors compared with normal adrenals from wild-type mice (**Supplementary Figure 6.6b**). The miRNA expression profiles obtained from normal murine

adrenal gland and both MYCN- and ALK^{F1174L}-driven neuroblastomas showed similar MYCN-driven patterns (**Figure 6.5d (II)**, **Supplementary Figure 6.7** and **Supplementary Table 6.4**). Of the 380 expressed miRNAs that were measured on the platform, 26 miRNAs were upregulated and 38 miRNAs were downregulated in LSL-MYCN;Dbh-iCre tumors compared with normal murine adrenal gland (**Supplementary Table 6.5**). Several miRNAs from the MYCN-induced miR-17–92 cluster (miR-17-5p, miR-18-5p, miR-20a-5p and miR-92a-3p) were significantly upregulated in LSL-MYCN;Dbh-iCre tumors compared with normal adrenals from wild-type mice (**Supplementary Figure 6.7b**). The conformity with human neuroblastoma is further supported by the observation that genes, differentially expressed between high- and low-risk human neuroblastomas, either without or with inclusion of MYCN-amplified tumors, are more significantly altered in LSL-MYCN;Dbh-iCre tumors compared with normal adrenals from wild-type mice (Kolmogorov–Shmirnov test, $P < 0.001$; **Figure 6.5e**). In summary, these observations support the relevance of our new MYCN-driven mouse model for the study of human neuroblastoma.

The mNB-A1 cell line, explanted from LSL-MYCN;Dbh-iCre tumors, reflects characteristics of its origin

In vitro cultured cells derived from a tumor of a LSL-MYCN;Dbh-iCre mouse presented neuronal structures resembling human neuroblastoma cells (**Figure 6.6a**). The presence of both MYCN and the Dbh-iCre transgene as well as Cre-mediated recombination in tumor-derived mNB-A1 cells was validated (**Figure 6.6b-c**). Furthermore, mNB-A1 cells were positive for luciferase expression as revealed by bioluminescence imaging (**Figure 6.6d**) and expressed MYCN mRNA and protein levels similar to LSL-MYCN;Dbh-iCre tumors (**Figure 6.6e-f**). To monitor their tumorigenic potential *in vivo*, mNB-A1 cells were inoculated into nude mice (**Figure 6.6g**). Bioluminescence imaging revealed that tumors from mNB-A1 cells maintained their luciferase activity (**Figure 6.6h**), and that luciferase imaging could be used to follow these tumors *in vivo*. Analysis of re-grafted tumors in nude mice revealed a strong correlation of tumor size with activity detected by luciferase imaging (**Supplementary Figure 6.8**).

Treatment of cultured mNB-A1 cells with JQ1, a pharmacological inhibitor with a high target potency against BET bromodomain proteins,[16] significantly reduced cell viability (**Figure 6.7a**).

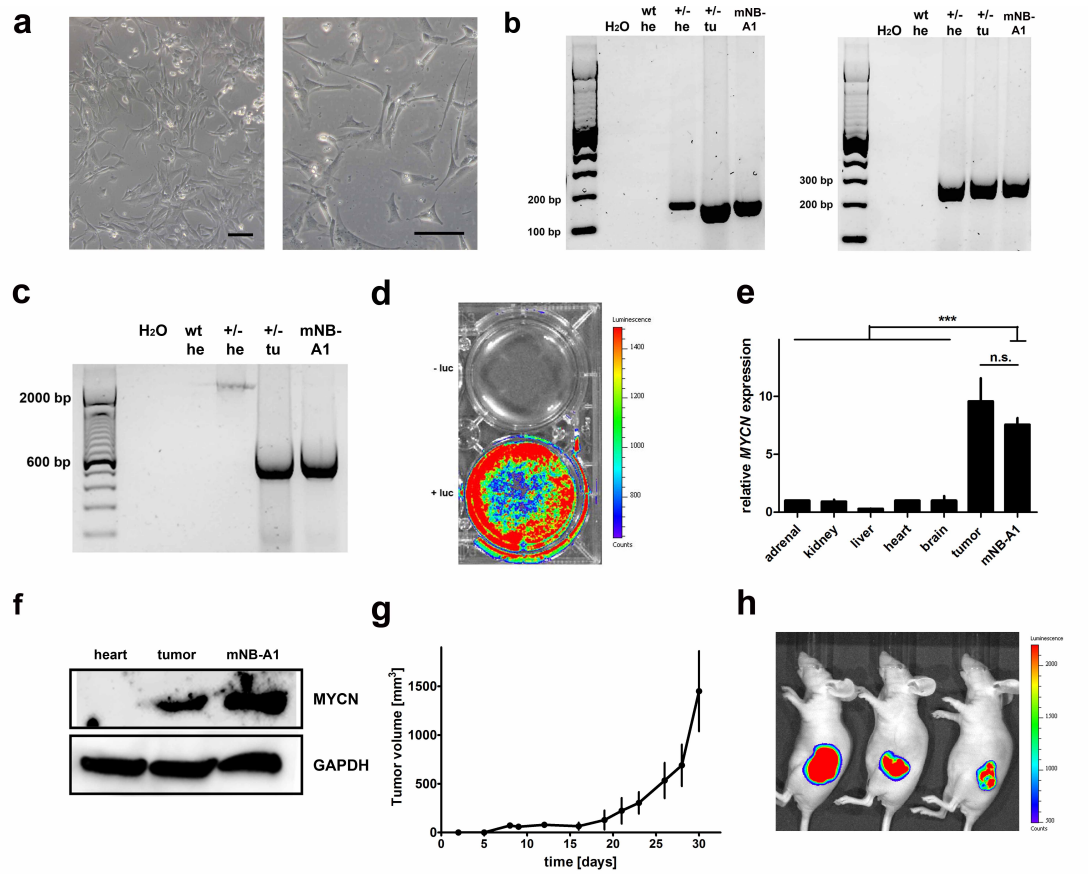

Figure 6.6. (a) Macroscopic images of cells cultivated after explantation of LSL-MYCN;Dbh-iCre tumors. Scale bars = 100 µm. **(b)** Representative genotyping PCR validating the MYCN knock-in allele (left) and the Dbh-iCre transgene (right) in cells cultured from murine neuroblastoma. Heart (he) from wild-type (wt) and heart (he) and tumor (tu) from heterozygous LSL-MYCN;Dbh-iCre mice (+/-) as controls. **(c)** PCR validating the removal of the transcriptional termination site 5′ of the MYCN allele in cells cultivated after explantation of LSL-MYCN;Dbh-iCre tumors. Wild-type (wt), heterozygous LSL-MYCN;Dbh-iCre (+/−), heart (he), tumor (tu). **(d)** Bioluminescence imaging of mNB-A1 cells. Luciferase activity: low = blue; high = red. luciferin (luc). **(e)** MYCN expression (qPCR) in mNB-A1 cells compared with various control tissues and to a representative LSL-MYCN;Dbh-iCre tumor. Expression was normalized to that in normal adrenal glands. Student's t-test: ***=P<0.001; NS = not significant. **(f)** Western blot analysis confirms MYCN expression in mNB-A1 cells compared with heart and LSL-MYCN;Dbh-iCre tumor. **(g)** Tumor growth after engraftment of 10^7 mNB-A1 cells into three nude mice at day 0. **(h)** Bioluminescence imaging of mNB-A1 cells growing in nude mice. Luciferase activity: low = blue, high = red.

Although MYCN expression in mNB-A1 cells remained unaltered by treatment with either JQ1 or the dimethyl sulfoxide (DMSO) control (**Figure 6.7b**), transcriptomic data closely mimic the observed transcriptional changes after JQ1 treatment of neuroblastoma cell lines[16] (**Figure 6.7e**). Furthermore, a strong reduction in MYCN signatures was observed, confirming the effect of JQ1 treatment on MYCN transcriptional programs (**Figure 6.7f** and **Supplementary Figure 6.9**). Treatment with MLN8237, a pharmacological inhibitor that decreases MYCN protein levels by abolishing autophosphorylation of Aurora A,[17] also significantly reduced cell viability (**Figure 6.7c**) and MYCN expression (**Figure 6.7d**).

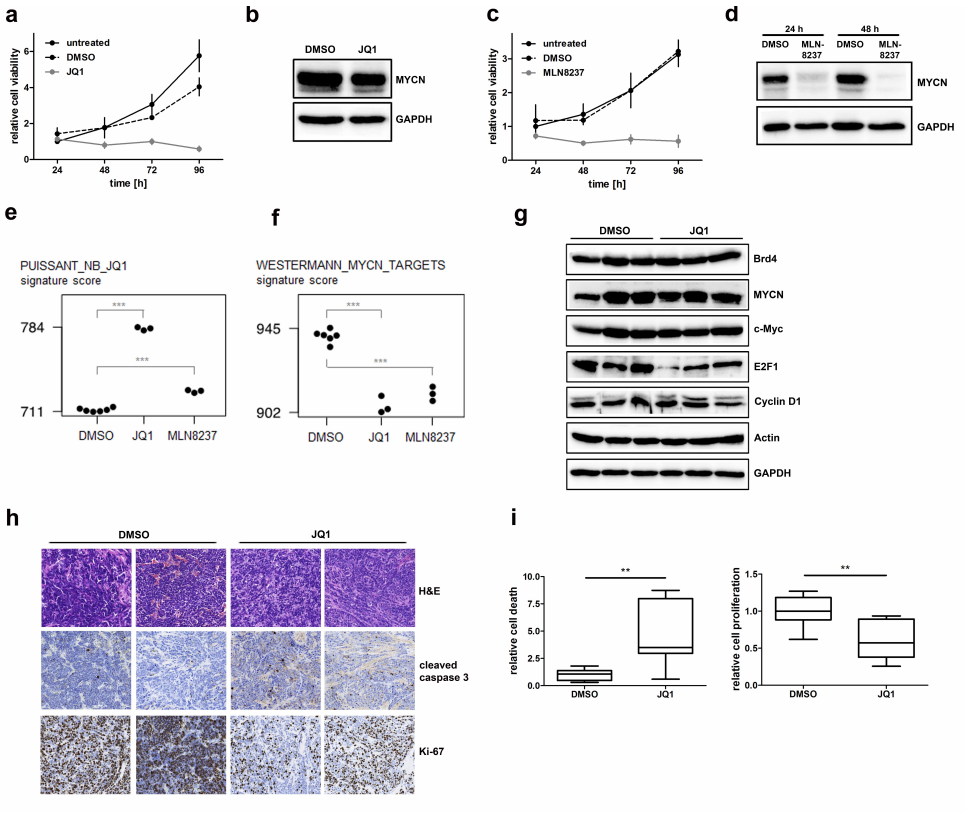

Figure 6.7. Treatment of mNB-A1 and re-grafted tumors. (a) JQ1 treatment of mNB-A1 cells significantly reduced cell viability in MTT assays compared with untreated or DMSO-treated cells. **(b)** Western blot analysis confirmed no MYCN protein regulation in mNB-A1 cells treated with JQ1 compared with DMSO-treated cells. **(c)** MLN8237 treatment of mNB-A1 cells significantly reduced cell viability in MTT assays compared with untreated or DMSO-treated cells. **(d)** Western blot analysis confirmed MYCN downregulation in mNB-A1 cells treated with MLN8237 compared with DMSO-treated cells. **(e, f)** A mRNA signature score established from genes differentially expressed after JQ1 treatment of neuroblastoma cell lines[16] **(e)**, and a MYCN mRNA signature score[14] **(f)** for mNB-A1 cells treated with either DMSO, JQ1 or MLN8237. **(g)** Western blot analyses of Brd4, MYCN, Myc, E2f1 and Cyclin D1 expression in re-grafted tumors from LSL-MYCN;Dbh-iCre mice treated with JQ1 or DMSO. Actin and Gapdh were used as loading controls. **(h)** Re-grafted tumors from JQ1- or DMSO-treated mice were examined histologically after hematoxylin/eosin (H&E) staining or immunostaining for cleaved caspase 3 (apoptotic cells) or Ki-67 (actively proliferating cells). Representative images are shown. **(i)** Bar graphs show the mean relative apoptosis (left) and proliferation (right) calculated from three representative images from each re-grafted tumor from groups of mice treated with either JQ1 or DMSO. Significance was calculated by Student's t-test: *P<0.05, **P<0.01, ***P<0.001.

Gene expression profiles of mNB-A1 cells after MLN8237 treatment show similarities with the transcriptional changes observed after JQ1 treatment of human neuroblastoma cell lines[16] (**Figure 6.7e**), and closer similarities to mNB-A1 cells treated with JQ1 (**Figure 6.7f** and **Supplementary Figure 6.9**). These data support a MYCN transcriptional program repression resulting from both MLN8237 or JQ1 treatment, although slight differences are observed, which is to be expected for treatment with compounds having a different mode of action. We conclude that cells derived from tumors of LSL-MYCN;Dbh-iCre mice retained their malignant capacity upon transplantation, and that growth remains depended on MYCN function, indicating oncogene addiction.

JQ1 treatment induces apoptosis and decreases proliferation of re-grafted tumors from LSL-MYCN;Dbh-iCre tumors

We next aimed to analyze whether JQ1 treatment also affects tumors from LSL-MYCN;Dbh-iCre mice *in vivo*. For that purpose, nude mice harboring re-grafted tumors from LSL-MYCN;Dbh-iCre mice were treated with JQ1. Western blotting of fresh-frozen re-grafted tumor lysates showed that JQ1 treatment did not suppress MYCN or Brd4 protein expression in the tumors (**Figure 6.7g**), but clearly downregulated E2f1 protein expression. Immunhistochemical analysis of the tumors revealed that JQ1 treatment also significantly decreased Mki67 (Ki-67) expression, an indicator of cell proliferation, and increased the level of cleaved caspase 3, indicating the induction of apoptosis (**Figure 6.7h-i**). Taken together, the effects of JQ1 treatment *in vitro* were recapitulated *in vivo*.

Discussion

Although treatment advances in many pediatric cancer types have resulted in increased survival of affected patients, the prognosis for advanced stage neuroblastoma remains poor, especially after tumor relapse.[18] Preclinical models to better understand the molecular features of aggressive neuroblastoma and that can be used to evaluate novel therapies are urgently needed. Here, we present a novel conditional MYCN-driven mouse model that resembles human neuroblastoma. Using Cre expression driven by the Dbh promotor, which is active specifically in noradrenergic neurons of the peripheral and central nervous system,[19] we restricted transgenic MYCN expression to the presumed tissue of neuroblastoma origin. Double-transgenic LSL-MYCN;Dbh-iCre mice developed tumors with a high incidence and regardless of strain background, thus overcoming one of the major limitations of existing models. Bioluminescence imaging identified tumors recapitulating human neuroblastoma localization and histology. LSL-MYCN;Dbh-iCre tumors also mimicked molecular marker expression and reflected chromosomal aberrations of human neuroblastomas. Interestingly, the most common genomic aberrations in human neuroblastomas, including gain of chromosome 17q, were also observed in tumors from LSL-MYCN;Dbh-iCre transgenic mice. Therefore, this mouse model offers the possibility for cross-species genomic analyses toward identifying the presumed oncogenic drivers on human chromosome 17q. In addition to a gain of the region of mouse chromosome 11, which is syntenic to human chromosome 17q, several other recurrent aberrations were observed that resemble aberrations observed in human neuroblastomas. Interestingly, chromosomal gains of human neuroblastomas are better recapitulated in our model than respective deletions. Specifically, loss of 1p36, a region frequently deleted in human MYCN-

amplified neuroblastomas, was not recapitulated in our model. Our findings are in line with previous findings in the TH-MYCN neuroblastoma mouse model.[20,21] Of note, numerical or partial gain of mouse chromo- some 11 resembling human chromosome 17q gain and amplification of the MYCN transgene was observed in both MYCN-driven mouse neuroblastoma models. In addition, gain of mouse chromosome 3 has been observed in all analyzed neuroblastoma mouse models to date.[15,20–22] Taken together, LSL-MYCN;Dbh-iCre mice develop neuroblastic tumors that share histological features and genomic alterations of human neuroblastomas.

Compared with the existing MYCN-driven mouse model of neuroblastoma, which expresses a human MYCN cDNA under the control of a rat tyrosine hydroxylase promoter,[6] the novel LSL-MYCN;Dbh-iCre bears several advantages. First, transgene integration is better defined in LSL-MYCN;Dbh-iCre mice. The ROSA26 locus is commonly used for the generation of genetically engineered knock-in mice, because it is ubiquitously expressed and a discontinuation of that locus causes no known phenotypic effect in mice.[23,24] In contrast, it is not known whether transgene integration into the distal region of chromosome 18, reported for the TH-MYCN mice, also causes positional effects that could possibly have an impact on tumorigenesis.[21] Second, tumors developing in TH-MYCN mice are limited to abdominal ganglion structures,[6] whereas LSL-MYCN;Dbh-iCre tumors develop predominantly from both adrenals, but also develop from the celiac and superior cervical ganglia, thus covering all locations in which human neuroblastomas arise. Third, TH-MYCN tumor penetrance is only high in a genetically near pure 129 × 1/SvJ strain background, probably due to differential expression of specific modifiers.[25] This hampers the combination with other transgenic mouse strains modifying neuroblastomagenesis, as they need to be backcrossed genetically to achieve the same tumor incidence. By contrast, the LSL-MYCN;Dbh-iCre model also develops tumors in other mouse strain backgrounds, such as C57Bl/6N, at a high frequency. Taken together, the novel LSL-MYCN;Dbh-iCre neuroblastoma mouse model overcomes the limitations of the only existing MYCN-driven neuroblastoma model, TH-MYCN.

Beyond the advantages discussed above, the new LSL-MYCN;Dbh-iCre is strikingly similar to the widely used TH-MYCN mouse model in regard to the occurrence of chromosomal alterations, mRNA and miRNA expression profiles. Therefore, subsequent experiments with the LSL-MYCN;Dbh-iCre mouse model can easily build on the many excellent results obtained with the TH-MYCN mouse model in the previous years. The LSL-MYCN;Dbh-iCre model also represents an excellent tool to evaluate new targeted therapies *in vivo*. However, the LSL-MYCN;Dbh-iCre mouse model can only be used to analyze those factors or compounds that regulate or interfere with the MYCN protein itself or MYCN downstream

signaling. Regulators of MYCN transcription or interactors with the MYCN mRNA, such as miRNAs targeting the MYCN 3′-untranslated region, cannot be analyzed in this model, as the MYCN cDNA that is ectopically expressed lacks any regulatory untranslated regions. A mouse model in which neuroblastomas are driven by over-expressed endogenous Mycn, such as the LSL-Lin28b;Dbh-iCre mouse model,[22] is more appropriate for the latter analyses.

We have used the LSL-MYCN;Dbh-iCre mouse cell line to evaluate two drugs, MLN8327 and JQ1, which are known to target MYCN. MLN8327 destabilizes the MYCN oncoprotein by inhibiting the interaction between MYCN and AURKA. We confirmed that MLN8327 treatment downregulates MYCN protein in our model cell line, leading to a strong reduction in cell viability and a decrease in the MYCN activity score. First, this confirms that cells derived from tumors arising in the LSL-MYCN;Dbh-iCre mice exhibit oncogene addiction to MYCN. Second, our results support and extend the preclinical evidence indicating MLN8327 as a promising targeted therapeutic agent to treat MYCN-amplified neuroblastoma. The mode of JQ1 action includes the down- regulation of MYC(N) mRNA transcription and, thereby, MYCN protein expression. As MYCN is ectopically expressed in our model system, a downregulation of MYCN expression after BRD4 inhibition is not necessarily expected. In line with this, we observed no change in MYCN expression after JQ1 treatment. Alternative mechanisms that could explain why JQ1 treatment still reduces cell viability in our model system include either MYCN-independent effects of JQ1 or the interference of JQ1 with MYCN-driven transcription rather than with transcription of the MYCN gene itself. The significant decrease of the MYCN activity score, which we observed following JQ1 treatment, implicates the latter effect, at least in combination with MYCN-independent effects of JQ1. P-TEFb has been previously demonstrated to be a factor required for MYC-driven transcription.[26,27] Therefore, P-TEFb is most likely also required for MYCN-driven transcription as well. As BRD4 is an important factor for P-TEFb recruitment,[28] we hypothesize that inhibiting Brd4 by JQ1 impairs recruitment of P-TEFb, and thereby attenuates MYC(N)-driven transcription. Although not in the focus and beyond the scope of this manuscript, this hypothesis should be taken into account and explored where it has weight for explaining JQ1 treatment results in future experiments attempting to finely assess the mode of action and side effects of JQ1. These should also help delineate the mechanism by which JQ1 decreases the MYCN signature score without downregulating MYCN protein levels.

A prerequisite for using LSL-MYCN;Dbh-iCre mice in preclinical research is assessing the dynamics of tumor development and a sufficient treatment window. With the dynamics of tumor development that we observed in LSL-MYCN;Dbh-iCre mice, the acceleration or delay

of tumor development as well as an increase or decrease in tumor incidence could be used as measurable end points of experimental manipulation, including the introduction of further genetic alterations. A treatment window must be defined to use the LSL-MYCN;Dbh-iCre mice for preclinical analysis of potential therapeutic compounds or therapeutic strategies. The treatment window is the time from tumor detection to the time the mouse succumbs to disease or must be killed due to tumor burden. Our ultrasonography experiments clearly indicate the presence of a sufficient treatment window in the LSL-MYCN;Dbh-iCre mouse model (Figure 6.2e), although the number of mice analyzed was too low to exactly define the boundaries of the treatment window. Exact delineation of the treatment window for the same animal model will also vary between studies, as it depends on the techniques used to detect and follow the tumor (palpation, luciferase, ultrasonography or nuclear resonance imaging), the end points used in the study (hyperplasia versus an established tumor) and the time at which a mouse must be killed due to tumor burden (ethical considerations and varying national animal protection regulations).

As genetic features of human neuroblastomas are preserved in LSL-MYCN;Dbh-iCre-induced tumors, positional approaches might help to identify other crucial driver genes in neuroblastoma development. Thus, a plethora of options is already available to uncover the full potential of LSL-MYCN;Dbh-iCre transgenic mice in terms of neuroblastoma genetics and future therapeutics, and we expect the LSL-MYCN;Dbh-iCre mouse model to be a valuable tool for the neuroblastoma research community. In fact, the LSL-MYCN mouse line has already been transferred to several laboratories, and is available on request to the research community. To prepare for a future expansion of requests, sperm and frozen embryos are being conserved to allow easier transfer, and the mouse line will be submitted to one of the available public repositories, such as the European Mouse Mutant Archive. As MYC(N) is a key driver of tumorigenesis not only in neuroblastoma, combination the conditional LSL-MYCN mouse with other cre-transgenic models bear the potential to also model tumorigenesis of other human malignancies.

Methods

Generation of LSL-MYCN mice and tumor detection

Human MYCN (Ensembl gene ID: ENSG00000134323) was cloned downstream of a chicken actin gene (CAG) promoter followed by loxP-flanked strong transcriptional termination site (LSL). The transgene was placed upstream of an internal ribosome entry site (IRES) and a second open reading frame coding for the luciferase gene (Fluc) in a

proprietary plasmid (Taconic-Artemis, Cologne, Germany). The CAG-LSL-MYCN-IRES-Fluc vector (LSL-MYCN) was introduced into the ROSA26 locus of B6S6F1 embryonic stem cells by recombinase-mediated cassette exchange (Figure 6.1a). Recombinant clones were isolated, validated by Southern blotting and mice were generated by injection into tetraploid blastocysts. LSL-MYCN mice were crossbred with Dbh-iCre mice.[19] Genotyping and confirmation of Cre-mediated recombination were performed as previously described.[15] Primer sequences are provided in Supplementary Table 1. Abdominal tumors were detected by weekly palpation, and confirmed by high- frequency ultrasonography using a Vevo2010 device (Visualsonics, Toronto, ON, Canada) and/or by in vivo luciferase imaging.[15] Time to tumor detection was displayed as tumor-free survival in Kaplan–Meier analysis. Growth curves for tumors were obtained by volume measurement using high-frequency ultrasonography.

Gene expression analysis

The RNeasy Micro Kit (Qiagen, Hilden, Germany) was used to isolate total mRNA from cells or tissue, and cDNA was generated by SuperScript II Reverse Transcriptase (Invitrogen, Darmstadt, Germany). qPCR was performed using the TaqMan Fast Advanced Master Mix (Applied Biosystems, Darmstadt, Germany) and the StepOnePlus Real-Time PCR System (Applied Biosystems) according to the manufacturer's instructions. *Cad1, MYCN, Dbh, Th* and *Phox2b* mRNA expression levels were normalized to endogenous *Gapdh* and calculated using the dd-Ct method using Biogazelle software (Biogazelle, Ghent, Belgium) as previously described.[29]

Western blot analysis

Cells or small tissue slices were lysed on ice in RIPA buffer (50 mM HEPES, 10 mM $NaCl_2$, 1% NP-40, 0.1% SDS and 1% Triton X-100) supplemented with cOmplete Protease Inhibitor Cocktail Tablets and PhosSTOP Phosphatase Inhibitor Cocktail Tablets (Roche, Mannheim, Germany) and 30 µg of the resulting proteins were separated on 10% SDS-PAGE then transferred to Amersham Hybond-C Extra (GE Healthcare, Solingen, Germany) membranes. Membranes were blocked in 5% milk powder in TBS-$T_{0.1}$ then incubated with primary antibodies against Brd4 (1:200; #sc48772; Santa Cruz, Heidelberg, Germany), E2f1 (1:1000; #AF4825; R&D Systems, Minneapolis, MN, USA) or MYCN (1:1000; #9405; Cell Signaling, Frankfurt am Main, Germany) and Actin (1:2,000; #A3853; Sigma-Aldrich, Taufkirchen, Germany) or Gapdh (1:2000; #MAB374; Millipore, Darmstadt, Germany) as a loading control. After washing twice with TBS-$T_{0.1}$, membranes were incubated 1h at room

temperature with horseradish peroxidase-conjugated secondary antibodies against mouse IgG (1:2000; #NA9310V; GE Healthcare), rabbit-IgG (1:2000; #NA9340V; GE Healthcare) or sheep IgG (1:2000; #HAF016; R&D Systems). Protein detection and visualization were performed as described previously.[30]

Immunhistochemistry and electron microscopy

Briefly, 3-µm-thick sections of formalin-fixed paraffin-embedded tumors and adrenals were deparaffinized, and antigen retrieval was performed by boiling the section in citrate buffer at pH 6 or EDTA at pH 9 for 20 min. Staining was performed as previously described[31] using anti-cleaved caspase 3 (#9661, Cell Signaling, 1:200), anti-tyrosine hydroxylase (ab76442; Abcam; 1:200), anti-Ki-67/Mib-1 (RM-9106, Dako Deutschland GmbH, Hamburg, Germany, 1:25) and anti-Ncam1 (ab6123; Abcam, Cambridge, UK; 1:500) as primary antibodies. Corresponding secondary antibody detection kits for reduced background in murine tissues were used (Histofine Simple Stain Mouse MAX PO, Medac, Hamburg, Germany), and antibody complexes were visualized using an automated stainer (LabVision Autostainer 480S, Thermo Scientific, Langenselbold, Germany). All slides were scanned with a Pannoramic 250 slide scanner (3D Histech.com Budapest, Hungary, Electron microscopy was performed as previously described.[32]

Array comparative genome hybridization (arrayCGH)

DNA was isolated using the DNeasy Blood & Tissue Kit (Qiagen) according to the manufacturer's instructions. ArrayCGH was performed using a 180K (AMADID 027411) mouse whole-genome arrays (n = 13; Agilent Technologies Santa Clara, CA, USA. Random primed labeling (BioPrime ArrayCGH Genomic Labeling System, Invitrogen) was used to label 400 ng of tumor DNA and matched control DNA with Cy3 and Cy5 dyes (Perkin Elmer, Waltham, MA, USA, respectively. Hybridization and washing were performed according to the manufacturer's instructions (Agilent Technologies). Fluorescence intensities were measured on an Agilent scanner (G2505C, Agilent Technologies). Data were extracted using the Feature Extraction v10.1.1.1 software program (Agilent Technologies), and further processed with arrayCGHbase (http://medgen.ugent.be/arraycghbase). Gains and losses were determined using the circular binary segmentation algorithm.[33,34]

mRNA expression profiling

Primary murine tumors, normal murine adrenals and treated mNB-A1 cells were profiled on Affymetrix Murine 430 version 2 oligonucleotide microarrays according to the manufacturer's

protocol. Microarray profiling results for eight LSL-MYCN;Dbh-iCre tumors have been deposited at the Gene Expression Omnibus under accession number GSE51297. Microarray profiling results for mNB-A1 cells have been deposited at Gene Expression Omnibus under accession number GSE57810. Profiles for three non- malignant adrenals from wild-type mice were used as controls. These profiles have been previously described by Molenaar et al.[22] Profiles were compared with mRNA profiles of tumors from ALK-transgenic and TH-MYCN mice that have been published previously.[15] Microarray.CEL files were normalized and summarized to gene levels using the Bioconductor repository of the R statistical language to do gcRMA normalization.[35] Probes with a log2 expression of o5 in o11 of the 14 samples were considered not expressed and filtered out. Only the probe with the highest average expression over all samples was retained for each gene.

miRNA expression profiling

Murine mature miRNA expression levels were quantified using the stem- loop reverse transcription-qPCR platform (Life Technology, Darmstadt, Germany). Briefly, 60 ng of total RNA was reverse transcribed using the rodent stem-loop RT Megaplex primer pools A and B (v2.0) followed by a 12-cycle pre-amplification according to the manufacturer's instructions. Pre-amplified cDNA was diluted and quantified using miRNA-specific Taqman assays (Life Technology) in a 3.5-µl qPCR reaction containing 1.5 µl of Taqman assay (1/17 dilution of 20X solution), 1.75µl Taqman gene expression master mix, 0.02 µl of cDNA and 0.23 µl of water on a 7900 HT qPCR system (Life Technology). Raw miRNA expression values were filtered using a Cq-cutoff of 32, and normalized using the global mean, as previously described.[36,37]

GSEA

The GSEA software was used to identify pathways or groups of functionally related genes deregulated in tumors from LSL-MYCN;Dbh-iCre mice compared with normal adrenal gland.[11,38] GSEA was run on the collections of 3272 curated gene sets (c2) from version 3.1 of the MSigDB.[39] Gene sets with less than 15 genes or more than 500 genes were excluded from the analysis. Gene sets with a false discovery rate $\leqslant 0.25$ and a nominal PP$\leqslant 0.05$ were considered significant. The gene ranking metric in the weighted enrichment score was the two-sided signal-to-noise ratio, and P-values were calculated using 1000 permutations of the phenotype.

Gene signature scores

Gene signature scores were calculated with adaptation of a previously reported algorithm.[40] The LSL-MYCN;Dbh-iCre signature was composed of the top 100 most differentially up- and downregulated genes in LSL-MYCN;Dbh-iCre tumors compared with normal adrenal gland. The signature score was calculated for a panel of 967 cancer cell lines in the Cancer Cell Line Encyclopaedia,[13] for which normalized gene expression data were downloaded from http://www.broadinstitute.org/ccle/home. Signature scores based on the expression values of MYC-regulated mRNAs or miRNAs, as previously defined by Westermann et al. and Mestdagh et al., respectively,[14,41] were calculated for a series of tumors from ALK^{F1174L},[15] LSL-MYCN;Dbh-iCre mice and normal adrenal gland tissue. Additional MYC (N) signatures, retrieved from curated gene sets (c2) from version 3.1 of the MSigDB,[39] were calculated for mNB-A1 cells treated with either JQ1, MLN8237 or DMSO. The published PUISSANT_NB_JQ1 signature[22], composed of the 316 genes differentially expressed in neuroblastoma cell lines upon JQ1 treatment, was calculated for mNB-A1 cells treated with JQ1, MLN8237 or DMSO.

Human neuroblastoma signature

A human neuroblastoma signature was generated using a published data set of 69 human primary neuroblastomas.[41] The signature was composed of the most differentially expressed genes (Rank Product analysis, $P < 0.001$) in high-risk compared with low-risk patients, either with or without inclusion of MYCN-amplified neuroblastomas, resulting in the human neuroblastoma signature and human non-MYCN-amplified neuroblastoma signature, respectively. To compare these gene signatures with expression data from LSL-MYCN;Dbh-iCre tumors, only genes with a known human and murine homolog were retained, yielding a list of 10 433 genes for further analysis.

Establishing of a cell line from a LSL-MYCN;Dbh-iCre tumor

Murine tumor was minced manually with scissors and the pieces digested with 2 mg/ml collagenase in PBS for 30 min at 37 °C. Tumor pieces were passed through sieves with different pore sizes (400, 100, 70 µm) to obtain a cell suspension. Cells were maintained in RPMI medium supplemented with 10% fetal calf serum, penicillin (100 U/ml), streptomycin (100 µg/ml), 1% N2 and 2% B27. The mNB-A1 cell line was in continuous culture for more than 4 months, and all experiments performed here have been obtained after 3–4 months in culture. Cells were seeded onto 96-well plates and treated with 250 nM JQ1 (BPS Bioscience, San Diego, CA, USA) or MLN8237 (Axon Medchem, Groningen, The

Netherlands). Metabolic activity was analyzed by 3-[4,5-dimethylthiazol-3-yl]-2,5-diphenyltetrazolium bromide (MTT) assay (Roche). We used this metabolic activity as a surrogate for the number of living cells, thus, cell viability.[42]

Engraftment of mNB-A1 cells into nude mice

Six-week-old female athymic NCR (nu/nu) mice were subcutaneously inoculated in the left flank with 10^7 cells derived from the LSL-MYCN;Dbh-iCre tumor suspended in 200µl BD Matrigel (BectonDickinson, Heidelberg, Germany). Mice were measured for tumor growth three times per week using the formula (breadth x length x height)/2.

JQ1 treatment of transplanted tumors from LSL-MYCN;Dbh-iCre mice

A Murine tumor was minced manually with scissors and the pieces were digested with 2mg/ml collagenase in PBS for 30min at 37°C. Tumor pieces were passed through a sieve with 400 µm pore size to obtain a cell suspension. Cells were washed with PBS and suspended in 1.5 ml Matrigel (BD Bioscience, Heidelberg, Germany) for subcutaneous inoculation (200 µl per mouse) into the left flank of 6-week-old female athymic (nu/nu) mice. Mice were treated with JQ1 (50 mg per kg body weight) or vehicle control (12.5% DMSO in PBS) twice daily by intraperitoneal injection for 3 consecutive days when the volume of the subcutaneous tumor reached 500–1000 mm^3, and animals were killed 4 h after the last injection. Half the tissue was snap-frozen in liquid nitrogen then stored at − 80 °C and the other half was formalin fixed and paraffin embedded for immunohistochemical analyses.

Statistical analysis

Statistical analyses were conducted using Graph Pad Prism 5.0 (GraphPad Software Inc, San Diego, CA, USA). Kaplan–Meier analyses were used to analyze overall survival. Mean relative apoptosis (calculated by positive staining for cleaved caspase 3) and proliferation (calculated by Ki-67 expression) in the transplanted LSL-MYCN;Dbh-iCre tumors from the control and JQ1-treated groups of mice was calculated from three representative images of each tumor using ImageJ 1.47 (National Institutes of Health, Bethesda, MD, USA). Significance was calculated by Student's t-test (*$P < 0.05$, **$P < 0.01$, ***$P < 0.001$). Differential gene expression analyses were performed using the RankProd package in the R statistical language.

Acknowledgements

We thank S Dreesmann, A Odersky, S Schäfers and N Solomentsew for excellent technical assistance and A Henssen for helpful discussions.

Funding. This work was supported by the National Genome Research Network of the German Ministry for Education and Research (NGFNplus grant #PKN-01GS0894-6 to JHS, AE and AS), the 7th framework European Union project, ASSET (contract #259348-2 to AE, FS and JHS), the German research council (SFB 832, A5 and Z1 to LCH), by the German Cancer Aid (Grant No 111301 to JHS), by the Agency for Innovation by Science and Technology (IWT PhD grant to AB and CK) and the Fund for Scientific Research Flanders (FWO post-doc grant to KDP).

References

1. Ora I, Eggert A. Progress in treatment and risk stratification of neuroblastoma: impact on future clinical and basic research. Semin Cancer Biol 2011; 21: 217–228.
2. Park JR, Eggert A, Caron H. Neuroblastoma: biology, prognosis, and treatment. Hematol Oncol Clin North Am 2010; 24: 65–86.
3. Jiang M, Stanke J, Lahti JM. The connections between neural crest development and neuroblastoma. Curr Top Dev Biol 2011; 94: 77–127.
4. Maris JM. Recent advances in neuroblastoma. N Engl J Med 2010; 362: 2202–2211.
5. Brodeur GM. Neuroblastoma: biological insights into a clinical enigma. Nat Rev Cancer 2003; 3: 203–216.
6. Weiss WA, Aldape K, Mohapatra G, Feuerstein BG, Bishop JM. Targeted expression of MYCN causes neuroblastoma in transgenic mice. EMBO J 1997; 16: 2985–2995.
7. Hansford LM, Thomas WD, Keating JM, Burkhart CA, Peaston AE, Norris MD et al. Mechanisms of embryonal tumor initiation: distinct roles for MycN expression and MYCN amplification. Proc Natl Acad Sci USA 2004; 101: 12664–12669.
8. Vandesompele J, Baudis M, De Preter K, Van Roy N, Ambros P, Bown N et al. Unequivocal delineation of clinicogenetic subgroups and development of a new model for improved outcome prediction in neuroblastoma. J Clin Oncol 2005; 23: 2280–2299.
9. Stallings RL, Howard J, Dunlop A, Mullarkey M, McDermott M, Breatnach F et al. Are gains of chromosomal regions 7q and 11p important abnormalities in neuro- blastoma? Cancer Genet Cytogenet 2003; 140: 133–137.
10. Schleiermacher G, Janoueix-Lerosey I, Ribeiro A, Klijanienko J, Couturier J, Pierron G et al. Accumulation of segmental alterations determines progression in neuroblastoma. J Clin Oncol 2010; 28: 3122–3130.
11. Subramanian A, Tamayo P, Mootha VK, Mukherjee S, Ebert BL, Gillette MA et al. Gene set enrichment analysis: a knowledge-based approach for interpreting genome-wide expression profiles. Proc Natl Acad Sci USA 2005; 102: 15545–15550.
12. Whiteford CC, Bilke S, Greer BT, Chen Q, Braunschweig TA, Cenacchi N et al. Credentialing preclinical pediatric xenograft models using gene expression and tissue microarray analysis. Cancer Res 2007; 67: 32–40.
13. Barretina J, Caponigro G, Stransky N, Venkatesan K, Margolin AA, Kim S et al. The Cancer Cell Line Encyclopedia enables predictive modelling of anticancer drug sensitivity. Nature 2012; 483: 603–607.
14. Westermann F, Muth D, Benner A, Bauer T, Henrich KO, Oberthuer A et al. Distinct transcriptional MYCN/c-MYC activities are associated with spontaneous regression or malignant progression in neuroblastomas. Genome Biol 2008; 9: R150.
15. Heukamp LC, Thor T, Schramm A, De Preter K, Kumps C, De Wilde B et al. Targeted expression of mutated ALK induces neuroblastoma in transgenic mice. Science translational medicine 2012; 4: 141ra91.
16. Puissant A, Frumm SM, Alexe G, Bassil CF, Qi J, Chanthery YH et al. Targeting MYCN in neuroblastoma by BET bromodomain inhibition. Cancer Discov 2013; 3: 308–323.
17. Brockmann M, Poon E, Berry T, Carstensen A, Deubzer HE, Rycak L et al. Small molecule inhibitors of aurora-a induce proteasomal degradation of N-myc in childhood neuroblastoma. Cancer Cell 2013; 24: 75–89.
18. Simon T, Berthold F, Borkhardt A, Kremens B, De Carolis B, Hero B. Treatment and outcomes of patients with relapsed, high-risk neuroblastoma: results of German trials. Pediatric Blood Cancer 2011; 56: 578–583.
19. Stanke M, Duong CV, Pape M, Geissen M, Burbach G, Deller T et al. Target- dependent specification of the neurotransmitter phenotype: cholinergic differ- entiation of sympathetic neurons is mediated in vivo by gp 130 signaling. Development 2006; 133: 141–150.
20. Weiss WA, Godfrey T, Francisco C, Bishop JM. Genome-wide screen for allelic imbalance in a mouse model for neuroblastoma. Cancer Res 2000; 60: 2483–2487.

21. Hackett CS, Hodgson JG, Law ME, Fridlyand J, Osoegawa K, de Jong PJ et al. Genome-wide array CGH analysis of murine neuroblastoma reveals distinct genomic aberrations which parallel those in human tumors. Cancer Res 2003; 63: 5266–5273.
22. Molenaar JJ, Domingo-Fernandez R, Ebus ME, Lindner S, Koster J, Drabek K et al. LIN28B induces neuroblastoma and enhances MYCN levels via let-7 suppression. Nat Genetics 2012; 44: 1199–1206.
23. Casola S. Mouse models for miRNA expression: the ROSA26 locus. Methods Mol Biol 2010; 667: 145–163.
24. Tchorz JS, Suply T, Ksiazek I, Giachino C, Cloetta D, Danzer CP et al. A modified RMCE-compatible Rosa26 locus for the expression of transgenes from exogenous promoters. PLoS One 2012; 7: e30011.
25. Rasmuson A, Segerstrom L, Nethander M, Finnman J, Elfman LH, Javanmardi N et al. Tumor development, growth characteristics and spectrum of genetic aberrations in the TH-MYCN mouse model of neuroblastoma. PLoS ONE 2012; 7: e51297.
26. Gargano B, Amente S, Majello B, Lania L. P-TEFb is a crucial co-factor for Myc transactivation. Cell Cycle 2007; 6: 2031–2037.
27. Eberhardy SR, Farnham PJ. Myc recruits P-TEFb to mediate the final step in the transcriptional activation of the cad promoter. J Biol Chem 2002; 277: 40156–40162.
28. Yang Z, He N, Zhou Q. Brd4 recruits P-TEFb to chromosomes at late mitosis to promote G1 gene expression and cell cycle progression. Mol Cell Biol 2008; 28: 967–976.
29. Schramm A, Vandesompele J, Schulte JH, Dreesmann S, Kaderali L, Brors B et al. Translating expression profiling into a clinically feasible test to predict neuro- blastoma outcome. Clin Cancer Res 2007; 13: 1459–1465.
30. Schulte JH, Bachmann HS, Brockmeyer B, Depreter K, Oberthur A, Ackermann S et al. High ALK receptor tyrosine kinase expression supersedes ALK mutation as a determining factor of an unfavorable phenotype in primary neuroblastoma. Clin Cancer Res 2011; 17: 5082–5092.
31. Schulte JH, Lim S, Schramm A, Friedrichs N, Koster J, Versteeg R et al. Lysine-specific demethylase 1 is strongly expressed in poorly differentiated neuroblastoma: implications for therapy. Cancer research 2009; 69: 2065–2071.
32. Schulte JH, Lindner S, Bohrer A, Maurer J, De Preter K, Lefever S et al. MYCN and ALKF1174L are sufficient to drive neuroblastoma development from neural crest progenitor cells. Oncogene 2012; 32: 1059–1065.
33. Menten B, Pattyn F, De Preter K, Robbrecht P, Michels E, Buysse K et al. arrayCGHbase: an analysis platform for comparative genomic hybridization microarrays. BMC Bioinformatics 2005; 6: 124.
34. Olshen AB, Venkatraman ES, Lucito R, Wigler M. Circular binary segmentation for the analysis of array-based DNA copy number data. Biostatistics 2004; 5: 557–572.
35. Gentleman RC, Carey VJ, Bates DM, Bolstad B, Dettling M, Dudoit S et al. Bioconductor: open software development for computational biology and bioinformatics. Genome Biol 2004; 5: R80.
36. Mestdagh P, Van Vlierberghe P, De Weer A, Muth D, Westermann F, Speleman F et al. A novel and universal method for microRNA RT-qPCR data normalization. Genome biology 2009; 10(6): R64.
37. De Preter K, Mestdagh P, Vermeulen J, Zeka F, Naranjo A, Bray I et al. miRNA expression profiling enables risk stratification in archived and fresh neuroblastoma tumor samples. Clin Cancer Res 2011; 17: 7684–7692.
38. Mootha VK, Bunkenborg J, Olsen JV, Hjerrild M, Wisniewski JR, Stahl E et al. Integrated analysis of protein composition, tissue diversity, and gene regulation in mouse mitochondria. Cell 2003; 115: 629–640.
39. Liberzon A, Subramanian A, Pinchback R, Thorvaldsdottir H, Tamayo P, Mesirov JP. Molecular signatures database (MSigDB) 3.0. Bioinformatics 2011; 27: 1739–1740.
40. Fredlund E, Ringner M, Maris JM, Pahlman S. High Myc pathway activity and low stage of neuronal differentiation associate with poor outcome in neuroblastoma. Proc Natl Acad Sci USA 2008; 105: 14094–14099.

41. Mestdagh P, Fredlund E, Pattyn F, Schulte JH, Muth D, Vermeulen J et al. MYCN/c-MYC-induced microRNAs repress coding gene networks associated with poor outcome in MYCN/c-MYC-activated tumors. Oncogene 2010; 29: 1394–1404.
42. Cimmino F, Schulte JH, Zollo M, Koster J, Versteeg R, Iolascon A et al. Galectin-1 is a major effector of TrkB-mediated neuroblastoma aggressiveness. Oncogene 2009; 28: 2015–2023.
43. Vandesompele J, Speleman F, Van Roy N, Laureys G, Brinskchmidt C, Christiansen H et al. Multicentre analysis of patterns of DNA gains and losses in 204 neuro- blastoma tumors: how many genetic subgroups are there?. Medical and pediatric oncology 2001; 36: 5–10.
44. Hong F, Wittner B, Breitling R, Smith C, Battke F et al. RankProd: Rank Product method for identifying differentially expressed genes with application in meta- analysis. R package version 2011; 2.34.0.

Supplements

Supplementary Tables

Supplementary tables of this manuscript are accessible through the following URL: https://goo.gl/OfGd8K

Supplementary Figures

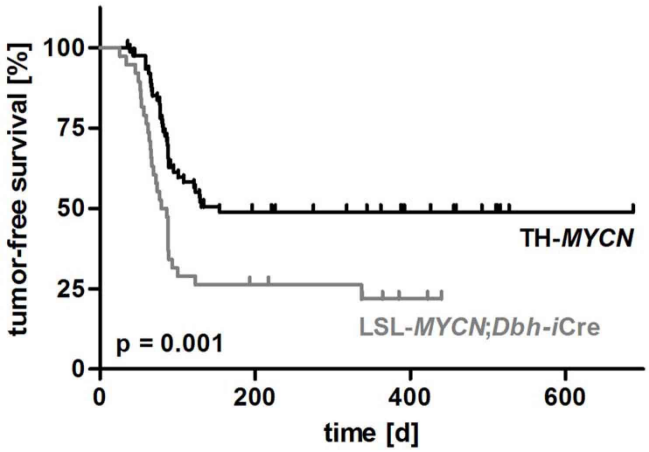

Supplementary Figure 6.1. Tumor incidence is higher in LSL-MYCN;Dbh-iCre mice than in TH-MYCN mice. Kaplan-Meier curves indicating time to detection of palpable tumors in mice heterozygous for TH-MYCN (strain background: 129x1/SvJ) and mice double-transgenic for LSL-MYCN;Dbh-iCre (mixed strain background: C57Bl6 predominant). Wilcoxon rank-sum test.

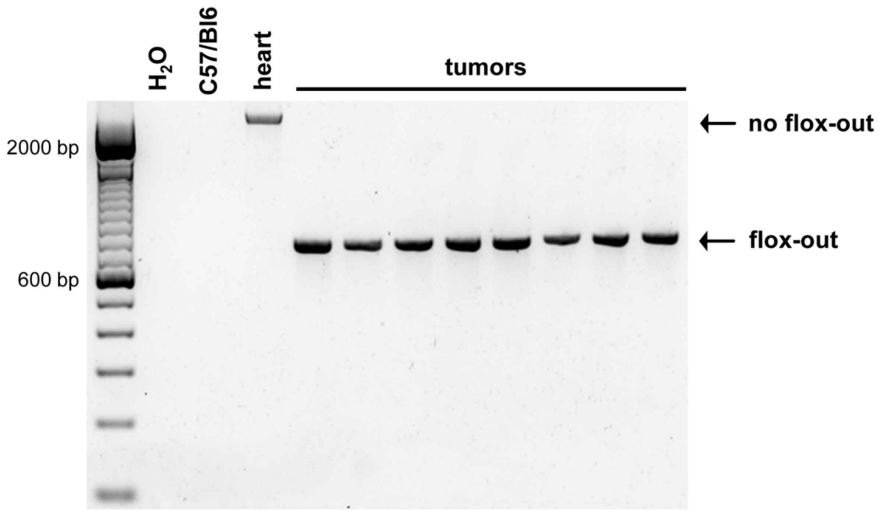

Supplementary Figure 6.2. Flox-out PCR. PCR validating the removal of the transcriptional termination site 5' of the MYCN allele in eight representative LSL-MYCN;Dbh-iCre tumors (Primers used: B1 and B2 – see **Figure 6.1a**).

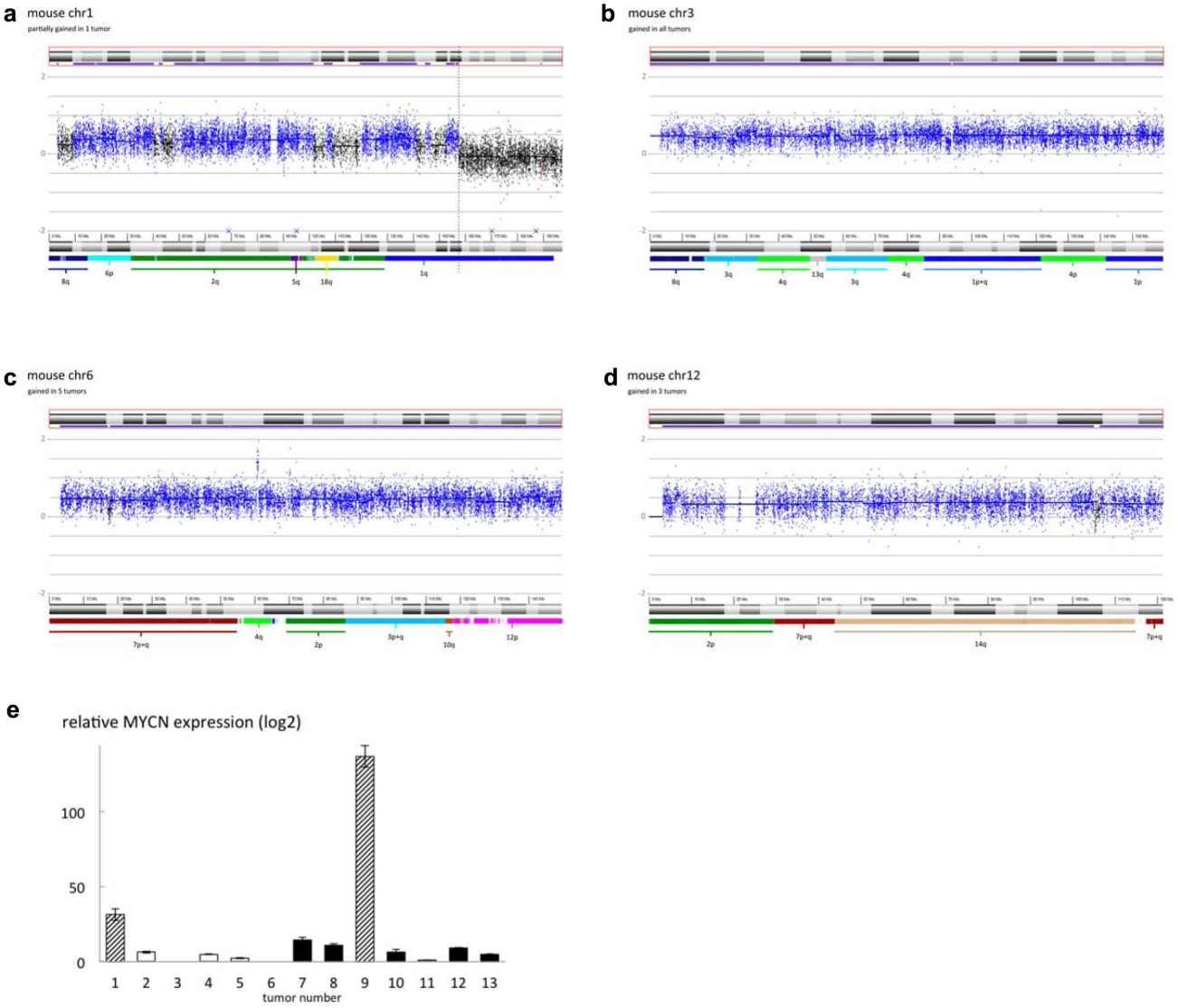

Supplementary Figure 6.3. Murine neuroblastoma tumors recapitulate genomic aberrations of human neuroblastoma tumors. (a) Tumor/control ratio plot for mouse chromosome 1 in tumor 10 shows partial chromosome 1 gain corresponding to partial gain of human chromosome 1p, 2q, 5q, 6p, 8q and 18q. **(b)** Tumor/control ratio plot for mouse chromosome 3 in tumor 6 shows gain of entire chromosome 3 corresponding to partial gain of human chromosome 1p and q, 3q, 4p and q, 8q and 13q. **(c)** Tumor/control ratio plot for mouse chromosome 6 in tumor 7 shows gain of entire chromosome 6 corresponding to partial gain of human chromosome 2p, 3p and q, 4q, 7p and q, 10q and 12p. **(d)** Tumor/control ratio plot for mouse chromosome 12 in tumor 9 shows gain of entire chromosome 12 corresponding to partial gain of human chromosome 2p, containing the endogenous Mycn locus, 7p and q, and 14q. **(e)** Relative MYCN expression levels in 13 murine neuroblastoma tumors. Tumors 1 and 9 (gray bars) harbor gain of chromosome 12, containing the murine Mycn locus.

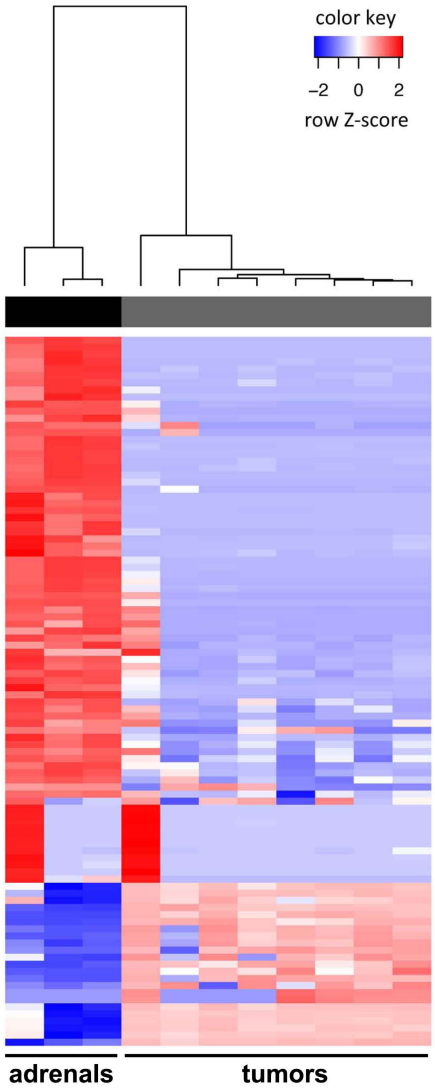

Supplementary Figure 6.4. Analysis of gene expression patterns from three normal adrenal glands and eight tumors from LSL-MYCN;Dbh-iCre mice using Affymetrix murine 430 Version2 oligonucleotide microarrays. Unsupervised hierarchical clustering using the 1% of genes with the highest standard deviations in expression across all samples revealed distinct clustering of adrenals and MYCN-driven tumors. Data are presented as row normalized.

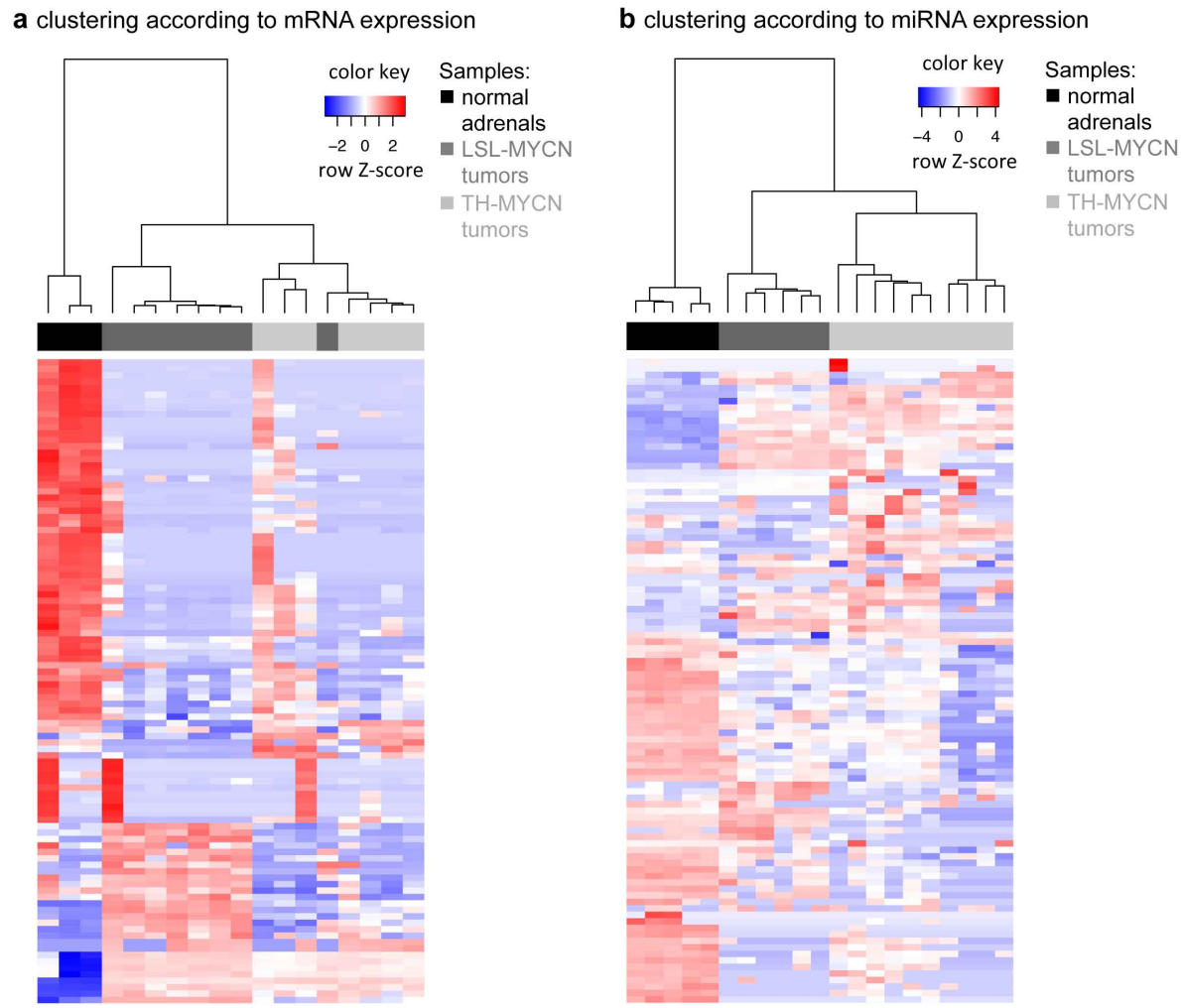

Supplementary Figure 6.5. Comparative analysis of the transcriptome of murine LSL-MYCN tumors and murine TH-MYCN tumors at (a) mRNA and (b) miRNA level.

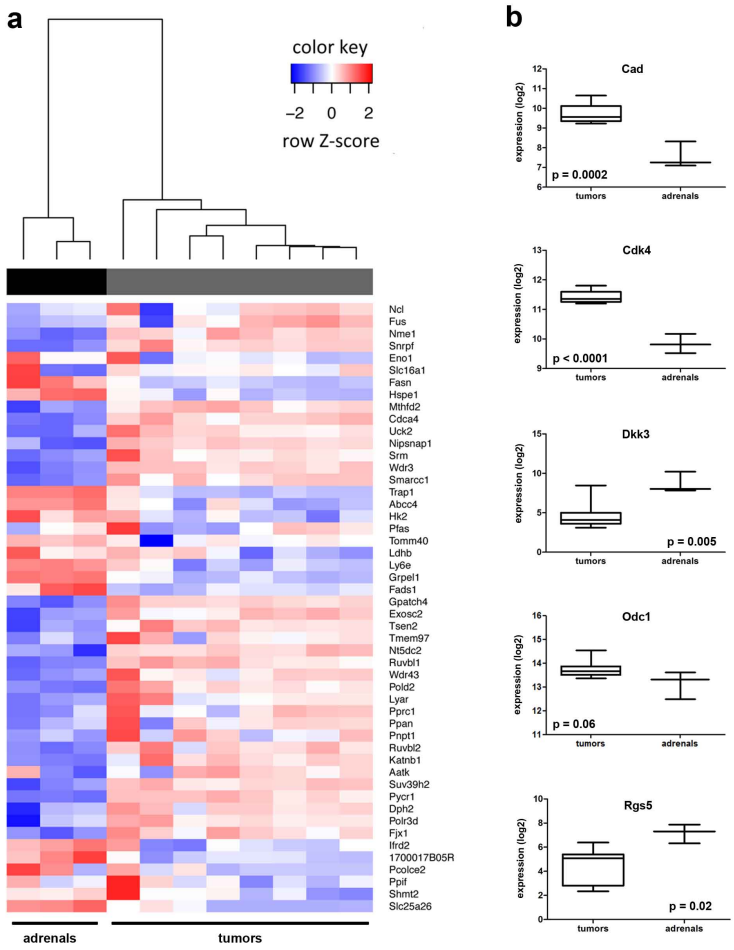

Supplementary Figure 6.6. (a) Analysis of gene expression patterns from three normal adrenal glands and eight tumors from LSL-MYCN;Dbh-iCre mice using Affymetrix murine 430 Version2 oligonucleotide microarrays. Hierachical clustering using MYCN mRNA signature published by Westermann *et al.*[32]. **(b)** Expression (log2) of MYCN upregulated (*Cad, Cdk4, Odc1*) and MYCN downregulated (*Dkk3, Rgs5*) target genes in MYCN-driven tumors compared to normal adrenals from wild type mice. Student's t-test.

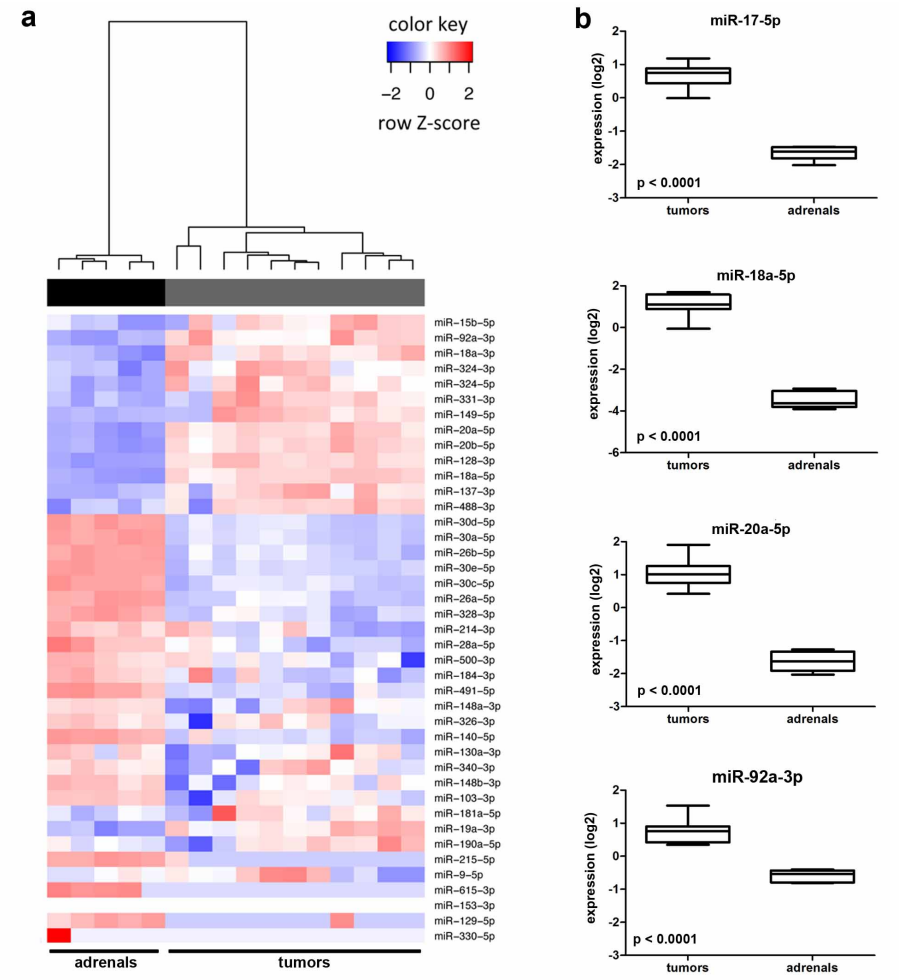

Supplementary Figure 6.7. (a) Analysis of miRNA expression patterns from five normal adrenal glands and eleven tumors from LSL-MYCN;Dbh-iCre mice using Affymetrix murine 430 Version2 oligonucleotide microarrays. Hierachical clustering was performed according to a published MYCN miRNA signature15. **(b)** Expression (log2) of miRNAs from the MYCN upregulated miR-17-92 cluster in tumors from LSL-MYCN;Dbh-iCre mice compared to normal adrenals from wild-type mice. Student's t-test.

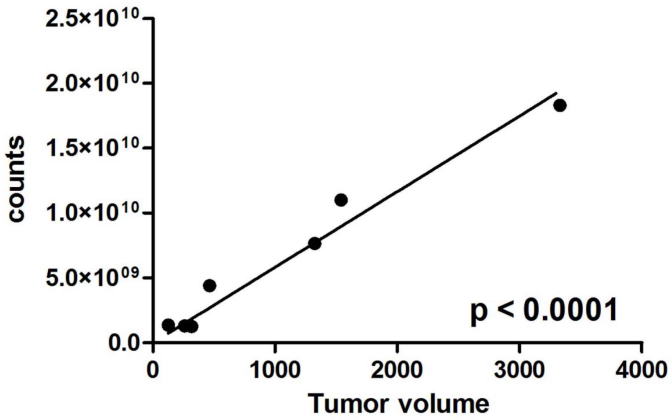

Supplementary Figure 6.8. Analysis of re-grafted tumors in nude mice revealed a strong correlation of tumor size with activity detected by luciferase imaging

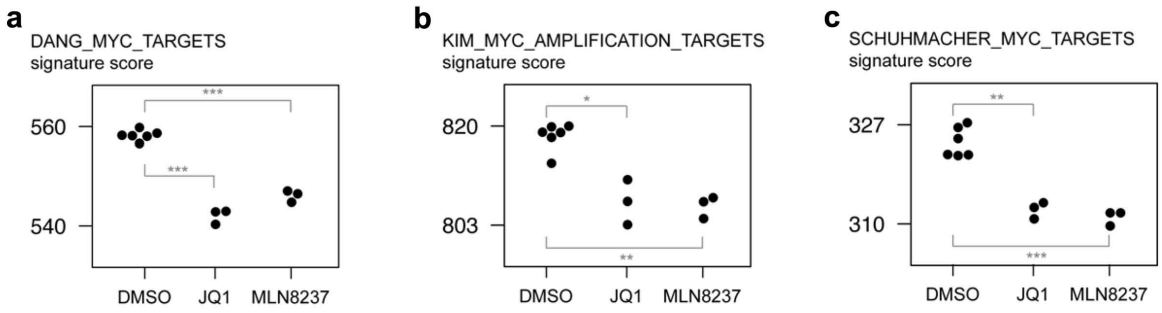

Supplementary Figure 6.9. Activity scores of three distinct MYC signatures in mNB-A1 cells treated with JQ1, MLN8237 or DMSO. Significant differences in activity scores are marked with (*); T-test, $P < 0.05$

Chapter 7

Discussion, future perspectives & conclusion

Table of content

Discussion

MYCN has been at the center of neuroblastoma research ever since the first discovery of its genomic amplification in high-risk neuroblastoma tumors. Amplification of *MYCN* is observed in 25% of cases and has served as the most well-known prognostic marker of neuroblastoma risk classification. Recent discoveries have further strengthened the central position of MYCN in neuroblastoma tumor biology. MYCN can be activated by a number of re-occurring events other than genomic amplification. Indeed, two neuroblastoma oncogenes that were identified more recently – ALK [1-4] and LIN28B [5] – enhance the MYCN pathway upon activation. LIN28B boosts MYCN levels via let-7 suppression [5] while ALK activates MYCN activity through several mechanisms, i.e. transcriptional activation [6], protein stability through GSK3ß and PP2A [7] and suppression of HBP1, a negative regulator of MYCN (Claeys et al., submitted). Taken together, current data place MYCN in the center of neuroblastoma oncogenesis, yet the oncogenic regulatory network driven by MYCN is still incompletely defined thus preventing to unlock the full therapeutic potential of the MYCN signaling pathway.

In the context of this thesis, we aimed to study and functionally characterize the regulatory network downstream of MYCN in neuroblastoma development. In the previous chapters, we reported our findings and proposed mechanistic models to integrate the data generated. This last chapter provides an overview of the conclusions, discusses open questions and offers perspectives for further research.

PLAG2 is a novel candidate oncogenic master regulator in MYCN-driven neuroblastoma tumorigenesis

One of the primary aims of my PhD was to gain novel insights into the regulatory networks that are driving early neuroblastoma oncogenesis and progression. To this end I successfully generated an *in vivo* MYCN time series mRNA and miRNA expression dataset through profiling of different stages of tumor development in the TH-MYCN mouse model. [8] This dataset – referred to as the "hyperplasia dataset" – played key roles in three papers that aimed to improve our understanding of the impact of MYCN on gene expression network in neuroblastoma.

My initial goal when engaging on this research project, was to shed light on miRNA-mRNA regulatory networks in neuroblastoma tumor development. At that point, our research group had contributed significantly to the understanding of miRNAs in neuroblastoma through mapping MYC/MYCN-regulated miRNAs [9] and elucidating the roles of the MYCN-activated oncogenic miR-17–92 cluster in neuroblastoma [10]. Through comparative cross-species

analysis of dynamic miRNA and mRNA expression data, the aim was to further build upon this expertise and to expand the knowledge on miRNA-mRNA networks in neuroblastoma development. The advantage of time-resolved or dynamic datasets over static datasets is the superior ability to understand and model biological processes, which are dynamic in nature. Owing to this advantage, a number of time series experiments have been performed in neuroblastoma cell lines, i.e. assessing the effects of perturbations on gene expression profiles. [11,12] However, *in vitro* studies may lead to results that do not necessarily recapitulate the conditions occurring in a living organism, thus warranting the study of biological processes in a more complex context. Despite the many benefits, time-series data also raise several experimental and computational challenges (reviewed in ref [13]). Moreover, the traditional gene expression data-analysis strategies yield long lists of differentially expressed genes – cancer signatures – that display a certain gene expression profile indicative for oncogenic or tumor-suppressive functions during carcinogenesis.

After assessing a number of advanced computational methods for integrating our time-series mRNA and miRNA expression, we decided to apply the MARINa algorithm to search for master regulators that drive gene networks during neuroblastoma development (see Chapter 3). In this approach, generating cancer signatures becomes only a starting point for a gene network analysis, where a causal regulatory model identifies the driver genes controlling the signatures and related phenotypes. In this thesis, the hyperplasia dataset was applied to generate gene signatures for neuroblastoma development, and gene expression data from a large set of primary neuroblastoma tumors was used to construct a causal neuroblastoma-specific regulatory model, using a bioinformatics approach that has not been previously applied in neuroblastoma. The MARINa algorithm relies strongly on the neuroblastoma-specific interactome that was reverse-engineered from gene expression data from primary neuroblastoma tumors using ARACNe. ARACNe is an information-theoretic method for identifying transcriptional interactions between gene products using gene expression profile data. Similar to other algorithms, ARACNe predicts potential functional associations among genes by identifying statistical dependencies between gene products. In this context, ARACNe has proven effective in identifying *bona fide* transcriptional targets, even in complex mammalian networks. [14] Given that the MARINa algorithm strongly relies on the outcome of the ARACNe algorithm, the limitations of ARACNe should be taken into account when interpreting the MARINa-inferred master regulators. More specifically, ARACNe can introduce false negatives for triplets of interacting genes as the algorithm will open all three-gene loops along the weakest interaction. Moreover, because mRNA abundance measurements only serve as a proxy for the interacting molecular species, the type of physical interactions corresponding to the irreducible statistical dependencies identified by

ARACNe are not always clear. Consequently, predictions made by ARACNe should be directly experimentally verified. [15]

Using the unique hyperplasia dataset in concert with this robust and innovative data-mining strategy (**Figure 3.2**), 22 master regulators of MYCN-driven neuroblastoma development were identified. Further characterization of these master regulators and their regulated neuroblastoma signatures highlighted MYB, E2F2, EZH2, PLAGL2 and MXD3 as master regulators of both MYCN-driven and MYCN-independent neuroblastoma development. Additionally, two synergistic master regulator pairs were identified. The data obtained in this study are highly exciting for several reasons. A number of inferred master regulators were previously described in relation to MYCN: for example MXD3 and E2F proteins can regulate MYCN expression [16,17]; MYCN amplified tumors are addicted to MYBL2, a family member of MYB displaying functional redundancy with MYB [18]; and EZH2 was shown to physically interact with MYCN at promoters of repressed target genes [19]. The identification of known MYCN interactors/regulators serves as a firm proof-of-principle for the value of the performed dynamic regulation analysis on data from developing MYCN driven tumors. One particularly interesting candidate master regulator identified is the C2H2-type zinc finger transcription factor **PLAGL2** (Pleiomorphic Adenoma-Like Protein 2) that is involved in cellular transformation and apoptosis. Of the inferred master regulators, PLAGL2 caught our attention for a number of reasons. First, while PLAGL2 is one of the top candidate master regulators in our study, only one published study has reported on the relationship between PLAGL2 and neuroblastoma. [20] Intriguingly, in their study, the authors found that overexpression of PLAGL2 cDNA – exogenously [20] or in response to iron depletion or hypoxia [21] – in a murine neuroblastoma cell line, Neuro2a, induces apoptosis through the induction of a pro-apoptotic factor, Nip3. This observation is in line with another report that investigated the effects of PLAGL2 overexpression in human promonocytic cells. [22] Here, PLAGL2 expression inhibited cell proliferation which correlated with an accumulation of cells in G1, apoptotic DNA-laddering, an increase in caspase 3, 8, and 9 activity, and a loss of mitochondrial transmembrane potential. Simultaneously, the authors observed a significant increase in the TP53 homologue, TP73, with PLAGL2 expression, possibly via direct activation of TP73 transcription. Both reports are inconsistent with the strong oncogenic role of PLAGL2 in a number of tumor entities [23-27], and with our data showing that high PLAGL2 expression strongly corresponds to poor survival of neuroblastoma patients (see Chapter 3, **Figure 3.3c**). However, such conflicting functionalities have been attributed to a number of oncogenes, including MYCN: conditional expression of MYCN in some MYCN non-amplified neuroblastoma cell lines has been shown to significantly inhibit cell growth and to induce apoptosis. [28] Supporting a putative oncogenic role for PLAGL2 in neuroblastoma is the

observation that enhanced PLAGL2 expression strongly suppresses neural stem cell differentiation while promoting their self-renewal capacity upon differentiation induction. [24] In their study, Zheng and colleagues found that PLAGL2 functions to activate WNT/β-catenin pathway while repression of WNT activation in PLAGL2-expressing NSCs sensitize them to differentiation. [24]

As indicated in Chapter 3, although we speculate that therapeutic targeting of the identified master regulators – and synergistic master regulator pairs – will contribute to the regression of both MYCN-driven and MYCN-independent neuroblastoma tumors, further mechanistic *in vitro* and *in vivo* experiments are needed to support the presumed oncogenic role of PLAGL2 in neuroblastoma. One possible approach is to screen for compounds that target the identified master regulators and test their efficacy and putative synergistic effects on neuroblastoma cell lines and the LSL-MYCN mouse model. Efforts such as *lincscloud* [†] that aims to develop comprehensive signatures of cellular states and tools to analyze them, can aid in the selection of candidate compounds to include in such screens. In addition, targeted knockdown or overexpression of the identified master regulators in neuroblastoma cell lines, followed by functional screens and gene expression analysis, will contribute to our understanding how deregulated master regulator expression can contribute to neuroblastoma development. To support the *in silico* findings, these experiments are currently ongoing at the CMGG.

While interesting candidate mRNA master regulators were identified, no miRNA master regulators could be inferred. Indeed, in literature, far less miRNAs than mRNAs, are considered as master regulators of a given phenotype. Several possible explanations can be proposed to explain our observation. First, multiple miRNAs can be involved in the regulation of one particular gene which may blur the effects when investigating the regulatory effects of one single miRNA. Secondly, it is well known that miRNAs act, not only by degrading their target mRNA but also by repressing translation (see also Chapter 1). The latter effect cannot be inferred from the datasets used in this study. While we failed to identify miRNA master regulators, the generation of the novel miRNA hyperplasia data set has proven to be an important resource for further studies addressing the role of miRNAs and their regulators in neuroblastoma development. More specifically, the miRNA hyperplasia data set proved to be an essential data mining resource as part of my endeavor to explore the regulatory miRNAome targeting two major neuroblastoma oncogenes, MYCN and LIN28B. In addition,

[†] cmap-broad.clue.io

I could make use of a powerful novel unbiased screening assay in order to identify miRNAs regulating target genes of choice (Van Peer *et. al.*, submitted).

Deciphering the MYCN and LIN28 targeting miRNome

In previous studies, individual miRNAs targeting MYCN have been identified. [29,30] Although the applied approach was valuable, it was biased towards canonical miRNA-mRNA interactions, identified by available prediction algorithms. In contrast, our approach was fully unbiased as it included the majority of miRNAs present in the miRBase repository (version 9.2, released in May 2007). Furthermore, the integration of the results from this unbiased screen with patient expression data allowed us to identify MYCN-targeting miRNAs in neuroblastoma context. This additional step is important as miRNAs are known to regulate their target genes in a highly tissue- and cell- type specific manner. Finally, we showed for the first time that MYCN specifically downregulates the miRNAs by which it is targeted, providing a mechanism to sustain its upregulated expression levels. Although our approach is unbiased, it still holds a number of limitations. First, as our 3'UTR library screen included the majority of miRNAs present in the miRBase version 9.2 (released in May 2007), it was limited to those miRNAs known at that time. Between May 2007 and June 2014, when the latest miRBase version (v21) was released, 2124 new human miRNAs were included in the repository, while 343 entries have been changed and 7 were deleted. [31] In addition, as we integrated the results from the 3'UTR library screen with human and murine miRNA expression data, our approach was further restricted to the miRNAs detected by the respective miRNA profiling platforms. Therefore, of the 2588 human miRNAs known to date (miRBase v21), only a small fraction of 187 miRNAs could be assessed. It should be noted however, that the vast majority of the newly detected miRNAs are often highly tissue specific.

Of the 12 MYCN-targeting miRNAs in neuroblastoma context, the majority were shown to be downregulated during MYCN-driven neuroblastoma development. Using the SHEP-MYCN-ER cell line with inducible MYCN activity, I could show that only two of these miRNAs (miR-29a-3p and miR-29c-3p) are directly downregulated upon induction of MYCN (**Figure 4.5**), suggesting that downregulation of MYCN-targeting miRNAs during tumor formation is likely to result from secondary (epi-)genetic events downstream of increased MYCN activity. Notably, for the let-7 family of miRNAs, it has been unclear whether these miRNAs could be considered as direct targets of MYCN. Some papers have suggested regulation of let-7 miRNAs by MYC [32,33], while others have argued against the direct regulation of let-7 by MYC [34]. Our findings described in Chapter 4 therefore greatly contribute to resolve this ongoing debate concerning miRNA-MYCN interregulatory control in neuroblastoma.

In Chapter 5, I further extend this understanding by demonstrating that the indirect regulation of the let-7 family of miRNAs occurs via induction of LIN28B. More precisely, I sought to identify whether LIN28B is regulated by MYCN in neuroblastoma via suppression of LIN28B-targeting miRNAs. Regulation of LIN28B by MYCN (or MYC) could offer an explanation for the observed regulation of let-7 miRNAs in MYC(N) driven systems. To this end, we performed a LIN28B 3'UTR-miRNA library screen and translated the results from this screen to the neuroblastoma context. Using a number of *in vitro* neuroblastoma models with controllable MYCN expression constructs, I showed that MYCN regulates the expression levels of the LIN28B-targeting miRNA miR-26a-5p (**Figure 7.1**). Notably, alterations of MYCN expression or activity did not affect the expression levels of the primary mir-26a transcripts. This indicates that altered miR-26a-5p levels are not the direct consequence of transcriptional activity of MYCN at the mir-26a promotor regions. Also here, downregulation of these LIN28B-targeting miRNAs during tumor formation is likely to result from secondary (epi-)genetic events downstream of increased MYCN activity (**Figure 7.1**). To our knowledge, these events are not yet identified, but elucidating them will increase our possibilities for developing new strategies for targeting MYCN in neuroblastoma. We believe that the discovery of the MYCN–miR-26–LIN28B regulatory axis in neuroblastoma marks LIN28B as an important effector of the MYCN oncogenic phenotype and underlines once more the importance of MYCN-regulated miRNAs in establishing the MYCN-driven oncogenic process. Consequently, LIN28B can be regarded as a prominent therapeutic target for MYCN-driven neuroblastoma tumors. Finally, given the role of both MYCN and LIN28B as *bona fide* stem cell markers, these novel findings are of broader significance for beyond cancer, notably in normal development and stem cell biology.

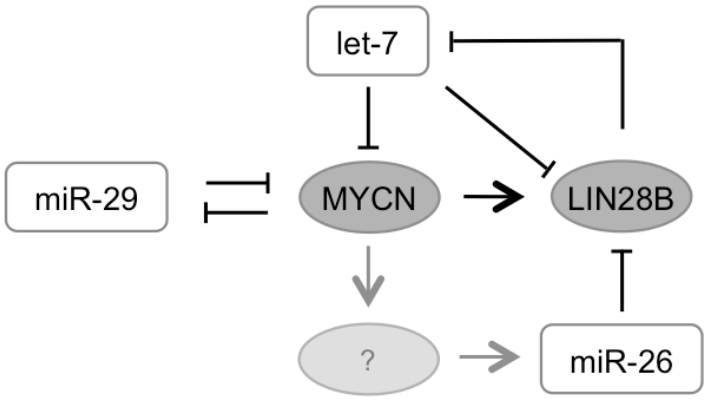

Figure 7.1: Schematic overview of the MYCN–LIN28B axis in neuroblastoma. The expression levels of MYCN and LIN28B are strongly interconnected via a network of miRNAs. A considerate number of these interactions have been established or confirmed in this thesis. The question mark represents a yet unknown factor in the proposed network.

Indeed, given the unbiased study design of both the MYCN 3'UTR-miRNA library screen and the LIN28B 3'UTR-miRNA library screen, the results generated in chapter 4 and 5 apply to regulation of MYCN and LIN28B in any cellular context; especially now that a myriad of high-throughput miRNA and gene expression data are publically available to translate this prioritization catalogue to any cellular context of interest.

Expanding cross species genomics through novel neuroblastoma transgenic animal models

Throughout this thesis, studying the genetic landscape of the well-established TH-MYCN mouse model has provided exciting new insights in the perturbed miRNA-mRNA networks in neuroblastoma. Although representing an excellent and broadly used tool, this mouse model holds some limitations related to the transgene integration site, the anatomical location of the observed tumors, implementation of *in vivo* imaging and tumor incidence in different genetic backgrounds. In Chapter 6, I therefore presented a novel mouse model – generated by our collaborators (Schulte lab, Essen, Germany) – with targeted Cre-conditional *MYCN* expression in the neural crest.

The Schulte lab developed a transgenic mouse strain harboring a floxed transcriptional termination cassette upstream of a *MYCN* allele integrated into the well-characterized ROSA26 locus, and observed no phenotype in the single transgenic mice. These mice were crossed with transgenic *Dbh*-iCre mice specifically expressing Cre recombinase in cells of the developing neural crest. Double-transgenic mice, termed LSL-*MYCN*;*Dbh*-iCre, developed tumors in all locations in which human neuroblastoma tumors arise. Tumor formation, enabled by transgenic luciferase expression, was monitored by ultrasound and bioluminescence imaging. Importantly, tumor incidence in LSL-*MYCN*;*Dbh-i*Cre mice was independent of the strain background. Using different molecular analyses, I showed that this novel neuroblastoma mouse model closely resembles the genomic aberrations and MYC-related mRNA and miRNA signatures occurring in human neuroblastoma tumors. Thus, potential neuroblastoma-relevant genes and miRNAs as well as novel treatment options can be investigated in a setting genetically mimicking human neuroblastoma. Combining this conditional LSL-*MYCN* mouse model with other transgenic mice carrying cancer-related or cancer-modifying alleles bear the potential to also give insights into other human *MYCN*-driven malignancies. I therefore anticipate that the LSL-*MYCN*;*Dbh-i*Cre neuroblastoma mouse will have a similar impact as the TH-*MYCN* mouse has had on the scientific community, and could functionally replace it as a model system. In addition, the Speleman lab in Ghent has also introduced the MYCN and mutant ALK zebrafish neuroblastoma model

which will allow further in depth cross species analyses in order to decipher perturbed regulatory networks in further depth as a prelude towards identification of novel therapeutic targets.

Future perspectives

I envision that the resources established in the frame of this thesis can be further exploited in a number of follow-up studies. First, the hyperplasia dataset can be further applied to ***prioritize candidate neuroblastoma oncogenes or tumor suppressor genes in a cross-species approach***. One such example is to prioritize candidate genes located on aberrant genomic regions in neuroblastoma tumors. Indeed, neuroblastoma is to a large extent a DNA copy number cancer type, and pinpointing the causal genes in these genomic aberrations has been hindered by the large size of these chromosomal gains and losses. In particular gain of chromosome 17 in the majority of aggressive neuroblastoma tumors [10,11] is an interesting chromosomal region for which the causal cooperative genes have not been unequivocally identified [12,13]. The commonly gained segment on chromosome 17 is completely synthetic to the distal part of mouse chromosome 11 that is gained in roughly one third of all LSL-*MYCN;Dbh-iCre* tumors (Chapter 6), strongly supporting a highly selective advantage of this cooperative event during tumor formation in this mouse model. As such, my PhD work has paved the way for the currently ongoing intensive research efforts in relation to several top ranked 17q candidate driver genes. For one of these genes, *BRIP1* {Fieuw:2014tv}, convincing *in vitro* data have been obtained and further in vivo studies in mice and zebrafish are ongoing (Van Hauwaert et al., unpublished).

Second, the hyperplasia dataset allowed to study the dynamic transcriptional landscape of TH-MYCN driven neuroblastoma and to identify a set of strong candidate master regulators synergistically implicated in MYCN-driven neuroblastoma development. Currently, the ***enhancer landscape*** linked to these master regulators is largely unknown. Enhancers are cis-regulatory elements that function to activate or repress target genes and prime genes for rapid induction for change of cellular state and have recently come prominently to the forefront of cancer research. Further, a central role for ***long noncoding RNAs*** in relation to enhancer activity and epigenetic control of active transcription is emerging. This additional level of epigenetic regulation has thus far not been extensively explored in the TH-MYCN transcriptional landscape study. Therefore, a full delineation of the enhancer landscape of MYCN-associated master regulators will unlock novel therapeutic potential for targeting MYCN overexpressing neuroblastoma tumors. Thus, the current study could be extended

with an in-depth analysis of the underlying (epi)genetic landscape during neuroblastoma development.

Finally, comparing the implications of perturbed MYCN activity in **the LSL-*MYCN;Dbh-iCre* mouse model** with similar insights obtained from ALK- or LIN28B- driven mouse and zebrafish tumors or the insights obtained in Chapter 3, could contribute to a more thorough understanding of both common and different effects of these important neuroblastoma oncogenes in the biology of this embryonic tumor.

Conclusion

The work in this thesis has significantly contributed to our understanding of the impact of MYCN activation in neuroblastoma tumor biology. As MYCN is the most important driver gene in neuroblastoma known to date, this will facilitate to the development of drugs suppressing neuroblastoma progression. While considered undrugable, at present multiple angles are being actively explored to target MYCN (see Chapter 1) and therefore the new insights of the present work can be directly applied to support such efforts. In addition, in this thesis I present the genomic characterization of a new MYCN-driven neuroblastoma mouse model, which overcomes a number of issues related to the previously only murine MYCN-driven neuroblastoma model and faithfully recapitulates the genetics of MYCN driven human neuroblastoma formation.

Therefore, the combination of the accomplishments in this thesis contributes to a more clear understanding of the genetic landscape of neuroblastoma and the molecular implications, generating opportunities for the development of targeted therapies. Indeed, through these and other efforts in the field, the understanding of the genetic basis of neuroblastoma is starting to keep up with advances in other cancer entities. Ultimately, this increased knowledge of normal and perturbed cell biology will lead to the development of more focused neuroblastoma therapies, characterized by an increased efficiency and decreased toxicity.

References

1. Chen, Y. *et al.* Oncogenic mutations of ALK kinase in neuroblastoma. *Nature* **455,** 971–974 (2008).
2. Janoueix-Lerosey, I. *et al.* Somatic and germline activating mutations of the ALK kinase receptor in neuroblastoma. *Nature* **455,** 967–970 (2008).
3. Mossé, Y. P. *et al.* Identification of ALK as a major familial neuroblastoma predisposition gene. *Nature* **455,** 930–935 (2008).
4. George, R. E. *et al.* Activating mutations in ALK provide a therapeutic target in neuroblastoma. *Nature* **455,** 975–978 (2008).
5. Molenaar, J. J. *et al.* LIN28B induces neuroblastoma and enhances MYCN levels via let-7 suppression. *Nat Genet* **44,** 1199–1206 (2012).
6. Schönherr, C. *et al.* Anaplastic Lymphoma Kinase (ALK) regulates initiation of transcription of MYCN in neuroblastoma cells. *Oncogene* **31,** 5193–5200 (2012).
7. Huang, M. & Weiss, W. A. Neuroblastoma and MYCN. *Cold Spring Harb Perspect Med* **3,** a014415–a014415 (2013).
8. Weiss, W. A., Aldape, K., Mohapatra, G., Feuerstein, B. G. & Bishop, J. M. Targeted expression of MYCN causes neuroblastoma in transgenic mice. *EMBO J* **16,** 2985–2995 (1997).
9. Mestdagh, P. *et al.* MYCN/c-MYC-induced microRNAs repress coding gene networks associated with poor outcome in MYCN/c-MYC-activated tumors. *Oncogene* **29,** 1394–1404 (2010).
10. Mestdagh, P. *et al.* The miR-17-92 MicroRNA Cluster Regulates Multiple Components of the TGF-β Pathway in Neuroblastoma. *Mol Cell* **40,** 762–773 (2010).
11. Valentijn, L. J. *et al.* Functional MYCN signature predicts outcome of neuroblastoma irrespective of MYCN amplification. *Proc Natl Acad Sci U S A* **109,** 19190–19195 (2012).
12. Kim, I. S., Choi, D.-K. & Do, J. H. Genome-wide temporal responses of human neuroblastoma SH-SY5Y cells to MPP+ neurotoxicity. *BioChip J* **7,** 247–257 (2013).
13. Bar-Joseph, Z., Gitter, A. & Simon, I. Studying and modelling dynamic biological processes using time-series gene expression data. *Nat Rev Genet* **13,** 552–564 (2012).
14. Margolin, A. A. *et al.* Reverse engineering cellular networks. *Nat Protoc* **1,** 662–671 (2006).
15. Margolin, A. A. *et al.* ARACNE: an algorithm for the reconstruction of gene regulatory networks in a mammalian cellular context. *BMC Bioinformatics* **7 Suppl 1,** S7 (2006).
16. Yun, J.-S., Rust, J. M., Ishimaru, T. & Díaz, E. A novel role of the Mad family member Mad3 in cerebellar granule neuron precursor proliferation. *Mol Cell Biol* **27,** 8178–8189 (2007).
17. Strieder, V. & Lutz, W. E2F proteins regulate MYCN expression in neuroblastomas. *J Biol Chem* **278,** 2983–2989 (2003).
18. Gualdrini, F. *et al.* Addiction of MYCN amplified tumours to B-MYB underscores a reciprocal regulatory loop. *Oncotarget* **1,** 278–288 (2010).
19. Corvetta, D. *et al.* Physical interaction between MYCN oncogene and polycomb repressive complex 2 (PRC2) in neuroblastoma: functional and therapeutic implications. *J Biol Chem* **288,** 8332–8341 (2013).
20. Mizutani, A., Furukawa, T., Adachi, Y., Ikehara, S. & Taketani, S. A zinc-finger protein, PLAGL2, induces the expression of a proapoptotic protein Nip3, leading to cellular apoptosis. *J Biol Chem* **277,** 15851–15858 (2002).
21. Furukawa, T. *et al.* Involvement of PLAGL2 in activation of iron deficient- and hypoxia-induced gene expression in mouse cell lines. *Oncogene* **20,** 4718–4727 (2001).
22. Hanks, T. S. & Gauss, K. A. Pleomorphic adenoma gene-like 2 regulates expression of the p53 family member, p73, and induces cell cycle block and apoptosis in human promonocytic U937 cells. *Apoptosis* **17,** 236–247 (2011).

23. Landrette, S. F. *et al.* Plag1 and Plagl2 are oncogenes that induce acute myeloid leukemia in cooperation with Cbfb-MYH11. *Blood* **105,** 2900–2907 (2005).
24. Zheng, H. *et al.* PLAGL2 regulates Wnt signaling to impede differentiation in neural stem cells and gliomas. *Cancer Cell* **17,** 497–509 (2010).
25. Yang, Y.-S., Yang, M.-C. W. & Weissler, J. C. Pleiomorphic adenoma gene-like 2 expression is associated with the development of lung adenocarcinoma and emphysema. *Lung Cancer* **74,** 12–24 (2011).
26. Sekiya, R. *et al.* PLAGL2 regulates actin cytoskeletal architecture and cell migration. *Carcinogenesis* **35,** 1993–2001 (2014).
27. Liu, B. *et al.* The role of pleomorphic adenoma gene-like 2 in gastrointestinal cancer development, progression, and prognosis. *Int J Clin Exp Pathol* **7,** 3089–3100 (2014).
28. Fulda, S., Lutz, W., Schwab, M. & Debatin, K. M. MycN sensitizes neuroblastoma cells for drug-induced apoptosis. *Oncogene* **18,** 1479–1486 (1999).
29. Wei, J. S. *et al.* The MYCN oncogene is a direct target of miR-34a. *Oncogene* **27,** 5204–5213 (2008).
30. Buechner, J. *et al.* Tumour-suppressor microRNAs let-7 and mir-101 target the proto-oncogene MYCN and inhibit cell proliferation in MYCN-amplified neuroblastoma. *Br J Cancer* **105,** 296–303 (2011).
31. Van Peer, G. *et al.* miRBase Tracker: keeping track of microRNA annotation changes. *Database* **2014,** bau080–bau080 (2014).
32. Chang, T.-C. *et al.* Widespread microRNA repression by Myc contributes to tumorigenesis. *Nature* **40,** 43–50 (2008).
33. Wang, Z. *et al.* MYC protein inhibits transcription of the microRNA cluster MC-let-7a-1~let-7d via noncanonical E-box. *J Biol Chem* **286,** 39703–39714 (2011).
34. Chang, T.-C. *et al.* Lin-28B transactivation is necessary for Myc-mediated let-7 repression and proliferation. *Proc Natl Acad Sci U S A* **106,** 3384–3389 (2009).

About the author

Personal information

Date of birth	May 18, 1987
Nationality	Belgian
Email address	anneleen.beckers@gmail.com
Twitter	twitter.com/AnneleenBC

Professional records

Project Manager and Data-analysis Expert at Biogazelle

Period	December 2014 - present
Location	Biogazelle NV, Zwijnaarde, Belgium

PhD fellow at Ghent University

Period	September 2010 - November 2014
Institute	Ghent University, Center for Medical Genetics, Ghent, Belgium
Funding	strategic basic research from the Agency of Promotion of Innovation by Science and Technology (IWT) (Project N° 101506)
Thesis	The role of miRNAs in neuroblastoma tumor initiation and progression
Promotors	prof. dr. Frank Speleman & prof. dr. ir. Katleen De Preter

Coach Effective Scientific Communication at Principiae

Period	April 2014
Content	Coaching PhD students in oral presentation skills, in cooperation with Jean-luc Doumont (Principiae)

Professional experiences abroad

March-April 2013	AG Pediatric Oncology Research Lab II, University Childrens Hospital Essen, Prof. Dr. Schulte J. H., Essen, Duitsland.

Education

Master of Science in Biomedical Sciences - Major Human Genetics

Period	September 2005 - June 2010
Institute	Ghent University, Ghent, Belgium
Thesis	The role of miRNAs and T-UCRs in neuroblastoma.
Promoters	prof. dr. Frank Speleman & prof. dr. ir. Katleen De Preter
Mentor	dr. ir. Pieter Mestdagh
Activities	Presidium Vlaamse Biomedische Kring (VBK)
Awards	Prize Prof. De Ridder: Prize awarded to the student with the greatest social and/or international engagement; elected by fellow students.

Scientific Achievements

Publications in A1 journals

Beckers A*, van peer G*, Carter DR, Mets E, Althoff K, Cheung BB, et al. MYCN-targeting miRNAs are predominantly downregulated during MYCN□driven neuroblastoma tumor formation. Oncotarget. 2014 Sep 16;5(0).

Althoff K*, **Beckers A*,** Bell E, Nortmeyer M, Thor T, Sprüssel A, et al. A Cre-conditional MYCN-driven neuroblastoma mouse model as an improved tool for preclinical studies. Oncogene. 2014 Sep 1.

Althoff K, **Beckers A**, Odersky A, Mestdagh P, Köster J, Bray IM, et al. MiR-137 functions as a tumor suppressor in neuroblastoma by downregulating KDM1A. Int J Cancer. 2013 Feb 7.

Althoff K, Lindner S, Odersky A, Mestdagh P, **Beckers A**, Karczewski S, et al. miR-542-3p exerts tumor suppressive functions in neuroblastoma by downregulating Survivin. Int J Cancer. 2014 Jul 21.

Van Peer G, Lefever S, Anckaert J, **Beckers A**, Rihani A, Van Goethem A, et al. miRBase Tracker: keeping track of microRNA annotation changes. Database. Oxford University Press; 2014 Jan 9;2014(0):bau080–0.

Henssen A, Thor T, Odersky A, Heukamp L, El-Hindy N, **Beckers A,** et al. BET bromodomain protein inhibition is a therapeutic option for medulloblastoma. Oncotarget. 2013 Nov;4(11):2080–95.

Bustin SA, Benes V, Garson J, Hellemans J, Huggett J, [...], **Beckers A**, et al. The need for transparency and good practices in the qPCR literature. Nature Methods. 2013 Nov;10(11):1063–7.

Rihani A, Van Maerken T, Pattyn F, van peer G, **Beckers A**, De Brouwer S, et al. Effective Alu Repeat Based RT-Qpcr Normalization in Cancer Cell Perturbation Experiments. Hoheisel JD, editor. PLoS ONE. Public Library of Science; 2013 Aug 14;8(8):e71776.

Abstracts and congress reports

Oral presentations

Beckers A., Carter D. R., Chueng B. B., Vandesompele J., Marshall G. M., De Preter K., Speleman F.: Time-resolved transcriptome analysis of TH-MYCN driven hyperplastic ganglia and tumors marks BRD3 as a novel candidate oncogene. Advances in Neuroblastoma Research 2014, Cologne, Germany, 13-16 May 2014.

Beckers A., Carter D. R., Ludwig A., Van Peer G., Chueng B. B., Vandesompele J., Marshall G. M., Shohet J. M., De Preter K., Speleman F.: The MYCN/ miR-26a-5p/ LIN28B regulatory axis explains MYCN-driven LIN28B upregulation during mouse neuroblastoma development. Oncopoint, Ghent, Belgium, xxx 2014.

Beckers A., De Preter K., Cheung B. B., Carter D. R., Van Peer G., De Brouwer S., Mestdagh P., Laureys G., Vandesompele J., Marshall G. M., Speleman F.: Dynamic regulation of miRNAs implicated in the MYCN-EZH2 regulatory axis during neuroblastoma tumor initiation and progression in a MYCN mouse model. Pediatric Cancer Research at the INTERFACE, Vienna, Austria, 6-8 June 2013.

Beckers A.: Time-resolved transcriptome analysis of TH-MYCN driven hyperplastic ganglia and tumors. ASSET GA meeting, Vienna, Austria, 9-11 June 2013.

Beckers A.: Studying neuroblastoma biology through omics analysis of NB mouse models. ENCCA-Neuroblastoma (NRC+) meeting, Amsterdam, The Netherlands, 27 May 2013.

Beckers A., Ongenaert M., Decock A., Kumps C., Pattyn F., Mestdagh P., Schulte J. H., Speleman F., De Preter K.: MiR-137 is epigenetically silenced in MYCN amplified neuroblastomas and targets the polycomb repressive complex 2 (PRC2) component EZH2. Advances in Neuroblastoma Research 2012, Toronto, Canada, 18-21 June 2012.

Poster presentations

Beckers A., Ludwig A., Van Peer G., Carter D. R., Chueng B. B., De Brouwer S., Vandesompele J., Marshall G. M., De Preter K., Shohet J. M., Speleman F. The MYCN/

miR-26a-5p/ LIN28B regulatory axis controls MYCN-driven LIN28B upregulation in neuroblastoma. Advances in Neuroblastoma Research 2014, Cologne, Germany, 13-16 May 2014.

Beckers A.*, Van Loocke W.*, Decock A., Ongenaert M., Vandesompele J., Speleman F., De Preter K.: Promoter DNA-methylation in the TH-MYCN neuroblastoma mouse model. Advances in Neuroblastoma Research 2014, Cologne, Germany, 13-16 May 2014.

Beckers A.*, Van Peer G.*, Carter D. R., Chueng B. B., Westermann F., Vandesompele J., Marshall G. M., De Preter K., Speleman F.: MYCN safeguards its upregulated expression through negatively controlling its upstream miRNAs. Advances in Neuroblastoma Research 2014, Cologne, Germany, 13-16 May 2014.

Beckers A., Decock A., Cheung B. B., Carter D. R., Van Peer G., De Brouwer S., Laureys G., Vandesompele J., Schulte J. H., Marshall G. M., Ongenaert M., De Preter K., SpelemanF. : The MYCN driven murine and human neuroblastoma methylome and dynamic regulation of chromatin regulators as a guide for epigenetic therapy. Cell Symposia: Cancer Epigenomics, Sitges, Spain, 6-8 October 2013.

Beckers A., De Preter K., Cheung B. B., Van Peer G., De Brouwer S., Mestdagh P., Laureys G., Vandesompele J., Marshall G. M., Speleman F. : Dynamic regulation of the mRNA and miRNAomes during MYCN driven neuroblastoma tumor formation yields novel insights into regulation of LIN28B expression. ASSET GA meeting, Vienna, Austria, 9-11 June 2013.

Beckers A., De Preter K., Cheung B. B., Carter D. R., Van Peer G., De Brouwer S., Mestdagh P., Laureys G., Vandesompele J., Marshall G. M., Speleman F.: Dynamic regulation of miRNAs implicated in the MYCN-EZH2 regulatory axis during neuroblastoma tumor initiation and progression in a MYCN mouse model. EMBO Conference Series: Chromatin and Epigenetics, Heidelberg, Germany, 8-12 May 2013.

Beckers A., De Wilde B., Ongenaert M., Kumps C., Schulte J. H., Vandesompele J., De Preter K., Speleman F. : Genome wide expression, mutation and methylation analysis validates three new mouse models for neuroblastoma targeting MYCN, ALK and LIN28B for pre-clinical studies. 13th Annual meeting of the Belgian Society of Human Genetics, Brussels, Belgium, 15 March 2013.

Beckers A., De Preter K., Cheung B. B., De Brouwer S., Van Peer G., Mestdagh P., Laureys G., Vandesompele J., Marshall G. M., Speleman F. : Identification of miRNAs implicated in neuroblastoma tumor initiation and progression through cross-species integrated genomic analysis. Keystone Symposia: Noncoding RNAs in Development and Cancer, Vancouver, Canada, 20-25 January 2013.

Beckers A., Ongenaert M., Decock A., Kumps C., Pattyn F., Neuroblastoma Research Consortium ., Mestdagh P., Schulte J. H., Speleman F., De Preter K.: MiR-137 is epigenetically silenced in MYCN amplified neuroblastomas and targets the polycomb repressive complex 2 (PRC2) component EZH2. Oncopoint, Ghent, Belgium, 23 May 2012.

Beckers A., Kumps C., Schramm A., Eggert A., Vandesompele J., De Preter K., Schulte J. H., Speleman F. : Accelerated TH-MYCN driven neuroblastoma formation in 129x1/SvJ mice is characterized by absence or very few cooperative genomic imbalances. Cancer Genomics, Heidelberg, Germany, 17-20 September 2011.

Beckers A., Kumps C., Schramm A., Eggert A., Vandesompele J., De Preter K., Schulte J. H., Speleman F. : Accelerated TH-MYCN driven neuroblastoma formation in 129x1/SvJ mice is characterized by absence or very few cooperative genomic imbalances. Mouse Molecular Genetics, Cambridge, Great-Britain, 17-20 September 2011.

Participations

12th Annual meeting of the Belgian Society of Human Genetics, Luttig, Belgium, 02 March 2012.
11th Annual meeting of the Belgian Society of Human Genetics, Louvain-La-Neuve, Belgium, 4 March 2011.

Mentorships

Pieter Bergez	“De toekomst van microRNA’s in de behandeling van kanker”: Z-lijn paper, 2de Bach geneeskunde, academiejaar 2010-2011. Promotor: Speleman F.
Marieke Labaere	“Optimalisatie van een mozaïsch muis model voor de studie van oncogene defecten in neuroblastoom”: Eindwerk voorgedragen tot het

behalen van het diploma master in de biomedische wetenschappen. Promotor: Speleman F.

Bieke Decaestecker "Studie van miRNAs betrokken in de ontwikkeling van neuroblastoom door middel van cross-species genomics analyses": Eindwerk voorgedragen tot het behalen van het diploma master in de biomedische wetenschappen. Promotor: De Preter K.

Brecht Dejaeghere "De interactie tussen omgevingsfactoren en epigenetica in de ontwikkeling van kanker". Z-lijn paper, 2de Bach geneeskunde, academiejaar 2012-2013. Promotor van de scriptie: De Preter K.

Simon Vanmeenen "De interactie tussen omgevingsfactoren en epigenetica in de ontwikkeling van kanker". Z-lijn paper, 2de Bach geneeskunde, academiejaar 2012-2013. Promotor van de scriptie: De Preter K. Begeleider : Beckers A.

Professional Training & Skills

Transferable skills

Coaching	course Coaching Oral Presentation (Principiae)
Writing	course Effective Written Documents (Principiae)
Presenting	course Effective Scientific Communication (Principiae)
Organization	course Personal Effectiveness (T.O.M.)
	course Leadership Foundation (Dan Steer)
	main organizer of a cycling event to sponsor childhood cancer research

Specialist training

course Introductory Statistics (IPVW)
course Analysis of Variance (IPVW)
course Datamining (UGent)
course Cytoscape (BITS - VIB)

Computer skills

Microsoft Office	Word, Excel, PowerPoint
Graphical tools	Adobe Illustrator
Data-analysis	R, GSEA, GenePattern, Ensembl